Universitat Politècnica de València
Departamento de Máquinas y Motores Térmicos

Doctoral Thesis

CFD MODELLING AND ANALYSIS OF THE PASSIVE PRE-CHAMBER IGNITION CONCEPT FOR FUTURE GENERATION SPARK-IGNITION ENGINES

Presented by:
Ibrahim Barbery Avila

Supervised by:
Prof. Ricardo Novella Rosa

in fulfillment of the requirements for the degree of
Doctor of Philosophy

Valencia, February 28th, 2023

Ph.D. Thesis

CFD MODELLING AND ANALYSIS OF THE PASSIVE PRE-CHAMBER IGNITION CONCEPT FOR FUTURE GENERATION SPARK-IGNITION ENGINES

Presented by: Ibrahim Barbery Avila
Supervised by: Prof. Ricardo Novella Rosa

Examination committee:

Chairman: Prof. Raúl Payri
Secretary: Dr. María Dolores Redel Macías
Examiner: Dr. Cinzia Tornatore

Reviewing board:

Dr. Darío López Pintor
Prof. Octavio Armas Vergel
Dr. Cinzia Tornatore

Valencia, February 28th, 2023

e

Para Ligia

Agradecimientos

Un doctorado no es simplemente una etapa de estudio, una carrera para publicar artículos o una manera de obtener un título, es un viaje de crecimiento personal donde intentamos empujar un poco los límites del conocimiento humano en un área específica, y como todo viaje se hace mucho más fácil al tener un buen guía. Yo tuve la suerte de contar con un tutor que más que guiarme en mi desarrollo profesional me ha ayudado a crecer como persona, enseñándome lecciones muy importantes sobre la vida y la familia. Por eso quiero empezar agradeciendo a mi director y amigo Ricardo, has sido un gran ejemplo para mí. También tengo que agradecer especialmente a mi tutor "no tan oficial" Josep Gómez, que me acogió como un hermano menor y me enseñó todo lo que se sobre motores y simulaciones CFD, ha sido un placer trabajar contigo y aprender de tí estos años.

Quiero darle las gracias al Instituto Universitario de Investigación CMT-Motores Térmicos por darme la oportunidad de realizar mi doctorado, en particular a su director el Dr. José María Desantes, mi jefe de línea el Dr. Jesús Benajes, varios profesores que me han acompañado durante mi formación como José Manuel Pastor y José María García Oliver, y todo el personal de secretaría que me han apoyado en mis tramites académicos y legales, en particular a Amparo Cutillas.

También debo reconocer a las personas que me apoyaron para realizar mi estancia de investigación en Sandia National Laboratories en Estados Unidos: Ales, Raja and Paul, thanks so much for your kind attention and all the knowledge that you shared with me during my time at SNL.

Mami, Papi, Vabi y Pamela, ustedes son mi mayor motivación en esta vida, gracias a ustedes soy todo lo que soy y para ustedes siempre irán todos mis triunfos, Dios no me pudo haber regalado una mejor familia, los amo.

A tí Eli, por haberme apoyado y acompañado durante mas de 3 años en mi etapa doctoral, gracias por tu comprensión, por tu paciencia y por ayudarme a crecer y salir de momentos tan difíciles.

Al resto de mi familia, mis tíos, primos y abuelos, gracias por estar siempre pendiente de mí, en especial a mi hermano Marcel con quien he tenido la alegría de compartir tantos momentos aquí en Valencia, y a mi abuelita Ligia, para quien va dedicada especialmente esta tesis.

A todos los amigos que me han acompañado en esta etapa, mis hermanos Sebas, Cesar y Tomas, de quienes he recibido tantos consejos y apoyo incondicional, y mis grandiosos compañeros de trabajo en CMT, Pablo, Cassio y Victor, gracias por hacer mis días de trabajo mucho más amenos.

Es importante destacar que esta tesis se ha desarrollado en el marco de una ayuda para la Formación de Personal Investigador (FPI) Subprograma 1 (PAID-01-19) financiada por la Universitat Politècnica de València.

Abstract

Since the irruption of electric vehicles in the automotive market as a clean and affordable transportation option, engine manufacturers have been looking for new ways to reduce the environmental footprint of current internal combustion engines (ICE's). Nowadays, most of the research efforts in passenger car applications focus on further developing spark-ignition (SI) engines to promote a new generation of high-performance and sustainable powertrains.

In this context, the pre-chamber ignition concept is becoming an attractive solution to increase the thermal efficiency of future light-duty SI engines, due to its inherent capability of enhancing the combustion process. Moreover, combining this ignition strategy with diluted mixtures (either with air or exhaust gases) has the potential to further improve the engine performance and reduce pollutant emissions. In particular, compared to active pre-chamber systems with an auxiliary fuel supply, the passive version provides advantages in terms of mechanical simplicity, packaging and cost-effectiveness. However, there are still major hurdles related to the understanding of the fundamental physicochemical aspects of the concept (turbulence, scavenging, energy conversion, jet dynamics, pre-chamber geometry...), that ultimately have limited the integration of this technology into production vehicles.

Therefore, this doctoral thesis intends to fill these knowledge gaps by using a state-of-the-art CFD model, validated with an extensive set of engine tests and following a simulation methodology specially developed for this research work. The obtained results were divided into three parts:

The first part evaluated a research single-cylinder SI engine, representative of light-duty applications, operating with the passive pre-chamber system in un-diluted stoichiometric conditions. Here, the impact of the engine operating point, spark timing and pre-chamber geometry over the physical and thermochemical processes that are involved in this combustion concept were evaluated.

The second part of the study focused on characterizing the concept in diluted conditions with air and exhaust gas re-circulation (EGR). The combustion evolution and energy distribution in the pre-chamber and main chamber for the experimental dilution limits were deeply analyzed. In addition, the use of hydrogen to extend the air-dilution limit was also assessed.

The final part of the investigation consisted in developing a potential technological application of this ignition concept from the acquired knowledge. Therefore, a pre-chamber design methodology combining 0D/1D and CFD numerical tools was developed and validated in the engine test bench. The

resulting pre-chamber offered good levels of thermal efficiency and was able to extend the EGR dilution limit.

This doctoral thesis represents a significant advancement in the frame of analyzing the impact of advanced ignition systems and their integration in ICE's in general, and in SI engines in particular, with the aim of improving the global features of these powerplants (efficiency and emissions), contributing to the effort that the scientific community is carrying out to mitigate the environmental impact of the transportation sector.

Resumen

Desde la irrupción de los vehículos eléctricos en el mercado automotriz como una opción de transporte limpia y asequible, los fabricantes de motores han estado buscando nuevas formas de reducir la huella ambiental de los actuales motores de combustión interna alternativos (MCIA). Hoy en día, la mayoría de las investigaciones en aplicaciones de vehículos de pasajeros se centran en desarrollar aún más los motores de encendido provocado (MEP) para promover una nueva generación de sistemas de propulsión sostenibles y de alto rendimiento.

En este contexto, el concepto de encendido de precámara se está convirtiendo en una solución atractiva para aumentar la eficiencia térmica de los futuros MEP para vehículos de pasajeros, debido a su capacidad de acelerar el proceso de combustión. Además, la combinación de esta estrategia de encendido con mezclas diluidas (ya sea con aire o gases de escape) tiene el potencial de mejorar aún más el rendimiento del motor. En particular, en comparación con los sistemas de precámara activa con suministro de combustible auxiliar, la versión pasiva ofrece ventajas evidentes en términos de simplicidad mecánica, ensamblaje y coste. Sin embargo, todavía existen importantes obstáculos relacionados con la comprensión de los aspectos fisicoquímicos fundamentales del concepto (turbulencia, aerodinámica, conversión de energía, dinámica de los chorros, geometría de precámara...), que en última instancia han limitado la integración de esta tecnología en producción.

Por lo tanto, esta tesis doctoral pretende extender el nivel de conocimiento de este concepto de encendido mediante el uso de un modelo CFD de última generación, validado con un extenso conjunto de medidas experimentales y siguiendo una metodología especialmente desarrollada para este trabajo de investigación. Los resultados obtenidos se dividieron en tres partes:

La primera parte evaluó un MEP monocilíndrico de investigación, representativo de vehículos automóviles, que integraba el concepto de precámara pasiva en condiciones estequiométricas sin dilución. Aquí se evaluó el impacto del punto de operación del motor, el avance del encendido y la geometría de la precámara sobre los procesos físicos y termoquímicos que intervienen en este concepto de combustión.

La segunda parte del estudio se centró en caracterizar el concepto en condiciones diluidas con aire y recirculación de gases de escape (EGR). Se analizó en profundidad la evolución del proceso de combustión y la distribución de energía en la precámara y cámara principal para los límites de dilución experimentales. Además, también se evaluó el uso de hidrógeno para ampliar el límite de dilución con aire.

La última etapa de la investigación consistió en evaluar una posible aplicación tecnológica de este concepto de encendido a partir de los conocimientos adquiridos. Por ello, se desarrolló una metodología de diseño de precámara que combina herramientas numéricas 0D/1D y CFD. Posteriormente, la metodología fue validada en el banco de ensayos del motor, y la precámara resultante ofreció buenos niveles de rendimiento térmico y fue capaz de extender el límite de dilución con EGR.

Con ello, la presente tesis doctoral supone un avance significativo en el campo del análisis del impacto de la integración de sistemas avanzados en MCIA en general, y en MEP en particular, con el objetivo de mejorar sus prestaciones, emisiones o rendimiento, contribuyendo al esfuerzo que está realizando la comunidad científica para mitigar el impacto ambiental del sector del transporte.

Resum

Des de la irrupció dels vehicles elèctrics en el mercat automotriu com una opció de transport neta i assequible, els fabricants de motors han estat buscant noves maneres de reduir la petjada ambiental dels actuals motors de combustió interna alternatius (MCIA). Hui dia, la majoria de les investigacions en aplicacions de vehicles de passatgers se centren a desenvolupar encara més els motors d'encesa provocada (MEP) per a promoure una nova generació de sistemes de propulsió sostenibles i d'alt rendiment.

En aquest context, el concepte d'encesa de precàmera s'està convertint en una solució atractiva per a augmentar l'eficiència tèrmica dels futurs MEP per a vehicles de passatgers, a causa de la seua capacitat d'accelerar el procés de combustió. A més, la combinació d'aquesta estratègia d'encesa amb mescles diluïdes (siga amb aire o productes de la combustió) té el potencial de millorar encara més el rendiment del motor. En particular, en comparació amb els sistemes de precàmera activa amb subministrament de combustible auxiliar, la versió passiva ofereix avantatges evidents en termes de simplicitat mecànica, assemblatge i cost. No obstant això, encara existeixen importants obstacles relacionats amb la comprensió dels aspectes fisicoquímics fonamentals del concepte (turbulència, aerodinàmica, conversió d'energia, dinàmica d'ejecció, geometria de precàmera...), que en última instància han limitat la integració d'aquesta tecnologia a la producció en sèrie.

Per tant, aquesta tesi doctoral pretén estendre el nivell de coneixement d'aquest concepte d'encesa mitjançant l'ús d'un model CFD d'última generació, validat amb un extens conjunt de mesures experimentals i seguint una metodologia especialment desenvolupada per a aquest treball de recerca. Els resultats obtinguts es divideixen en tres parts.

La primera part estudia un MEP monocilíndric d'investigació, representatiu dels vehicles actuals d'automoció, que integra el concepte de precàmera passiva en condicions estequiomètriques sense dilució. Ací s'avalua l'impacte del punt d'operació del motor, l'avanç de l'encesa i la geometria de la precàmera sobre els processos físics i termoquímics que intervenen en aquest concepte de combustió.

La segona part de l'estudi se centra a caracteritzar el concepte en condicions diluïdes amb aire i recirculació de gasos produïts per la combustió (EGR). S'analitza en profunditat l'evolució del procés de combustió i la distribució d'energia en la precàmera i en cambra principal per als límits de dilució experimentals. A més, també s'avalua l'ús d'hidrogen per a ampliar el límit de dilució amb aire.

L'última etapa de la investigació consisteix a avaluar una possible aplicació tecnològica d'aquest concepte d'encesa a partir dels coneixements adquirits. Per això, es desenvolupa una metodologia de disseny de precàmera que combina eines numèriques 0D/1D i CFD. Posteriorment, la metodologia és validada al banc d'assajos del motor, on la precàmera resultant ofereix bons nivells de rendiment tèrmic i és capaç d'estendre el límit de dilució amb EGR.

Amb això, la present tesi doctoral suposa un avanç significatiu en el camp de l'anàlisi de l'impacte de la integració de sistemes avançats en MCIA en general, i en MEP en particular, amb l'objectiu de millorar les seues prestacions, emissions o rendiment, contribuint a l'esforç que està realitzant la comunitat científica per a mitigar l'impacte ambiental del sector del transport.

List of publications

Following the work performed in the framework of this doctoral thesis and its associated projects, the following journal and conference papers have been published in chronological order:

- Novella, R., Gomez-Soriano, J., Barbery, I., Libert, C., & Dabiri, M. (2019). "*Understanding Passive Turbulent Jet Ignition Concept for Automotive Applications*". CONVERGE User Conference 2019, Barcelona, Spain.

- Novella, R., Gomez-Soriano, J., Raga, P., & Barbery, I. (2019). "*A CFD modeling study for improving the understanding of the Turbulent Jet Ignition concept for next generation SI engines*". HPC Spanish Combustion Workshop, 2nd edition, Barcelona, Spain.

- Novella, R., Pastor, J., Gomez-Soriano, J., Barbery, I., Libert, C., Rampanarivo, F., & Dabiri, M. (2020). "*Experimental and Numerical Analysis of Passive Pre-Chamber Ignition with EGR and Air Dilution for Future Generation Passenger Car Engines*" (No. 2020-01-0238). SAE Technical Paper. DOI: https://doi.org/10.4271/2020-01-0238.

- Benajes, J., Novella, R., Gomez-Soriano, J., Barbery, I., Libert, C., Rampanarivo, F., & Dabiri, M. (2020). "*Computational assessment towards understanding the energy conversion and combustion process of lean mixtures in passive pre-chamber ignited engines*". Applied Thermal Engineering, 115-501. DOI: https://doi.org/10.1016/j.applthermaleng.2020.115501.

- Novella, R., Gomez-Soriano, J., Barbery, I., Libert, C., Rampanarivo, F., & Dabiri, M. (2020). "*Definition of the configuration for future CNG SI engines operating with the passive pre-chamber ignition concept*". SIA Powertrain & Electronics Conference.

- Benajes, J., Novella, R., Gomez-Soriano, J., Barbery, I., Libert, C., Rampanarivo, F., & Dabiri, M. (2021). "*Advantages of hydrogen addition in a passive pre-chamber ignited SI engine for passenger car applications*". International Journal of Energy Research. DOI: https://doi.org/10.1002/er.6648.

- Novella, R., Gomez-Soriano, J., Barbery, I., & Libert, C. (2022); "*Numerical analysis of the passive pre-chamber ignition concept for light duty applications*". Applied Thermal Engineering, 118610. DOI: https://doi.org/10.1016/j.applthermaleng.2022.118610.

Contents

List of Figures

List of Tables

Nomenclature

Acronyms

A/V	Ratio between the total area of the holes and the pre-chamber volume.
AI	Auto-ignition.
AMR	Adaptive mesh refinement.
aST	After the Spark timing.
aTDC	After the Top dead center.
BDC	Bottom dead center.
CA10-90	Combustion duration.
CA10	Crank-angle for 10% of fuel burnt.
CA50	Crank-angle for 50% of fuel burnt.
CA90	Crank-angle for 90% of fuel burnt.
CAD	Crank-angle degree.
CCV	Cycle-to-cycle variability.
CFD	Computational Fluid Dynamics.
CI	Compression ignition.
CO_2	Carbon dioxide.
COV	Coefficient of variance.
CO	Carbon monoxide.
DI	Direct injection.
EAE	Energy available for ejection.
ECFM	Extended Coherent Flamelet Model.
EGR	Exhaust gas re-circulation.

EVO	Exhaust valve opening.
H_2	Hydrogen.
HC	Unburned hydrocarbons.
HRR	Heat release rate.
HR	Heat release.
ICE	Internal combustion engine.
IMEP	Indicated mean effective pressure.
IVC	Intake valve closing.
IVO	Intake valve opening.
LES	Large Eddy Simulations.
MBT	Maximum break torque.
MC	Main chamber.
NO_x	Nitrogen oxides.
OP	Operating point.
PC	Pre-chamber.
PFI	Port fuel injection.
PRF	Primary Reference Fuel.
Q_{wall}	Heat losses through the pre-chamber walls.
RGF	Residual Gas Fraction.
RON	Research Octane Number.
SD	Standard deviation.
SI	Spark ignition.
ST	Spark timing.
TDC	Top dead center.
TJI	Turbulent jet ignition.
TKE	Turbulent kinetic energy.
TKI	Tabulated kinetics of ignition.
TWC	Three-Way Catalyst.
URANS	Unsteady Reynolds-averaged Navier Stokes.

Greek symbols

Δp	Pressure difference between the pre-chamber and main chamber.
ΔCA10-90	Difference between the combustion duration of a given pre-chamber design and the combustion duration of the reference pre-chamber.

ϵ	Dissipation rate of the turbulent kinetic energy.
γ	Specific heat ratio.
λ	Relative air-to-fuel equivalence ratio.
Σ	Flame surface density.
σIMEP	Variability of the IMEP.
τ	Time for the flame to reach the holes of the pre-chamber.

Latin symbols

$\bar{c}$	Volume progress variable of the ECFM model.
$\tilde{c}$	Mass progress variable of the ECFM model.
Da	Damköhler number.
Ka	Karlovitz number.
l_f	Laminar flame thickness.
l_t	Integral length scale.
Re	Reynolds number.
S_L	Laminar flame speed.
$t*$	Time it takes the jet to reach the farthest wall distance of the main chamber.
u'	Turbulence RMS velocity.

"Simplicity is the ultimate sophistication"
Leonardo Da Vinci

Chapter 1

Introduction

Energy, one of the most important properties of the universe that has allowed mankind to evolve and develop the industrialized civilization we now live in. From the electricity in our houses to the way we go to work, today's society is completely energy dependent. Additionally, the urbanization of emerging countries and the rapid growth of human population are keeping the industry in a constant adaptation process. According to the United Nations, the global population, which today accounts for 7.6 billion people, is expected to grow by one billion people in the next decade, and increase approximately 29% by 2050, reaching a population of almost ten billion people [1]. Furthermore, one of the most important consequences that this is expected to create is an increased demand of energy and natural resources worldwide.

To highlight this issue, the Energy Information Administration (EIA) of the United States has made projections of the energy consumption by different sectors for the upcoming decades, in their International Energy Outlook report of 2021 [2]. As shown in the top of Figure 1.1, the industrial and transportation sectors are the major consumers of energy both in countries that belong and don't belong to the Organization for Economic Cooperation and Development (OECD), with a growing trend projected towards 2030. Interestingly, despite the escalating adoption of renewable sources, by 2050 most means of energy production are still expected to be fossil fuel dependent, as evidenced by the bottom plots of the aforementioned figure. Thus, society may be facing a considerable hike in the generation of Carbon Dioxide (CO_2), only attributed to this increasing energy demand.

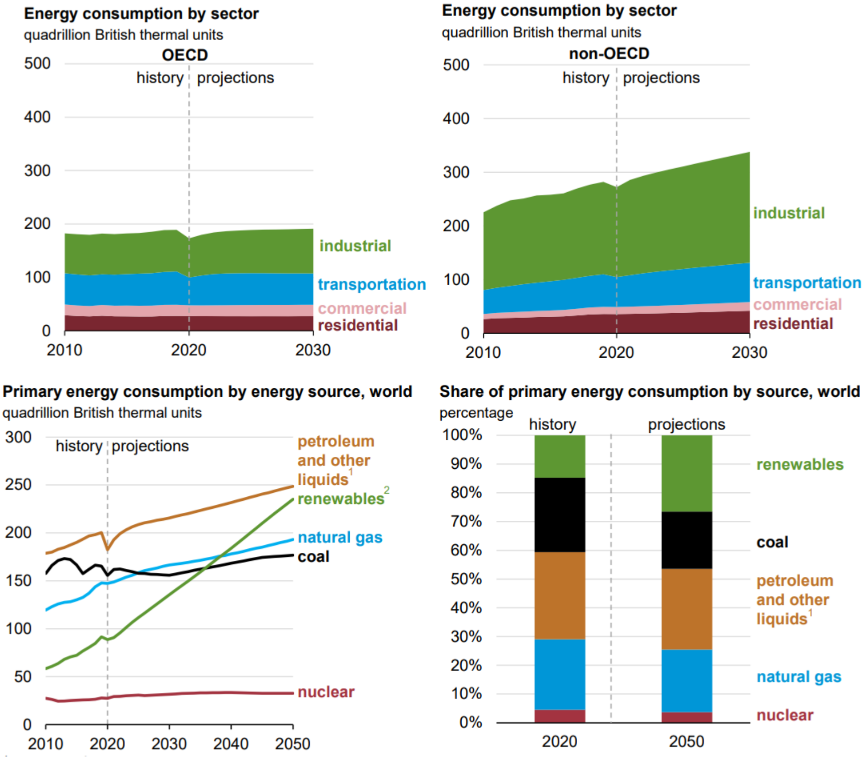

Figure 1.1: Energy consumption by sector and primary sources of energy production [2]

Being one of the major greenhouse gases (GHG), the projected increase of CO_2 is generating great concerns about the environmental footprint of these gases and their consequences over global warming. According to Hansen et al. [3], human activities have made the global surface temperature escalate at a rate of 0.2°C per decade since the 1980s, having increased almost 1°C in the post-industrial age. Global warming is causing several issues around the world, and each year the global surface temperature gets closer to levels that could potentially constitute a dangerous climate change, leading to the extermination of many species, changing the sea levels and affecting human life as we know it. Thus, humanity's motivation to find alternatives for reducing the CO_2 emissions generated by the industry has never been higher.

Particularly, the transportation sector alone accounts for almost 25% of the GHG emissions in the European Union (EU), where the vast majority of these gases are produced in road transportation by heavy-duty and light-duty or

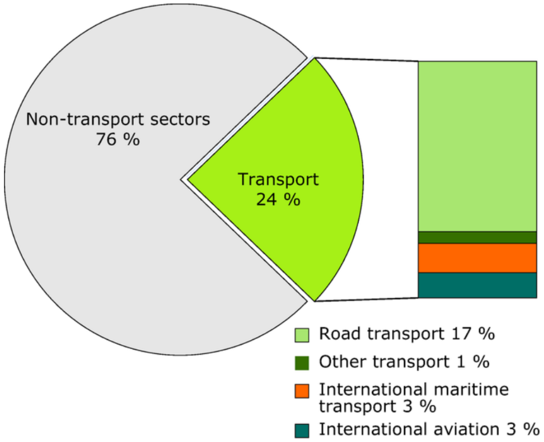

Figure 1.2: Contribution of greenhouse gases by non-transportation and transportation sectors according to the European Environment Agency [4]

passenger car vehicles [4]. This is illustrated in Figure 1.2, with data gathered by the European Environment Agency. After the sharp decrease of the GHG emissions in 2017 [5], transportation was the only major European economic sector that showed and increase in GHG. In 2018, the levels of GHG from transportation were 29% above the 1990 levels. Since then, and considering that modern vehicle technologies such as Battery Electric Vehicles (BEVs) or Fuel Cell Electric Vehicles (FCEVs) are still decades away from being majorly adopted by most countries, many research efforts have been dedicated to optimizing the current technical definitions of Internal Combustion Engines (ICE), as a potential mid-term solution for reducing the CO_2 emissions of this sector.

1.1 General scope of Internal Combustion Engines

To understand the context in which this research work is framed and highlight the interest of the subject that will be addressed, the reader must be introduced to the current landscape of Internal Combustion Engines, specifically for passenger car vehicles. In this sense, Figure 1.3 presents an analysis of the European motor vehicle market, comparing the information gathered by the European Association of Automobile Manufacturers (ACEA) on new vehicle sales in the European Union for the first half of 2021 with those for the same period in 2022 [6].

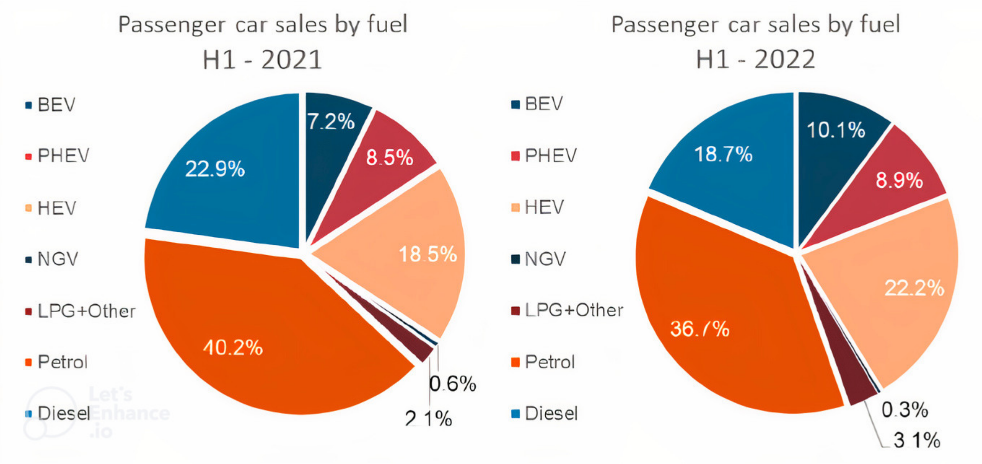

Figure 1.3: Passenger car sales in the European Union during the first semester of 2021 and 2022 [6]

It can be seen that despite the evident increase in the sale of electric vehicles (from 7% to 10% of the total), sales of vehicles powered by ICE are still leading the market, especially in the case of Spark Ignition (SI) engines. According to this data, the market share of SI engines in this type of vehicles represents approximately 67% of the total, assuming that the vast majority of Plug-in Hybrid Electric Vehicles (PHEV) and non-plug-in Hybrid Electric Vehicles (HEV) are equipped with this type of engine, and it has remained practically constant (from 67.2% to 67.8%). However, the market share of Compression Ignition (CI) engines has dropped significantly (from 22.9% to 18.7%), and it looks like this downward trend will continue in the short term. The main reason behind this trend is the excessive nitrogen oxides (NO_x) and particulate matter (PM) emissions that are generated by modern diesel vehicles [7], and the extra-cost of the after-treatment systems required in these vehicles to fulfill current European standards. On the other hand, after-treatment systems for SI engines are much cheaper. Among these, the Three-Way Catalyst (TWC) has proven to be a fundamental technology for controlling tailpipe NO_x emissions [8, 9], evolving in the direction of reducing thermal inertia to reach its working temperature more quickly, reducing the emissions of polluting gases during cold-start.

Another interesting comparison between SI and CI engines is presented in Figure 1.4, where the ideal thermodynamic working cycles are plotted for

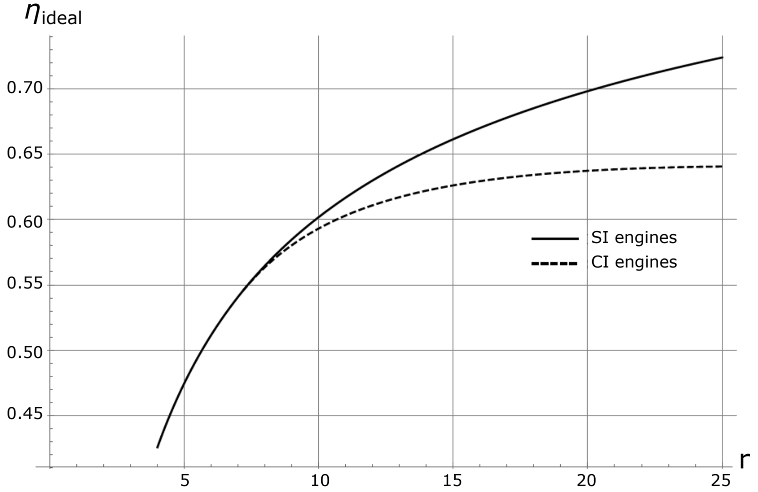

Figure 1.4: Comparison between ideal thermal efficiencies of SI and CI engines computed according to their respective thermodynamic cycles

each of these propulsive systems against the geometric compression ratio (r). These curves highlight how, at a same compression ratio, SI engines provide higher levels of efficiency than CI engines. Nevertheless, for the former powerplants the main bottleneck is the maximum compression ratio that they can achieve, which typically ranges from 8:1 to 12:1 due to knocking combustion limitations, an abnormal phenomenon that appears during the operation of SI engines and compromises their mechanical integrity [10]. This explains why equivalent CI engines usually show higher levels of thermal efficiency, given that they can operate with compression ratios that range between 18:1 and 23:1. Therefore, there is a need to continue optimizing SI engines, fundamentally in terms of thermal performance (directly related to fuel consumption and CO_2 emissions), since it is expected that they will continue to form part of most of the propulsive systems for motor vehicles at least until 2035 in the European Union, but probably much longer in other geographic regions.

1.2 Seeking the improvement of future generation spark-ignition engines

In this context, there are several advances that have been implemented or at least proposed to improve the characteristics of SI engines over the last few years. Direct injection systems, variable valve timing systems (VVT), increased compression ratio and exhaust gas re-circulation (EGR) are already fully integrated, and have been instrumental for increasing the thermal performance and the specific power generation of these engines. Among the options that are not yet widespread are water injection, variable compression ratio systems, use of carbon neutral fuels like hydrogen (H_2) or ammonia (NH_3) and operation in lean mixture conditions, which have shown their potential to further optimize performance and/or specific power, but are still with a technological complexity and/or a notable economic cost that makes their mass deployment extremely difficult.

The use of dilution strategies like EGR or lean mixtures (dilution with excess air) are of particular interest for modern passenger car vehicles. These strategies have the potential to increase the thermal efficiency of the engine by reducing the heat losses through the combustion chamber walls and enabling throttle-less operation, which reduces the pumping losses at part-load conditions [11]. Using EGR has the advantage of being compatible with the TWC, given that the mixture composition would still maintain a stoichiometric air-to-fuel equivalence ratio (λ=1), while using air dilution has the additional benefit of increasing the specific heat ratio (γ) of the mixture, which is directly proportional to the engine's thermal efficiency [12].

Nevertheless, the integration of these dilution strategies intrinsically implies a general deterioration of the combustion process, including the ignition stage. However, in reality, the inductive type ignition system (coil – spark plug) of SI engines for automotive applications has hardly undergone significant changes beyond the technological update of its components, the increase in potential difference and the energy that can be deposited between the electrodes. Therefore, the recent interest of the scientific community and the automotive industry in promoting research to further develop the introduction of EGR and lean combustion into modern vehicles, justifies the need to investigate in parallel non-conventional ignition concepts that allow to ensure a suitable combustion process even in very unfavorable conditions, and thus explore the real limits of these strategies.

Based on the previous discussion, the pre-chamber ignition concept arises as part of these non-conventional ignition systems. Having historically shown its potential to optimize the ignition process in unfavorable conditions [13], specially in high-power stationary powerplants [14], the pre-chamber ignition concept is considered as a promising candidate for increasing the thermal efficiency, improving fuel economy and reducing the CO_2 emissions of future generation SI engines. Particularly, the passive version of this technology (which will be explained in detail during the following chapters) can be easily adapted to current versions of many commercial engines. However, in the current literature, there still exists an important knowledge gap regarding the physical and thermochemical processes that are involved in this ignition concept, which has limited the successful integration of this technology in passenger car vehicles.

1.3 Thesis objective

In light of the aforementioned context, the main focus of this thesis will be the detailed study of the passive pre-chamber ignition concept for light-duty engine applications. In this sense, the main objective of the work can be defined as *characterizing the physical and thermochemical phenomena that drive the combustion process of passive pre-chambers in light-duty SI engines, both in un-diluted and diluted conditions.* This research is born to shorten the knowledge gap between the scientific principals that are found in the literature and the real-world applications of this technology, in order for it to penetrate further into the automotive market as a potential solution for improving the thermal efficiency and fuel economy of future vehicles, in hopes of reducing the environmental footprint of the transportation sector.

Most of the current investigations in the field of Internal Combustion Engines combine experimental campaigns with computational models in order to gather the most knowledge from the performed activities. In this sense, the use of Computational Fluid Dynamics (CFD) has become fundamental in the design of technological advances for ICE's, due to the capability of these complex numerical models to produce quantitative predictions of detailed fluid-flow phenomena such as turbulence, heat transfer and chemical reactions [15]. For this reason, a state-of-the-art CFD model was selected as the main tool for the activities carried out during this thesis, complemented with experimental data and simplified numerical tools to analyze in depth the characteristics of the passive pre-chamber ignition concept.

Finally, in order to fulfill the primary objective of this investigation, a set of partial objectives were defined to target several aspects of the pre-chamber system:

- **Study of the pre-chamber scavenge and flow field**: In order to understand certain details of the combustion process and the dilution tolerance, the air-management of the pre-chamber gases and the generation of turbulence inside the pre-chamber was studied by non-reacting

CFD simulations. The model was implemented with a set of dynamic tracers in order to analyze the gas exchange process during the open and closed cycles.

- **Analysis of the combustion process and energy conversion of the passive pre-chamber ignition concept in un-diluted stoichiometric conditions**: This objective is imperative for establishing a baseline understanding of the concept in terms of the energy conversion inside the pre-chamber, evolution of the flame, characteristics of the ejected jets, main chamber ignition and the general development of the combustion process in the main chamber. For this purpose, the CFD combustion model was calibrated with experimental results in order to guarantee the reliability of the numerical simulations. A sweep of engine operating conditions (load/speed) was also performed to make a full characterization of the concept.

- **Impact of the pre-chamber geometry over the scavenge and combustion process**: Understanding the influence of several geometric features of the pre-chamber over the involved physical and thermochemical processes is critical for addressing the shortcomings of the concept. In this case, both the basic geometric parameters (such as pre-chamber volume, number of holes and hole diameter) and more detailed geometric parameters (such as hole orientation, layout of the holes and position of the spark plug) were evaluated with the CFD model.

- **Compatibility with air and EGR dilution strategies**: After analyzing the concept in un-diluted conditions, the same studies were performed with EGR and air-dilution, in order to obtain a better grasp of the concept's performance in conditions where the combustion process is compromised.

- **Development of a numerical methodology to design and optimize passive pre-chambers for light-duty engines**: This objective represents the technological result of the thesis. With the gathered knowledge of the aforementioned aspects, and in order to take a step forward towards implementing this system in passenger car vehicles, it is important to provide a design pathway for optimizing the performance of the concept in a given SI engine architecture. Thus, a computational methodology combining 1D and CFD numerical tools was developed for this purpose and validated in the engine test bench.

1.4 Thesis outline

After providing the context for the investigation and explaining the aspects to be covered in the studies of the passive pre-chamber system (**Chapter 1**), the general outline of the research is summarized in Figure 1.5, from the methodology adopted for implementing the CFD model, to the activities performed in each chapter to address the partial objectives set for the thesis. The most relevant content of each chapter is described below:

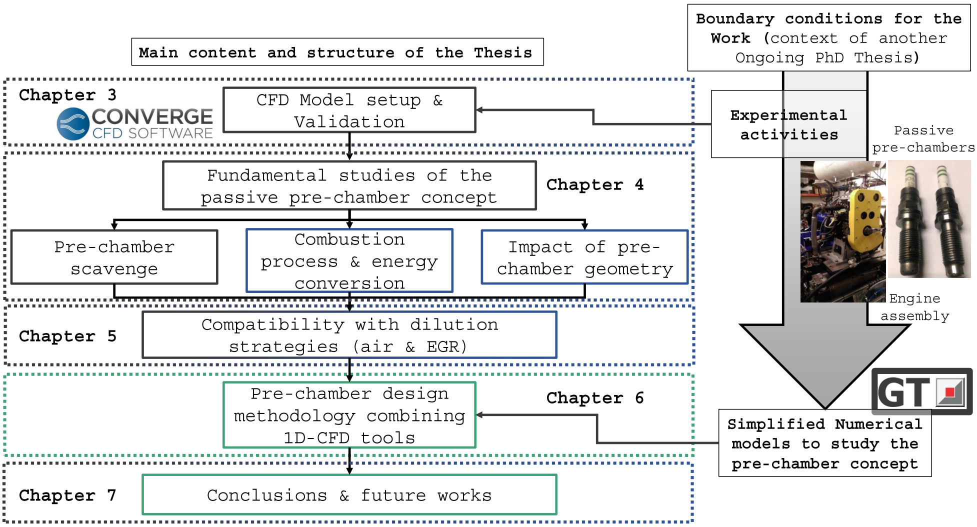

Figure 1.5: Thesis outline

Chapter 2 presents the fundamental characteristics of the combustion process in traditional SI engines, along with several strategies that are currently being investigated to improve the performance of these powerplants. Moreover, a brief review of the pre-chamber ignition concept is also presented in this chapter, highlighting the applications of this technology throughout the years and the state-of-the-art.

Chapter 3 describes the tools used for the investigation. This chapter starts by presenting the experimental facilities, characteristics of the studied engine and the simplified numerical models, all of which are used as boundary conditions in the following chapters to perform the detailed studies of the passive pre-chamber concept with the CFD model (see Figure 1.5 for reference). Then, the CFD model is introduced, together with all the numerical schemes and physical models (turbulence, combustion...) used to perform the simulations. Lastly, the modeling methodology is described and the validation of the numerical solution against experimental data is presented for several operating conditions and EGR/air dilution rates.

Chapter 4 presents the fundamental studies of the passive pre-chamber ignition concept in terms of scavenging, flow-field analysis, combustion and energy management. The results are compared at three different engine load/speed conditions, and a spark timing sweep is performed at low load/speed conditions to asses the compatibility of the concept with catalyst warm-up under cold-start conditions. A study of different pre-chamber geometric features is also presented in this chapter, evaluating the impact of pre-chamber volume, number of holes and hole orientation over the combustion process. Multi-cycle LES simulations are performed in a simplified computational domain to asses the influence of two pre-chamber designs, with very different internal flow-fields, over the cycle-to-cycle variability (CCV) of the combustion process. For these simulations only the pre-chamber combustion was considered.

In **Chapter 5** the acquired knowledge is complemented with simulations at two EGR rates (10% and 20%) and lean mixtures (λ=1.6 and λ=1.9). These studies allowed to understand the limitations of the concept when operating in combustion-compromised conditions, to better asses the compatibility of the passive pre-chamber system with dilution strategies. A potential solution for overcoming the air-dilution limit is also explored in this chapter, by adding small quantities of hydrogen to the intake port in order to improve the laminar flame speeds of the mixture. three gasoline/hydrogen blends are simulated and the impact over the combustion process is analyzed.

Chapter 6 presents the numerical methodology developed for optimizing the design of passive pre-chambers. This methodology starts by performing 0D/1D simulations with a GT-Power model of the engine and an in-house 1D jet model, assuming several simplified hypothesis for evaluating a wide array of pre-chamber geometries (in terms of volume and hole diameter) in two operating conditions. Thereafter, the set of pre-chambers is narrowed down and the most promising candidates are selected to be evaluated in the CFD model. In this stage, several combustion simulations are carried out in order to optimize the design in terms of more specific geometric features for improving both the performance of the concept and the tolerance of the final design to EGR dilution. The combustion stability of the final pre-chamber candidate is also evaluated using the multi-cycle LES methodology introduced in Chapter 4. Finally, the design methodology is validated by manufacturing the selected pre-chamber and testing it in the real engine.

Lastly, **Chapter 7** summarizes the most relevant findings and main conclusions of the research work. In addition, some ideas for future investigations are proposed from the knowledge and experience acquired during the development of this thesis.

References

[1] (UN), United Nations. *World population projected to reach 9.8 billion in 2050, and 11.2 billion in 2100.* 2017.

[2] Nalley, S and LaRose, A. *International Energy Outlook 2021 (IEO2021).* 2021.

[3] Hansen, James et al. “Global temperature change”. In: *Proceedings of the National Academy of Sciences* 103.39 (2006), pp. 14288–14293.

[4] (EEA), European Environment Agency. *Transport sector contribution to total GHG emissions (EEA-32).* 2009.

[5] Zhongming, Zhu, Linong, Lu, Xiaona, Yao, Wangqiang, Zhang, Wei, Liu, et al. “Transport: increasing oil consumption and greenhouse gas emissions hamper EU progress towards environment and climate objectives”. In: (2020).

[6] (ACEA), European Association Of Automobile Manufacturers. *Data on motor vehicle sales in the European Union in 2021 and 2022, compiled by ACEA.* 2022.

[7] O’Driscoll, Rosalind, Stettler, Marc EJ, Molden, Nick, Oxley, Tim, and ApSimon, Helen M. “Real world CO2 and NOx emissions from 149 Euro 5 and 6 diesel, gasoline and hybrid passenger cars”. In: *Science of the total environment* 621 (2018), pp. 282–290.

[8] Wang, Jihui, Chen, Hong, Hu, Zhicheng, Yao, Mingfa, and Li, Yongdan. “A review on the Pd-based three-way catalyst”. In: *Catalysis Reviews* 57.1 (2015), pp. 79–144.

[9] Ashok, B, Kumar, A Naresh, Jacob, Ashwin, and Vignesh, R. “Emission formation in IC engines”. In: *NOx Emission Control Technologies in Stationary and Automotive Internal Combustion Engines.* Elsevier, 2022, pp. 1–38. DOI: `https://doi.org/10.1016/B978-0-12-823955-1.00001-2`.

[10] Pan, Jiaying et al. “LES analysis for auto-ignition induced abnormal combustion based on a downsized SI engine”. In: *Applied Energy* 191 (2017), pp. 183–192.

[11] Germane, Geoff J, Wood, Carl G, and Hess, Clay C. “Lean combustion in spark-ignited internal combustion engines-a review”. In: (1983).

[12] Heywood, John B. *Internal Combustion Engine Fundamentals. N. York: McGraw-Hill.* 1988.

[13] Toulson, Elisa, Schock, Harold J, and Attard, William P. *A review of pre-chamber initiated jet ignition combustion systems.* Tech. rep. SAE Technical Paper, 2010. DOI: `https://doi.org/10.4271/2010-01-2263`.

[14] Heyne, S., Meier, M., Imbert, B., and Favrat, D. “Experimental investigation of prechamber autoignition in a natural gas engine for cogeneration”. In: *Fuel* 88.3 (2009), pp. 547–552. DOI: `https://doi.org/10.1016/j.fuel.2008.09.032`.

[15] Versteeg, Henk Kaarle and Malalasekera, Weeratunge. *An introduction to computational fluid dynamics: the finite volume method.* Pearson education, 2007.

Chapter 2

Fundamentals and literature review

Before diving into the detailed description of the tools used for the research and the results obtained throughout this thesis, it is important to establish some fundamental concepts about the combustion process in SI engines, as well as a bibliographical review of the passive pre-chamber ignition system and the evolution of this technology throughout history. Therefore, this chapter aims to provide the context in which the current scientific work is framed, and to supply the basic knowledge for the reader to be able to comprehend the complex physical and technological concepts used in the following chapters. On that note, Sections 2.1 and 2.2 explain the fundamentals of turbulent premixed combustion and several strategies for increasing the thermal efficiency and reducing the emissions of modern SI engines, while Section 2.3 presents a historical review of pre-chamber technology, the state-of-the-art of the passive version of this system and the knowledge gaps that are intended to be filled with this thesis.

2.1 Combustion in spark-ignition engines

A critical aspect that determines the behavior and characteristics of the combustion process is the flow-field in which this process takes place. In ICE applications the majority of the flow-fields are turbulent, where the Reynolds number is high, indicating that the inertial forces are considerably larger than the viscous forces and perturbations in the flow increase in magnitude. This leads to a fluid motion where particles do not move along ordered layers as in laminar flows.

Turbulence is one of the most complex phenomena found in physics, which is intrinsically characterized by different scale three-dimensional rotational flow structures called *turbulent eddies*. The size range of these structures depends on the Reynolds number. Furthermore, the largest eddies found in the flow are known as the integral scale, which are the most energetic vortexes. Thereafter, as the vortex stretching process takes place, the larger eddies are broken down into smaller vortexes and the kinetic energy is sequentially transferred. Ultimately, the smallest eddies, also known as the Kolmogorov scales, correspond to vortexes from which the kinetic energy is dissipated into heat due to the friction between adjacent fluid layers. This transition from largest to smallest eddies can be interpreted as an energy cascade, where the conservation of the momentum is guaranteed [1, 2].

The aforementioned characteristics are the basis of several models that have been extensively developed to describe the physics of turbulent flows, since the governing (instantaneous) equations, despite being fully known, are practically impossible to resolve due to the complex nature of the problem. These turbulence models will be described in detail in Chapter 3.

Now, in the case of port fuel injected (PFI) SI engines, the main charge is well mixed at the moment of ignition (homogeneous air-fuel blend), and the design of the ports is usually made to induce a tumble motion that generates a highly turbulent environment. Therefore, the combustion mode that takes place is a turbulent premixed combustion, where the flame front interacts with the turbulent eddies (even at the Kolmogorov scales). These mutual interactions between chemistry and turbulence lead to an increase in the mass consumption rate and the flame surface [3], due to the gradients generated by the flow motion that influence the chemical production. In this context, Borghi [4], Peters [5] and other authors have introduced a taxonomy for different flame regimes in turbulent premixed combustion, by comparing the laminar flame scales with the characteristic turbulent scales. Based on this comparison, several dimensionless numbers have been defined and are used to separate the combustion regimes.

Firstly, the Reynolds number is the ratio of the inertial forces to the viscous forces. Thus, for turbulent flows, a turbulent Reynolds number (Re) can be defined by Equation 2.1, where l_t is the integral length scale (or largest turbulent eddy length scale in m), $u^{'}$ is the turbulence intensity (or turbulent velocity fluctuations in m/s) and v is the kinematic viscosity (or momentum diffusivity in m^2/s).

$$Re = \frac{u^{'} l_t}{v} \tag{2.1}$$

Moreover, The Damköhler number, Da, is a measure of the macroscopic turbulence on a chemical reaction. It is defined in Equation 2.2 as the ratio of the integral time scale, τ_f, to the characteristic chemical reaction time scale, τ_c, where l_f is the laminar flame thickness and S_L is the laminar flame speed.

$$Da = \frac{\tau_f}{\tau_c} = \frac{l_t/u^{'}}{l_f/S_L} \tag{2.2}$$

The Karlovitz number, Ka, refers the turbulence intensity $u_k^{'}$ and the length scale l_k to the smallest turbulent eddies (Kolmogorov scale). It corresponds to the ratio of the characteristic chemical reaction time scale, τ_c, and the Kolmogorov time scale, τ_k.

$$Ka = \frac{\tau_c}{\tau_k} = \frac{u_k^{'}/l_k}{S_L/l_f} \tag{2.3}$$

Assuming equal mass diffusivity, D, for all reacting species, the Karlovitz number presented in Equation 2.3 can also be expressed by Equation 2.4.

$$Ka = \frac{l_f^2/D}{l_k^2/D} = \frac{l_f^2}{l_k^2} \tag{2.4}$$

Moreover, the Kolmogorov time scale can be defined by Equation 2.5, with $\epsilon = u^{'2}/\tau_f$ being the dissipation rate of turbulent kinetic energy.

$$\tau_k = (v/\epsilon)^{1/2} \tag{2.5}$$

Considering the same diffusivity mechanism for energy, mass and momentum it is useful to take a Schmidt number of unity. This parameter is defined as the ratio of momentum diffusivity to mass diffusivity, therefore:

$$v = D = S_L l_f \tag{2.6}$$

Finally, substituting Equations 2.5 and 2.6 in 2.3, the Karlovitz number can be recast by Equation 2.7, which is linked to Equations 2.1 and 2.2 by the relation shown in Equation 2.8.

$$Ka = (u^{'}/S_L)^{3/2}(l_f/l_t)^{1/2} \tag{2.7}$$

$$Re = Da^2Ka^2 \tag{2.8}$$

At this point, the combustion regime diagram proposed by Borghi, Peters and other authors can now be discussed, which is shown in Figure 2.1. The axis of this graph are plotted in logarithmic scales, the straight line denoted by Re=1 separates the laminar combustion regime (Re<1) from five turbulent combustion regimes (Re>1) that will be discussed in the following bullet-points:

- *Wrinkled Flamelets*: when $u^{'}<S_L$ the eddy structures are not able to enter inside the flame. As such, the laminar flame propagation dominates over the flame corrugations by turbulence (extremely low turbulent velocities).

- *Corrugated Flamelets*: when $u^{'}>S_L$, Da>1 and Ka<1 the flame thickness is smaller compared to the smallest turbulent scale, thus the entire flame is embedded within the Kolmogorov eddies. Hence, the turbulent motions can corrugate the flame front but cannot distort the inner flame layer.

- *Thickened Wrinkled Flames*: when Da>1 and Ka>1 the smallest eddies can enter the reactive flame region (pre-heat zone) but still cannot enter into the inner flame structure. This phenomenon leads to the formation of pockets of fresh and burnt gases, and the flame can no longer be identified as a laminar flame.

- *Thickened Flames*: when Da<1 the mixing of fresh and burned gases is very fast, provoking multiple and distributed reaction zones inside the unburned gas. The rate of these reactions is limited by chemistry.

- *Thick Flames or Broken Reaction Zones*: in this case the Kolmogorov eddies become smaller than the inner layer thickness, l_δ, therefore the turbulence can enter into the inner reaction layer and extinguish the flame.

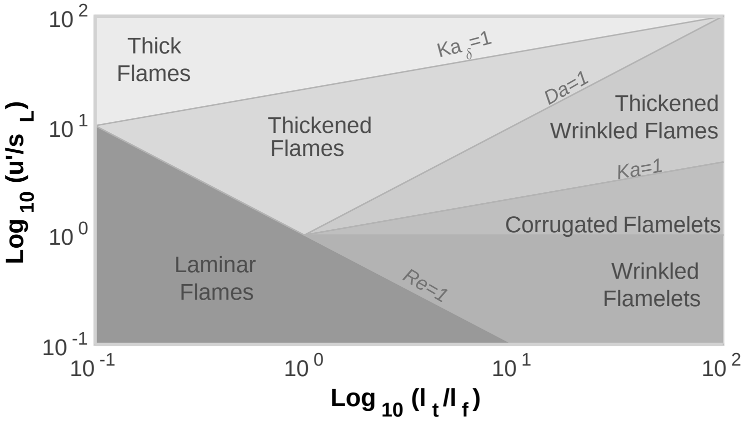

Figure 2.1: Turbulent premixed combustion regime diagram

To characterize the boundary conditions of this last turbulent regime, it is required to introduce a second Karlovitz number. Following the same structure as Equation 2.4, the Karlovitz delta, Ka_δ, can be defined by Equation 2.9.

$$Ka_\delta = \frac{l_\delta^2}{l_k^2} \tag{2.9}$$

Thus, the line denoted by Ka_δ=1 is a boundary between the previously described *thickened flames* regime (Ka_δ<1) and the *thick flames* regime (Ka_δ>1). In this limit, the inner flame thickness, l_δ, equals the size of the Kolmogorov eddies, l_k. Usually, for most premixed flames it is estimated that $\delta = l_f / l_\delta \approx 10$. Using this definition along with Equation 2.4, the Equation 2.9 can be rewritten as $Ka_\delta = \delta^2 Ka$. Therefore, the transition between *thickened flames* and *broken reaction zones* corresponds to a threshold for $Ka \approx 100$.

In outline, *corrugated flamelets* and *thickened-wrinkled flames* are the typical turbulent regimes where combustion develops in SI engine applications. A visual representation of this process is presented in Figure 2.2, where the ignition spot creates an initial flame kernel that starts propagating as a small sphere and afterwards the Kolmogorov eddies wrinkle the flame, leading to an augmented flame surface that increases the burning rates. Therefore, the turbulent flame speed, S_T, is higher than the laminar flame speed, S_L.

$$S_T = S_L + u' \tag{2.10}$$

$$S_T = f S_L \tag{2.11}$$

Historically, many experiments have been carried out on this topic to better understand the relationship between these two velocities. From these studies, several empirical correlations have been proposed, such as the work from Abdel-Gayed et al. and Gulder [6, 7] (Equation 2.10), and the expression presented in Equation 2.11, where f represents a turbulence corrective factor that is defined as the ratio between the instantaneous flame surface, A, and the average flame surface, A_T.

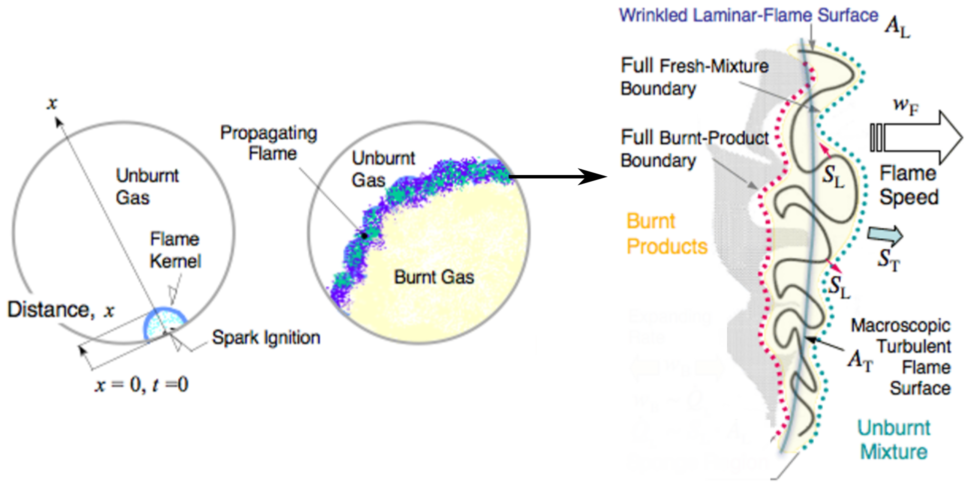

Figure 2.2: Representation of the flame propagation in an SI engine [8]

However, in the case of the pre-chamber ignition concept, the behavior of the flame in the combustion regime diagram can change significantly depending on the operating conditions (engine load/speed, mixture composition...), due to the complex physical and thermochemical phenomena involved in the combustion process. This makes it a complicated system to model numerically, which will be further explored along Chapters 4 and 5 of this thesis.

2.2 Modern strategies for improving the efficiency of SI engines

As was briefly stated in Chapter 1, the automotive sector has currently a high demand of SI engines, given that they are the main propulsion system of most passenger car vehicles. Thus, since these powerplants will continue to form part of the motor vehicle market during the next couple of decades (at least), manufacturers have shown great interest in developing technologies that allow to increase their thermal performance, reducing the fuel consumption and CO_2 emissions in order to meet the ever-changing environmental standards. In this framework, the use of diluted mixtures, such as lean burn or exhaust gas re-circulation (EGR), have been extensively studied for SI engine applications. The following subsections will present a general overview of these concepts, highlighting their advantages, drawbacks, and also some alternatives for overcoming these weaknesses.

2.2.1 Dilution strategies

The first dilution strategy that will be explained is lean burn, which consists in burning the fuel with an excess of air [9]. In this case the relative air-to-fuel equivalence ratio (λ), defined as the ratio between the real air-to-fuel ratio and the stoichiometric air-to-fuel ratio, is greater than the stoichiometric value (λ=1).

The main advantages of this combustion strategy are:

- Firstly, the specific heat ratio (γ), defined as the ratio between the heat capacity at constant pressure and the heat capacity at constant volume (C_P/C_v), increases as the excess of air rises [10], which will result in a greater thermal efficiency according to the ideal Otto cycle formulation, presented in Equation 2.12 [11]. In this equation, CR represents the compression ratio, defined as the maximum cylinder volume divided by the volume of the combustion chamber at Top Dead Center (TDC).

$$\eta_{th} = \frac{W}{Q} = 1 - \frac{1}{CR^{\gamma-1}} \tag{2.12}$$

- Moreover, as the amount of air increases, the λ value can be directly controlled by the injected fuel mass, which provides two clear benefits on the engine performance: on one hand, the fuel consumption is reduced, and on the other hand, the pumping losses decrease as the engine can be operated in less throttled conditions [12, 13].

- Another important benefit is the reduction of the heat losses through the chamber walls, since the combustion temperatures reached during the burning process decrease as the λ increases.
- Furthermore, this strategy also results in lower nitrogen oxides (NO_x) emissions, since the formation these oxides is blocked as combustion occurs at lower temperatures. This trend continues as the excess of air increases, resulting in even lower NO_x emissions. Nevertheless, reaching NO_x levels that comply with the current European standards would require the engine to be operated at very high λ values, which exceed the lean limit operation of the conventional SI concept.

Building on the previous bullet-point, the disadvantages of excess air begin to appear as the λ approaches the dilution limit:

- At the lean limit, the engine begins to face a high number of misfiring cycles that compromise its regular operation and power output. The low flammability limits of most conventional fuels used in SI engines (gasoline, CNG...) causes an increased cycle-to-cycle variability (CCV) and poor combustion stability when operating at high λ values.
- Another cause of poor combustion stability would be the slower flame speeds that lean mixtures provide. The partial burning caused by these low flame speeds affect the flame kernel growth and its propagation, leading to the aforementioned misfiring cycles in which the fuel is not successfully ignited, and therefore no power output is obtained [14].
- Misfiring cycles have two important consequences: on one hand, they cause a substantial reduction in the achieved indicated mean effective pressure (IMEP), and on the other hand, they increase the emitted hydrocarbons (HC) and carbon monoxide (CO) emissions [15].
- An important technological drawback associated to lean burn is the incompatibility with the Three-Way Catalyst, given that this device requires a stoichiometric air-fuel mixture to operate properly.

These main disadvantages of the lean burn strategy, along with the restrictive pollutant regulations, have hindered the integration of this technology into production engines. However, the recent development of enhanced ignition systems and advanced combustion concepts have raised the interest in using the lean burn proposal in the context of SI engines.

The second dilution strategy that will be described is EGR. In this case, the objective is to reduce the thermal formation of nitrogen monoxide (NO) by increasing the total amount of combustion products retained in the cylinder at the Intake Valve Closing (IVC) [16]. As with the air-dilution strategy, the decreased formation of nitrogen oxides comes from the lower combustion temperatures reached in the cylinder, given that the air-fuel mixture with EGR burns at slower rates. Particularly, the NO_x levels can be further reduced if the EGR is previously cooled [17].

$$EGR = \frac{\dot{m}_{EGR}}{\dot{m}_{int}}100 \tag{2.13}$$

The percentage of EGR can be calculated by Equation 2.13, where $\dot{m}_{EGR}$ is the recirculated exhaust mass flow and $\dot{m}_{int}$ is the total intake mass flow. This approach is usually implemented by boosting the intake pressure to keep the amount of air admitted into the engine. Furthermore, some of the advantages of this dilution strategy are:

- The increase of the thermal efficiency due to the reduction of heat losses, product of the lower combustion temperatures, combined with a reduction in the pumping work caused by the higher intake manifold pressure.
- Additionally, although EGR changes the mixture composition, it does not entail a variation in the air-to-fuel equivalence ratio, given that the total admitted air is maintained. Therefore, the engine can be operated at stoichiometric conditions, which allows the use of the Three-Way Catalyst in order to control the output NO_x emissions. This feature has allowed manufacturers to integrate this strategy into current passenger car vehicles, given that the technological complexity is reduced and it is more viable compared to lean burn.
- Moreover, the addition of EGR can also be used to avoid knocking issues, as well as enabling the use of higher compression ratios.

The disadvantages of EGR also stem from the fact that the combustion process is deteriorated:

- The slower burn rates lead to increased cycle-to-cycle dispersion, and due to these higher levels of CCV, there is a tolerance limit where the benefits in terms of thermal efficiency are lost.

- The main causes for the loss of combustion stability are the lower flammability limit and the reduction in the flame speed.
- Also, the combustion duration is prolonged as the EGR rate increases, which affects the obtained power in an undesirable way. This makes it necessary to use advanced spark timings in order to recover suitable levels of thermal efficiency.

Ultimately, despite the differences in the way of implementing both dilution approaches, the general advantages are similar whether the mixture is diluted with air or EGR. However, the main bottleneck for both technologies is the worsening of the combustion process, which prevents exploring the real limits of each strategy for improving the engine performance. Thus, enhancing either the ignition system or the combustion process becomes critical in order to extend the dilution limit and obtain the most benefits out of these strategies.

2.2.2 Ignition systems

Currently, the latest generation of SI engines increasingly use technological solutions and strategies aimed at optimizing the air-management process (variable distribution), mixture formation (combination of direct and indirect injection) and combustion (diluted mixtures with EGR or with air) in order to maximize their efficiency. Therefore, there is a strong demand for improvement of the ignition event in these engines since, in certain scenarios, the limited capacity of the conventional ignition concept (coil - spark plug) does not allow to reach the full potential of some of the aforementioned technologies [18]. In particular, the implementation of combustion with diluted mixtures significantly hinders the ignition and flame propagation process, which requires significant enhancements in the ignition system.

Consequently, research in the field of ignition systems has been brought to the fore in the development of high-efficiency SI engines. The tendencies have been directed to increasing the provided power of the ignition source, extending the duration of the energy input, generating multiple ignition spots, rising the initial ignition volume and actively managing the supplied power. In this section, non-conventional ignition systems are classified into 5 groups:

- Ignition by high energy spark [19–23].
- Nanosecond repetitively pulsed (NRP) discharge ignition [24–26].

- Radio frequency (RF) plasma ignition [27, 28].
- Laser-induced plasma ignition [29].
- Pre-chamber ignition (described in detail in Section 2.3).

Figure 2.3 shows the classification and most important characteristics of the ignition systems available for SI engines, including their level of maturity and the main challenges that they face [30].

A non-conventional ignition system must be reliable, low cost and have reduced energy consumption. Nowadays, it is indisputable that the conventional spark plug ignition system, after a century of refinement, continues to dominate the market. Despite their potential to improve the combustion process, non-conventional ignition systems must cope with the conflicting demands for both performance and reliability, in addition to meeting the particular needs of the different loads at which the engine operates. The lifespan of the spark plug is another important limitation as the energy and duration of the discharge increase. The erosion of the electrodes comes from pulverization or sputtering (erosion by high voltage) and oxidation (thermal erosion) [31], but the lifespan of the spark plug can be increased with the use of new materials and designs [32].

For ignition systems to minimize electrode erosion, ignition events at high-energy, to the extent that they generate thermal plasma, should only be applied when really necessary, depending on the specific operating conditions. Also, as the rate of erosion by sputtering is relatively low, non-thermal plasma ignition is generally considered more resistant to the erosion.

With the aim of improving the ignition process, or even facilitating the implementation of combustion concepts otherwise unreliable in new generation SI engines, where the need to maximize efficiency prevails, ignition systems have progressed at a rapid pace during the last years. High energy spark ignition systems allow the increase in power, energy and/or duration of the plasma [33]. Additionally, the increase in space between the spark plug electrodes potentially offers a greater ignition volume, leading to an increased production of active radicals.

Among non-thermal plasma ignition systems, i.e. nanosecond transient plasma [34], radio frequency corona ignition [35] and plasma induced by microwaves [36], the radio frequency corona igniter is the one that presents a greater adaptability to changing thermodynamic conditions within the combustion chamber.

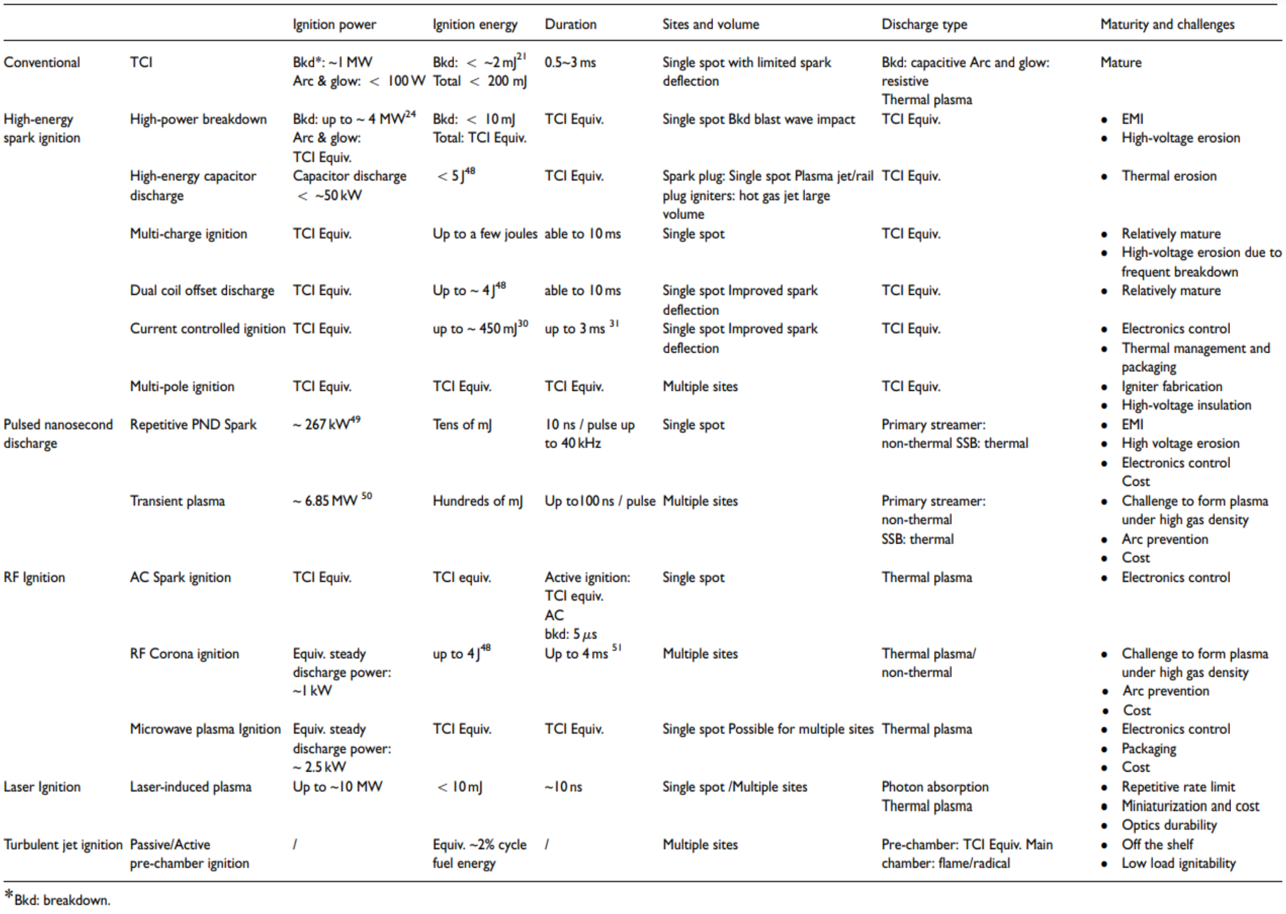

		Ignition power	Ignition energy	Duration	Sites and volume	Discharge type	Maturity and challenges
Conventional	TCI	Bkd*: ~1 MW Arc & glow: < 100 W	Bkd: < ~2 mJ[21] Total < 200 mJ	0.5~3 ms	Single spot with limited spark deflection	Bkd: capacitive Arc and glow: resistive Thermal plasma	Mature
High-energy spark ignition	High-power breakdown	Bkd: up to ~ 4 MW[24] Arc & glow: TCI Equiv.	Bkd: < 10 mJ Total: TCI Equiv.	TCI Equiv.	Single spot Bkd blast wave impact	TCI Equiv.	• EMI • High-voltage erosion
	High-energy capacitor discharge	Capacitor discharge < ~50 kW	< 5 J[48]	TCI Equiv.	Spark plug: Single spot Plasma jet/rail plug igniters: hot gas jet large volume	TCI Equiv.	• Thermal erosion
	Multi-charge ignition	TCI Equiv.	Up to a few joules	able to 10 ms	Single spot	TCI Equiv.	• Relatively mature • High-voltage erosion due to frequent breakdown
	Dual coil offset discharge	TCI Equiv.	Up to ~ 4 J[48]	able to 10 ms	Single spot Improved spark deflection	TCI Equiv.	• Relatively mature
	Current controlled ignition	TCI Equiv.	up to ~ 450 mJ[30]	up to 3 ms [31]	Single spot Improved spark deflection	TCI Equiv.	• Electronics control • Thermal management and packaging
	Multi-pole ignition	TCI Equiv.	TCI Equiv.	TCI Equiv.	Multiple sites	TCI Equiv.	• Igniter fabrication • High-voltage insulation
Pulsed nanosecond discharge	Repetitive PND Spark	~ 267 kW[49]	Tens of mJ	10 ns / pulse up to 40 kHz	Single spot	Primary streamer: non-thermal SSB: thermal	• EMI • High voltage erosion • Electronics control Cost
	Transient plasma	~ 6.85 MW [50]	Hundreds of mJ	Up to100 ns / pulse	Multiple sites	Primary streamer: non-thermal SSB: thermal	• Challenge to form plasma under high gas density • Arc prevention • Cost
RF Ignition	AC Spark ignition	TCI Equiv.	TCI equiv.	Active ignition: TCI equiv. AC bkd: 5 μs	Single spot	Thermal plasma	• Electronics control
	RF Corona ignition	Equiv. steady discharge power: ~1 kW	up to 4 J[48]	Up to 4 ms [51]	Multiple sites	Thermal plasma/ non-thermal	• Challenge to form plasma under high gas density • Arc prevention • Cost
	Microwave plasma Ignition	Equiv. steady discharge power: ~ 2.5 kW	TCI Equiv.	TCI Equiv.	Single spot Possible for multiple sites	Thermal plasma	• Electronics control • Packaging • Cost
Laser Ignition	Laser-induced plasma	Up to ~10 MW	< 10 mJ	~10 ns	Single spot /Multiple sites	Photon absorption Thermal plasma	• Repetitive rate limit • Miniaturization and cost • Optics durability
Turbulent jet ignition	Passive/Active pre-chamber ignition	/	Equiv. ~2% cycle fuel energy	/	Multiple sites	Pre-chamber: TCI Equiv. Main chamber: flame/radical	• Off the shelf • Low load ignitability

*Bkd: breakdown.

Figure 2.3: Classification and characteristics of ignition systems [30]

Laser ignition offers excellent ability to ignite extremely diluted mixtures, due to the high-power energy deposition and the possibility of creating multiple ignition points [37]. The Laser-induced plasma breakdown is facilitated in a high-density environment due to the greater photon absorption.

Pre-chamber ignition systems show promising potential to mitigate knocking combustion, as well as to extend the dilution limit of the engine, although this potential is very different depending on whether the system is active or passive. This will be further elaborated in the following section.

In short, non-conventional ignition technologies have clear advantages over the conventional spark ignition concept in terms of their compatibility with strategies that compromise the combustion process (such as dilution of the mixture with both EGR and air), although in different measures depending on the specific characteristics of the combustion system. Therefore, the new generation ignition systems are considered necessary for increasing the efficiency of future SI engines.

2.3 The pre-chamber ignition concept

As was briefly mentioned in Chapter 1, SI engines offer worse levels of efficiency and fuel consumption in comparison to equivalent CI engines. The main reasons are the low compression ratio (between 8:1 and 12:1) and the need to operate the engine with a stoichiometric air-to-fuel equivalence ratio. The octane number of the fuel and the intrinsic tendency of knocking combustion determine the limit of the compression ratio [38], while the constraints that make it necessary to operate the engine at λ=1 are related to the need of maintaining an adequate flame propagation speed, to achieve high levels of combustion efficiency [39], and the use of the Three-Way Catalyst as an after-treatment system to control the $\mathrm{NO_x}$ emissions [40].

Furthermore, the pre-chamber ignition concept, also known as Turbulent Jet Ignition (TJI) [41, 42], is presented as a very promising alternative to overcome the aforementioned limitations of SI engines and extend the synergies of these propulsion systems with the dilution strategies presented in Section 2.2. This technology has been adopted in a range of applications that span from high power stationary powerplants [43] to automotive vehicles [44].

2.3.1 General characteristics of pre-chamber combustion

The pre-chamber ignition concept uses a conventional spark plug to ignite a determined amount of air-fuel mixture in a dedicated volume (pre-chamber), which is connected to the combustion chamber (main chamber) through a set of holes [45]. As combustion progresses within the pre-chamber, the pressure in this region rises and a series of hot gaseous jets are ejected through the holes into the main chamber, forcing the onset of combustion in multiple zones and also sweeping a large part of the main chamber volume with a high shear of turbulence [46]. The typical evolution of the pre-chamber and main chamber pressure is presented in Figure 2.4, along with a 3D sketch showing the development of the jets inside the main chamber as combustion progresses.

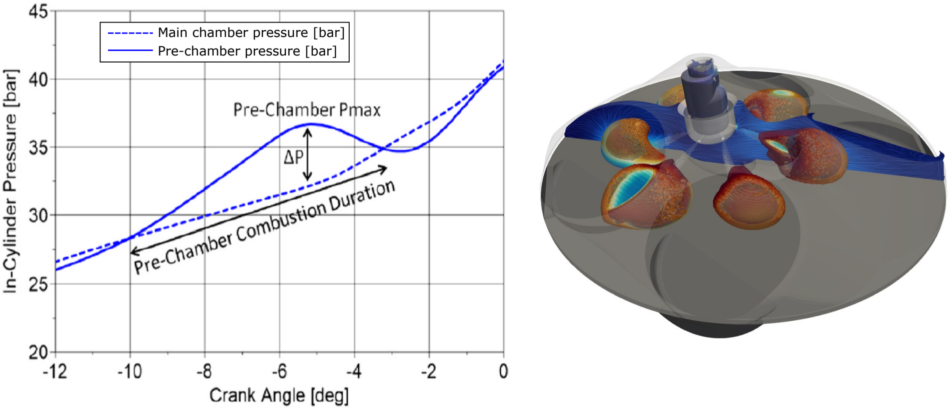

Figure 2.4: Typical evolution of the pre-chamber pressure trace (left) [47] and development of the jets in the main chamber (right).

Under suitable conditions, combustion in the main chamber operating with the pre-chamber ignition concept shows an extremely low dispersion and is significantly faster compared to the conventional spark ignition system [48]. In addition, this accelerated combustion is also favorable to mitigate the knocking tendency, which allows to increase the compression ratio in order to improve the thermal efficiency of the engine [49]. In general, these characteristics are what make the pre-chamber ignition concept a strategy of great interest to solve the fundamental problems of combustion with diluted mixtures, related to the difficulty of assuring a suitable ignition and flame propagation process.

The features of the ejected jets have been thoroughly studied in stationary chambers [50, 51], rapid compression and expansion machines (RCM) [52] and heavy duty engine applications [53] using optical techniques. Starting from these studies, it is concluded that the penetration of the jets, their duration and the characteristics of the reaction zone inside of them are aspects that strongly condition the performance of the pre-chamber ignition concept. All of these features are fundamentally dependent on the thermochemical properties of the mixture, the employed fuel, the internal geometry of the pre-chamber, the volume, the number of holes and their diameter, and the position of the ignition source (spark plug) in the pre-chamber [54].

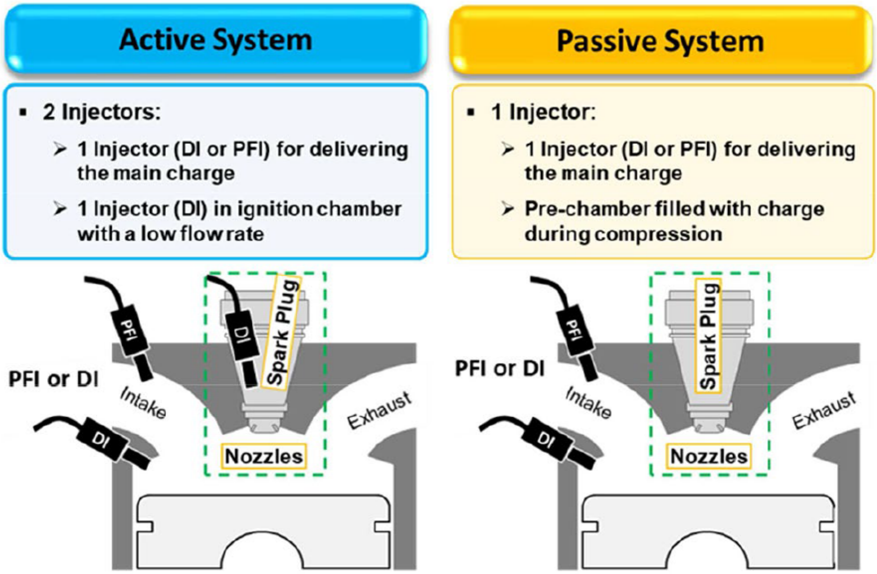

Figure 2.5: Diagram of the versions of the pre-chamber ignition concept. Passive system (right) and active system (left) [55].

As Figure 2.5 shows, the pre-chamber ignition concept can be implemented according to two approaches. In the active system, fuel is supplied directly into the pre-chamber through an additional injection system, so that the λ in this region is kept at optimum levels around stoichiometric conditions, regardless of the value defined for the main chamber charge. In this version of the concept, the high reactivity of the jets ejected from the pre-chamber favors the ignition and the development of the combustion process in the main chamber, even in extremely unfavorable conditions, allowing to burn conventional fuels (gasoline) with λ values between 2.0 and 2.4. Other benefits associated with the active system are the stratification of the mixture and the abrupt reduction of HC and NO_x emissions [56].

In the passive system, there is no additional fuel contribution in the pre-chamber, so its air-to-fuel ratio is not directly controlled [52]. In indirect injection (PFI) engines, the value of λ is essentially the same in the pre-chamber and in the main chamber, while in direct injection (GDI) engines, differences in λ between both chambers can be generated to some extent by adjusting the relative position of the injector with respect to the pre-chamber. This difference in the value of λ in the pre-chamber between both approaches allows the air-dilution limit to be noticeably higher for the active version compared to the passive version of this technology.

The pre-chamber ignition concept in its two versions has been extensively studied due to its remarkable benefits in terms of the combustion process [57, 58]. In particular, the higher burning rates, the lower cycle-to-cycle variability and its ability to operate under extremely lean conditions make the active approach an interesting technology. However, the additional cost of duplicating the injection system compromises its integration in SI engines for passenger car applications, in which costs are critical and can determine the success or failure of this version of the concept. In outline, the key advantage of the passive version is its mechanical simplicity, which makes it a reliable and low-cost system, facilitating its integration in the current versions of many commercial engines, since the pre-chamber can be mounted directly into the conventional spark plug housing. However, some aspects still need to be investigated as they represent a challenge for the passive system, such as the gas exchange process (filling and scavenging) in the pre-chamber, the limits of the concept in terms of maximum dilution with EGR or with air, the applicability at low engine load/speeds (idle conditions), and the compatibility with spark timing delay in order to accelerate the activation of the Three-Way Catalyst under starting conditions [59].

For this reason, the passive pre-chamber concept seems to be a promising solution for passenger car vehicles, as long as its performance in the entire engine operating range and its compatibility with other strategies aimed at optimizing the thermal efficiency and pollutant emissions for light-duty applications are ensured.

2.3.2 Historical review of pre-chamber technology

Active pre-chamber applications

The first practical application of the pre-chamber system was reported in the second decade of the twentieth century by Harry R. Ricardo [61], for

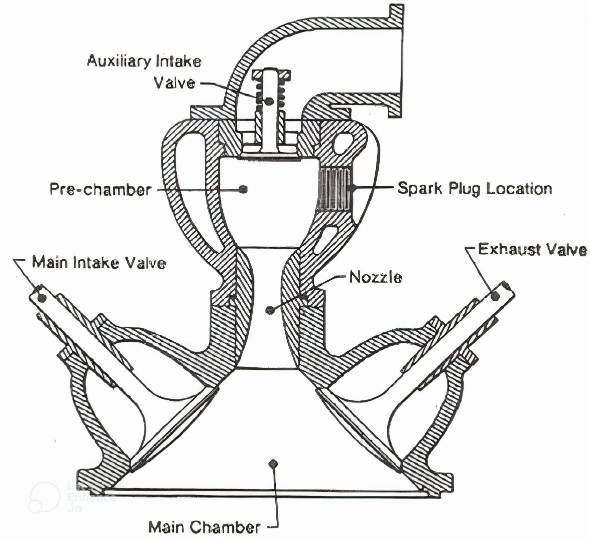

Figure 2.6: Ricardo Dolphin engine with a divided combustion chamber [60].

a two-stroke Ricardo Dolphin engine that used a pre-chamber cavity and a conventional spark plug to initiate combustion [60]. A sketch of the cylinder head is presented in Figure 2.6, where the pre-chamber is connected to the main chamber through a large convergent-divergent nozzle, and an auxiliary valve is used to scavenge the pre-chamber with a rich air-fuel mixture. Results from these studies showed higher burning rates operating with a lean mixture in the main charge, however, there was some loss of efficiency at part-load conditions due to the pneumatic mechanism of the pre-chamber valve.

A particularity of this design is that it uses a large pre-chamber (over 10% of the main chamber volume). Therefore, subsequent applications that were inspired by the Ricardo Dolphin configuration, and proposed technological adjustments to improve the performance of this engine, were also based on large volume pre-chambers [62]. Among these, the three-valve engine patented by Caleb E. Summers [63] introduced a mechanically actuated auxiliary valve and a larger nozzle, to avoid the admission of lean mixture into the pre-chamber. Moreover, Albert Bagnulo [64] proposed a dual-chamber engine with a nozzle layout that induced a swirling motion inside the pre-chamber, to generate a higher stratification of the charge in this region.

Many other authors patented engines with large pre-chambers [65–67], however, as the fuel injection system replaced the old carburetor system, the auxiliary valve was removed and engines with smaller pre-chambers started to be developed. In the 1970's, several manufacturers released engines that integrated the active pre-chamber technology. One of the early successes was the Compound Vortex Controlled Combustion (CVCC) system designed by Honda [68]. This engine added branch conduits into the torch passage, which led to a simultaneous reduction of NO_x, CO and HC emissions. Thus, the CVCC system was able to comply with the 1975 emission standards without a catalytic converter [69].

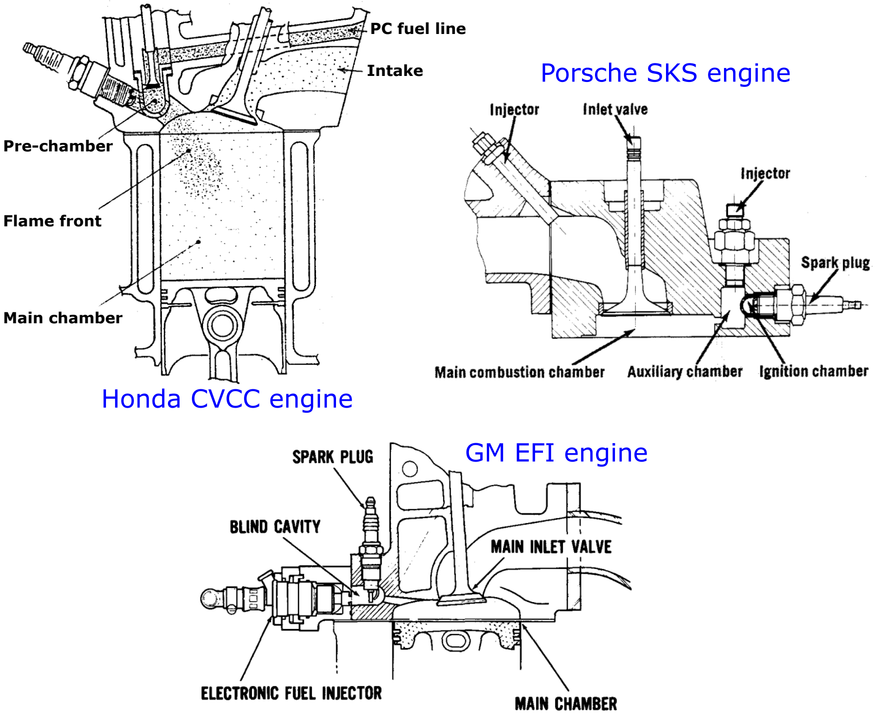

Figure 2.7: Configuration of the cylinder head for the Honda CVCC engine [68] (upper-left), the Porsche SKS engine [70] (upper-right) and the GM EFI Torch Ignition engine [71] (bottom).

Thereafter, in 1975 Porsche developed a stratified charge engine with their Stable Kernel of Combustion (SKS) system [70, 72]. In this case, the pre-chamber integrated a direct injection system to obtain a rich mixture (λ between 0.4 and 0.8), whereas the main chamber operated with λ values between 1.5 and 3.0. The emissions of a standard 911 engine were reduced without significantly compromising the specific fuel consumption, however, the HC levels were still above those required by legislation.

Moreover, General Motors (GM), Volkswagen and Ford also patented engines with this technology [71, 73, 74]. GM developed a system called Electronic Fuel Injection (EFI) Torch Ignition, which included a pre-chamber with a horizontal fuel injector and nozzle. On the other hand, the device designed by Volkswagen used a spherical pre-chamber with a tangential nozzle to generate swirl, similar to the configuration proposed by Albert Bagnulo in 1947 but with a pre-chamber injection system (PCI). Sketches for the Honda CVCC engine, the Porsche SKS engine and the GM EFI Torch Ignition engine are presented in Figure 2.7

An important characteristic of the CVCC engine was that it used a large diameter for the pre-chamber nozzle, which enabled a continuous flame front propagation from the pre-chamber towards the main chamber. However, in this same decade pre-chamber configurations with smaller nozzles started to emerge, that were able to ignite the main charge with a fast and active jet.

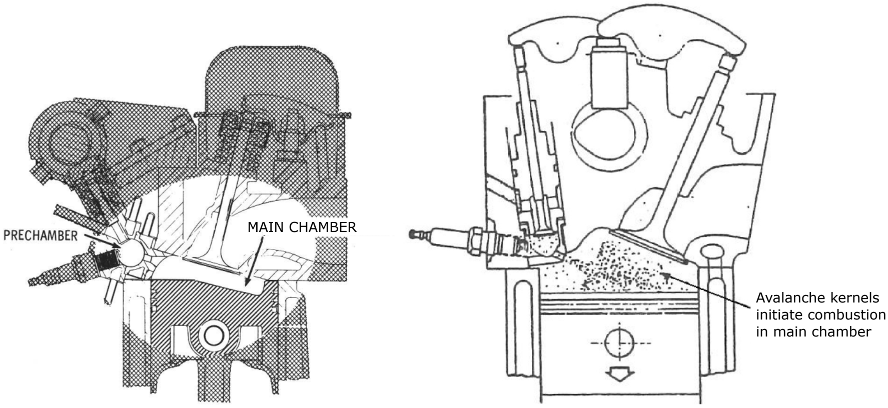

Figure 2.8: Configuration of the cylinder head for the JISCE engine [75] (left) and the LAG engine [76] (right).

Davis et al. [75] employed this principle to develop a Jet Ignition Stratified Charge Engine (JISCE), in which several experimental analysis and combustion diagnostics were performed. Afterwards, Lev Ivanovich Gussak introduced an ignition concept by incomplete combustion products, which highlighted the importance of active radicals for igniting the main charge [77, 78]. Gussak used this concept to develop an engine which he called LAG (Russian initials for Avalanche Activated Combustion) [76, 79, 80]. This system made use of a considerably smaller pre-chamber (about 2%-3% of the combustion chamber volume) than the ones developed to that date. Both the configurations of the JISCE and the LAG engine are presented in Figure 2.8.

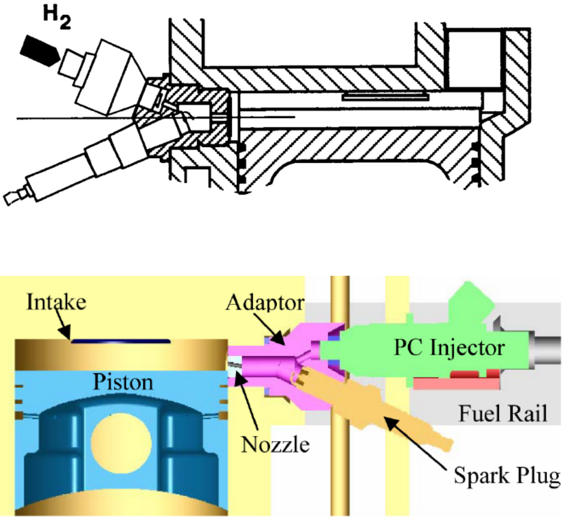

Figure 2.9: Early configuration of the Hydrogen Assisted Jet Ignition concept [81] (top) and updated version by Toulson et al. [82] (bottom).

A huge leap forward was taken in the 1990's by Harry C. Watson and Grant Lumsden, when they introduced a system called Hydrogen Assisted Jet Ignition (HAJI) [81, 83, 84]. This concept enabled a conventional gasoline engine to be operated in ultra-lean conditions (λ>2) by fueling the pre-chamber with hydrogen, which generated a high-speed jet with chemically active radicals (H and OH). The lean limit was identified when the Coefficient of Variation (COV) of the Indicated Mean Effective Pressure (IMEP) exceeded 10%. Several particularities of this system included the use of a pre-chamber with less than 2% of the clearance volume (even 1% in some cases), hydrogen supplied around 2%-3% of the main chamber energy, a lean limit extension up to λ=5, good combustion stability (less than 2% of COV IMEP) at ultra-lean conditions, significantly lower NO_x formation and improved engine efficiency [85, 86].

Years later, Toulson et al. carried out experimental campaigns of the HAJI system on a single cylinder research engine with different pre-chamber and main chamber fuels [82]. In these studies it was found that besides hydrogen, other more readily available fuels, such as Liquified Petroleum Gas (LPG) or Compressed Natural Gas (CNG), also allowed an important lean limit extension compared to the conventional SI concept. A sketch of the early HAJI system is shown in the upper-part of Figure 2.9, as well as the updated version from Toulson et al. in the bottom-part.

One of the most recent applications of pre-chamber technology is the Turbulent Jet Ignition (TJI) system developed by MAHLE Powertrain [87, 88]. This concept arose as an alternative to overcome the hurdles of the HAJI system for enabling a successful lean operation but using commercial fuels for the pre-chamber scavenge (gasoline, propane, CNG...). A very particular pre-chamber design was manufactured with several small holes connected to the main chamber for the jet ignition process. The diameter of the holes is between 1 mm and 1.25 mm, while the pre-chamber volume is kept roughly at 2% of the clearance volume to minimize HC emissions and heat losses. An electronically controlled direct injector was placed within the pre-chamber to supply the fuel. A detailed sketch of this design is presented in Figure 2.10, along with the integration of the system into the cylinder head [56].

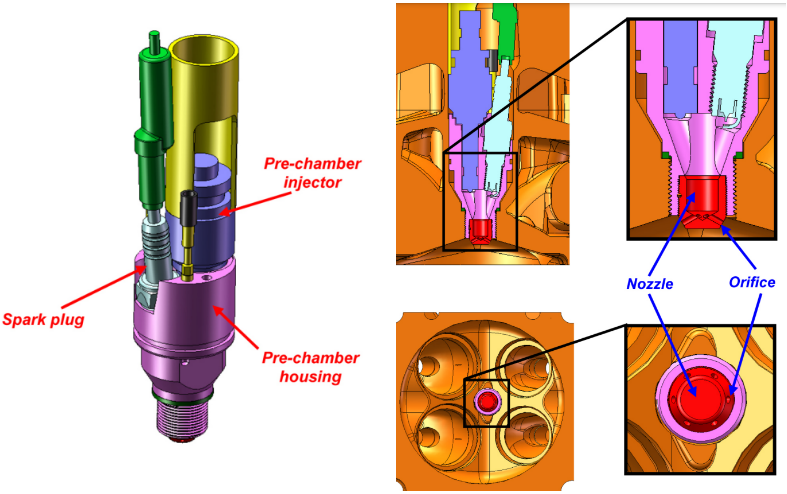

Figure 2.10: MAHLE Turbulent Jet Ignition (TJI) system [56].

Several dedicated studies of this system were carried out by Attard et al. [39, 89, 90], and the results for a λ sweep in a gasoline-fueled SI engine at part-load conditions (1500 rpm and 3.3 bar IMEP) are shown in Figure 2.11 [56]. This image highlights that the MAHLE active jet ignition system is able to extend the lean limit by over 50% compared to the regular spark plug before reaching the stability threshold, using propane as the pre-chamber fuel. The thermal efficiency of the engine and the output NO_x emissions were considerably improved, while the HC emissions were kept at similar levels as the conventional SI concept until $\lambda \approx 1.8$. Despite being very expensive and technologically complex for commercial use, several patents of the TJI system have been adopted since 2015 by Formula-1 racing teams [42].

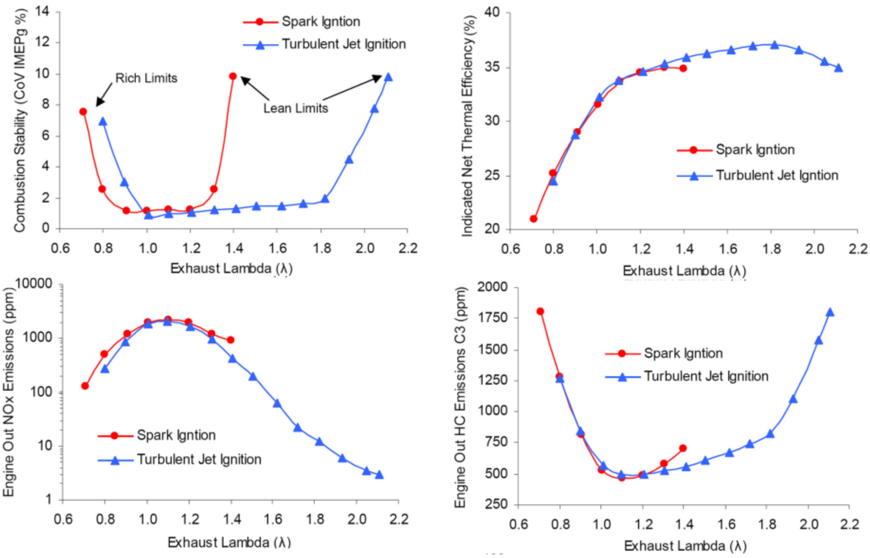

Figure 2.11: Results of the MAHLE TJI system compared to the conventional spark plug for a λ sweep at 1500 rpm and 3.3 bar IMEP [56].

In addition, during the past 3 years MAHLE has continued doing research on the active TJI system to improve its performance at part-load conditions [91], and optimize the air-to-fuel equivalence ratio across the entire engine map [47].

Passive pre-chamber applications

Active pre-chamber applications became popular because they were able to ignite lean mixtures without much effort, however, the high cost and technological complexities of these systems motivated the research and development of passive (or un-scavenged) pre-chamber applications, mainly due to their mechanical simplicity and lower assembly costs. This concept removes the auxiliary pre-chamber fueling system, and usually only includes a spark plug to initiate combustion in this region. Thus, the pre-chamber is filled with main chamber gases during the compression stroke, which represents some disadvantages from a thermodynamic point of view compared to the active approach.

The first engines that integrated passive pre-chambers were called torch cell ignition systems, such as the Turbulence Generating Pot (TGP) developed

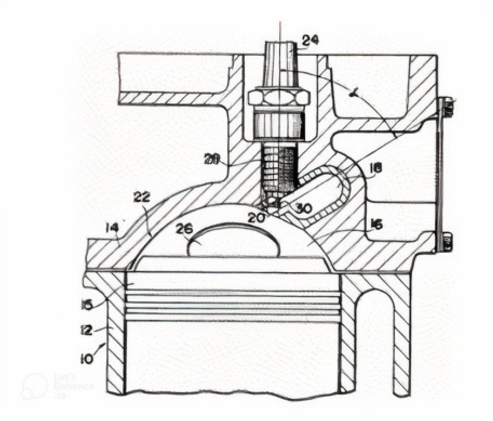

Figure 2.12: Sketch of the Turbulence Generating Pot [92].

by Toyota [93]. In the 1970's Noguchi et al. [94] and Sanda et al. [92] patented an engine with this TGP system, which allowed to increase the lean operating range compared to the conventional SI concept. Figure 2.12 shows a sketch of the aforementioned TGP engine. In the same decade General Motors [95], Ford [96, 97] and Volkswagen [98] also developed torch cell ignition engines. However, these devices were still based on large pre-chamber designs (around 10% of the combustion chamber volume).

Thereafter, as the need to improve the combustion process in highly diluted conditions became more critical, many of the technological advances focused on using other strategies to complement the passive pre-chamber system. One example from the early 1980's is the lean-burn SI engine with a catalytic pre-chamber investigated by Rychter et al. [99]. The cylinder head configuration with the passive catalytic pre-chamber is presented in Figure 2.13. The purpose of this strategy is to use a catalytic coating in the pre-chamber to induce some pre-reactions and accelerate the flame speeds, while simultaneously reducing the energy required for ignition [100, 101]. Later investigations conducted by Jarosiński et al. [102, 103] showed a reduction in HC and NO_x emissions as the lean limit was extended for this type of engines, in addition to a 33% improvement in the fuel consumption.

Moreover, during the same decade Reinhard Latsch from Bosch Stuttgart developed a swirled chamber spark plug [105]. As shown in Figure 2.14, the pre-chamber was designed to fit an M14 spark plug with four tangential nozzles to induce the swirling motion, in addition to a central hole. This system was inspired by the Avalanche Activated Combustion concept introduced by

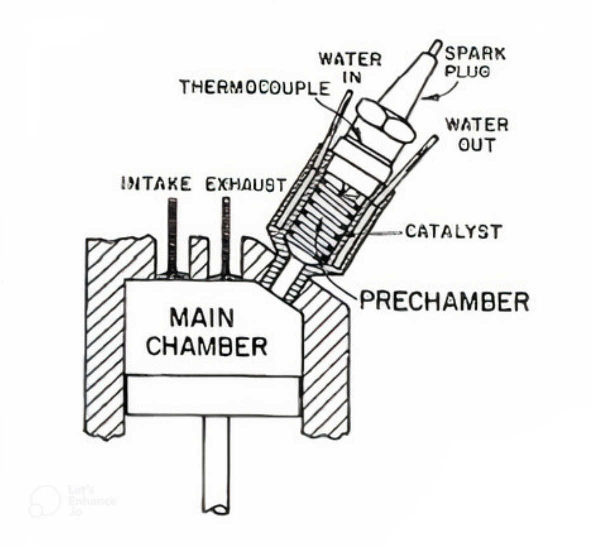

Figure 2.13: Layout of the cylinder head with a catalytic pre-chamber [101].

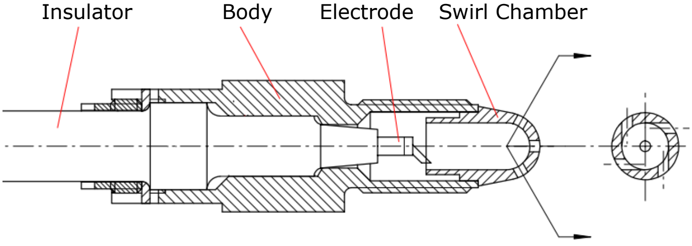

Figure 2.14: Sketch of the swirled chamber spark plug [104].

Gussak [77] (LAG engines). Several researches conducted in the 1980's [106–108] demonstrated that the burn rates were improved with this pre-chamber configuration, allowing to achieve higher thermal efficiency levels at low engine loads, especially if the geometric features of the pre-chamber are set properly.

Building on the swirled chamber spark plug, Weng et al. [110] started working on a configuration in 1999 to further improve the performance of this concept, by adding a direct injection strategy in the main chamber. This system was called Bowl Pre-chamber Ignition (BPI), and it consisted in generating a lean mixture from an initial injection during the intake stroke, and using a bowl-shaped piston to accumulate a small amount of extra fuel mass from a secondary injection event during the compression stroke. This way, a

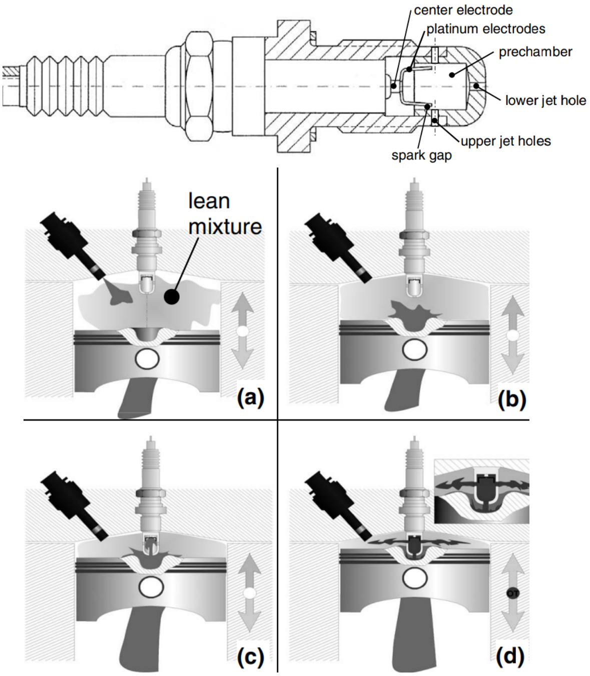

Figure 2.15: Stages of the BPI system: (a) Secondary injection during the compression stroke, (b) Accumulation of rich air-fuel mixture in the piston bowl, (c) Filling of the pre-chamber, (d) Ignition and jet ejection [109].

richer air-fuel mixture is transferred to the pre-chamber in the final stages of the compression, improving the burning rates as the mixture is ignited in this region. The secondary injection only provided 5% of the total fuel mass.

Figure 2.15 shows a schematic representation of this process along with the employed pre-chamber, which consists of several holes manufactured near the middle-section of this volume and a bottom hole oriented towards the piston bowl. This concept enabled a lean limit extension up to $\lambda = 1.7$ without compromising the levels of HC emissions [111]. What's more, Kettner et al. [109] showed that it can be used with adequate levels of EGR dilution to improve the fuel consumption at part-load conditions.

During the past two decades, advancements in High Performance Computing (HPC) has highlighted the importance of using numerical models to study both basic and complex physical phenomena in many engineering applications. In the frame of the passive pre-chamber system, the experimental limitations of studies performed in the 20th century hindered the potential

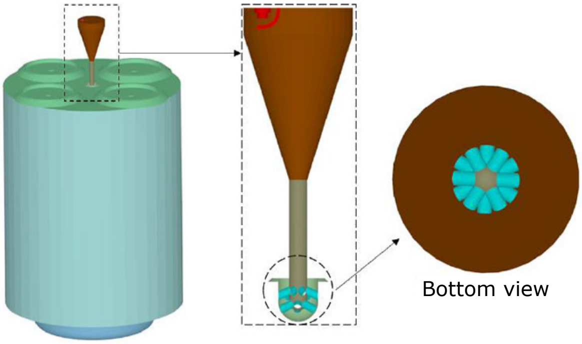

Figure 2.16: 3D CFD model of the KAUST narrow throat pre-chamber [112].

of truly understanding the underlying physicochemical characteristics of the concept. Thus, the development of 3D Computational Fluid Dynamics (CFD) models can help to gain further insight on these aspects.

In this sense, many researches have been focused on modelling the pre-chamber concept with CFD in a variety of applications [113–119]. Furthermore, one of the most interesting investigations in recent years has been carried out at the King Abdullah University of Science and Technology (KAUST), where a narrow throat pre-chamber with a conical body has been evaluated in a heavy-duty engine fueled with natural gas [120, 121]. The computational domain for the CFD simulations performed with the KAUST pre-chamber is shown in Figure 2.16, where the particular design includes two rows of nozzles that are slightly displaced along the pre-chamber throat.

Silva et al. [112] assessed the effects of the throat diameter, nozzle diameter and nozzle length over the combustion process in both chambers. The results revealed that the nozzle and throat diameters had an important impact on the pre-chamber pressurization and the duration of the ejection process (until the flow reversal), while the nozzle length had a minor impact on these features, giving an interesting degree of freedom to design the nozzles in favor of their mechanical integrity. This type of studies exhibit the capabilities of 3D simulations to evaluate detailed geometrical aspects of the pre-chamber, as well as their impact over the phenomena related to turbulence and chemistry, which are essential for optimizing the performance of the concept.

One of the major hurdles that has prevented the integration of the passive pre-chamber system into commercial passenger car engines is related to the characteristic small size of the pre-chamber, which has important limitations under conditions where the combustion process is compromised due to the

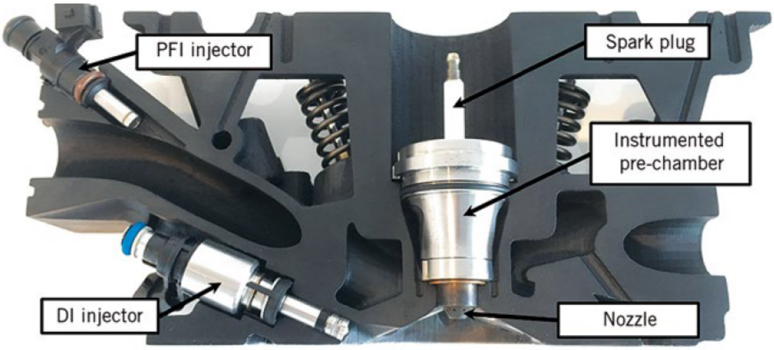

Figure 2.17: Cylinder head assembly of the MAHLE passive jet ignition system [122].

low amount of fuel (part-loads) or the worsened thermochemical properties of the mixture (flame extinction that leads to misfires and high cycle-to-cycle variability). Due to several aspects that are still not fully understood, the compatibility of the passive pre-chamber concept with strategies such as air/EGR dilution and spark timing delay for catalyst activation under cold-start conditions has been limited for light-duty applications [123].

In the last three years MAHLE Powertrain has been developing a passive version of their Turbulent Jet Ignition system, with the particular cylinder head design shown in Figure 2.17 in order to fit the pre-chamber spark plug. Encouraging results of this concept have been reported by Cooper et al. [55, 122], where the passive pre-chamber has shown good knock mitigation capabilities, increased power output, reduced specific fuel consumption at high loads and several improvements at part-loads. Some of these results are presented in Figure 2.18, for an engine load sweep at 4000 rpm and stoichiometric conditions. Here, it is clearly observed how the passive pre-chamber system is able to maintain optimum CA50 values from 4 bar up to 16 bar of BMEP, with low levels of COV IMEP and high pressure rises. Additionally, Cooper has also reported that an optimization of the internal pre-chamber geometry combined with the use of Miller Cycle, increased compression ratio and suitable levels of EGR can extend the synergies of the concept with catalyst warm-up at low loads [55].

Nevertheless, there is still a lack of detailed information about how to achieve good synergies with strategies like air/EGR dilution and spark timing delay at low load/speed conditions. An extensive comprehension of aspects such as turbulence generation and scavenging of residuals inside the

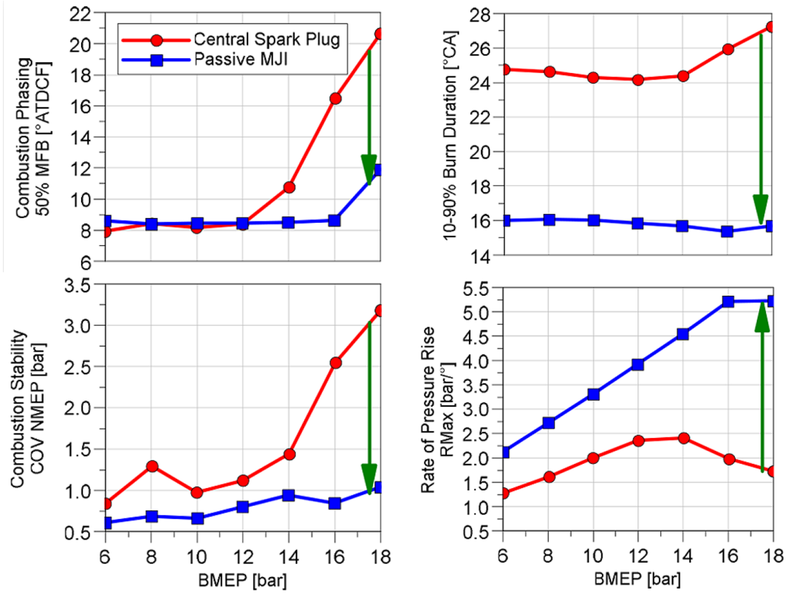

Figure 2.18: Results of the MAHLE passive jet ignition system over an engine load sweep at 4000 rpm [122].

pre-chamber, energy conversion, thermo-fluid dynamics of the jets and overall behavior of the combustion process, is necessary for developing a design path that would allow to optimize the concept's performance. Thus, evaluating the aforementioned physicochemical phenomena by advanced CFD simulations, in order to extract the key features of this ignition system, is the main knowledge gap that will be addressed in this PhD thesis.

2.4 Summary

During this chapter, several important concepts to understand the studies performed in this research work have been introduced, starting with the fundamental characteristics of the turbulent premixed combustion process that takes place in spark-ignition engines. Furthermore, the construction of the flame regime diagram proposed by Borghi [4], Peters [5] and other authors was explained by defining several dimensionless numbers, such as the Damköhler number (Da) and the Karlovitz number (Ka), that are based on comparing the laminar flame scales with the characteristic turbulent scales and separate 5 turbulent combustion regimes. Typically, *corrugated flamelets*, where Da>1 and Ka<1, and *thickened-wrinkled flames*, where Da>1 and Ka>1, are the turbulent regimes where combustion develops in SI engines.

Thereafter, some strategies for improving the thermal efficiency and pollutant emissions of SI engines were presented. The first consisted in using diluted mixtures (either with air or exhaust gases) to reduce the heat losses through the chamber walls by achieving lower combustion temperatures, in addition to reducing the pumping work at part-load conditions by enabling throttle-less operation. using EGR dilution has the advantage of being compatible with the Three-Way Catalyst for controlling the engine output NO_x emissions, since the air-fuel mixture can maintain a stoichiometric equivalence ratio. Nevertheless, both air-dilution and EGR deteriorate the combustion process as the dilution rate increases, leading to misfiring cycles and important stability issues. In light of this, the second strategy that was proposed was the use of non-conventional ignition systems to overcome the hurdles of diluted mixtures by enhancing the combustion process. 5 groups of high-energy ignition systems were presented with a brief literature review of each one, highlighting the pre-chamber ignition concept as a potential solution for future passenger car engines.

Thus, the final part of this chapter focused on describing the characteristics of the pre-chamber ignition system. This strategy separates the combustion chamber into two regions, a pre-chamber (where the spark plug is placed) and a main chamber (where most of the air-fuel mixture is located), which are connected through one or more nozzles. The combustion initiates in the pre-chamber, and as the flame reaches the nozzles, hot gaseous jets are ejected towards the main chamber, providing a multi-zone ignition with a large flame surface. Therefore, this concept is able to achieve faster burning rates and lower levels of cyclic dispersion compared to the conventional spark plug, which allows to mitigate the knocking tendency and burn leaner mixtures.

The pre-chamber system can be implemented according to two approaches: active systems, where auxiliary fuel is supplied directly into the pre-chamber, and passive systems, where there is no additional fuel contribution into the pre-chamber. Since the 1920's, several versions of the active pre-chamber system have been used in SI engine applications, given that this concept has shown the capability of burning extremely lean mixtures (λ>2) as the ejected jets are always in favorable conditions due to the dedicated fuel scavenge in the pre-chamber. However, the additional expenses and technological complexity of integrating the pre-chamber fuel supply system compromises the use of this approach for commercial passenger car engines (where costs are critical).

On the other hand, the passive pre-chamber concept has a mechanical simplicity that provides good adaptability for many current SI engine architectures, given that it can share the same housing as the conventional spark plug. This has motivated many studies throughout history to further develop this technology. Nevertheless, for light-duty applications, the characteristic small size of the pre-chamber has shown relevant drawbacks under conditions where the combustion process is compromised due to the low amount of fuel (part-loads) or the worsened thermochemical properties of the mixture (flame extinction that leads to misfires and high cycle-to-cycle variability). This has limited the ability of the concept to achieve high levels of air/EGR dilution and the compatibility with spark timing retard at loads consistent with idle and cold-start conditions for accelerating the catalyst activation.

Despite recent studies have reported that an optimization of the internal pre-chamber geometry can help to extend the synergies with the aforementioned engine strategies [55], there is still limited information about features like turbulence, scavenging of internal residuals, thermochemical properties of the mixture, energy conversion, dynamics of the jets and overall behavior of the combustion process, that are necessary to understand in order to optimize the pre-chamber design and improve the performance of the concept. This represents the main knowledge gap that is intended to be filled in this PhD thesis, using CFD as the main tool for analyzing the aforementioned physicochemical characteristics of this ignition strategy, to take a step in the direction of developing this technology for future passenger car applications.

References

[1] Richardson, Lewis Fry. *Weather prediction by numerical process.* University Press, 1922.

[2] Kolmogorov, Andrey Nikolaevich. “The local structure of turbulence in incompressible viscous fluid for very large Reynolds numbers”. In: *Cr Acad. Sci. URSS* 30 (1941), pp. 301–305.

[3] Poinsot, Thierry and Veynante, Denis. *Theoretical and numerical combustion.* RT Edwards, Inc., 2005.

[4] Borghi, R. “On the structure and morphology of turbulent premixed flames”. In: *Recent advances in the Aerospace Sciences.* Springer, 1985, pp. 117–138.

[5] Peters, Norbert. “The turbulent burning velocity for large-scale and small-scale turbulence”. In: *Journal of Fluid mechanics* 384 (1999), pp. 107–132.

[6] Abdel-Gayed, RG, Bradley, D, and Lau, AKC. “The straining of premixed turbulent flames”. In: *Symposium (International) on Combustion.* Vol. 22. 1. Elsevier. 1989, pp. 731–738.

[7] Gülder, Ömer L. “Turbulent premixed flame propagation models for different combustion regimes”. In: *Symposium (International) on Combustion.* Vol. 23. 1. Elsevier. 1991, pp. 743–750.

[8] Extracted: *https://glanze.sakura.ne.jp/propagate.html.*

[9] Heywood, John B. *Internal Combustion Engine Fundamentals. N. York: McGraw-Hill.* 1988.

[10] Ayala, Ferrán A, Gerty, Michael D, and Heywood, John B. *Effects of combustion phasing, relative air-fuel ratio, compression ratio, and load on SI engine efficiency.* Tech. rep. SAE Technical Paper, 2006.

[11] Payri González, Francisco and Desantes Fernández, José M$^{\text{a}}$. *Motores de combustión interna alternativos.* Editorial Universitat politécnica de valencia, 2011.

[12] Germane, Geoff J, Wood, Carl G, and Hess, Clay C. “Lean combustion in spark-ignited internal combustion engines-a review”. In: (1983).

[13] Attard, William P and Blaxill, Hugh. *A lean burn gasoline fueled prechamber jet ignition combustion system achieving high efficiency and low NOx at part load.* Tech. rep. SAE Technical Paper, 2012. DOI: `https://doi.org/10.4271/2012-01-1146`.

[14] Quader, Ather A. “Lean combustion and the misfire limit in spark ignition engines”. In: *SAE transactions* (1974), pp. 3274–3296.

[15] Stadler, Andreas, Wessoly, Maximilian, Blochum, Sebastian, Härtl, Martin, and Wachtmeister, Georg. “Gasoline fueled pre-chamber ignition system for a light-duty passenger car engine with extended lean limit”. In: *SAE International Journal of Engines* 12.3 (2019), pp. 323–340.

[16] Wei, Haiqiao, Zhu, Tianyu, Shu, Gequn, Tan, Linlin, and Wang, Yuesen. “Gasoline engine exhaust gas recirculation–A review”. In: *Applied energy* 99 (2012), pp. 534–544.

[17] Toulson, Elisa, Watson, Harry C, and Attard, William P. “The effects of hot and cool EGR with hydrogen assisted jet ignition”. In: *Asia Pacific Automotive Engineering Conference*. 2007-01-3627. 2007.

[18] Reitz, Rolf D et al. *IJER editorial: The future of the internal combustion engine*. 2020.

[19] Han, Sung Bin, Choi, Kyu Hoon, Ra, Sung Oh, Lee, Sang Joon, and Lee, Jong Tai. *Ignitability and combustion characteristics of the multi spark capacitor discharge ignitor for a lean burn engine*. Tech. rep. SAE Technical Paper, 1995.

[20] Hese, Martin, Tschöke, Helmut, Breuninger, Tobias, Altenschmidt, Frank, and Winter, Harald. “Influence of a Multispark Ignition System on the inflammation in a Spray-guided Combustion Process”. In: *SAE International Journal of Fuels and Lubricants* 2.2 (2010), pp. 376–386.

[21] Alger, Terrence, Gingrich, Jess, Mangold, Barrett, and Roberts, Charles. “A continuous discharge ignition system for EGR limit extension in SI engines”. In: *SAE International Journal of Engines* 4.1 (2011), pp. 677–692.

[22] Hayashi, Naoto, Sugiura, Akimitsu, Abe, Yuya, and Suzuki, Kotaro. “Development of ignition technology for dilute combustion engines”. In: *SAE International Journal of Engines* 10.3 (2017), pp. 984–994.

[23] Han, Xiaoye, Yu, Shui, Tjong, Jimi, and Zheng, Ming. “Study of an innovative three-pole igniter to improve efficiency and stability of gasoline combustion under charge dilution conditions”. In: *Applied Energy* 257 (2020), p. 113999.

[24] Pancheshnyi, Sergey V, Lacoste, Deanna A, Bourdon, Anne, and Laux, Christophe O. "Ignition of propane–air mixtures by a repetitively pulsed nanosecond discharge". In: *IEEE Transactions on Plasma Science* 34.6 (2006), pp. 2478–2487.

[25] Lefkowitz, Joseph K et al. "Schlieren imaging and pulsed detonation engine testing of ignition by a nanosecond repetitively pulsed discharge". In: *Combustion and Flame* 162.6 (2015), pp. 2496–2507.

[26] Tanoue, Kimitoshi et al. "Development of a novel ignition system using repetitive pulse discharges: application to a SI Engine". In: *SAE International Journal of Engines* 2.1 (2009), pp. 298–306.

[27] Heise, Volker, Farah, Philippe, Husted, Harry, and Wolf, Edgard. *High frequency ignition system for gasoline direct injection engines.* Tech. rep. SAE Technical Paper, 2011.

[28] Mariani, Antonio and Foucher, Fabrice. "Radio frequency spark plug: An ignition system for modern internal combustion engines". In: *Applied energy* 122 (2014), pp. 151–161.

[29] Bradley, D, Sheppard, CGW, Suardjaja, IM, and Woolley, R. "Fundamentals of high-energy spark ignition with lasers". In: *Combustion and Flame* 138.1-2 (2004), pp. 55–77.

[30] Yu, Shui and Zheng, Ming. "Future gasoline engine ignition: A review on advanced concepts". In: *International Journal of Engine Research* 22.6 (2021), pp. 1743–1775.

[31] Nishioka, Shin, Hanashi, Ken, and Okabe, Shinichi. *Super ignition spark plug with wear resistive electrode.* Tech. rep. SAE Technical Paper, 2008.

[32] Maly, Rudolf R and Herweg, Rüdiger. "Spark ignition and combustion in four-stroke gasoline engines". In: *Flow and combustion in reciprocating engines.* Springer, 2008, pp. 1–66.

[33] Dale, J De, Checkel, MD, and Smy, PR. "Application of high energy ignition systems to engines". In: *Progress in energy and combustion science* 23.5-6 (1997), pp. 379–398.

[34] Shiraishi, Taisuke, Urushihara, Tomonori, and Gundersen, Martin. "A trial of ignition innovation of gasoline engine by nanosecond pulsed low temperature plasma ignition". In: *Journal of Physics D: Applied Physics* 42.13 (2009), p. 135208.

[35] Suess, M, Guenthner, M, Schenk, M, and Rottengruber, HS. “Investigation of the potential of corona ignition to control gasoline homogeneous charge compression ignition combustion”. In: *Proceedings of the Institution of Mechanical Engineers, Part D: Journal of Automobile Engineering* 226.2 (2012), pp. 275–286.

[36] Wang, Zhi, Huang, Jian, Wang, Qiang, Hou, Lingyun, and Zhang, Guixin. “Experimental study of microwave resonance plasma ignition of methane–air mixture in a constant volume cylinder”. In: *Combustion and Flame* 162.6 (2015), pp. 2561–2568.

[37] Dodd, Robert et al. “Laser ignition of an IC test engine using an Nd: YAG laser and the effect of key laser parameters on engine combustion performance”. In: *Lasers in Engineering* 17.3 (2007), pp. 1554–2971.

[38] Attard, William P, Konidaris, Steven, Hamori, Ferenc, Toulson, Elisa, and Watson, Harry C. *Compression Ratio Effects on Performance, Efficiency, Emissions and Combustion in a Carbureted and PFI Small Engine.* Tech. rep. SAE Technical Paper, 2007.

[39] Attard, William P and Parsons, Patrick. “Flame kernel development for a spark initiated pre-chamber combustion system capable of high load, high efficiency and near zero NOx emissions”. In: *SAE International Journal of Engines* 3.2 (2010), pp. 408–427.

[40] Wang, Jihui, Chen, Hong, Hu, Zhicheng, Yao, Mingfa, and Li, Yongdan. “A review on the Pd-based three-way catalyst”. In: *Catalysis Reviews* 57.1 (2015), pp. 79–144.

[41] Toulson, Elisa, Schock, Harold J, and Attard, William P. *A review of pre-chamber initiated jet ignition combustion systems.* Tech. rep. SAE Technical Paper, 2010. DOI: `https://doi.org/10.4271/2010-01-2263`.

[42] Alvarez, Carlos Eduardo Castilla, Couto, Giselle Elias, Roso, Vinıcius Rückert, Thiriet, Arthur Braga, and Valle, Ramon Molina. “A review of prechamber ignition systems as lean combustion technology for SI engines”. In: *Applied Thermal Engineering* 128 (2018), pp. 107–120. DOI: `https://doi.org/10.1016/j.applthermaleng.2017.08.118`.

[43] Heyne, S., Meier, M., Imbert, B., and Favrat, D. “Experimental investigation of prechamber autoignition in a natural gas engine for cogeneration”. In: *Fuel* 88.3 (2009), pp. 547–552. DOI: `https://doi.org/10.1016/j.fuel.2008.09.032`.

[44] Attard, William P, Bassett, Michael, Parsons, Patrick, and Blaxill, Hugh. *A new combustion system achieving high drive cycle fuel economy improvements in a modern vehicle powertrain.* Tech. rep. SAE Technical Paper, 2011.

[45] Gentz, Gerald, Thelen, Bryce, Litke, Paul, Hoke, John, and Toulson, Elisa. "Combustion visualization, performance, and CFD modeling of a pre-chamber turbulent jet ignition system in a rapid compression machine". In: *SAE International Journal of Engines* 8.2 (2015), pp. 538–546.

[46] Gentz, Gerald, Gholamisheeri, Masumeh, and Toulson, Elisa. "A study of a turbulent jet ignition system fueled with iso-octane: Pressure trace analysis and combustion visualization". In: *Applied energy* 189 (2017), pp. 385–394. DOI: `https://doi.org/10.1016/j.apenergy.2016.12.055`.

[47] Peters, Nathan, Subramanyam, Sai Krishna Pothuraju, Bunce, Michael, Blaxill, Hugh, and Cooper, Adrian. "Optimization of lambda across the engine map for the purpose of maximizing thermal efficiency of a jet ignition engine". In: *SAE International Journal of Advances and Current Practices in Mobility* 2.2020-01-0278 (2020), pp. 3140–3150.

[48] Attard, William P and Blaxill, Hugh. "A single fuel pre-chamber jet ignition powertrain achieving high load, high efficiency and near zero NOx emissions". In: *SAE International Journal of Engines* 5.3 (2012), pp. 734–746.

[49] Attard, William P, Blaxill, Hugh, Anderson, Eric K, and Litke, Paul. "Knock limit extension with a gasoline fueled pre-chamber jet igniter in a modern vehicle powertrain". In: *SAE International Journal of Engines* 5.3 (2012), pp. 1201–1215.

[50] Biswas, Sayan and Qiao, Li. "Ignition of ultra-lean premixed hydrogen/air by an impinging hot jet". In: *Applied energy* 228 (2018), pp. 954–964. DOI: `https://doi.org/10.1016/j.apenergy.2018.06.102`.

[51] Biswas, Sayan and Qiao, Li. "Ignition of ultra-lean premixed H2/air using multiple hot turbulent jets generated by pre-chamber combustion". In: *Applied Thermal Engineering* 132 (2018), pp. 102–114. DOI: `https://doi.org/10.1016/j.applthermaleng.2017.11.073`.

[52] Xu, Guoqing, Kotzagianni, Maria, Kyrtatos, Panagiotis, Wright, Yuri M, and Boulouchos, Konstantinos. “Experimental and numerical investigations of the unscavenged prechamber combustion in a rapid compression and expansion machine under engine-like conditions”. In: *Combustion and Flame* 204 (2019), pp. 68–84.

[53] Tang, Qinglong et al. “Optical diagnostics on the pre-chamber jet and main chamber ignition in the active pre-chamber combustion (PCC)”. In: *Combustion and Flame* 228 (2021), pp. 218–235.

[54] Allison, PM, De Oliveira, M, Giusti, Andrea, and Mastorakos, Epaminondas. “Pre-chamber ignition mechanism: Experiments and simulations on turbulent jet flame structure”. In: *Fuel* 230 (2018), pp. 274–281.

[55] Cooper, Adrian, Harrington, Anthony, Bassett, Michael, Reader, Simon, and Bunce, Michael. *Application of the passive MAHLE jet ignition system and synergies with miller cycle and exhaust gas recirculation.* Tech. rep. SAE Technical Paper, 2020.

[56] Attard, William P, Fraser, Neil, Parsons, Patrick, and Toulson, Elisa. “A turbulent jet ignition pre-chamber combustion system for large fuel economy improvements in a modern vehicle powertrain”. In: *SAE International Journal of Engines* 3.2 (2010), pp. 20–37.

[57] Zhu, Sipeng, Akehurst, Sam, Lewis, Andrew, and Yuan, Hao. “A review of the pre-chamber ignition system applied on future low-carbon spark ignition engines”. In: *Renewable and Sustainable Energy Reviews* 154 (2022), p. 111872.

[58] Santos, Nathália Duarte Souza Alvarenga, Alvarez, Carlos Eduardo Castilla, Roso, Vinıcius Rückert, Baeta, José Guilherme Coelho, and Valle, Ramon Molina. “Combustion analysis of a SI engine with stratified and homogeneous pre-chamber ignition system using ethanol and hydrogen”. In: *Applied Thermal Engineering* 160 (2019), p. 113985.

[59] Sens, M et al. “Pre-chamber ignition and promising complementary technologies”. In: *27th Aachen colloquium automobile and engine technology.* 2018.

[60] Turkish, Michael C. “3-valve stratified charge engines: Evolvement, analysis and progression”. In: *SAE Transactions* (1974), pp. 3483–3503.

[61] Ricardo, Harry R. “Recent research work on the internal-combustion engine”. In: *SAE Transactions* (1922), pp. 1–93.

[62] Turkish, Michael C. “Prechamber and valve gear design for 3-valve stratified charge engines”. In: *SAE Transactions* (1975), pp. 2827–2856.

[63] Summers, C. E. *Internal Combustion Engine.* U.S. Patent 1568638, Jan. 1926.

[64] Bagnulo, A. *Engine with Stratified Mixture.* U.S. Patent 2422610, Jun. 1947.

[65] Mallory, M. *Internal Combustion Engine.* U.S. Patent 2121920, Feb. 1938.

[66] Broderson, N. O. *Method of operating internal-combustion engines.* U.S. Patent 2690741, Oct. 1954.

[67] Barnard, A. and Brewer, C. D. *mprovements in or relating to internal combustion engines.* British Patent No. 948686, Feb. 1964.

[68] Date, T, Yagi, S, Ishizuya, A, and Fujii, I. *Research and Development of the Honda CVCC engine. SAE Paper 740605.* 1974.

[69] Norbye, JP and Dunne, J. “Honda’s New CVCC Car Engine Meets’ 75 Emissions Now”. In: *Popular Science Magazine* (1973), pp. 79–81.

[70] Garret, Thomas Kenneth. *Automotive Fuels And Fuels Systems.* 1994.

[71] Wyczalek, Floyd A, Harned, John L, Maksymiuk, S, and Blevins, Jerry R. *EFI prechamber torch ignition of lean mixtures.* Tech. rep. SAE Technical Paper, 1975.

[72] Garrett, T Ken. “Porsche stratified charge engine”. In: *Environmental Science & Technology* 9.9 (1975), pp. 826–830.

[73] Brandstetter, Walter R et al. “THE VOLKSWAGEN PCI STRATIFIED CHARGE CONCEPT. RESULTS FROM THE 1, 6 LITER AIR COOLED ENGINE”. In: (1974).

[74] Scussel, AJ, Simko, AO, and Wade, WR. “The Ford PROCO engine update”. In: *SAE Transactions* (1978), pp. 2706–2725.

[75] Davis, GC, Krieger, RB, and Tabaczynski, Rodney J. “Analysis of the flow and combustion processes of a three-valve stratified charge engine with a small prechamber”. In: *SAE Transactions* (1974), pp. 3534–3550.

[76] Gussak, LA, Karpov, VP, and Tikhonov, YV. “The application of lag-process in prechamber engines: SAE paper 790692”. In: *Passenger Car Meeting & Exposition, SAE International, Warrendale, PA, United States.* 1979.

[77] Gussak, LA, Ryabikov, OB, Politenkova, GG, and Furman, GA. "Effect of adding individual combustion products on combustion of methane—Air mixture". In: *Bulletin of the Academy of Sciences of the USSR, Division of chemical science* 22 (1973), pp. 2128–2128.

[78] Gussak, LA. "High chemical activity of incomplete combustion products and a method of prechamber torch ignition for avalanche activation of combustion in internal combustion engines". In: *SAE transactions* (1975), pp. 2421–2445.

[79] Gussak, LA and Turkish, MICHAEL C. "LAG-process of combustion and its application in automobile gasoline engines". In: *Proc. IMechE C*. Vol. 257. 1976.

[80] Gussak, LA. *The role of chemical activity and turbulence intensity in prechamber-torch organization of combustion of a stationary flow of a fuel-air mixture*. Tech. rep. SAE Technical Paper, 1983.

[81] Lumsden, Grant and Watson, Harry C. "Optimum Control of an SI engine with a= 5 capability". In: *SAE paper* 950689 (1995).

[82] Toulson, Elisa. *Applying alternative fuels in place of hydrogen to the jet ignition process*. University of Melbourne, Department of Mechanical Engineering, 2008.

[83] Watson, HC. *International Patent. Application PCT/AU92/00552*. Tech. rep. PCT/AU92/00552, 1992.

[84] Watson, Harry C. *Internal combustion engine ignition device*. US Patent 5,611,307. 1997.

[85] Lawrence, Jeremy and Watson, Harry C. "Hydrocarbon emissions from a HAJI equipped ultra-lean burn SI engine". In: *SAE transactions* (1998), pp. 6–12.

[86] Dober, GG. "Modelling the flame enhancement of a HAJI equipped spark ignition engine". In: *SAE No. 99091* (1999).

[87] Attard, William. *Turbulent jet ignition pre-chamber combustion system for spark ignition engines*. US Patent 8,857,405. 2014.

[88] Bunce, Michael, Blaxill, Hugh, and Attard, William. *Turbulent jet ignition pre-chamber combustion system for spark ignition engines*. US Patent 9,353,674. 2016.

[89] Attard, William P and Parsons, Patrick. "A normally aspirated spark initiated combustion system capable of high load, high efficiency and near zero NOx emissions in a modern vehicle powertrain". In: *SAE International Journal of Engines* 3.2 (2010), pp. 269–287.

[90] Attard, William P, Kohn, Jacob, and Parsons, Patrick. “Ignition energy development for a spark initiated combustion system capable of high load, high efficiency and near zero NOx emissions”. In: *SAE International Journal of Engines* 3.2 (2010), pp. 481–496.

[91] Bunce, Michael, Cairns, Alasdair, and Blaxill, Hugh. “The use of active jet ignition to overcome traditional challenges of pre-chamber combustors under low load conditions”. In: *International Journal of Engine Research* 22.11 (2021), pp. 3325–3339.

[92] Sanda, S. and Nakamura, N. *Internal combustion engine provided with pre-combustion chamber.* U.S. Patent 4048973, Sep. 1977.

[93] Konishi, M., Nakamura, N., Oono, E., and Baika, T. “Effects of a Prechamber on NOx Formation Process in the SI Engine”. In: *1979 Automotive Engineering Congress and Exposition.* SAE International, 1979. DOI: `https://doi.org/10.4271/790389`.

[94] Noguchi, M., Sanda, S., and Nakamura, N. “Development of Toyota Lean Burn Engine”. In: *1976 Automobile Engineering Meeting.* SAE International, 1976. DOI: `https://doi.org/10.4271/760757`.

[95] Wyczalek, Floyd A, Frank, Daniel L, and Neuman, John G. “Plasma jet ignition of lean mixtures”. In: *SAE Transactions* (1975), pp. 856–868.

[96] Adams, TG. “Theory and evaluation of auxiliary combustion (torch) chambers”. In: *SAE Transactions* (1978), pp. 2328–2339.

[97] Adams, Tim G. *Torch ignition for combustion control of lean mixtures.* Tech. rep. SAE Technical Paper, 1979.

[98] Brandstetter, Walter. “The Volkswagen lean burn pc-engine concept”. In: *SAE Transactions* (1980), pp. 1804–1821.

[99] Rychter, TJ, Saragih, R, Lezański, T, and Wojcicki, S. “Catalytic activation of a charge in a prechamber of a SI lean-burn engine”. In: *Symposium (International) on Combustion.* Vol. 18. 1. Elsevier. 1981, pp. 1815–1824.

[100] Beyerlein, Steven Ware. *Catalytic charge activation in a lean-burn internal combustion engine.* Washington State University, 1987.

[101] Beyerlein, Steven W and Wojcicki, Stanislaw. “A lean-burn catalytic engine”. In: *SAE transactions* (1988), pp. 1040–1051.

[102] Jarosinski, J and Wojcicki, S. *Investigation of a lean-burn piston engine with catalytic prechamber and recirculation of combustion products.* Tech. rep. American Society of Mechanical Engineers, New York, NY (United States), 1995.

[103] Jarosiński, Józef, Łapucha, Ryszard, Mazurkiewicz, Jacek, and Wójcicki, Stanisław. “Investigation of a lean-burn piston engine with catalytic prechamber”. In: *SAE transactions* (1996), pp. 226–233.

[104] Geiger, José, Pischinger, Stefan, Böwing, Robert, Koß, Hans-Jürgen, and Thiemann, Jörg. “Ignition systems for highly diluted mixtures in SI-engines”. In: *SAE transactions* (1999), pp. 1099–1110.

[105] Latsch, Reinhard. “The swirl-chamber spark plug: a means of faster, more uniform energy conversion in the spark-ignition engine”. In: *SAE transactions* (1984), pp. 365–377.

[106] Latsch, Reinhard and Schlembach, Hans. *Externally ignited internal combustion engine.* US Patent 4,218,992. 1980.

[107] Benedikt, Walter, Latsch, Reinhard, and Schlembach, Hans. *Separately ignited internal combustion engine with at least one main combustion chamber and an ignition chamber.* US Patent 4,416,228. 1983.

[108] Latsch, Reinhard, Schlembach, Hans, and Scherenberg, Dieter. *Method for igniting lean fuel-air mixtures and an apparatus to perform the method.* US Patent 4,513,708. 1985.

[109] Kettner, Maurice et al. “A new flame jet concept to improve the inflammation of lean burn mixtures in SI engines”. In: *SAE transactions* (2005), pp. 1549–1557.

[110] Weng, Volker et al. “Investigation on the Bowl-Prechamber-Ignition (BPI) Concept in a Direct Injection Gasoline Engine at Part Load”. In: *Design of Racing and High-Performance Engines—1998-2003* (1999), p. 463.

[111] Kettner, Maurice et al. *The BPI flame jet concept to improve the inflammation of lean burn mixtures in spark ignited engines.* Tech. rep. SAE Technical Paper, 2004.

[112] Silva, Mickael et al. *Effects of geometry on passive pre-chamber combustion characteristics.* Tech. rep. SAE Technical Paper, 2020.

[113] Thelen, Bryce Charles, Gentz, Gerald, and Toulson, Elisa. *Computational study of a turbulent jet ignition system for lean burn operation in a rapid compression machine.* Tech. rep. SAE Technical Paper, 2015.

[114] Thelen, Bryce Charles and Toulson, Elisa. *A computational study of the effects of spark location on the performance of a turbulent jet ignition system.* Tech. rep. SAE Technical Paper, 2016.

[115] Assanis, Dimitris, Engineer, Nayan, Neuman, Paul, and Wooldridge, Margaret. *Computational development of a dual pre-chamber engine concept for lean burn combustion.* Tech. rep. SAE Technical Paper, 2016.

[116] Muller, Matias, Freeman, Corbin, Zhao, Peng, and Ge, Haiwen. "Numerical simulation of ignition mechanism in the main chamber of turbulent jet ignition system". In: *Internal Combustion Engine Division Fall Technical Conference.* Vol. 51999. American Society of Mechanical Engineers. 2018, V002T06A010.

[117] Xu, Guoqing, Wright, Yuri Martin, Schiliro, Michele, and Boulouchos, Konstantinos. "Characterization of combustion in a gas engine ignited using a small un-scavenged pre-chamber". In: *International Journal of Engine Research* (2018), p. 1468087418798918. DOI: `https://doi.org/10.1177/1468087418798918`.

[118] Malé, Quentin et al. "Large eddy simulation of pre-chamber ignition in an internal combustion engine". In: *Flow, Turbulence and Combustion* (2019), pp. 1–19.

[119] Kim, Joohan et al. "Assessment of turbulent combustion models for simulating prechamber ignition in a natural Gas engine". In: *Journal of Engineering for Gas Turbines and Power* 143.9 (2021).

[120] Sanal, Sangeeth et al. *A Numerical Study on the Ignition of Lean CH 4/Air Mixture by a Pre-Chamber-Initiated Turbulent Jet.* Tech. rep. SAE technical paper, 2020.

[121] Hlaing, Ponnya et al. "Effect of pre-chamber enrichment on lean burn pre-chamber spark ignition combustion concept with a narrow-throat geometry". In: (2020).

[122] Cooper, Adrian, Harrington, Anthony, Bassett, Michael, and Pates, David. *Knock Mitigation Benefits Achieved through the Application of Passive MAHLE Jet Ignition Enabling Increased Output under Stoichiometric Operation.* Tech. rep. SAE Technical Paper, 2021.

[123] Sens, Marc and Binder, Emanuel. "Pre-chamber ignition as a key technology for future powertrain fleets". In: *MTZ worldwide* 80.2 (2019), pp. 44–51.

Chapter 3

Tools and methodology

This chapter presents the numerical and experimental tools used in the research environment that was designed for performing the studies of the passive pre-chamber ignition concept, as well as the adopted methodology for combining these tools in a coherent way according to their own characteristics and extract the most information out of each one. The primary focus will be on the description of the CFD model (Section 3.3), given that this is the main tool used for the analysis. A detailed explanation of the most relevant physical models that were considered for performing the CFD simulations will be presented (Sections 3.3.1, 3.3.2 and 3.3.3), as well as the simulation procedures that were followed (Section 3.3.4) and the mesh independence study (Section 3.3.5).

3.1 Methodology outline

The general outline of the research activities was presented in Figure 1.5, however, in reality, the process followed along this thesis was not so linear. Several iterations between the numerical and experimental tools are performed in each chapter, in order to obtain the most accurate overview of the concept's underlying physics. As the reader may perceive, the results of Chapters 4, 5 and 6 are based on numerical simulations. Thus, ensuring that these simulations are representative of the real physics of the engine is a critical aspect in order to extract meaningful conclusions. For this reason, the first step of the investigation consisted of calibrating the CFD combustion model to accurately reproduce the experimental trends (Section 3.3.6). This was performed in three relevant engine operating conditions (load/speed), both for improving the reliability of the model and to carry out the analysis in a wide region of the engine map, making for a better characterization of the concept. The research can then be divided into three major parts. The first one (Chapter 4) consisted of evaluating the concept in un-diluted stoichiometric conditions, analyzing the impact of the engine operating point, spark timing and pre-chamber geometry over the physical and thermochemical processes that are involved in this combustion system. Thereafter, the characteristics of the concept in diluted conditions were studied (Chapter 5). In this case, the numerical model was also validated against experimental results using EGR and air-diluted mixtures, allowing to explore the synergies of the passive pre-chamber concept with these strategies. The third and final stage of the investigation (Chapter 6) consisted of developing a technological application for the acquired knowledge during Chapters 4 and 5. For this purpose, an iterative design methodology combining 0D/1D and CFD numerical tools was developed and validated in the engine test bench. The main goal of this methodology is to obtain a pre-chamber design to both optimize the performance of the concept and improve the compatibility with EGR dilution.

Now, following a logical order, the tools used as boundary conditions for the research (experimental engine and simplified numerical models) will be explained first, followed by the detailed description of the CFD modelling platform.

3.2 Experimental facilities and simplified numerical models

Several experimental campaigns have been performed during the years in which this thesis has been carried out. However, the dedicated analysis of these experiments are in the framework of another ongoing PhD thesis. Moreover, the aforementioned thesis also makes use of simple 0D/1D models to perform basic studies of the passive pre-chamber concept and complement the experimental data. These studies include the evaluation of basic geometric parameters of the pre-chamber and their impact on jet-ejection features. Nevertheless, the spatiallity of the combustion process and pre-chamber flow-dynamics is not attainable with these 1D models. Therefore, in order to get a complete understanding of the most relevant physical aspects of the concept, both the real engine test results and simplified numerical models are used as inputs for supporting the analysis performed during this research work with the detailed 3D-CFD model.

3.2.1 Test bench and engine characteristics

The experimental environment is made up of a small-displacement turbocharged single-cylinder SI research engine, representative of those currently found in passenger cars, and a fully equipped test bench designed to operate this type of engines. The full details of the experimental facilities can be found in several investigations published in the literature [1, 2]. Figure 3.1 shows a schematic representation of the engine test cell, including the intake and exhaust lines and several of the measurement devices and instrumentation that has been installed for monitoring the most relevant engine parameters during the operation. It is important to point out that a pre-chamber pressure transducer was not available for this research, and thus only the cylinder, exhaust and intake pressures were monitored.

The intake system has an Atlas Copco ZA-1 water-cooled, oil-free rotary-screw external compressor, with a maximum pressure of 4 bar and a maximum flow rate of 450 m^3/h. This device is associated with an Atlas Copco FD 380 W dryer, in charge of eliminating any moisture that the compressed air could contain by means of a condensation process, cooling the air to a temperature of 280K. This system has a 500-liter plenum (at the outlet of the dryer) and another one of 250 liters (near the inlet of the engine) to attenuate the pressure pulses generated by the compression system. The intake temperature is regulated with a conditioning system made up of a 2 kW electrical resistance and a refrigeration unit capable of extracting 4 kW of thermal power. The exhaust system is much simpler, with a 50-litre plenum to condition the flow before reaching the pneumatic knife gate valve that regulates the exhaust back-pressure experienced by the engine.

Table 3.1: Main properties of the gasoline fuel.

Type	**Gasoline RON95**
H/C ratio [mol/mol]	1.761
Stoichiometric A/F [-]	14.374
Lower Heating Value (LHV) [MJ/kg]	42.493
Density (15°C) [kg/m^3]	843.8
Reduced formula ($C_xH_yO_z$)	7.594 (x) - 13.376 (y) - 0.0 (z)

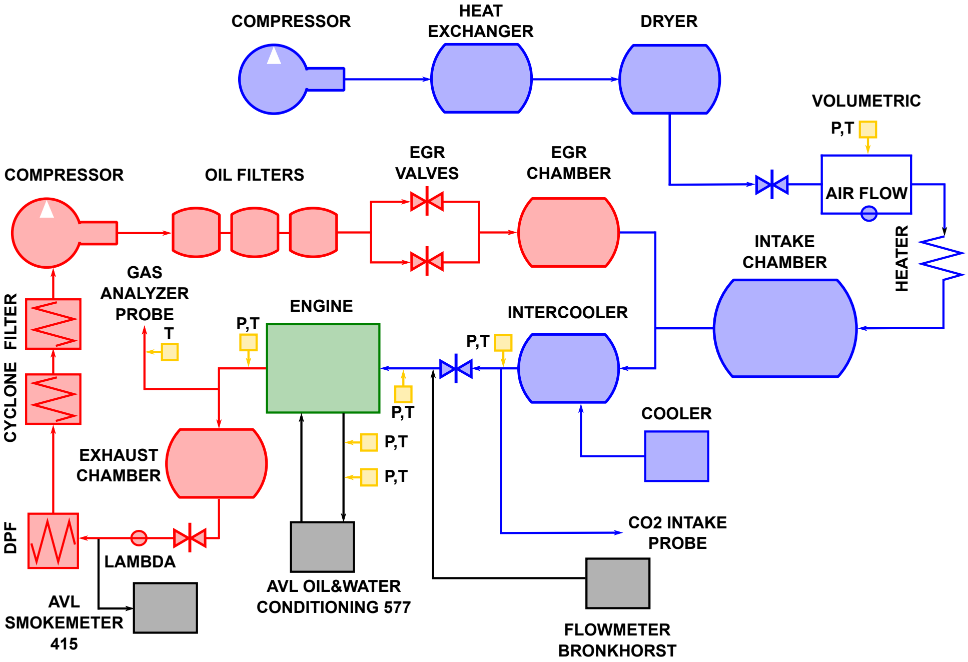

Figure 3.1: Layout of the engine test cell

The liquid fuel supply system has an AVL 733S fuel mass meter and an AVL 753 conditioning system, necessary to keep the fuel temperature as constant as possible, in order to avoid measurement errors associated with density variations. A RON95 (95 Research Octane Number) calibrated gasoline has been used as fuel for the research activities, with the specifications found in Table 3.1.

The EGR system is low pressure, to allow a smooth re-circulation of exhaust gases even when the pressure difference between the exhaust and intake is unfavorable. This system has an Atlas Copco GA VSD screw compressor with a maximum pressure of 12.75 bar and a maximum flow-rate of 135 m^3/h. The characteristics of other relevant instrumentation and measurement devices are shown in Table 3.2.

An in-house 0D combustion diagnostics tool (CALMEC) is used to solve the first law of thermodynamics taking the cylinder as control volume, obtaining the instantaneous evolution of the energy released by the progress of combustion from the in-cylinder pressure signal [3–5]. Global parameters such as the Indicated Mean Effective Pressure (IMEP), maximum cylinder pressure ($P_{\max}$), pressure gradient ($dP/d\alpha$) and combustion stability indicators (COV

Table 3.2: Meassurement devices and instrumentation

Variable	Equipment
Engine torque	HBM T10F (0-500 Nm)
Air flow-rate	ELSTER G-100 RVG (0.05-160 m^3/h)
Fuel mass flow-rate	AVL 733S (0-150 Kg/h)
Cylinder pressure	KISTLER 6061B (0-250 bar)
Intake/Exhaust pressure	KISTLER 4045A (0-5 bar)
Exhaust emissions	HORIBA MEXA 7100 DEGR

IMEP and σIMEP) are derived directly from the analysis of the cylinder pressure signal, while the start of combustion (SoC) and the main burning angles (CA10, CA50, CA90) are obtained from the law of heat release (HR) and the heat release rate (HRR). This calculation also includes sub-models to account for heat transfer losses, mechanical deformations, and blow-by losses.

The four-stroke single-cylinder research engine corresponds to a version of the HR12 three-cylinder engine developed and marketed by the Renault company, conveniently modified and adapted to suit the requirements of this project. Table 3.3 collects the most relevant specifications of the engine. It is important to highlight that the engine is equipped with an indirect injection system, with the injector located in the intake manifold (PFI), at a distance of about 270 mm from the port entrance. This solution has been chosen to ensure the maximum level of homogeneity in the air/fuel mixture, avoiding the impact that the local stratification of equivalence ratio could generate over the combustion process.

Table 3.3: Main specifications of the engine.

Engine	4-stroke SI
Number of cylinders [-]	1
Displacement [cm^3]	404
Bore – Stroke [mm]	80.0 – 80.5
Connecting rod length [mm]	156
Compression ratio (geometric) [-]	13.4:1
Valvetrain [-]	DOHC
Number of valves/cylinder [-]	2 intake and 2 exhaust
Fuel injection system [-]	PFI (P_{max} 6 bar)

As mentioned in Chapter 2, one of the advantages of the passive pre-chamber ignition concept consists in the possibility of directly integrating the pre-chamber without having to modify the cylinder head, since the conventional spark plug and the pre-chamber can perfectly share the same seat and

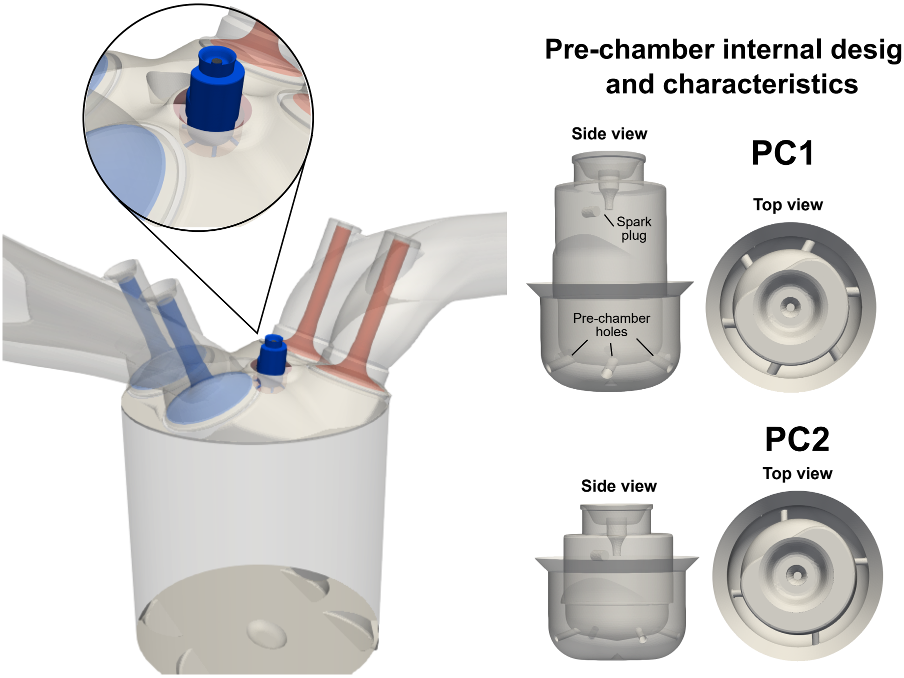

Figure 3.2: Schematic of the cylinder and pre-chamber geometry

location on the engine. In this way, the engine can be switched from operating with the conventional ignition concept to the passive pre-chamber ignition concept very easily, significantly reducing both the time and the cost of the experimental activities. Figure 3.2 shows a schematic view of the cylinder, highlighting the location of the housing for the pre-chamber on the cylinder head, which in this case is metric twelve (M12). This figure also shows the internal design of the pre-chambers, with a view from the side and from the top. For the initial test campaigns, four pre-chamber designs were evaluated, maintaining the same internal geometry and only changing the volume, number of holes and hole diameter. From the top view of the pre-chambers it is also noticeable that the holes are offseted with respect to each other. This tangential angle between the hole axis and the center of the pre-chamber was kept constant at 12.5° for each of the designs. The pre-chambers were labled from 1 to 4, and the basic characteristics of each design is shown in Table 3.4, highlighting the reference pre-chamber (**PC1**) for performing the CFD model validation. The last column of the table shows the relation between the total transversal area of the pre-chamber holes and the pre-chamber volume (A/V ratio), this is an important parameter that will be analyzed in Chapter 4.

Table 3.4: Pre-chamber designs and specifications.

ID	Volume [mm^3]	Holes [-]	Diameter [mm]	A/V ratio [1/m]
PC1	**600**	**6**	**0.7**	**3.9**
PC2	350	4	0.7	4.4
PC3	350	4	0.5	2.2
PC4	950	6	0.5	1.2

The experimental campaign considered for the thesis was composed of the operating conditions shown in Table 3.5. These three points are characteristic of relevant operating conditions in passenger cars, gathering a complete diagonal of the engine map, making them appropriate for a full characterization of the concept. The high load/speed operating point (OP1=4500 rpm, 12.8 bar IMEP) is representative of full throttle operation, the medium load/speed operating condition (OP2=2000 rpm, 6.8 bar IMEP) is a point of regular operation in a passenger car, and the low load/speed operating point (OP3=1350 rpm, 3.3 bar IMEP) is characteristic of idle or cold-start conditions.

Finally, the measurement methodology consisted in adjusting the injected fuel mass to obtain the target IMEP operating with the conventional SI system, and keeping this fuel mass constant for the subsequent pre-chamber tests. Then, a Spark Timing (ST) sweep was performed until the Maximum Brake Torque (MBT) was reached, or by contrast, until a continued ST advance was prevented by knocking combustion. Aditionally, both EGR and air dilution sweeps were performed in each operating point for establishing the dilution limits of each pre-chamber design.

Table 3.5: Operating conditions for the baseline experiments.

Operating points	OP1	OP2	OP3
Engine speed [rpm]	4500	2000	1350
IMEP [bar]	12.8	6.8	3.3
Injected fuel [mg/cc]	28.4	15.3	8.4
λ [-]	1	1	1
EGR rate [%]	0	0	0
Spark Timing [CAD BTDC]	10	11.8	22
Intake pressure [bar]	1.1	0.68	0.39
Exhaust pressure [bar]	1.07	1.04	1.01
Coolant and oil temperature [K]	363	360	360

3.2.2 0D/1D engine model (GT-Power)

A model of the engine was built on a 0D/1D simulation platform using GT-Power [1]. This model was developed to study the thermo-fluid dynamic evolution in both the pre-chamber and the main chamber, with low computational-cost simulations. The characteristics of this model have been described in the previous reference, so only the most relevant aspects that allow to understand its application in this research work are highlighted here.

The model includes all of the systems that make up the test cell described in section 3.2.1, a submodel of the single-cylinder research engine and a submodel for the pre-chamber. Here, both the pre-chamber and the main chamber are modeled as 0D volumes, where the equations of conservation of mass, species and energy are solved, and which are connected by means of 1D ducts that represent each of the pre-chamber holes. In this way, after implementing the corresponding equations in the model, it has been possible to determine at the outlet of the holes the temporal evolution of the parameters that govern the dynamics of the gaseous jets ejected between the pre-chamber and the main chamber (mass flow, momentum flux...).

This model reproduces the evolution of the pressure in the pre-chamber and in the main chamber, together with the gas exchange between them, based on the profile of the heat release rates imposed in both chambers. Since there is no pressure transducer in the pre-chamber, the HRR inside this volume is imposed by a Wiebe function [6]. In the main chamber, the HRR obtained from the experimental pressure signal is imposed, for the corresponding operating condition.

In the context of this research, the model is used in Chapter 6 to evaluate, in a short time frame, many combinations of pre-chamber volumes and hole diameters by imposing different HRR profiles for each one, assuming several hypothesis regarding the start of combustion in the main chamber and the burn duration of the Wiebe profile.

This model has been calibrated by contrasting its results with the engine test data and adjusting the coefficients related to the permeability and/or heat transfer of the different elements, until a reasonable agreement was reached between the simulated and experimental pressure profiles. Figure 3.3 shows the results of this calibration for OP1 and OP3. This validation confirms the capacity of the model to accurately reproduce the experimental pressure trends, which is why it is considered adequate for the analysis that is intended to be carried out in Chapter 6.

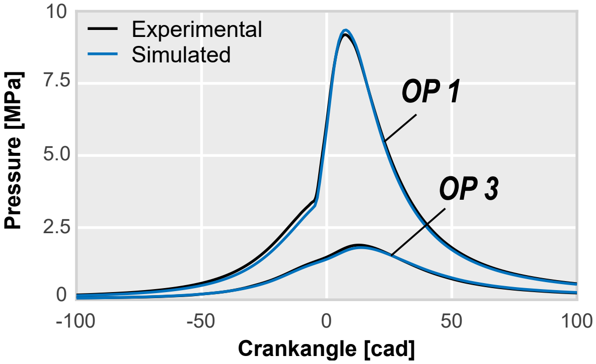

Figure 3.3: Validation of the GT-Power model [7]

3.2.3 1D gaseous jet model (DICOM)

To estimate the macroscopic characteristics of the gaseous jets ejected from the pre-chamber towards the main chamber, a 1D jet model (DICOM) developed at the IUI CMT-Research Institute has been used [8–11]. Considering that most of the applications of this tool have been oriented towards simulating the characteristic liquid jets of CI engines (diesel-like sprays), several adaptations were made to the model in order to study the characteristics of the pre-chamber gaseous jets. A detailed description of this model can be found in the previous references, so only those aspects that are considered relevant in the context of the present study are described here.

The jets ejected from the pre-chamber are modeled as a gas stream injected through the pre-chamber holes into the main gas-filled chamber, therefore, an ideal gas equation of state is used along with an approximation of low Mach in terms of compressibility. The inputs of the 1D jet model include the time evolution of the mass and momentum fluxes through the pre-chamber holes, which are obtained from the results of the simulations performed with the 0D/1D engine model described in section 3.2.2.

While in diesel-like sprays a low temperature flow is injected into a high temperature environment, in this case a jet of high temperature fluid (in the range of 1500K according to the 0D/1D simulations of the engine) coming from the pre-chamber is ejected towards the main chamber, where the ambient temperature is lower (around 700K) [12].

For the purposes of this research, the model is used to obtain information related to jet penetration predictions in Chapter 6. Therefore, the most critical parameters to be considered for the simulations are the momentum flux at the exit of the pre-chamber holes and the main chamber density, since these govern the dynamics of the jet. In the most simplified scenario, a non-reactive gaseous jet could be considered as a flow of constant density [13], therefore, the impact of the temperature and the composition of the gas at the exit of the holes are considered of a secondary order (they are kept constant).

The boundary conditions of the main chamber, in which the gaseous jet from the pre-chamber is ejected, consist of transient profiles of density and temperature that are also obtained from the results of the simulations carried out with the 0D/1D GT-Power engine model. One of the most critical parameters for the application of this 1D jet model is the cone angle, which is often used as a fit parameter to experimental penetration data [14]. Here, a constant cone angle of 25° was determined, after several iterations with the 3D-CFD model for performing the 1D jet model calibration. Although in the experiments and in the 3D model it is possible to expect interactions between the gaseous jets ejected from the pre-chamber and the walls of the combustion chamber, this model only considers the propagation of a free jet, without taking into account said interactions.

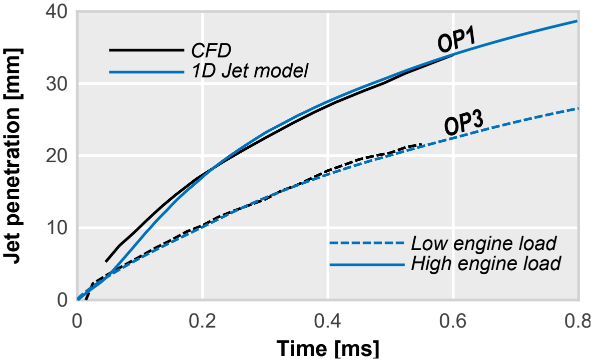

Figure 3.4: Validation of the 1D Jet model [7]

The model validation against the results from the 3D-CFD simulations is shown in Figure 3.4 for OP1 and OP3, verifying the reliability of the penetration data obtained with this simplified 1D jet model for performing the analysis that will be presented in Chapter 6.

It is important to highlight that both the 1D gaseous jet model and the 0D/1D GT-Power model are only used as boundary conditions for this research work, given that the development of these tools and their extensive use for evaluating different aspects of the passive pre-chamber concept are in the frame of another ongoing PhD thesis [1, 7].

3.3 CFD model implementation

3.3.1 Description of the numerical model

Given the complex nature of the passive pre-chamber ignition concept in terms of flow-dynamics, chemistry and turbulence, a three-dimensional modelling environment is considered as the most suitable approach to study this system. However, modelling Internal Combustion Engines can be challenging given that the computational domain is composed of mobile parts (piston, valves...). Therefore, the model was implemented in the commercial CFD code CONVERGE [15]. This software has been widely adopted in the ICE community due to its capacity to simulate moving boundaries and the integrated Adaptive Mesh Refinement (AMR) tool, that allows the computational mesh to be scaled in run-time to improve the resolution of relevant physical and thermodynamic properties of the flow.

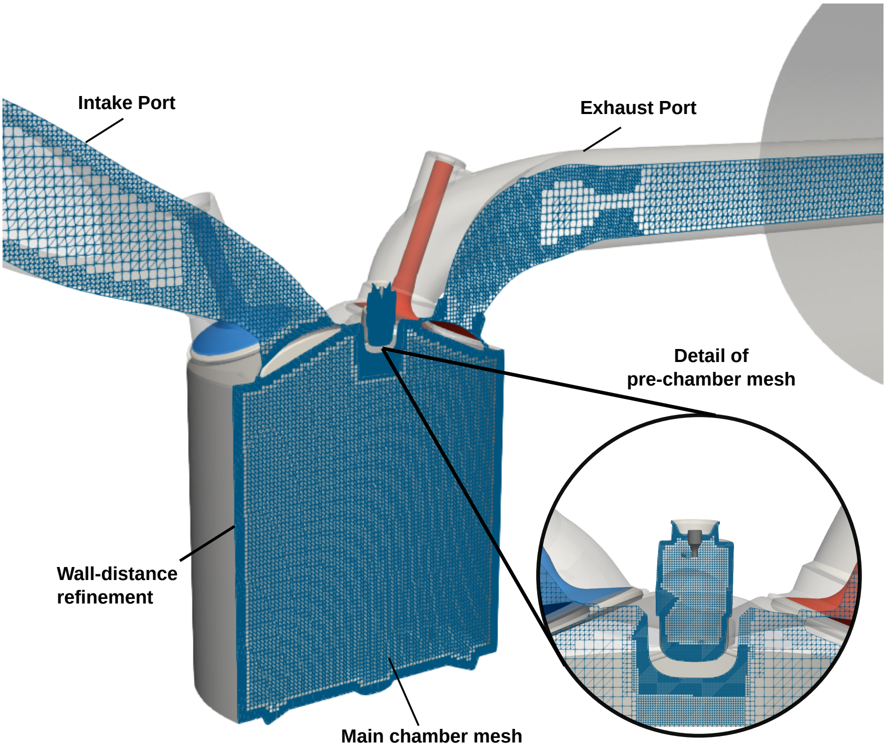

Figure 3.5: Computational domain and mesh details

A detailed 3D-sketch of the single-cylinder engine was used to generate the computational domain shown in Figure 3.5, including the pre-chamber and the intake/exhaust port geometries for performing complete cycle simulations. This way, a realistic recreation of the flow field can be achieved for the combustion simulations.

The mesh discretization was done by the cut-cell Cartesian method available in the CFD code. The base cell size throughout the domain was of 4 mm. However, the mesh has been refined in the most critical regions in terms of flow conditions, such as the intake and exhaust ports, where the size of the cells is 2 mm, and within the cylinder itself, with a cell size of 1 mm. In turn, to improve boundary layer predictions, the cells near the cylinder walls, including the piston, cylinder head and the valves, have been reduced to 0.5 mm. The cells in the pre-chamber were refined to 0.25 mm and 0.125 mm near the walls of this region. Additionally, an adaptive refinement (AMR) has been implemented to improve the resolution of the mesh based on the velocity and temperature sub-grid scales of 1 m/s and 2.5 K respectively, down to a minimum cell size of 0.125 mm. This allows to better capture the details associated with the dynamics of the pre-chamber jets and the combustion process. Finally, the mesh was refined to a size of 0.0625 mm in a 1 mm radius sphere located at the spark plug, to improve the resolution of the initial flame kernel and the start of combustion. This mesh configuration is summarized in Table 3.6, and was selected after performing an extensive literature review on SI engine modelling [16–23], and based on previous investigations carried out by the author [24, 25]. The convergence of the computational mesh is demonstrated with the mesh independence study performed in Section 3.3.5.

Table 3.6: configuration of the computational mesh.

Computational region	**Cell size**
Intake port	2 mm
Exhaust port	2 mm
Cylinder	1 mm
Cylinder walls/Piston/Valves	0.5 mm
Pre-chamber	0.25 mm
Pre-chamber walls & holes	0.125 mm
Spark plug gap	0.0625 mm
AMR sub-grid criteria	**Minimum cell size**
Temperature: 2.5 K	0.125 mm
Velocity: 1 m/s	0.125 mm

A numerical approximation needs to be used in order to solve the governing transport equations for mass, momentum, energy and species in each cell of the domain. CONVERGE uses the finite volume method [26] for this purpose. Moreover, The resolution of these transport equations is done by an iterative procedure with a Pressure Implicit with Splitting of Operators (PISO) algorithm [27]. The spatial discretization of the computational domain is performed with a second-order central difference scheme, while a first order implicit scheme was employed for temporal discretization.

In terms of physical models, the Redlich-Kwong equation of state [28] was selected to calculate the compressible flow properties. The wall heat-transfer model developed by Angelberger et al. [29] was used to account for heat losses through the boundaries of the computational domain. And finally, the two most relevant physical models that were setup to perform the simulations were the turbulence and combustion models. These will be explained in detail along the following sections.

3.3.2 Turbulence modelling framework

As explained in Chapter 2, the combustion process in SI engines takes place in a highly turbulent environment, thus, an adequate prediction of the in-cylinder turbulence field is critical in order to properly reproduce the combustion evolution [30]. In fluid mechanics, the characterization of turbulence is an extremely complex and delicate process, given that it convectively enhances the mixing rate of momentum, energy and species [31, 32], which changes significantly the characteristics of the flow-field.

An intrinsically unsteady turbulent flow is characterized by 3D rotational flow structures of different sizes called turbulent eddies. Furthermore, in the frame of CFD simulations, several models have been developed based on the characteristic scales of the turbulent eddies that they are able to resolve and the treatment that is given to the turbulent flow-field [33, 34]. For the purposes of this investigation, two of the most important turbulence models will be described.

Unsteady Reynolds Averaged Navier Stokes (URANS):

URANS models make a statistical treatment of the fluctuations around the ensamble-averaged values of the flow variables [35]. These fluctuations are considered to be small and due to turbulence, therefore, the complete range of the turbulent scales (eddies of all sizes) is modelled and not resolved. In this framework, the flow variables are decomposed in two terms as shown in

Equation 3.1, where u_i is the instantaneous velocity, $\bar{u}_i$ the ensemble mean and $u_i^{'}$ the fluctuating component.

$$u_i = \bar{u}_i + u_i^{'} \tag{3.1}$$

URANS models introduce an un-closed term in order to account for the effects of turbulent interactions in the classical conservation equations. This term is known as the Reynolds stress tensor (τ_{ij}), and in order to determine it, additional transport equations need to be solved together with the governing Navier-Stokes equations [36, 37]. In this sense, an eddy-viscosity-based two-equation turbulence model, namely the Re-Normalization Group variant of the k-ϵ model (**RNG k-**ϵ), was selected for this research [38].

The turbulence lentgh scale for this model is expressed in terms of the turbulent kinetic energy (k) and the dissipation rate of this energy (ϵ) according to Equation 3.2, with C_μ being a user-defined model constant.

$$le = C_\mu^{3/4}\frac{k^{3/2}}{\varepsilon} \tag{3.2}$$

The Reynolds stress tensor is given by Equation 3.3, where S_{ij} is the mean strain rate tensor and μ_t is the turbulent viscosity. Thus, in order to determine the turbulent viscosity and close Equation 3.3, two transport equations are defined for the turbulent kinetic energy and its dissipation rate (Equations 3.4 and 3.5 respectively). In these equations, Pr is the Prandtl number, S is a source term defined by the user and S_s represents the source term that accounts for interactions with the discrete phase. The $C_{\varepsilon i}$ terms are model constants that account for compression and expansion, and R is determined with Equations 3.6 and 3.7.

$$\tau_{ij} = 2\mu_t S_{ij} - \frac{2}{3}\delta_{ij}\left(\rho k + \mu_t\frac{\partial \tilde{u}_i}{\partial x_i}\right) \tag{3.3}$$

$$\frac{\partial \rho k}{\partial t} + \frac{\partial(\rho u_i k)}{\partial x_i} = \tau_{ij}\frac{\partial u_i}{\partial x_j} + \frac{\partial}{\partial x_j}\left(\frac{\mu+\mu_t}{Pr_k}\frac{\partial k}{\partial x_j}\right) - \rho\varepsilon + \frac{C_s}{1.5}S_s \tag{3.4}$$

$$\begin{aligned}\frac{\partial \rho \varepsilon}{\partial t} + \frac{\partial(\rho u_i \varepsilon)}{\partial x_i} = \frac{\partial}{\partial x_j}\left(\frac{\mu+\mu_t}{Pr_\varepsilon}\frac{\partial \varepsilon}{\partial x_j}\right) + C_{\varepsilon 3}\rho\varepsilon\frac{\partial u_i}{\partial x_i} + \\ \left(C_{\varepsilon 1}\frac{\partial u_i}{\partial x_j}\tau_{ij} - C_{\varepsilon 2}\rho\varepsilon + C_s S_s\right)\frac{\varepsilon}{k} + S - \rho R\end{aligned} \tag{3.5}$$

$$R = \frac{C_\mu \eta^3 (1 - \eta/\eta_0)}{(1 + \beta \eta^3)} \frac{\varepsilon^3}{k} \tag{3.6}$$

$$\eta = \frac{k}{\varepsilon} |S_{ij}| = \frac{k}{\varepsilon} \sqrt{2 S_{ij} S_{ij}} \tag{3.7}$$

This model is well suited to describe the behavior of the characteristic in-cylinder turbulent flow-field of ICE's [39, 40]. Additionally, given that it works with a statistical approach and mean values of the flow variables, the associated computational cost is considerably lower compared to other turbulence models, which has promoted its wide usage in the scientific community and the automotive industry for aiding in the design and evaluation of different engine technologies. For this reasons, and considering that the purpose of this thesis is to study the global characteristics of the passive pre-chamber combustion and perform some optimizations to this system, the majority of the CFD simulations were carried out in a URANS framework.

Large Eddy Simulations (LES):

This approach arose as a partial solution to address the shortcomings of RANS models. In this case, a low-pass spatio-temporal filtering of the Navier-Stokes equations is performed in order to separate the large and small-scale turbulent structures [41, 42]. Then, according to the applied filter (Δ), the larger turbulent scales that are above this filter are directly resolved with the complete instantaneous Navier-Stokes equations (mean flow + fluctuations due to turbulence). On the other hand, the small-scale turbulence is modelled by what is known as a Sub-grid Scale (SGS) stress model [43].

Thus, the decomposition of the flow-field in a LES framework is done by considering a resolved component and a sub-grid component. This can be represented by Equation 3.1 considering $\bar{u}_i$ as the resolved velocity field and $u_i^{'}$ as the sub-grid velocity field. Thereafter, by including the LES decomposition into the classical momentum conservation equation, the resulting expression is shown in Equation 3.8. In this case, the over-bars are used to denote filtered parameters (Pressure, density, velocity...). The stress tensors σ_{ij} and τ_{ij} are described by Equations 3.9 and 3.10.

$$\frac{\partial \left(\bar{\rho} \tilde{u}_i\right)}{\partial t} + \frac{\partial \left(\bar{\rho} \tilde{u}_i \tilde{u}_j\right)}{\partial x_j} = -\frac{\partial \bar{P}}{\partial x_i} + \frac{\partial \bar{\sigma}_{ij}}{\partial x_j} - \frac{\partial \tau_{ij}}{\partial x_j} \tag{3.8}$$

Now, the majority of LES models focus on resolving the sub-grid stress tensor (τ_{ij}). In the context of this investigation, a **Dynamic Structure** sub-grid LES approach has been considered for modelling this tensor [44]. This model expresses τ_{ij} as a function of the sub-grid turbulent kinetic energy by adding a transport equation for this parameter (Equation 3.11), and solving it by an iterative procedure.

$$\bar{\sigma}_{ij} = \mu(\frac{\partial \widetilde{u}_i}{\partial x_j} + \frac{\partial \widetilde{u}_j}{\partial x_i}) - \frac{2}{3}\mu\frac{\partial \widetilde{u}_k}{\partial x_i}\delta_{ij} \tag{3.9}$$

$$\tau_{ij} = \overline{\rho}(\widetilde{u_i u_j} - \widetilde{u_i}\widetilde{u_j}) \tag{3.10}$$

$$\frac{\partial k}{\partial t} + \bar{u}_i\frac{\partial k}{\partial x_i} = -\tau_{ij}\frac{\partial \bar{u}_i}{\partial x_j} - \epsilon + \frac{\partial}{\partial x_i}(\frac{\nu_t}{\sigma_k}\frac{\partial k}{\partial x_i}) \tag{3.11}$$

In order to determine which turbulence model should be used in a simulation, it is critical to establish the application of the specific case study, as well as the demands that must be covered by the numerical model. For example, although a RANS approach is perfectly suitable for characterizing the global behavior of the flow-dynamics and combustion process in SI engines through single-cycle simulations, the underlying hypothesis of the model does not allow it to account for multi-cycle combustion instabilities due to large turbulent scales. Alternatively, LES models, due to their capacity to resolve these large scale eddies, are better suited for analyzing the flow-field variations in multiple engine cycles, and their impact over the combustion process [45, 46].

In CFD simulations, the spatial filter of a LES model, that determines the size of the largest eddies to be resolved, is directly related to the size of the computational mesh. Thus, the cells of the domain should be small enough to allow a meaningful amount of energy to be resolved. This represents the major bottleneck of the LES approach, given that the employed mesh is typically composed by millions of cells, resulting in a considerable demand of computational power, which in term results unpractical for many applications.

Nevertheless, in the frame of this thesis, a clever methodology has been developed to perform multi-cycle combustion simulations using a LES approach in a simplified computational domain. This method is described in Chapter 4 and used to study the cycle-to-cycle variations of two pre-chamber designs that generate very different internal flow patterns.

3.3.3 Combustion model description

Recreating the turbulent premixed combustion of an SI engine in a CFD simulation is a challenging matter. In order to accurately describe this process an appropriate combustion model needs to be employed, that is able to account for the set of complex chemical reactions during the burning process and their interactions with the in-cylinder flow field. Nowadays, most CFD codes have two modelling approaches for performing this task. The first one is a Well Stirred Reactor (WSR) or SAGE combustion model [47, 48], which utilizes a detailed chemistry solver and computes the source term of the energy equation by the method proposed by Turns [49]. In this approach, the reaction rates of all species considered in the calculation are estimated with a multi-step chemical kinetics mechanism, which contains a set of elementary reactions that describe the overall chemical reaction. Additionally, the CFD solver needs to compute the transport equations for each species involved in the simulation, thus, depending on the amount of species/reactions that are contained in the mechanism, this model can be very computationally expensive.

The second modelling approach that has been widely extended in the scientific community consists of flamelet-based models [50, 51]. These models characterize the propagation of the flame front by the use of *Progress Variables*, which are essentially additional transported species that track the position of the flame while separating the computational domain into un-burned and burned regions by large scale stratification of chemical species. This approach has the advantage of significantly reducing the associated computational time as it does not account for detailed chemistry, therefore, the only species transport equations that are solved are those required by each particular model, which are considerably less than those involved in the SAGE model.

In the frame of modelling pre-chambers, both WSR and flamelet models have been used and provided encouraging results [52, 53]. However, a particularity of the pre-chamber ignition concept is that the flame can evolve in different regimes of the Borghi diagram [54, 55] during the combustion process. Thus, given the limitations of the different combustion models to accurately describe the flame evolution under different combustion regimes [56], no clear consensus has yet been reached regarding which model gives the most accurate predictions and the correct reproduction of all involved phenomena. Nevertheless, given the small-scale turbulence that develops inside the pre-chamber, flamelet models are better equipped to deliver a good match between experiments and simulations as they take into account both large-scale and small-scale turbulence [57], whereas the WSR model does not utilize an explicit turbulent combustion closure for the chemical reaction rates [58].

Considering the previous discussion, an extension of the Coherent Flamelet Model proposed by Marble and Broadwell [59], namely the Extended Coherent Flamelet Model (**ECFM**) [60], has been selected to carry out the activities of this thesis, given that it has demonstrated to perform well for simulating the pre-chamber ignition concept in both RANS and LES frameworks [61, 62]. This model tracks the position of the flame front by solving a transport equation for the flame surface density (Σ).

$$\frac{\partial \Sigma}{\partial t} + \frac{\partial u_i \Sigma}{\partial x_i} = \frac{\partial}{\partial x_i}\left(\frac{\mu}{S_c}\frac{\partial (\Sigma/\bar{\rho})}{\partial x_i}\right) + (P_1 + P_2 + P_3)\Sigma - D + P_k \tag{3.12}$$

$$P_1 = \alpha K_t \tag{3.13}$$

$$P_2 = \frac{2}{3}\frac{\partial \tilde{u}_i}{\partial x_i} \tag{3.14}$$

$$P_3 = \frac{2}{3}\bar{S}_l \frac{1-\tilde{c}}{\tilde{c}}\Sigma \tag{3.15}$$

$$D = \beta \bar{S}_l \frac{\Sigma^2}{1-\bar{c}} \tag{3.16}$$

$$\tilde{c} = \frac{\sum_i \tilde{Y}_i^b}{\sum_i \tilde{Y}_i^u + \sum_i \tilde{Y}_i^b} \tag{3.17}$$

$$\bar{c} = \frac{\rho}{\rho_b}\tilde{c} \tag{3.18}$$

Aside from the classical unsteady convection and diffusion terms, the transport equation 3.12 introduces additional terms (P_i) to account for several properties of the flame, a destruction term D and a source term P_k.

P_1 in Equation 3.13 models the production of flame surface by the effects of turbulent stretch along the flame front. In this equation, α is a user-defined constant of the model, and the turbulent stretch K_t is calculated as a function of the turbulent kinetic energy (k), the dissipation rate of this energy (ε), the turbulence RMS velocity ($u^{'}$), the laminar flame speed (S_L), the laminar flame thickness (l_f) and the integral length scale (l_t).

P_2 (Equation 3.14) accounts for the effects of thermal expansion and curvature of the flame. P_3 (Equation 3.15) represents the flame surface production due to mean flow dilation. In this term, $\bar{S}_l$ is the volume-averaged laminar flame speed, while $\tilde{c}$ is the mass progress variable which is calculated by Equation 3.17, where $\tilde{Y_i^b}$ represents the burned species mass fraction and $\tilde{Y_i^u}$ represents the mass fraction of un-burned species. Finally, the term D of Equation 3.16 is a corrective parameter that accounts for the destruction of flame surface due to consumption. In this equation, β is a model constant defined by the user and $\bar{c}$ is the volume progress variable, calculated in function of the mass progress variable by Equation 3.18.

Another crucial aspect of the combustion model is the way that the ignition is treated. For this thesis, the ECFM model was coupled with the Impossed Streatch Spark Ignition Model (ISSIM) developed by Colin and Truffin [63]. This model uses a simplified electrical circuit of the inductive-coil system to simulate the discharge of the spark divided in three phases: The breakdown and arc phases, which are modeled by considering an instantaneous deposition of energy in the gas with the approach proposed by Duclos and Colin [64], and the glow phase, which is accounted for by solving the ordinary differential equation of the electrical circuit. Ultimately, this model converts a user-specified energy input into a sphere with a reference flame surface density, in order to start the flame propagation through the transport equation for Σ. Additionally, the model includes a tunable constant to account for the initial wrinkling of the flame kernel, which directly increases or reduces the reference flame surface density.

Given that the ECFM model does not include a detailed chemistry solver, a different approach is required to compute the thermo-chemical properties of the flame. In this case, a set of four-dimensional tables were integrated into the combustion model to account for these properties. The generation of these tables was performed with a series of 0D/1D calculations that will be explained below.

0D homogeneous reactor simulations for auto-ignition delay

In order to account for knocking combustion, the ECFM model requires a Tabulated Kinetics Ignition (TKI) table, with values for the auto-ignition (AI) delay of the air-fuel mixture in a wide range of pressure, temperature, equivalence ratio and mixture composition (four dimensions). Thus, a 0D homogeneous reactor model, available in the CFD code, was used to perform these calculations, assuming isobaric conditions. It should be noted that the

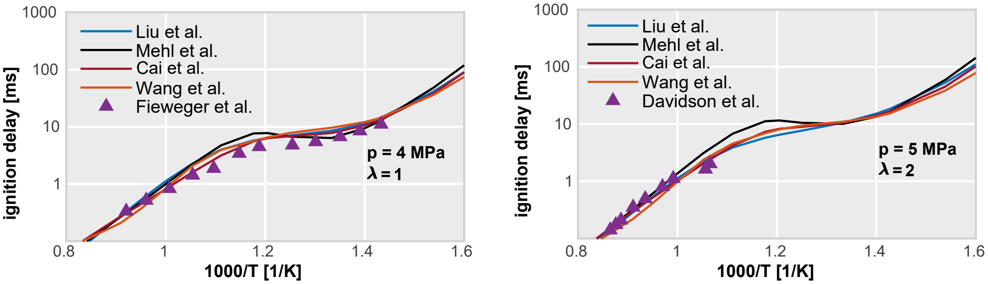

Figure 3.6: 0D homogeneous reactor simulation results for auto-ignition delay. Several chemical kinetics mechanisms are compared with experimental data at the same conditions.

ignition delay for these calculations was defined as the time necessary to increase the temperature of the mixture by 400K from its initial value [65].

Several chemical kinetic mechanisms available in the literature for Primary Reference Fuels (PRF) were used to carry out the 0D simulations, considering pure iso-octane as the gasoline fuel surrogate [66–69]. The calculations were compared with experimental data at high pressures of 4 MPa and 5 MPa (closer to engine-like conditions), for both stoichiometric and lean mixtures [70, 71]. This comparison is shown in Figure 3.6, where very little differences are observed among the selected mechanisms. Thus, the reduced mechanism of 44 species and 139 reactions developed by Liu et al. [66] was chosen to generate the ignition delay table, due to its good balance between computational time and accuracy of the results.

1D laminar flame speed calculations

The ECFM model also requires values for the laminar flame properties (laminar flame speed and laminar flame thickness) in order to accurately predict the combustion rates of the modelled flame front. Although these values are generally estimated through empirical correlations, these equations tend to underestimate the laminar flame speeds in actual engine operating conditions. Therefore, tabulated values of these properties were generated by a 1D model of a freely propagating flame in a channel with fixed cross-sectional area. This tool was available in the CFD code, and allowed to perform multiple calculations for different combinations of pressure, temperature, equivalence ratio and mixture composition.

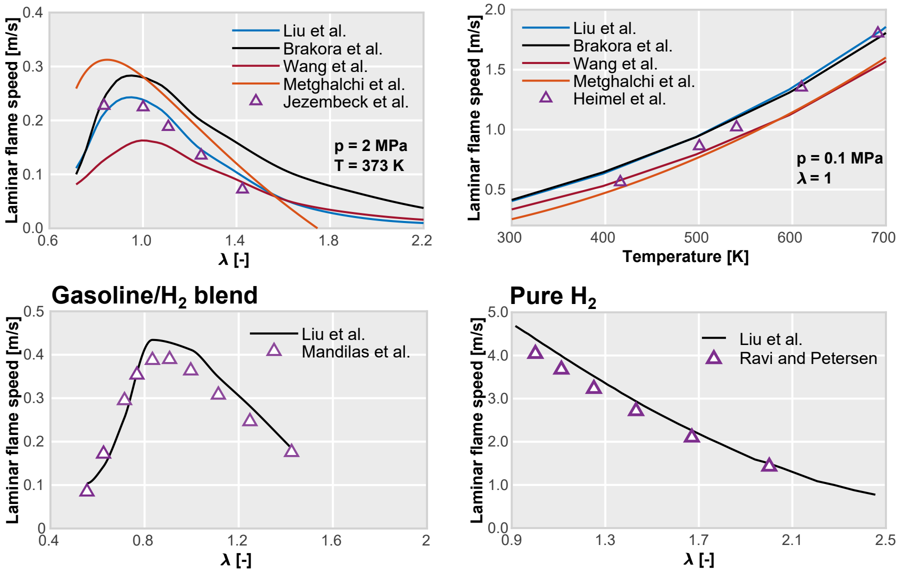

Figure 3.7: 1D laminar flame speed simulation results. Several chemical kinetics mechanisms are compared with experimental data at the same conditions. the bottom row shows the results for pure hydrogen and a gasoline/hydrogen blend.

Once more, the results of several kinetic mechanisms for Primary Reference Fuels [66, 69, 72] were compared with the experiments performed by Jerzembeck et al. [73] and Heimel et al. [74]. The upper row of Figure 3.7 shows the contrast between these 1D simulations and the experimental data, where the calculations with the correlation proposed by Metghalchi and Keck [75] were also included for reference. In this case, it is clearly observed that the mechanism from Liu et al. [66] provides the most accurate predictions of the laminar flame speeds, particularly in engine-like conditions (high temperatures and pressures), thus, it was again selected for generating the data table.

Additionally, Chapter 5 will present a study of the passive pre-chamber concept operating with gasoline/hydrogen fuel blends under lean conditions. Furthermore, ensuring that the employed mechanism can also predict accurate flame speed values for these gasoline/hydrogen blends is necessary to improve the reliance of the model. For this purpose, the bottom row of Figure 3.7 presents the 1D simulation results for a mixture of 95% gasoline and 5% H_2

(in Molar fraction) on the left, and the results for pure hydrogen combustion on the right. These calculations are compared with the data gathered by Mandilas et al. [76] and Ravi and Petersen [77], showing that the mechanism from Liu et al. is able to capture very well the experimental trends, even at high λ values.

These 0D/1D validations of the auto-ignition delay and laminar flame speed exhibit the preciseness of the model for reproducing the combustion fundamentals of pure gasoline fuel and gasoline/hydrogen blends, which provides a good starting point to extract reliable conclusions from the CFD simulations.

Table 3.7: Summary of the CFD model setup.

Physical models	
Combustion	ECFM (*with tabulated values for flame properties*)
Laminar flame speed table	PRF mechanism from Liu et al. [66]
Auto-ignition delay table	PRF mechanism from Liu et al. [66]
Ignition	Imposed Stretch Spark Ignition Model (ISSIM)
Turbulence	URANS RNG k-ϵ
Heat Transfer	Angelberger
Equation of state	Redlich-Kwong
Numerical schemes	
Spatial discretization	Second-order central difference scheme
Temporal discretization	First-order central difference scheme
Coupling between transport equations	PISO algorithm

3.3.4 Simulation methodology

After describing the physical models and numerical solvers implemented in the CFD code, which are summarized in Table 3.7, a methodology for performing the simulations needed to be established. For this research, the calculations were carried out in two parts, a non-reacting case followed by a reactive simulation. The first part consisted in modelling the full engine cycle (open + closed cycles), in order to study the characteristics of the in-cylinder flow dynamics and the pre-chamber filling/emptying without the influence of combustion reactions. For this case, the complete geometry of the cylinder shown in Figure 3.8 was used, which included the intake/exhaust ports and valves.

The second part focused on analyzing the combustion process. Furthermore, only the closed cycle was considered for these simulations. The bottom-right corner of Figure 3.8 shows the reduced computational domain in which the reactive cases were calculated, where the cylinder is closed by the valve

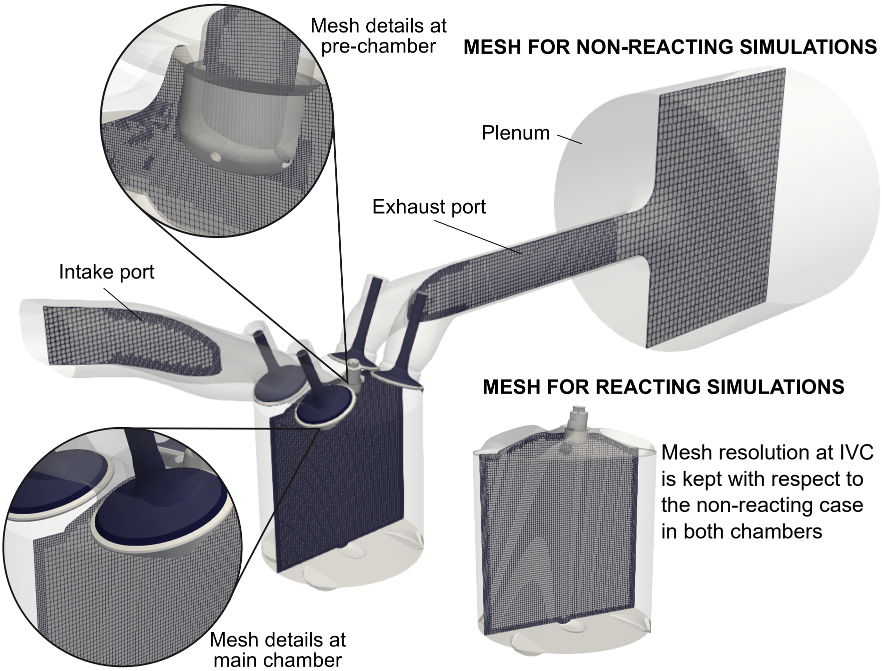

Figure 3.8: Computational domain for non-reacting and reacting simulations

seats and the port geometries have been removed. It is important to highlight that the mesh resolution in both the cylinder and the pre-chamber was maintained with respect to the non-reactive case at the moment of initialization. Moreover, the thermodynamic properties, characteristics of the flow field and stratification of species in the cylinder and pre-chamber were taken from an instantaneous solution generated in the non-reactive case.

This methodology allowed to reduce the computational expense of the simulations while still maintaining a high reliability on the numerical solution. Now, the setup for each case will be explained in the following sub-sections.

Setup for the non-reacting simulations

Obtaining a correct estimation of the velocity field and the generation of turbulence inside the cylinder is mandatory for the combustion model to reproduce the actual physics of the flame. Therefore, the open cycle needs to be accounted for when simulating SI engines, in order to perform reliable studies. The configuration of these non-reacting cases was done based on the corresponding experimental data for each simulated operating point.

The simulations started at the Exhaust Valve Opening (EVO), 146 Crankangle degrees (CAD) after the combustion Top Dead Center (aTDC) of the previous cycle, and were carried out until the EVO of the following cycle. During these calculations, the combustion model was deactivated. The purpose of performing the complete cycle simulation rather than just the open cycle, was to study the scavenging of residual gases and evolution of the flow field in the pre-chamber during the compression stroke, given that the passive version of this technology does not have a dedicated fuel scavenge in the pre-chamber region.

The initial pressures for each region of the domain were taken directly from the measured pressure signals in the cylinder, intake and exhaust ports at the EVO. As can be seen in Figure 3.8, the intake port was cut-off at the position of the pressure sensor in order to model the inflow boundary condition with the instantaneous intake pressure profile. On the other hand, the outflow boundary condition was modeled by a constant exhaust back-pressure and a large plenum to simulate the pressure waves generated in this conduct. This method was found to be the best way to reproduce the real acoustics of the engine.

The temperatures in the intake and exhaust manifolds were also monitored during the experimental campaign. Thus, these temperatures were used to initialize the intake and exhaust regions of the CFD model, and also as constant inflow/outflow boundary conditions. However, as the temperature inside the cylinder was not monitored, this parameter was estimated through the combustion diagnosis tool described in Section 3.2.1. This tool has integrated sub-models to account for the filling-emptying of the cylinder and intake/exhaust short-circuit, that calculate the mass flow-rate from the pressure difference between these regions, then, the in-cylinder temperature can be estimated from the trapped mass by the ideal gas equation of state [3, 78]. Moreover, the temperatures of the domain walls were estimated for each operating condition by the lumped heat transfer model developed by Torregrosa et al. [79].

Regarding the treatment of chemical species, pure iso-octane was used as the gasoline fuel surrogate. Also, considering that the engine was port fuel injected, and that the injection takes place almost 30 cm away from the port entrance and well before the Intake Valve Opening (IVO), a perfectly premixed air-fuel blend was initialized in the intake region, with the species concentration according to the relative air-to-fuel equivalence ratio of the simulated operating point. Thus, although injection modelling was not performed, the adopted approach was considered to be well-representative of the experimental

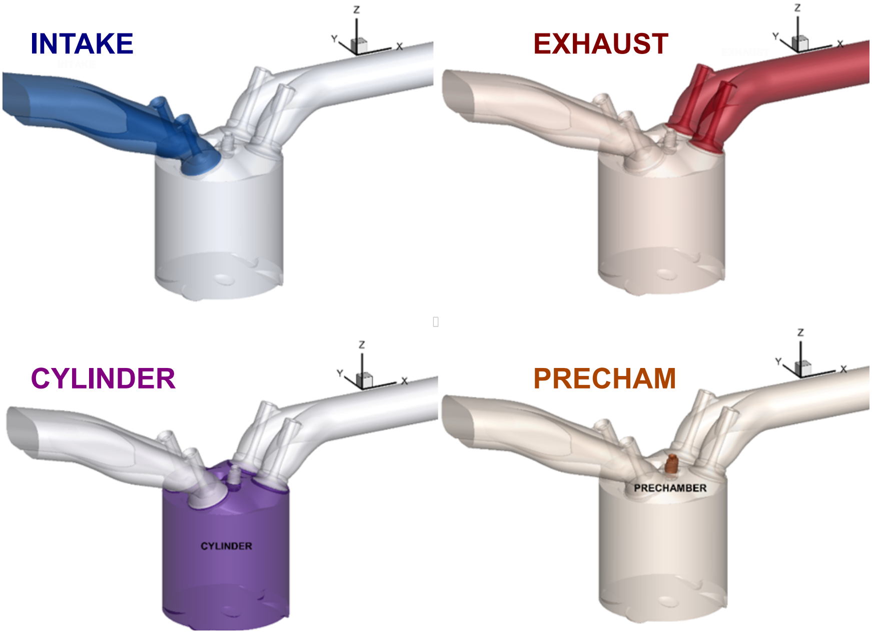

Figure 3.9: Transported passives initialized in each region of the computational domain

conditions. However, the stratification of internal residual gases can have a relevant impact over the combustion process. Furthermore, these were taken into account by initializing both the exhaust and cylinder regions with 100% of combustion residuals from the previous cycle, again, with the species concentration corresponding to the experimental λ value. It is important to point out that the pre-chamber region was initialized with the same pressure, temperature and species concentration of the cylinder.

A particular post-processing strategy devised for this research consisted in initializing *transported passives* in each region of the computational domain, in order to study the gas exchange process between these regions. Essentially, transported passives can also be seen as *dynamic tracers*, which are defined as calculated quantities that move with the flow, coupled in space and time with mass, momentum and energy, but don't affect the calculation of temperature and species concentration [15]. Furthermore, the four regions of the domain were associated with each dynamic tracer shown in Figure 3.9: INTAKE, EXHAUST, CYLINDER and PRECHAM respectively. These transported passives were uniformly initialized in every cell of the corresponding region with a value of 1, therefore, as the valves open, fractions of each tracer are passed to different regions following the direction of the flow. This was particularly useful to track the amount of mass coming from the intake (fresh air-fuel mixture), and evaluate how the pre-chamber was filled with these gases.

Finally, in order to have a reference of how the cases were setup, Table 3.8 shows the configuration of the simulation for OP2 (see Table 3.5 for reference).

Table 3.8: Initial parameters of the non-reactive case for OP2 (2000 rpm, 6.8 bar IMEP, λ=1 without EGR).

Region	**Cylinder**	**Intake**	**Exhaust**	**Pre-chamber**
Pressure [Pa]	191982	71389	104000	191982
Temperature [K]	1490	303	855	1490
YIC_8H_{18} [-]	0.0	0.06224	0.0	0.0
YO_2 [-]	0.0	0.2179	0.0	0.0
YN_2 [-]	0.7198	0.7198	0.7198	0.7198
YCO_2 [-]	0.1918	0.0	0.1918	0.1918
YH_2O [-]	0.08834	0.0	0.08834	0.08834
INTAKE [-]	0.0	1.0	0.0	0.0
EXHAUST [-]	0.0	0.0	1.0	0.0
CYLINDER [-]	1.0	0.0	0.0	0.0
PRECHAM [-]	0.0	0.0	0.0	1.0

Setup for the reacting simulations

The closed-cycle simulations were initialized at the Intake Valve Closing (IVC), 170 Crankangle degrees before the combustion Top Dead Center (bTDC), and finished at the EVO. Here, the combustion model was re-activated and the ignition was set to the corresponding experimental spark timing of the simulated operating point.

A mapping approach is used to start these cases, which consisted in initializing the cylinder and pre-chamber regions with an instantaneous solution coming from the non-reactive simulation at the IVC. This allowed to maintain the velocity and turbulence fields, stratification of species, transported passives and the thermodynamic properties that were generated in the computational domain during the open cycle, in order to have realistic conditions at the moment of ignition. Furthermore, the initialization of species, pressure, temperature and flow variables was not done explicitly for these cases. Additionally, the wall temperatures were also kept with respect to the non-reactive simulation.

Table 3.9: Initial parameters of the reactive case for OP2 (2000 rpm, 6.8 bar IMEP, λ=1 without EGR).

Parameter at IVC	**Experimental**	**Simulation**	**Difference** [%]
Pressure [Pa]	57482.8	58483.1	1.5
Temperature [K]	352.3	346.8	1.6
Trapped mass [mg]	257.6	259.2	0.6
air mass [mg]	223.1	223.6	0.2
Fuel mass [mg]	15.33	14.66	-
λ [-]	1.01	1.01	-
LHV [MJ/Kg]	42.5	44.4	-
Energy released [J]	650.1	650.8	-

For the purpose of closing the gap between the simulated conditions and the real engine tests as much as possible, a special adjustment was made to the initial fuel mass of the simulation by a temperature scaling factor. This procedure consisted in correcting the fuel mass in order to release the same amount of energy as the experimental case, considering that the Lower Heating Values (LHV) of iso-octane and the RON95 gasoline used in the experiments were different.

Thus, after applying the aforementioned correction, the initial parameters for the simulation corresponding to OP2 (see Table 3.5 for reference) were gathered in Table 3.9, contrasted against the measured experimental data (cylinder pressure, air mass and injected fuel mass) and the data estimated from the combustion diagnosis tool (trapped mass and cylinder temperature). This table highlights the accuracy of the modelling approach for recreating the experimental conditions, given that the differential values between all the compared parameters are below 2%. It is interesting to point out that despite the adjusted fuel mass, the air mass to maintain stoichiometry barely changes. This is due to the fact that the ratio between the stoichiometric air-to-fuel equivalence ratio of gasoline (14.374) and iso-octane (15.035) is very similar to the ratio between the lower heating values of these two fuels (shown in Table 3.9).

Finally, another special post-processing strategy based on dynamic tracers was developed for these simulations. In this case, a User Defined Function (UDF) was programmed into the CFD code to configure a transported passive species in the pre-chamber region at the moment of the jet ejection (after the start of combustion). This passive was initialized with value of 1 once the calculation detects an inversion of the flow between the main chamber and pre-chamber. Thus, it is possible to track the amount of mass coming from the pre-chamber that entrains the main chamber charge.

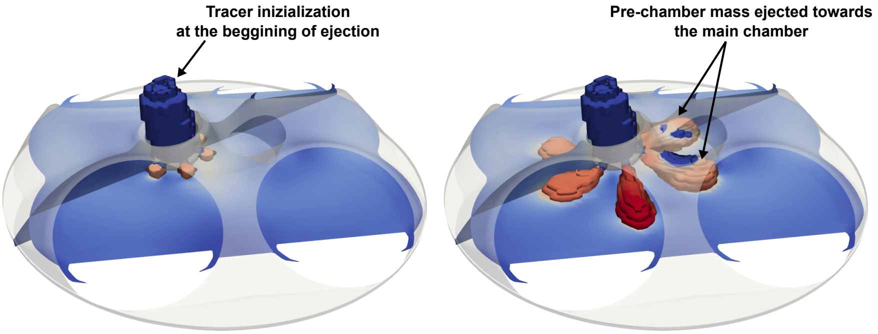

Figure 3.10: Dynamic tracer for tracking the position of the pre-chamber jets

Figure 3.10 shows a visual representation of the aforementioned dynamic tracer, with a snapshot corresponding to the beginning of the ejection process and another one where the jets are more developed. To establish the boundaries of the ejected jets an entrainment threshold of 1/1000 of the tracer's mass fraction was found to be appropriate to represent these limits. This post-processing variable allowed to perform novel studies by quantifying the energy released within the limits of the jets, the penetration and morphology of these jets and the lag between the start of ejection and the main chamber ignition.

3.3.5 Mesh independence study

One of the most important aspects in a CFD simulation is the definition of the computational mesh. This configuration was presented in Section 3.3.1, based on previous research experience and a thorough literature review. However, the accuracy of the numerical solution must always be balanced with the computational cost of the simulations.

As commented in Section 3.3.1, the CFD code uses the cut-cell Cartesian algorithm to create an orthogonal mesh based on hexahedrons, this ensures both high computational efficiency and mesh quality, but the size of the grid must be selected by the user depending on the application. Furthermore, this section presents a mesh independence study to ensure that the selected discretization of the domain does not affect the computation of thermodynamic and flow variables.

For this purpose, three meshes were evaluated, changing the base grid size in the cylinder. The calculations were performed following the methodology described in Section 3.3.4, simulating each mesh in both non-reacting and reacting conditions. The grid resolution in both simulations was kept equal to maintain consistency, at least until the spark timing of the reacting simulation when the mesh resolution starts to increase due to the temperature based AMR. Table 3.10 shows the studied meshes, highlighting the reference mesh described in Section 3.3.1 and including the cells at IVC and the computational time associated to each mesh.

Table 3.10: Characteristics of the studied meshes. The base grid size is referred to the cells in the cylinder

Base grid size	Cells at IVC	Computational time @64 processors
2 mm	602566	33 hours
1 mm	**1301803**	**74 hours**
0.5 mm	5811415	172 hours

In order to study the grid convergence, the solution of relevant variables for performing the analysis that is intended to be carried out in this thesis must be plotted. Therefore, the cylinder pressure trace, which is the main thermodynamic variable used to perform the validation of the CFD model in the next section, was considered for the independence study. Additionally, given that the generation of turbulence inside the pre-chamber is a phenomenon that affects significantly the propagation of the flame in this region, driving the subsequent jet ejection process and the ignition of the main chamber, the turbulent kinetic energy (TKE) in the pre-chamber was also evaluated.

Figure 3.11 shows the simulation results for these variables. From here, it is clearly observed that the base grid size of 2 mm underestimates by approximately 25% the pressure peak compared to the reference case of 1 mm base grid size. This in turn, results in a slightly delayed phasing of the pressure signal, which can be explained by the slower combustion process due to the considerable under-prediction of the pre-chamber TKE (around 70%), which is likely to produce a slower flame propagation in the pre-chamber and therefore, a delayed ignition of the main chamber. On the other hand, refining the grid to a much higher resolution with a base cell size of 0.5 mm, does not entail a significant change in the pressure profile or the TKE generation inside the pre-chamber. Thus, given that the base grid size of 1 mm proved to produce reliable results while considerably improving the computational time (see Table 3.10 for reference), this mesh was selected to perform the research activities of this thesis.

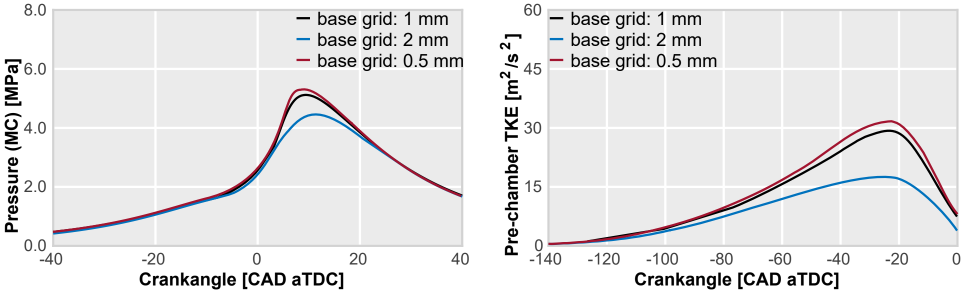

Figure 3.11: Mesh convergence for 3 base grid sizes in the cylinder. The main chamber pressure and pre-chamber TKE are plotted.

3.3.6 Model validation

After verifying the convergence of the numerical solution against relevant calculation parameters in the previous section, the final part of this chapter will focus on validating the CFD model against the experimental data. This is a fundamental step to ensure that the results are representative of the physical reality, and to provide a good support for the studies that will be presented in the following chapters.

Furthermore, in order to get a complete overview of the concept in different regions of the engine map, the three operating points presented in Table 3.5 were simulated, following the procedure explained in Section 3.3.4. Both the experiments and simulations were carried out with the reference pre-chamber tagged as PC1 in Table 3.4. These simulations were performed at stoichiometric conditions, with the corresponding MBT spark timing of each particular operating point.

The results from the simulations are shown in Figure 3.12, along with the experimental pressure signals and the HRR traces estimated from these signal with the combustion diagnosis tool described in Section 3.2.1. The measured in-cylinder pressure is averaged over 250 consecutive firing cycles. Overall, a very good agreement can be appreciated among the simulated and experimental curves for the three operating conditions. In particular, OP1 shows a minimal over-prediction of the peak cylinder pressure, however, it is within the range of the cycle-to-cycle variations for this running point. The remaining operating points (OP2 and OP3) show a very precise match between the two pressure curves.

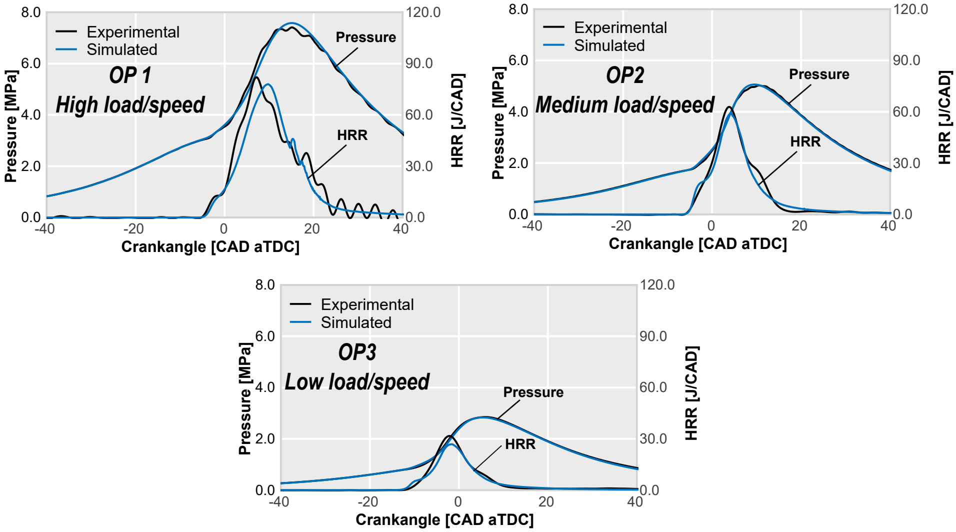

Figure 3.12: Validation of the CFD model in the tested operating conditions

The HRR traces also show a similar behavior in terms of ignition timing, peak burn rate and combustion duration. Nevertheless, these signals should only be taken as a reference and not as a strict validation parameter, given that the experimental HRR is a simple estimation performed with a different software. Thus, the performance of the computational model has been verified, and more detailed information can be extracted from these simulations in order to understand the characteristics of this ignition system.

Table 3.11: Comparison of indicated parameters for the baseline simulations and experiments.

Operating point	**IMEP** [bar] **Experimental**	**Simulated**	**Indicated eff.** [%] **Experimental**	**Simulated**
OP1	12.8	12.91	43.4	43.5
OP2	6.8	6.78	41.5	41.4
OP3	3.3	3.33	36.0	36.2

In order to have a quantitative assessment of the model, Table 3.11 presents a comparison of the indicated mean effective pressure and the gross indicated efficiency between experiments and simulations. This table shows little differences among the results for the indicated parameters in each operating condition, which further proves the robustness of the numerical solution.

An analysis of the air and EGR dilution limits is intended to be carried out in Chapter 5, thus, another important aspect to consider for these activities is the performance of the model under diluted conditions.

Modelling the passive pre-chamber ignition concept in highly diluted conditions has important challenges, given that there are complex physical phenomena occurring during the combustion process that need to be accounted for. One example of this was demonstrated by Yamaguchi et al [80] and Biswas et al. [81], with studies of the turbulent jet ignition process performed in a constant volume chamber. They showed that for high dilutions and reduced hole diameters, the flame could be totally or partially quenched when exiting towards the main chamber, which initiates the chain-branching reactions by active radicals. This in term, delays the combustion onset in the main chamber.

According to Poinsot et al. [82], the ECFM model uses a flame speed correction factor when the flame approaches the domain walls, which should be able to account for the extinction phenomena. However, in reality, simulating the flame propagation through these narrow channels is extremely complicated, given that the flame can evolve in unfavorable combustion regimes. Furthermore, ensuring that the model is also reproducing the global behavior of the engine in these conditions is crucial in order to properly study the underlying physics of the concept.

For this purpose, rather than performing blind simulations with different dilution levels, the experimental dilution sweeps were considered. Two air-dilution points (λ=1.4 and λ=1.6) for OP1 and two EGR rates (10% and 20%) at stoichiometric conditions for OP2 were modelled and contrasted against the experimental data. Figure 3.13 shows this comparison in terms of in-cylinder pressure and HRR. It is interesting to point out that the plots at the right-side of the figure (λ=1.6 and 20% EGR) are the corresponding dilution limits for those operating points. In general terms, the model fairly catches the measured pressure signal, showing a similar behavior during the combustion process and a correct estimation of the maximum pressure in all the simulated conditions. For the case of 20% EGR however, the model slightly overestimates the pressure peak.

Table 3.12 presents the same indicated parameters that were previously compared for the operating points in un-diluted stoichiometric conditions. In this case, the simulations show a good match with the experimental values at moderate levels of dilution (λ=1.4 and 10% EGR), however, as the dilution rate increases, the model starts to underestimate these values. This can be explained by the HRR traces of Figure 3.13 for λ=1.6 and 20% EGR, given

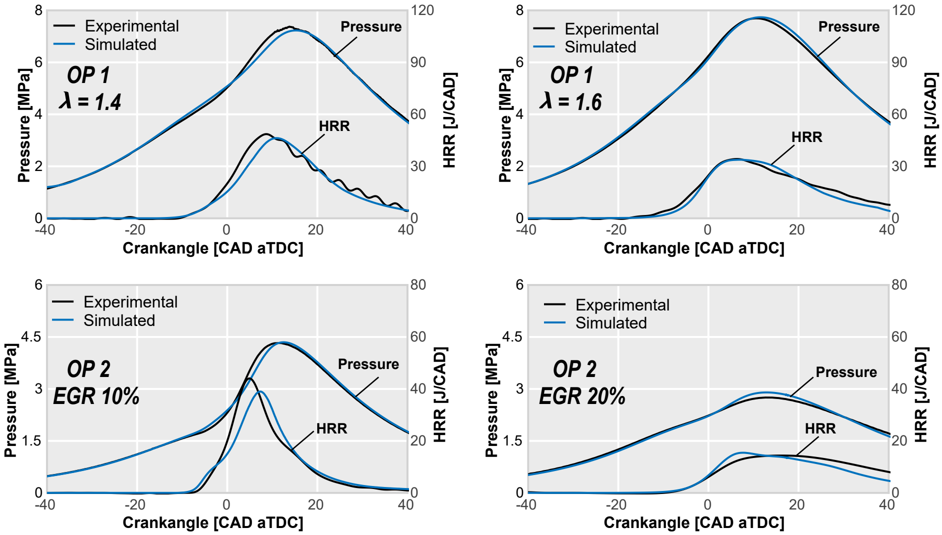

Figure 3.13: Validation of the CFD model in diluted conditions

Table 3.12: Comparison of indicated parameters for the simulations and experiments with air/EGR dilution.

Operating point	**IMEP** [bar] **Experimental**	**Simulated**	**Indicated eff.** [%] **Experimental**	**Simulated**
OP1 λ=1.4	12.8	12.74	44.2	44.0
OP1 λ=1.6	12.8	12.61	43.0	42.3
OP2 EGR 10%	6.8	6.78	40.5	40.4
OP2 EGR 20%	6.8	6.62	39.0	38.1

that the numerical solution shows an under-prediction of the burn rates for these cases during the expansion stroke. Nevertheless, for the scope of the studies that will be presented in this research, the model is considered to be behaving well enough to extract meaningful conclusions.

3.4 Summary

Along this chapter, the experimental environment and numerical tools used during this research to perform the fundamental studies of the passive pre-chamber ignition concept have been described. The studies are based on 3D-CFD simulations, combined with real engine test results and simplified numerical models to address the most critical aspects of the system's underlying physics and design features.

With the target of verifying the reliability of the numerical results, an extensive description and validation of the CFD model has been performed, paying special attention to the mesh configuration, turbulence and combustion models.

The majority of the simulations are carried out in a URANS framework, given that it allows to reproduce the global characteristics of the in-cylinder flow-field for single-cycle combustion simulations at a reduced computational cost. Nevertheless, a dedicated study of the pre-chamber's cycle-to-cycle variations will also be presented in the following chapters by using a LES turbulence model.

The ECFM model is employed for modelling the combustion process, coupled with the ISSIM model for spark-ignition. However, as this is a flamelet based model and detailed chemical kinetics are not solved, the auto-ignition delay and laminar flame speed values were calculated from set of 0D/1D simulations for a wide array of pressure, temperature, equivalence ratio and mixture composition. Thereafter, four-dimensional data tables were generated from these results to provide them as inputs for the ECFM model. Several chemical kinetics mechanisms for PRF were used for the simulations, and compared with experimental data in order to determine the most suitable mechanism for generating the tables. Ultimately, the mechanism from Liu et al [66] provided the most accurate predictions, and the laminar flame speed was also validated for combustion with pure hydrogen and gasoline/hydrogen fuel blends.

The mesh independence study demonstrated the convergence of thermodynamic and flow variables with a base grid size of 1 mm for the cells inside the cylinder. A mesh with a base grid size of 2 mm showed to significantly under-predict the cylinder pressure and pre-chamber TKE, while a mesh with 0.5 mm base grid size resulted in a considerable increase in computational time while the calculated parameters barely changed.

An efficient modelling methodology was developed by dividing the simulations into non-reacting and reacting cases. The former simulated the complete engine cycle, while the latter only considered the closed-cycle, and thus was carried out in a reduced computational domain without the port and valve geometries. However, these closed-cycle simulations were initialized by a mapping approach from an instantaneous solution generated from the open-cycle simulation, in order to have a proper recreation of the flow-field at the moment of ignition. This allowed to improve the computational time while maintaining representative results, and also to study the effects of the pre-chamber flow-dynamics with and without the influence of the combustion process.

Finally, following the aforementioned methodology, the complete model validation was performed for three relevant engine operating points in undiluted stoichiometric conditions: 12.8 bar IMEP @4500 rpm (OP1), 6.8 bar IMEP @2000 rpm (OP2), and 3.3 bar IMEP @1350 rpm (OP3). Additionally, the model was also validated in two air-diluted conditions for OP1 (λ=1.4 and λ=1.6) and two EGR rates for OP2 (10% and 20% EGR). In all cases, the model was able to accurately reproduce the experimental pressure profile, providing a solid foundation for the analysis that will be presented during the following chapters.

References

[1] Benajes, J et al. “Evaluation of the passive pre-chamber ignition concept for future high compression ratio turbocharged spark-ignition engines”. In: *Applied Energy* 248 (2019), pp. 576–588. doi: `https://doi.org/10.1016/j.apenergy.2019.04.131`.

[2] López, JJ et al. “Advantages of the unscavenged pre-chamber ignition system in turbocharged natural gas engines for automotive applications”. In: *Energy* 218 (2021), p. 119466. doi: `https://doi.org/10.1016/j.energy.2020.119466`.

[3] Lapuerta, M., Armas, O., and Hernández, J.J. “Diagnosis of DI Diesel combustion from in-cylinder pressure signal by estimation of mean thermodynamic properties of the gas”. In: *Applied Thermal Engineering* 19.5 (1999), pp. 513–529. doi: `https://doi.org/10.1016/S1359-4311(98)00075-1`.

[4] Payri, F., Molina, S., Martín, J., and Armas, O. “Influence of measurement errors and estimated parameters on combustion diagnosis”. In: *Applied Thermal Engineering* 26.2 (2006), pp. 226–236. doi: `https://doi.org/10.1016/j.applthermaleng.2005.05.006`.

[5] Olmeda, Pablo, Martın, Jaime, Novella, Ricardo, and Carreño, Ricardo. “An adapted heat transfer model for engines with tumble motion”. In: *Applied Energy* 158 (2015), pp. 190–202.

[6] Galindo, J, Climent, H, Plá, B, and Jiménez, VD. “Correlations for Wiebe function parameters for combustion simulation in two-stroke small engines”. In: *Applied thermal engineering* 31.6-7 (2011), pp. 1190–1199.

[7] Novella, R, Gomez-Soriano, J, Martinez-Hernandiz, PJ, Libert, C, and Rampanarivo, F. “Improving the performance of the passive pre-chamber ignition concept for spark-ignition engines fueled with natural gas”. In: *Fuel* 290 (2021), p. 119971. doi: `https://doi.org/10.1016/j.fuel.2020.119971`.

[8] Pastor, José V, López, J Javier, Garcıa, José M, and Pastor, José M. “A 1D model for the description of mixing-controlled inert diesel sprays”. In: *Fuel* 87.13-14 (2008), pp. 2871–2885.

[9] Desantes, JM, Pastor, JV, Garcıa-Oliver, JM, and Pastor, JM. “A 1D model for the description of mixing-controlled reacting diesel sprays”. In: *Combustion and Flame* 156.1 (2009), pp. 234–249.

[10] Pastor, Jose V, Garcia-Oliver, Jose M, Pastor, Jose M, and Vera-Tudela, W. "One-dimensional diesel spray modeling of multicomponent fuels". In: *Atomization and sprays* 25.6 (2015).

[11] Desantes, José M, Garcıa-Oliver, José M, Xuan, Tiemin, and Vera-Tudela, Walter. "A study on tip penetration velocity and radial expansion of reacting diesel sprays with different fuels". In: *Fuel* 207 (2017), pp. 323–335.

[12] Garcia-Oliver, Jose Maria et al. "An experimental and one-dimensional modeling analysis of turbulent gas ejection in pre-chamber engines". In: *Fuel* 299 (2021), p. 120861.

[13] Desantes, Jose Maria, Payri, Raul, Salvador, Francisco Javier, and Gil, Antonio. "Development and validation of a theoretical model for diesel spray penetration". In: *Fuel* 85.7-8 (2006), pp. 910–917.

[14] Pickett, Lyle M et al. "Relationship between diesel fuel spray vapor penetration/dispersion and local fuel mixture fraction". In: *SAE International Journal of Engines* 4.1 (2011), pp. 764–799.

[15] *CONVERGE 2.4 Theory Manual.* CONVERGENT SCIENCE Inc. 2018.

[16] Malé, Quentin et al. "Large eddy simulation of pre-chamber ignition in an internal combustion engine". In: *Flow, Turbulence and Combustion* (2019), pp. 1–19.

[17] Ye, Ying et al. "A Mapping Approach for Efficient CFD Simulation of Low-Speed Large-Bore Marine Engine with Pre-Chamber and Dual-Fuel Operation". In: *Energies* 14.19 (2021), p. 6126.

[18] Xu, Guoqing, Hanauer, Christophe, Wright, Yuri M, and Boulouchos, Konstantinos. *CFD-simulation of ignition and combustion in lean burn gas engines.* Tech. rep. SAE Technical Paper, 2016.

[19] Broatch, A, Olmeda, P, Margot, Xandra, and Gómez-Soriano, Josep. "Numerical simulations for evaluating the impact of advanced insulation coatings on H2 additivated gasoline lean combustion in a turbocharged spark-ignited engine". In: *Applied Thermal Engineering* 148 (2019), pp. 674–683.

[20] Ravindran, Arun C and Kokjohn, Sage L. "Combining machine learning with 3D-CFD modeling for optimizing a DISI engine performance during cold-start". In: *Energy and AI* 5 (2021), p. 100072.

[21] Guo, Hengjie, Torelli, Roberto, Szybist, James P, and Som, Sibendu. “CFD modeling of pre-spark heat release in a boosted direct-injection spark-ignition engine”. In: *International Journal of Engine Research* (2021), p. 14680874211044110.

[22] Ge, Haiwen et al. “CFD optimization of the pre-chamber geometry for a gasoline spark ignition engine”. In: *Frontiers in Mechanical Engineering* 6 (2021), p. 599752.

[23] Silva, Mickael et al. “Computational assessment of effects of throat diameter on combustion and turbulence characteristics in a pre-chamber engine”. In: *Applied Thermal Engineering* 212 (2022), p. 118595.

[24] Benajes, J et al. “Computational assessment towards understanding the energy conversion and combustion process of lean mixtures in passive pre-chamber ignited engines”. In: *Applied Thermal Engineering* 178 (2020), p. 115501. DOI: `https://doi.org/10.1016/j.applthermaleng.2020.115501`.

[25] Novella, R, Gomez-Soriano, J, Barbery, I, and Libert, C. “Numerical analysis of the passive pre-chamber ignition concept for light duty applications”. In: *Applied Thermal Engineering* (2022), p. 118610.

[26] Versteeg, Henk Kaarle and Malalasekera, Weeratunge. *An introduction to computational fluid dynamics: the finite volume method.* Pearson education, 2007.

[27] Issa, Raad I. “Solution of the implicitly discretised fluid flow equations by operator-splitting”. In: *Journal of computational physics* 62.1 (1986), pp. 40–65.

[28] Redlich, Otto and Kwong, Joseph NS. “On the thermodynamics of solutions. V. An equation of state. Fugacities of gaseous solutions.” In: *Chemical reviews* 44.1 (1949), pp. 233–244.

[29] Angelberger, C, Poinsot, T, and Delhay, B. *Improving near-wall combustion and wall heat transfer modeling in SI engine computations.* Tech. rep. SAE Technical Paper, 1997. DOI: `https://doi.org/10.4271/972881`.

[30] Peters, Norbert. *Turbulent combustion.* Cambridge university press, 2000.

[31] Cant, RS. “SB Pope, Turbulent Flows, Cambridge University Press, Cambridge, UK”. In: *Combustion and Flame* 125 (2001), pp. 1361–1362. DOI: `http://dx.doi.org/10.1016/S0010-2180(01)00244-9`.

[32] Launder, Brian Edward and Spalding, Dudley Brian. "The numerical computation of turbulent flows". In: *Numerical prediction of flow, heat transfer, turbulence and combustion.* Elsevier, 1983, pp. 96–116.

[33] Wilcox, David C et al. *Turbulence modeling for CFD.* Vol. 2. DCW industries La Canada, CA, 1998.

[34] Sodja, Jurij. "Turbulence models in CFD". In: *University of Ljubljana* (2007), pp. 1–18.

[35] Yusuf, Siti Nurul Akmal, Asako, Yutaka, Sidik, Nor Azwadi Che, Mohamed, Saiful Bahri, and Japar, Wan Mohd Arif Aziz. "A short review on rans turbulence models". In: *CFD Letters* 12.11 (2020), pp. 83–96.

[36] Shih, Tsan-Hsing, Liou, William W, Shabbir, Aamir, Yang, Zhigang, and Zhu, Jiang. "A new k- eddy viscosity model for high reynolds number turbulent flows". In: *Computers & fluids* 24.3 (1995), pp. 227–238.

[37] Wilcox, David C. "Formulation of the kw turbulence model revisited". In: *AIAA journal* 46.11 (2008), pp. 2823–2838.

[38] Yakhot, Victor and Orszag, Steven A. "Renormalization group analysis of turbulence. I. Basic theory". In: *Journal of scientific computing* 1.1 (1986), pp. 3–51. DOI: `https://doi.org/10.1007/BF01061452`.

[39] d'Adamo, A, Breda, S, Berni, F, and Fontanesi, S. "The potential of statistical RANS to predict knock tendency: Comparison with LES and experiments on a spark-ignition engine". In: *Applied Energy* 249 (2019), pp. 126–142.

[40] Ravindran, Arun C, Kokjohn, Sage L, and Petersen, Benjamin. "G-equation based ignition model for direct injection spark ignition engines". In: *International Journal of Engine Research* 23.8 (2022), pp. 1339–1352.

[41] Pope, Stephen B. "Ten questions concerning the large-eddy simulation of turbulent flows". In: *New journal of Physics* 6.1 (2004), p. 35.

[42] Pomraning, Eric Douglas. *Development of large eddy simulation turbulence models.* The University of Wisconsin-Madison, 2000.

[43] Menon, S, Yeung, P-K, and Kim, W-W. "Effect of subgrid models on the computed interscale energy transfer in isotropic turbulence". In: *Computers & fluids* 25.2 (1996), pp. 165–180.

[44] Pomraning, Eric and Rutland, Christopher J. "Dynamic one-equation nonviscosity large-eddy simulation model". In: *AIAA journal* 40.4 (2002), pp. 689–701.

[45] Vermorel, Olivier et al. “Towards the understanding of cyclic variability in a spark ignited engine using multi-cycle LES”. In: *Combustion and flame* 156.8 (2009), pp. 1525–1541.

[46] Chen, Ceyuan, Pal, Pinaki, Ameen, Muhsin, Feng, Dengquan, and Wei, Haiqiao. “Large-eddy simulation study on cycle-to-cycle variation of knocking combustion in a spark-ignition engine”. In: *Applied Energy* 261 (2020), p. 114447.

[47] Ravindran, Arun C and Kokjohn, Sage L. “The challenges of using detailed chemistry model for simulating direct injection spark ignition engine combustion during cold-start”. In: *International Journal of Engine Research* (2021), p. 14680874211045968.

[48] Silva, Mickael et al. *Effects of geometry on passive pre-chamber combustion characteristics*. Tech. rep. SAE Technical Paper, 2020.

[49] Turns, Stephen R et al. *Introduction to combustion*. Vol. 287. McGraw-Hill Companies New York, NY, USA, 1996.

[50] Posch, Stefan, Winter, Hubert, Zelenka, Jan, Pirker, Gerhard, and Wimmer, Andreas. “Development of a tool for the preliminary design of large engine prechambers using machine learning approaches”. In: *Applied Thermal Engineering* 191 (2021), p. 116774. DOI: `https://doi.org/10.1016/j.applthermaleng.2021.116774`.

[51] d’Adamo, A, Iacovano, C, and Fontanesi, S. “Large-Eddy simulation of lean and ultra-lean combustion using advanced ignition modelling in a transparent combustion chamber engine”. In: *Applied Energy* 280 (2020), p. 115949.

[52] Feyz, ME, Hasti, VR, Gore, JP, and Nalim, MR. “Large eddy simulation of hot jet ignition in moderate and high-reactivity mixtures”. In: *Computers & Fluids* 183 (2019), pp. 28–37.

[53] Xu, Guoqing, Wright, Yuri Martin, Schiliro, Michele, and Boulouchos, Konstantinos. “Characterization of combustion in a gas engine ignited using a small un-scavenged pre-chamber”. In: *International Journal of Engine Research* (2018), p. 1468087418798918. DOI: `https://doi.org/10.1177/1468087418798918`.

[54] Borghi, R. “On the structure and morphology of turbulent premixed flames”. In: *Recent advances in the Aerospace Sciences*. Springer, 1985, pp. 117–138.

[55] Borghi, Roland. “Turbulent combustion modelling”. In: *Progress in energy and combustion science* 14.4 (1988), pp. 245–292.

[56] Poinsot, Thierry and Veynante, Denis. *Theoretical and numerical combustion.* RT Edwards, Inc., 2005.

[57] Kim, Joohan et al. “Assessment of turbulent combustion models for simulating prechamber ignition in a natural Gas engine”. In: *Journal of Engineering for Gas Turbines and Power* 143.9 (2021).

[58] Pal, Pinaki, Keum, SeungHwan, and Im, Hong G. “Assessment of flamelet versus multi-zone combustion modeling approaches for stratified-charge compression ignition engines”. In: *International Journal of Engine Research* 17.3 (2016), pp. 280–290.

[59] Marble, Frank E and Broadwell, James E. *The coherent flame model for turbulent chemical reactions.* Tech. rep. PURDUE UNIV LAFAYETTE IN PROJECT SQUIDHEADQUARTERS, 1977.

[60] Boudier, P, Henriot, S, Poinsot, T, and Baritaud, T. “A model for turbulent flame ignition and propagation in spark ignition engines”. In: *Symposium (International) on Combustion.* Vol. 24. 1. Elsevier. 1992, pp. 503–510. DOI: `https://doi.org/10.1016/S0082-0784(06)80064-0`.

[61] Benajes, J, Novella, R, Gomez-Soriano, J, Barbery, I, and Libert, C. “Advantages of hydrogen addition in a passive pre-chamber ignited SI engine for passenger car applications”. In: *International Journal of Energy Research* 45.9 (2021), pp. 13219–13237. DOI: `https://doi.org/10.1002/er.6648`.

[62] Syrovatka, Zbynek, Vitek, Oldrich, Vavra, Jiri, and Takats, Michal. *Scavenged pre-chamber volume effect on gas engine performance and emissions.* Tech. rep. SAE Technical Paper, 2019.

[63] Colin, O and Truffin, K. “A spark ignition model for large eddy simulation based on an FSD transport equation (ISSIM-LES)”. In: *Proceedings of the Combustion Institute* 33.2 (2011), pp. 3097–3104. DOI: `https://doi.org/10.1016/j.proci.2010.07.023`.

[64] Duclos, JM and Colin, O. “(2-25) Arc and Kernel Tracking Ignition Model for 3D Spark-Ignition engine calculations ((SI-7) SI Engine Combustion 7-Modeling)”. In: *The Proceedings of the International symposium on diagnostics and modeling of combustion in internal combustion engines 01.204.* The Japan Society of Mechanical Engineers. 2001, p. 46. DOI: `https://doi.org/10.1299/jmsesdm.01.204.46`.

[65] Bounaceur, Roda et al. “Prediction of auto-ignition temperatures and delays for gas turbine applications”. In: *Journal of Engineering for Gas Turbines and Power* 138.2 (2016).

[66] Liu, Yao-Dong, Jia, Ming, Xie, Mao-Zhao, and Pang, Bin. “Enhancement on a skeletal kinetic model for primary reference fuel oxidation by using a semidecoupling methodology”. In: *Energy & Fuels* 26.12 (2012), pp. 7069–7083. DOI: `https://doi.org/10.1021/ef301242b`.

[67] Mehl, Marco, Pitz, William J, Westbrook, Charles K, and Curran, Henry J. “Kinetic modeling of gasoline surrogate components and mixtures under engine conditions”. In: *Proceedings of the Combustion Institute* 33.1 (2011), pp. 193–200. DOI: `https://doi.org/10.1016/j.proci.2010.05.027`.

[68] Cai, Liming and Pitsch, Heinz. “Optimized chemical mechanism for combustion of gasoline surrogate fuels”. In: *Combustion and flame* 162.5 (2015), pp. 1623–1637. DOI: `https://doi.org/10.1016/j.combustflame.2014.11.018`.

[69] Wang, Hu, Yao, Mingfa, and Reitz, Rolf D. “Development of a reduced primary reference fuel mechanism for internal combustion engine combustion simulations”. In: *Energy & Fuels* 27.12 (2013), pp. 7843–7853. DOI: `https://doi.org/10.1021/ef401992e`.

[70] Fieweger, K, Blumenthal, Ro, and Adomeit, G. “Self-ignition of SI engine model fuels: a shock tube investigation at high pressure”. In: *Combustion and Flame* 109.4 (1997), pp. 599–619. DOI: `https://doi.org/10.1016/S0010-2180(97)00049-7`.

[71] Davidson, DF, Gauthier, BM, and Hanson, RK. “Shock tube ignition measurements of iso-octane/air and toluene/air at high pressures”. In: *Proceedings of the Combustion Institute* 30.1 (2005), pp. 1175–1182.

[72] Brakora, Jessica and Reitz, Rolf D. *A comprehensive combustion model for biodiesel-fueled engine simulations.* Tech. rep. SAE Technical Paper, 2013. DOI: `https://doi.org/10.4271/2013-01-1099`.

[73] Jerzembeck, S, Peters, N, Pepiot-Desjardins, Pitsch, and Pitsch, H. “Laminar burning velocities at high pressure for primary reference fuels and gasoline: Experimental and numerical investigation”. In: *Combustion and Flame* 156.2 (2009), pp. 292–301. DOI: `https://doi.org/10.1016/j.combustflame.2008.11.009`.

[74] Heimel, Sheldon and Weast, Robert C. “Effect of initial mixture temperature on the burning velocity of benzene-air, n-heptane-air, and isooctane-air mixtures”. In: *Symposium (international) on combustion.* Vol. 6. 1. Elsevier. 1957, pp. 296–302.

[75] Metghalchi, Mohamad and Keck, James C. "Burning velocities of mixtures of air with methanol, isooctane, and indolene at high pressure and temperature". In: *Combustion and flame* 48 (1982), pp. 191–210.

[76] Mandilas, C, Ormsby, MP, Sheppard, CGW, and Woolley, R. "Effects of hydrogen addition on laminar and turbulent premixed methane and iso-octane–air flames". In: *Proceedings of the combustion institute* 31.1 (2007), pp. 1443–1450.

[77] Ravi, Sankaranarayanan and Petersen, Eric L. "Laminar flame speed correlations for pure-hydrogen and high-hydrogen content syngas blends with various diluents". In: *International Journal of Hydrogen Energy* 37.24 (2012), pp. 19177–19189.

[78] Benajes, Jesús, Olmeda, Pablo, Martın, Jaime, and Carreño, Ricardo. "A new methodology for uncertainties characterization in combustion diagnosis and thermodynamic modelling". In: *Applied Thermal Engineering* 71.1 (2014), pp. 389–399. DOI: `https://doi.org/10.1016/j.applthermaleng.2014.07.010`.

[79] Torregrosa, A, Olmeda, P, Degraeuwe, By, and Reyes, M. "A concise wall temperature model for DI Diesel engines". In: *Applied Thermal Engineering* 26.11-12 (2006), pp. 1320–1327. DOI: `https://doi.org/10.1016/j.applthermaleng.2005.10.021`.

[80] Yamaguchi, Shigeki, Ohiwa, Norio, and Hasegawa, Tatsuya. "Ignition and burning process in a divided chamber bomb". In: *Combustion and flame* 59.2 (1985), pp. 177–187.

[81] Biswas, Sayan and Qiao, Li. "Ignition of ultra-lean premixed H2/air using multiple hot turbulent jets generated by pre-chamber combustion". In: *Applied Thermal Engineering* 132 (2018), pp. 102–114. DOI: `https://doi.org/10.1016/j.applthermaleng.2017.11.073`.

[82] Poinsot, TJ, Haworth, Daniel Connell, and Bruneaux, Gilles. "Direct simulation and modeling of flame-wall interaction for premixed turbulent combustion". In: *Combustion and flame* 95.1-2 (1993), pp. 118–132.

Chapter 4

Characterization of the passive pre-chamber concept

"Simplicity is the ultimate sophistication", this is a very famous quote from Leonardo Da Vinci that can be philosophically interpreted at many levels. In the context of this thesis, one may state that: achieving the most simplified version of a system usually entails a very elaborate journey to understand the system's most fundamental aspects, in order to remove all the unnecessary complexities. This can be translated to the pre-chamber concept by comparing the active and passive approaches.

The active pre-chamber concept is composed of a more elaborate system, where basically the generation of optimum jets is always guaranteed due to the pre-chamber fueling (no mysteries here). On the other hand, the passive pre-chamber concept, being a more simplified system, requires an extensive comprehension of the scavenging, flow-dynamics and design features that will strongly condition the combustion process.

Thus, this chapter presents the fundamental aspects associated with this ignition strategy, based on the studies performed with the validated 3D-CFD model that was introduced in Chapter 3. This will serve as a starting point to understand the limitations of this technology for its use in passenger car applications, and also to asses its compatibility with other engine strategies. The first part of the chapter will show a dedicated analysis in un-diluted stoichiometric conditions, considering only one operating point. Thereafter, the impact of different operating conditions is evaluated, as well as the influence of spark timing and several design parameters over the relevant physical and thermochemical processes involved.

4.1 Studies of the passive pre-chamber concept in un-diluted stoichiometric conditions

Several studies performed from the experimental campaigns [1, 2] have demonstrated that the pre-chamber concept provides considerable advantages compared to the conventional SI concept, in terms of thermal efficiency, when operating at high load/speed conditions (OP1 in Table 3.5). This is mainly due to the faster combustion rates achieved with the pre-chamber, that overcome the knocking limitations of the conventional SI system in these conditions. Furthermore, this operating point was selected to carry out the first part of the research activities.

4.1.1 Analysis of the pre-chamber scavenge and flow field

The pre-chamber scavenge is one of the most critical aspects to address in the passive version of this technology. Given that there is not a dedicated fuel injection in the pre-chamber, the replacement of burned gases with fresh mixture is mainly controlled by the flow-dynamics between the pre-chamber and main chamber during the compression stroke. This can be observed in the left-side plot of Figure 4.1, where the evolution of the transported passives defined in Section 3.3.4 is shown for the pre-chamber region. From here, it can be seen that despite having some gas exchange during the intake stroke, where some fresh gases are able to enter the pre-chamber, the main filling process is generated due to the force of the piston during the compression (when the slope of the INTAKE curve increases).

These curves are taken from the non-reacting simulations, and can help to quantify the maximum amount of intake mixture that is able to enter the pre-chamber for a given operating condition. Thus, the residual gas fraction (RGF) that remains in the pre-chamber can be defined as the difference between the INTAKE passive and the sum of the remaining passives (Equation 4.1). This parameter is shown on the right-side plot of Figure 4.1, highlighting that at TDC the pre-chamber has 9.3% of residuals remaining from the previous combustion cycle. This has significant implications for strategies like EGR dilution where a spark advance is needed, given that as the combus-

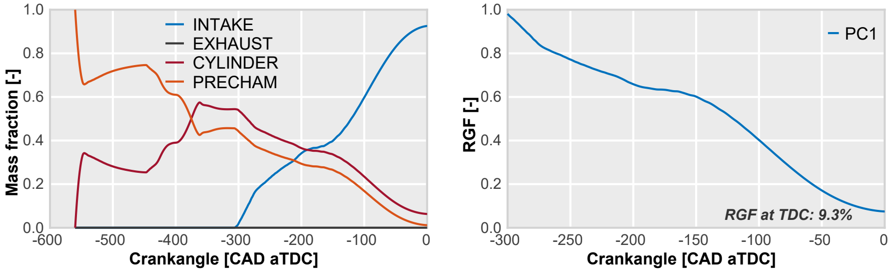

Figure 4.1: Evolution of the transported passives in the pre-chamber region.

tion starts at earlier crankangles (before TDC), it will take place in a more unfavorable environment due to these internal residuals.

$$RGF = INTAKE - (EXHAUST + CYLINDER + PRECHAM) \quad (4.1)$$

Moreover, the spatial distribution of the residual gases is another important aspect to consider. For this purpose, Figure 4.2 shows the RGF stratification inside the pre-chamber for two different crankangles referenced to the combustion TDC, compared to the RGF stratification for the conventional SI system in the same operating conditions. This figure highlights a fundamental difference between these ignition concepts. On one hand, for the SI system, despite the possibility of having some mixture stratification, the amount of residuals remains basically constant after the intake stroke, with a reasonably homogeneous distribution in the combustion chamber. Furthermore, advancing the spark timing does not entail a considerable change in the amount of residuals encountered by the initial flame kernel, nor in the later stages of the combustion process.

However, for the passive pre-chamber concept, both the amount of residuals and their stratification are higher, specially when moving towards advanced spark timings. The snapshots of Figure 4.2 show that in -10 CAD the average residuals in the pre-chamber are 4% higher than the conventional SI concept, and when advancing to -25 CAD this difference increases to 6%. This situation is even more evident when analyzing the amount of residuals in the spark plug gap, where they increase from 13.4% to 20% by advancing the spark timing from -10 CAD to -25 CAD. This will limit the compatibility of the concept with spark advance, and therefore, with conditions where advancing

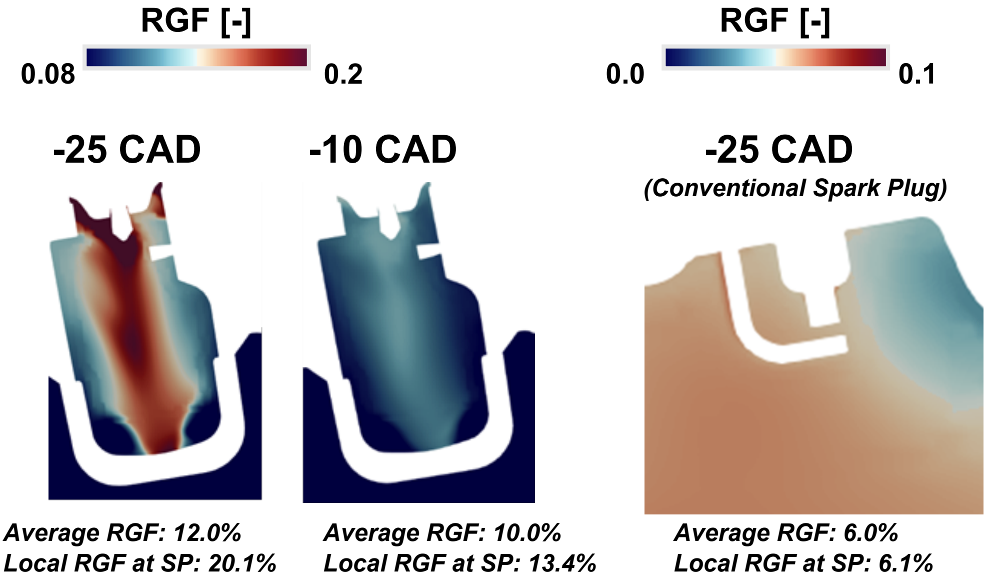

Figure 4.2: Visualization of the residual gas fraction inside the pre-chamber at different crankangles. The RGF for the conventional Spark Plug is also shown for reference.

the spark is necessary to properly phase the combustion (lower load/speeds or EGR diluted conditions).

Another relevant flow variable to study is the Turbulent Kinetic Energy (TKE) inside the pre-chamber. Since the passive system will essentially share the same mixture composition as the main chamber, operating in conditions that compromise the combustion process in this region, like using air or EGR dilution, will directly translate these issues to the pre-chamber. Thus, the generation of turbulence is something that can help to overcome this situation by improving the turbulent flame speeds in the pre-chamber.

In Figure 4.3 the evolution of the TKE and the velocity magnitude inside the pre-chamber are plotted. The black curves correspond to the volume-averaged values in this region, and the blue curves correspond to the averaged values in a 1 mm box located at the spark plug gap. It is confirmed how the temporal evolution of these flow parameters is also controlled by the compression stroke. However, as the piston approaches the top dead center (from -20 CAD), the TKE starts to have a sharp decrease due to the friction between the gas and the pre-chamber walls.

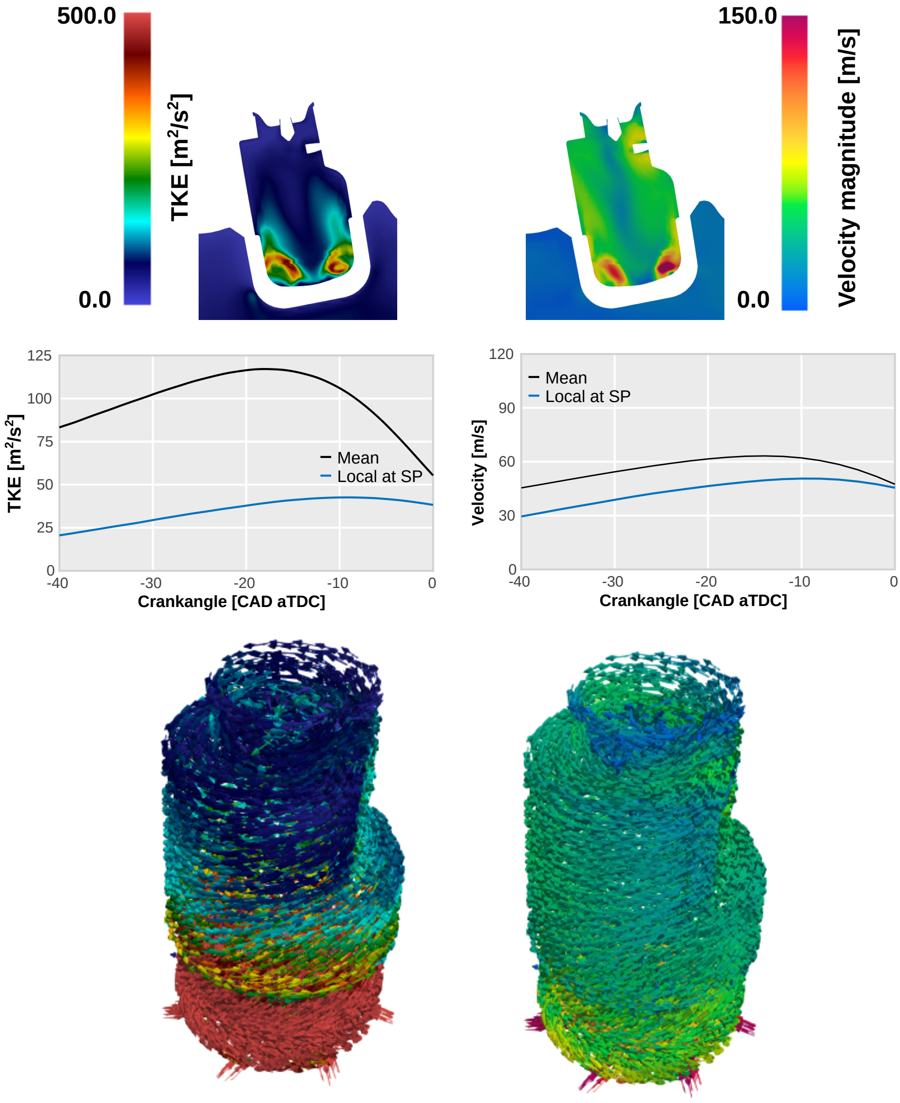

Figure 4.3: Pre-chamber TKE and velocity. The average and local values at the spark plug gap are plotted and the local distribution of these variables are shown at -10 CAD

Another important aspect is the spatial heterogeneity caused by the vortex that is generated from the swirling motion of the pre-chamber holes, which produces significant differences between the mean values of the TKE and those observed in the spark plug gap. This can be appreciated in the top snapshots of Figure 4.3, where the flow patterns for the velocity and TKE are shown at -10 CAD. From these images it is clearly observed that the high values of TKE are generated in the bottom of the pre-chamber due to the flow stretching through the holes, and are dissipated as the flow moves towards the electrodes. The velocity follows a similar pattern, but without having such a high difference with the values at the top of the pre-chamber. The bottom part of Figure 4.3 shows a representative 3D-sketch of these variables, to highlight the direction of the flow and the high swirl that rises along the pre-chamber walls.

This analysis presents another problem of the passive pre-chamber concept in relation to the spark timing. In this case, if the spark is triggered very close to TDC or during the expansion stroke, the levels of turbulence in the pre-chamber will be drastically reduced, and also the available energy in this region will start to decrease, due to the mass transfer towards the main chamber as a consequence of the piston's suction during its downward movement. Thus, both the RGF and the TKE are parameters that will strongly influence the pre-chamber combustion process and ignition of the main chamber, depending on the moment when the spark is triggered. This will be further explored in Sections 4.2 and 4.3.

4.1.2 Analysis of the combustion process

After analysing the pre-chamber scavenge and flow-field with the non-reactive simulations, the reactive cases can be used to study the combustion process. Furthermore, the first stage of this analysis will consist on describing the temporal evolution of the thermodynamic variables in both the pre-chamber and main chamber, as well as the flow-dynamics between them during the jet ejection process. For this purpose, the left-side plots of Figure 4.4 present the pre-chamber and main chamber pressure traces along with the difference between them ($\Delta \mathrm{p} = \mathrm{P}_{\mathrm{PC}}$ - P_{MC}), while the right side of the figure shows the pre-chamber and main chamber HRR.

Four well-differentiated phases are identified from the pressure curves: (I) filling of the pre-chamber, (II) ejection, (III) re-flux and (IV) emptying. The filling process (I) is controlled by the pressure generated in the main chamber during the compression stroke, and as will be seen in Sections 4.2 and 4.3, the pressure difference between both chambers during this stage depends on both the geometry of the pre-chamber (relationship between the cross-sectional area of the holes and the volume) and the engine speed.

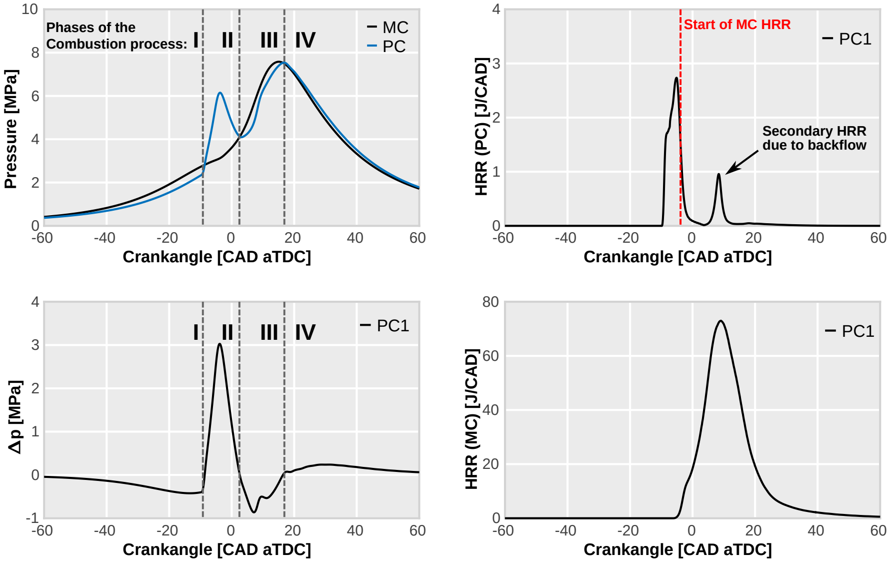

Figure 4.4: Evolution of the pressure and HRR during the pre-chamber and main chamber combustion.

The duration of the ejection process (II) is around 12 to 15 CAD for this regime of 4500 rpm, and is fundamentally controlled by the pressure difference between the two chambers. This pressure difference quickly reverses as the energy input and mass transferred by the pre-chamber combustion comes to an end, and the main chamber pressure suddenly increases after the ignition occurs in this region. The ejection process is the one that actually drives the main chamber ignition, and the evolution of the combustion process in this chamber will be conditioned by the characteristics of the jets generated during this stage.

The re-flux stage (III) is not always observed, since it depends on the relationship between the evolution of the main chamber combustion and the expansion it undergoes due to the movement of the piston. However, if this stage occurs, there is usually a backflow HRR in the pre-chamber, due to the mass that is re-entering this region and the remaining fuel that was not consumed during the ejection. Finally, the pre-chamber emptying stage (IV) is generally irrelevant for the combustion process in the main chamber, but it is obviously necessary to be able to replace the residual gases in the pre-chamber by unburned mixture.

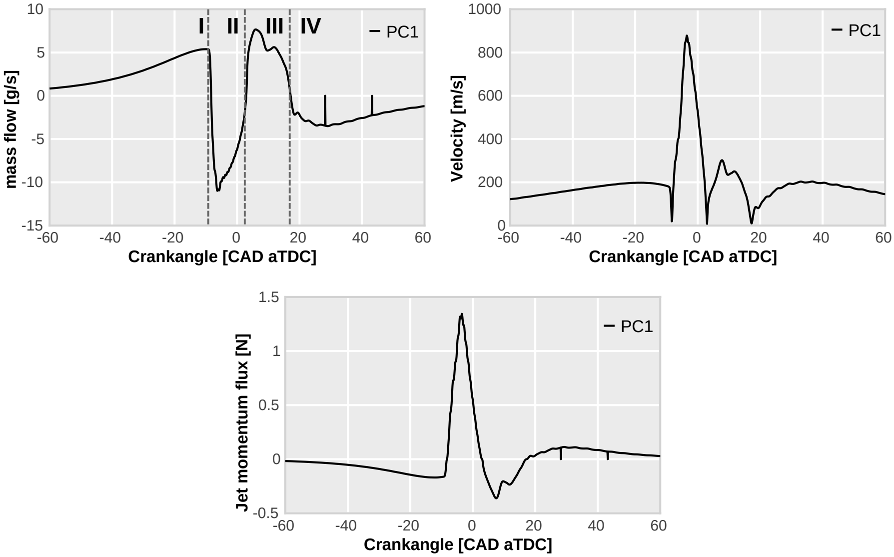

Figure 4.5: Flow-dynamics between the pre-chamber and main chamber. The Jet momentum flux is calculated as the product between the mass flow rate and the velocity through the pre-chamber holes.

Moreover, Figure 4.5 shows the features of the jets ejected from the pre-chamber. The mass flow rate and the velocity are calculated by placing monitor boxes of 0.3 mm at the exit of the holes and averaging these variables in those volumes. Thereafter, the jet momentum flux is calculated as the product between the computed mass flow rate and the velocity through the pre-chamber holes. From here, the four stages that were previously defined for the pre-chamber combustion are again observed, and the jet momentum can be used (along with the Δp) as a parameter to quantify the strength of the jets. However, it is sometimes helpful to decompose this parameter, given that a high momentum profile can be achieved by either having an elevated mass flow, which is usually given by having big holes, or a high velocity profile, which is often the product of a fast combustion process in the pre-chamber.

Moving on, the spatial evolution of the combustion process inside the two chambers is presented in Figure 4.6, where the structural differences between them can be appreciated. In this figure, the position of the flame is tracked by coloring the source term of the energy equation, and the scale is normalized to the maximum HRR in each region for visualization purposes. Additionally, the boundaries of the ejected jets are identified by a green contour line,

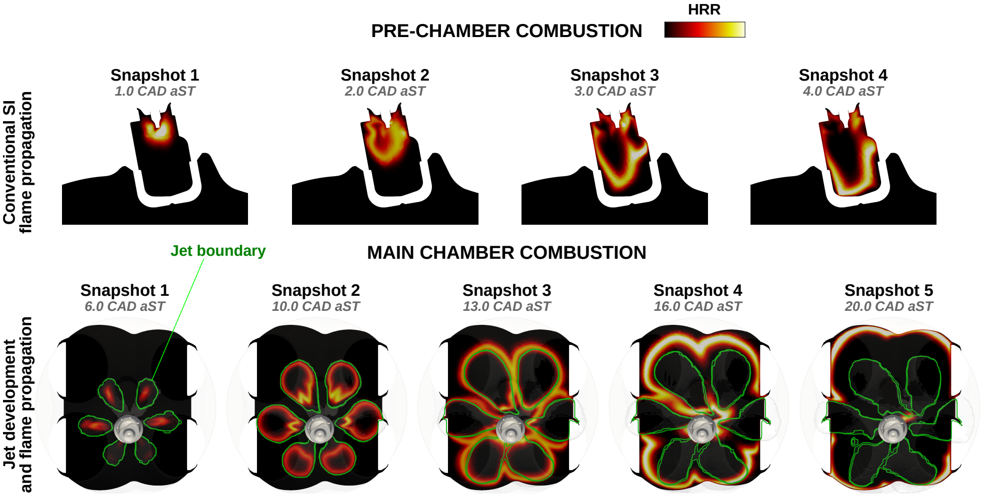

Figure 4.6: Visualization of the combustion process in both chambers.

which corresponds to the threshold of the user-defined dynamic tracer that was programmed into the CFD code and explained in Section 3.3.4.

In these conditions, the flame inside the pre-chamber develops very fast, reaching the holes between 4 and 5 CAD after the spark timing (CAD aST). This process follows a conventional SI combustion pattern, with the difference of occurring in an environment with very particular fluid dynamic conditions, as shown in Figure 4.3. Thus, the flow heterogeneity inside the pre-chamber causes an evident distortion of the flame front in this region.

Thereafter, the combustion in the main chamber starts inside of the ejected jets and rapidly progresses to their limits. From the third snapshot of the main chamber combustion, it is seen how the flame is able to surpass the jet boundaries and starts progressing according to a conventional flame propagation. However, the duration of the ejection process is very limited according to Figures 4.4 and 4.5, which causes the momentum flux to stop being supplied to the jets, and thus begins to slow down their rate of penetration until a complete stop.

To better analyze the aforementioned sequence, Figure 4.7 shows the temporal evolution of the penetration for the jets and the flame front. The top-left corner of the figure presents a sketch of the combustion chamber, highlighting the jets that are plotted on the right-side graph. It is interesting to note that the position of the pre-chamber is not co-axial with the cylinder axis. This

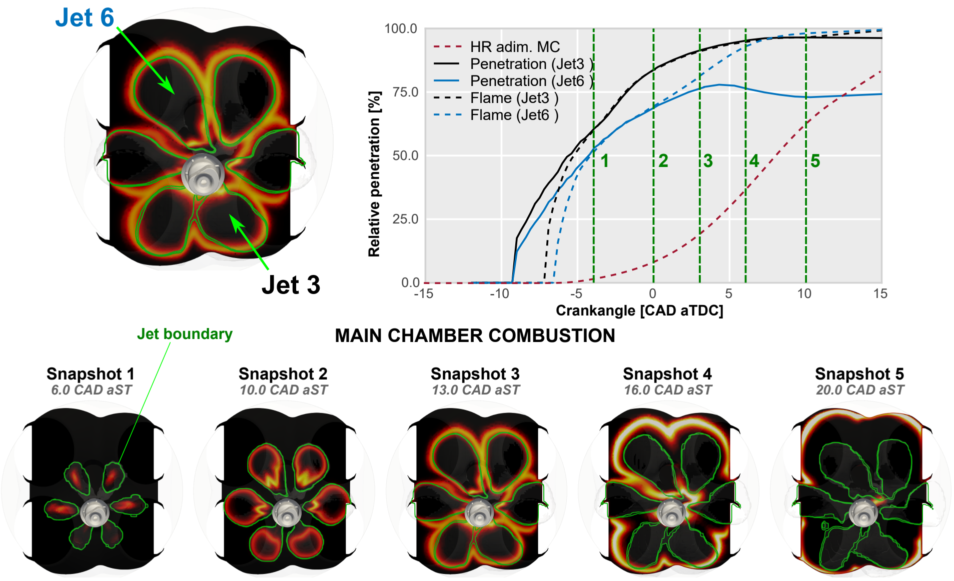

Figure 4.7: Evolution of the jets and flame penetration. two jets are plotted with different paths to travel in the combustion chamber, along with the flame associated to each jet. The normalized HR in the main chamber is also shown.

causes the problem to lose symmetry, with some jets having to travel a short path and others a long one to reach the cylinder walls. Thus, the penetrations included in this figure have been normalized to the respective wall distance of each particular jet. The normalized HR in the main chamber has also been included for reference.

The blue curves of Figure 4.7 correspond to the jet with the longest path to travel in the combustion chamber (Jet 6), while the black curves correspond to a jet with a shorter path (Jet 3). Additionally, the solid lines are related to the penetration of the jet, while the dashed lines show the penetration of the flame. The vertical lines of the plot represent the 5 snapshots shown at the bottom of the figure.

A couple of interesting ideas can be extracted from this figure. First, there is a short lag (around 1 CAD) between the triggering of the spark (at -10 CAD) and the beginning of the jet ejection. However, this process begins at the same time for all of the jets, given that it is mainly produced by the pre-chamber pressurization.

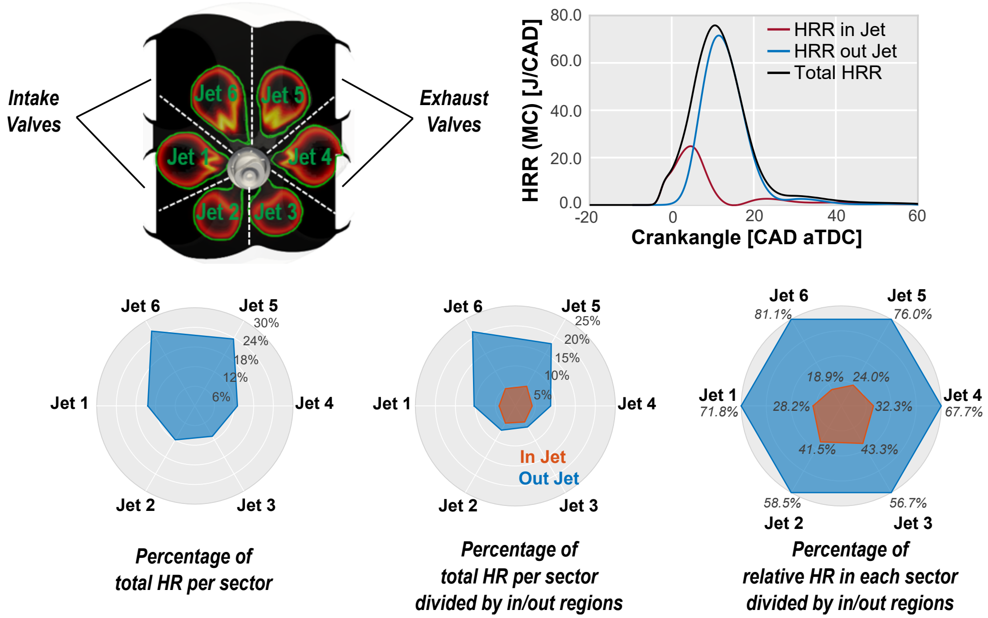

Percentage of total HR per sector

Percentage of total HR per sector divided by in/out regions

Percentage of relative HR in each sector divided by in/out regions

Figure 4.8: Main chamber energy distribution. The energy consumed inside and outside of the jets is quantified for each sector of the main chamber, according to the division presented in the top-left corner.

On the other hand, depending on the local evolution of the combustion process in the pre-chamber, the flame starts to come out of some holes sooner than others, as shown by the onset of the flame penetrations in Figure 4.7. Nevertheless, each flame is able to reach the corresponding jet limits at approximately the same time (around 1 to 3 CAD after the ejection starts). Afterwards, jets that must travel a short path (Jet 3) are able to reach the cylinder walls, while jets that must travel a long path (Jet 6) do not reach these walls, and the flame front must progress freely once it escapes the influential boundaries of the jet.

At this point, the potential of using the user-defined dynamic tracer to study the pre-chamber jet features has been proven. Furthermore, a deeper analysis can be made by quantifying the amount of the main chamber charge that is consumed within the limits of the jets, and how much of this charge is burned outside the jet boundaries according to a conventional flame front propagation process. To illustrate this study, Figure 4.8 shows the main chamber HRR profile divided into two contributions. The red curve corresponds to the energy released inside the jets, the blue curve shows the energy consumed outside the jets and the black curve is the total HRR.

These curves highlight that most of the combustion (specifically over 70% of the burned fuel) takes place outside of the jet entrainment region. It can be affirmed that in these operating conditions (λ=1 and 0% EGR), where the thermodynamic properties in the main chamber are favorable enough to sustain a fast flame propagation, the ejected jets act as a “super-spark”, starting the combustion process in a volumetric region orders of magnitude larger than the localized ignition generated by the conventional SI concept. However, once the combustion starts, it is the fluid-dynamics and thermochemical conditions downstream of the jets that dominate the rest of the process.

Given the asymmetric nature of the problem, due to the installation limitations of the pre-chamber over the cylinder head, the energy distribution in the main chamber is another interesting aspect to analyze. Furthermore, an angular representation of the combustion chamber was made, dividing this region into six sectors of 60° according to the sketch shown at the top-left corner of Figure 4.8. Thereafter, the polar graphs presented at the bottom of the figure were generated.

The left-side graph shows the percentage of energy consumed in each sector relative to the total energy released in the main chamber. This plot confirms that around 50% of the main chamber charge is consumed in sectors 5 and 6, corresponding to the jets with the longest path to travel in the combustion chamber. Moreover, the middle graph divides the percentage of energy released in each sector into the contributions inside and outside of the jet boundaries. From here, the small share of released energy within the limits of the jets can be again appreciated. However, an interesting trend is observed for jets 2 and 3, where the energy consumed by those jets is almost half of the total energy released in their corresponding sectors. This can be better analyzed from the last polar graph, where the relative contribution of energy released inside and outside of each jet is plotted with respect to the total energy of each sector. Thus, as jets 2 and 3 are closer to the chamber walls, they are able to burn over 40% of the fuel in their respective regions. On the other hand, for jets 5 and 6, only 19% and 24% of the energy is released within the jet limits, as the momentum flux stops to drive the jet development and they are not able to penetrate further into the main chamber.

This study has shown that the pre-chamber location over the cylinder head has an important impact on both the energy distribution and the combustion process in the main chamber. Having an asymmetrical installation, where the pre-chamber is offseted with respect to the cylinder axis, will directly translate

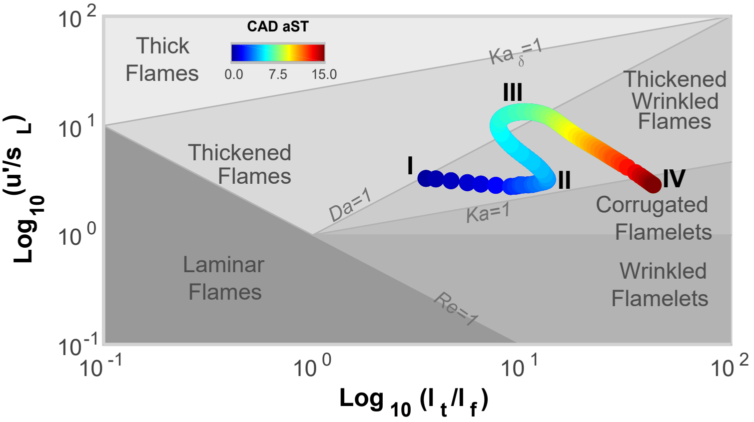

Figure 4.9: Evolution of the flame structure during the combustion process in the Borghi-Peters diagram.

into some of the jets not being able to reach the cylinder walls. Thus, the flame front will need to sweep a high percentage of the main chamber volume without the aid of the highly turbulent jets. This can represent a potential issue in conditions where the thermochemical and fluid-dynamic properties downstream of the jets are compromised.

Moving forward, the evolution of the flame regime throughout the combustion process is shown in Figure 4.9, in order to characterize the flame structure during the different stages of this process. The aforementioned figure presents the diagram proposed by Borghi and Peters [3, 4], where they introduced a taxonomy for the different flame regimes in premixed combustion. This diagram is made by comparing the characteristic length scales (l_t and l_f) along with the turbulent intensity ($u^{'}$) and laminar flame speed (S_L).

In the frame of the performed CFD simulations, the flame thickness (l_f) and laminar flame speeds were extracted from the data table generated from the 1D flame speed calculations for the ECFM combustion model (see Section 3.3.3). On the other hand, the integral length scale (l_t) and turbulent intensity were computed through the RANS turbulence model, with the equations described in Section 3.3.2 as a function of the modelled turbulent kinetic energy and the dissipation rate of this energy. These four variables were spatially averaged along the flame front during each time step of the simulation.

The colored dots of Figure 4.9 represent the time frame relative to the moment of ignition. From here, three stages are identified to analyze the combustion evolution. From (I) to (II), the flame develops inside the pre-chamber region, progressing initially in the *thickened wrinkled flames* regime, where the Kolmogorov scales are larger than the flame thickness and the flame structure is suitable for most SI engine applications. This stage ends quickly, after 3 to 5 CAD in this particular operating condition. Later on, from (II) to (III), as the flame stretches through the pre-chamber holes and begins to develop in the main chamber, it momentarily shifts towards the *thickened flames* regime, where some eddies can penetrate into the diffusive layer of the flame structure. However, the flame quickly stabilizes from (III) to (IV), and returns to the *thickened wrinkled flames* regime. Then, during the final stages, the flame develops in the *corrugated flamelets* regime, just as a conventional SI combustion process.

This figure exhibits the multi-regime flame evolution of the passive pre-chamber concept, which is an important characteristic of this ignition strategy that will be further explored in Chapter 5, in order to analyze the combustion process in diluted conditions.

4.1.3 Energy balance of the pre-chamber during the ejection process

Finally, to close this section, an energetic analysis of the pre-chamber is proposed. For this purpose, an energy balance during the jet ejection process has been performed, given that this stage is the one that will be truly relevant for the main chamber ignition.

The energy management during the pre-chamber combustion can be divided into four contributions: The energy that is used for effectively igniting the main chamber (**EAE**) in the form of a flame or as hot combustion products, the energy that is lost by heat transfer through the pre-chamber walls ($\mathbf{Q_{wall}}$), the unburned fuel left inside the pre-chamber at the end of ejection (**Unburnt**), and the non-reacting mass that is lost during the first stages of the ejection process (**Inert**) due to the pressurization of the pre-chamber. These variables are quantified in Figure 4.10, from the start of combustion until the flow reverses due to the main chamber pressure rise. The left bar shows the absolute energy values of each contribution, where the red, orange, yellow and blue blocks are associated to each of the previously defined parameters (in the same order). These values are then normalized with respect to the total energy available at the beginning of the pre-chamber combustion (full length of the left-side bar), and from here the right-side bar is generated, showing the relative share of each energy parameter. Additionally, the bottom part of

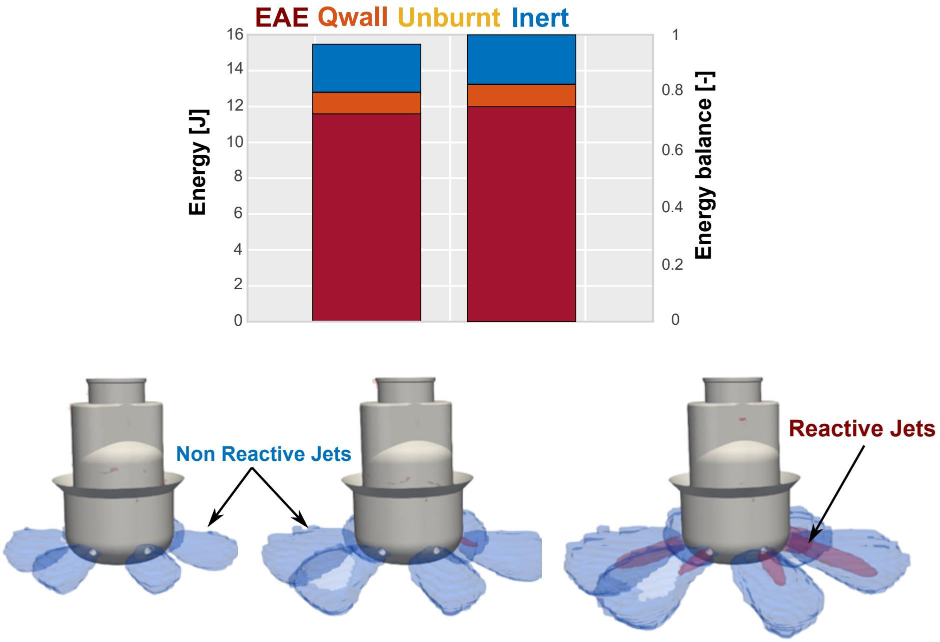

Figure 4.10: Pre-chamber energy balance during the ejection process.

Figure 4.10 shows a schematic visualization of the non-reacting jets that are ejected first (Inert), followed by the reacting jets that are able to produce the ignition (EAE).

The first two energy parameters are related to the burned fuel. The EAE is calculated by integrating the HRR inside the pre-chamber from the start of combustion until the end of ejection, while the heat transfer through the pre-chamber walls is estimated with Angelberger's model [5], by integrating the pre-chamber boundary heat profile between the start of combustion and the end of ejection. Then, the following parameters are associated with the unburned mixture. On one hand, the fuel mass remaining in the pre-chamber at the end of ejection was multiplied by the Lower Heating Value (LHV) in order to compute the energy that remains unused in this region (Unburnt), whereas the fuel lost due to non-reacting ejection (Inert) was computed by a surface integral at the exit of each hole, accumulating the escaped fuel mass from the beginning until the end of the ejection process.

Several interesting conclusions can be drawn from this figure. Firstly, the unburned mixture remaining in the pre-chamber in this particular operating point is negligible (less than 1% of the total energy), given that the flame is able to sweep the whole pre-chamber volume due to the high levels of turbulence in this region. Secondly, the share of heat transfer through the walls of the pre-chamber during this period is very low as well (roughly 8%), since the combustion happens so fast that there is hardly any time available. This implies that there is some flexibility to design the thermal management system of the pre-chamber in terms of energy losses, as long as the combustion process in this region is not significantly deteriorated. Moreover, there is a relevant energy loss associated with the mass of mixture that is ejected under inert conditions (around 20% in this case), which basically depends on the time it takes for the flame front to reach the bottom of the pre-chamber, where the holes are located.

Thus, an important aspect that derives from this study is the need for the flame to quickly reach the holes and avoid ejecting non-reacting mass, since this fuel initially does not help to ignite the main chamber. Furthermore, this can be achieved by either promoting an accelerated combustion process in the pre-chamber (enhancing the turbulence or thermochemical properties in this region), or by keeping the location of the spark plug reasonably close to the holes, being especially relevant in the case of pre-chambers with long axial lengths (large volumes and limited internal diameters by the metric of the cylinder head housing).

4.2 Impact of the engine operating conditions

After establishing a baseline understanding of the pre-chamber fluid-dynamics, energy conversion and the combustion process at high load-speed conditions (OP1), expanding the research to other operating points is crucial in the path towards implementing this technology in passenger car engines. Therefore, this section compares the simulation results of the three running points described in Table 3.5, which are representative of real engine conditions. Afterwards, a dedicated spark timing sweep study at low load/speed conditions (OP3) will be presented, to assess the compatibility of the concept with catalyst warm-up.

4.2.1 Pre-chamber combustion features

The first part of the analysis is focused on the pre-chamber combustion features. Thus, Figure 4.11 presents the most relevant parameters of this process:

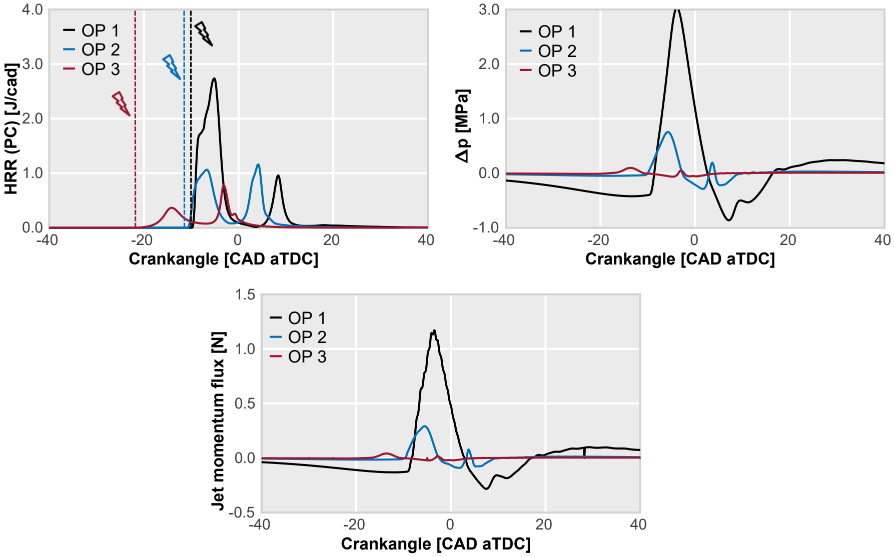

Figure 4.11: Pre-chamber combustion parameters. The temporal evolution of the HRR profile, Δp and jet momentum flux are shown for each operating point.

the pre-chamber HRR, the Δp and the jet momentum flux. Additionally, the HRR plot shows the spark timing of each case with a vertical line in the same color (black for OP1, blue for OP2 and red for OP3), which corresponds to the MBT spark timing in each running point.

The chemical HRR for each operating condition allows to identify important differences between them in terms of combustion onset, burning rates and duration. Aside from the evident contrast among the maximum HRR values for the three running points, the start of combustion relative to the spark timing also presents a higher lag as the engine load/speed decreases. These effects can be attributed to two main aspects: the local distribution of fluid-dynamic conditions (as will be seen in Figure 4.12), and the difference in fuel energy at the moment of ignition (as will be shown in Figure 4.13). The pre-chamber combustion process not only relies on the available energy, but also on the consumption rates of that energy. Therefore, the flow-field parameters like the residual gases or generation of turbulence will have a relevant impact over the burning rates.

An interesting trend is found by analyzing the HRR during the re-flux stage, caused by the main chamber back-pressure. From here, it is observed that as the engine load/speed decreases, the second HRR peak reaches higher values relative to the main HRR during the ejection. This secondary release of energy is mainly attributed to the mass injected back into the pre-chamber during the back-flow, and the unburned fuel that was left in this region after the ejection (as will be seen in Figure 4.13).

Moreover, the jet ejection parameters (Δp and momentum flux) show a similar pattern according to the HRR profiles. Thus, as can be expected, the slower burning rates at lower load/speed conditions compromise the pre-chamber pressurization and the ejection process. This can be appreciated in the jet momentum curves, where the peak value for OP1 is 4 and 10 times higher than the maximum momentum flux for OP2 and OP3 respectively. Another observable trend is the pressure losses during the pre-chamber filling, that increase for higher engine load/speeds, which is reasonable since the circulation of the gas through the pre-chamber holes is compromised. This occurs fundamentally due to the behavior of the holes that act as nozzles, blocking the flow in a given engine speed regime depending on the relationship between the total cross-sectional area of the holes and the pre-chamber volume (A/V ratio), as will be confirmed in Section 4.3 dedicated to the study of the pre-chamber geometry.

This initial study leads to the conclusion that as the jet features are significantly worsened at low load/speed conditions, the performance of the concept in this running point will be compromised.

Going further into the analysis, Figure 4.12 presents the temporal evolution of the relevant flow-variables (RGF and TKE) averaged in the pre-chamber region, along with snapshots of these variables showing their local distribution for each operating condition at -20 CAD. Both the instantaneous curves and the local visualizations highlight the deteriorated flow-field as the engine load/speed decreases. The percentage of residual gases at TDC increases from 9% in OP1 to 20% in OP3. On top of that, the concentration of these residuals in the spark plug gap at -20 CAD is close to 30% for OP3. This considerably compromises the laminar flame speeds and the combustion development in the pre-chamber region [6, 7], hindering the generation of high-quality jets.

Additionally, the pre-chamber TKE is a parameter that significantly enhances the flame propagation in this region. Thus, as the average TKE levels inside the pre-chamber are almost eight times lower in OP3 compared to OP1, the turbulent flame speeds in the former operating point will be considerably reduced. From the local snapshots included below the instantaneous TKE

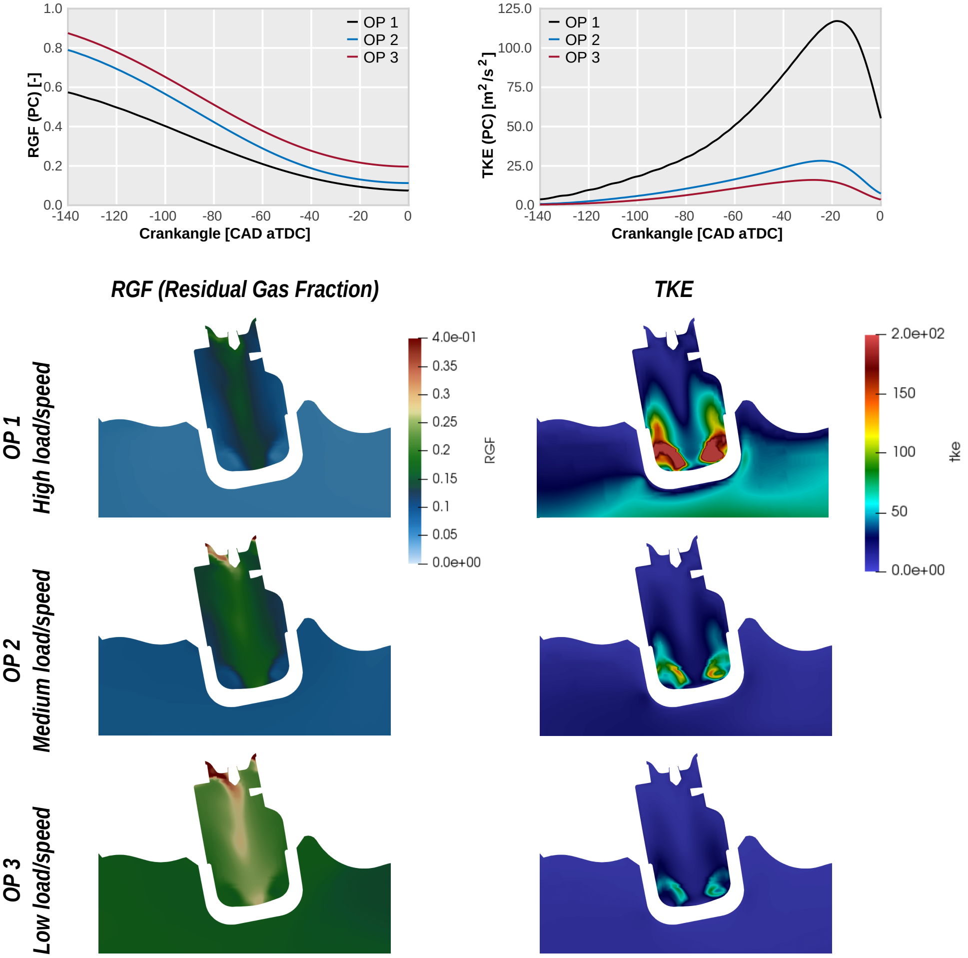

Figure 4.12: Distribution of the residual gas fraction and turbulent kinetic energy in the pre-chamber. The volume-averaged values are plotted at the top, while the local snapshots are shown at -20 CAD for each operating point.

curves, it can be seen that the turbulence flow pattern is maintained among the three cases, changing only in intensity. Furthermore, as the high TKE values generated at the bottom of the pre-chamber are quickly dissipated as the flow moves towards the electrodes, once the flame starts to progress at low engine load/speed conditions, it will encounter even lower levels of turbulence.

This inherent deterioration of the pre-chamber flow conditions when operating at low engine load/speeds is one of the reasons behind the slower

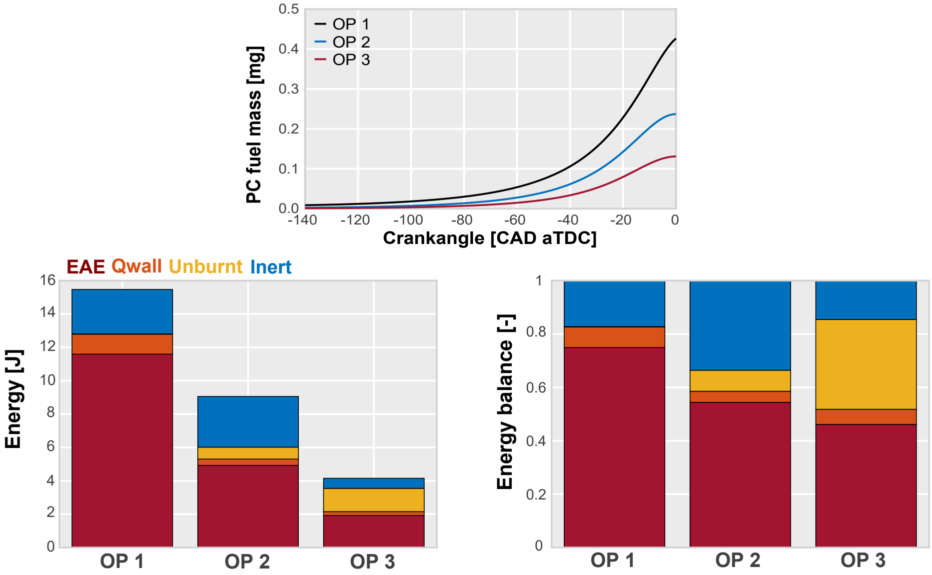

Figure 4.13: Pre-chamber energy balance during the ejection process. The energy conversion is shown for each operating condition, and the evolution of the pre-chamber fuel mass is plotted at the top.

burn rates observed in Figure 4.11. However, another important aspect is the energy available for ignition, as well as the management of that energy.

Therefore, Figure 4.13 shows the evolution of the fuel mass inside the pre-chamber during the compression stroke, along with the energy balance performed for each operating condition during the ejection process, keeping the same nomenclature that was described in Figure 4.10. Inspecting the top plot confirms how the amount of fuel inside the pre-chamber depends on the engine load. Since the injected fuel per cycle decreases for lower loads, the pre-chamber is also filled with less fuel mass in these conditions. Moreover, as OP3 triggers the spark at an earlier stage to achieve a suitable combustion phasing in the main chamber, the initial energy available in the pre-chamber for this operating point will be further reduced. This remark can be appreciated with the full length of the bar graphs in the bottom-left corner, where OP3 shows almost 4 times less energy than OP1 at the beginning of the pre-chamber combustion.

Decomposing the available energy into the 4 contributions explained in Figure 4.10, can help to understand how much of this energy is actually being used for the main chamber ignition in each operating condition. OP1 for example, is clearly the most efficient point in terms of both absolute energy and energy conversion. This is highlighted with the bottom-right corner bar graphs, where the relative share of each energy parameter with respect to the total energy is plotted. At high load/speed conditions, due to the higher turbulence levels and improved scavenge that allow the flame front to sweep the whole pre-chamber volume, over 70% of the available energy is used to ignite the main chamber. Also, despite having the highest heat losses due to the elevated pre-chamber temperatures reached during the combustion, the unburned fuel and the fuel lost in inert conditions account for less than 20% of the initial energy.

On the other hand, for OP2 (medium load/speed conditions) the effective energy used for ignition is reduced to 55%. What's more, the fuel mass lost during the non-reactive ejection increases to 33%. In this point, the pressure in the pre-chamber still builds up relatively fast, however, the worsened flow conditions compared to OP1 causes the flame front to progress more slowly towards the holes, which translates into a higher amount of mass being lost under inert conditions.

Finally, OP3 not only shows the lowest amount of energy but also the worst energy management. In this point, only 45% of the initial energy is used for main chamber ignition. Additionally, despite having the lowest share of energy lost in non-reacting conditions (due to the slow pre-chamber pressurization), the share of unburned fuel remaining at the end of ejection represents over 30% of the available energy. This is a consequence of the higher residuals and lower levels of turbulence, that causes a deterioration in the flame propagation process. The increase in unburned fuel at lower engine load/speeds also confirms the decrease in combustion rates shown in Figure 4.11.

4.2.2 Main chamber combustion features

Now, the effect of the previous trends over the performance of the jets and the combustion development in the main chamber will be analyzed. For this purpose, Figure 4.14 shows the same plots that were presented in Figure 4.8, in this case for each operating condition. The HRR profiles are shown at the top, divided into the contributions inside and outside of the jet boundaries, while the three rows of polar graphs correspond to each representation of the energy distribution in the main chamber that was discussed in Figure 4.8.

From the HRR traces, it can be seen that despite the pronounced differences in absolute values, the distribution between the energy released inside

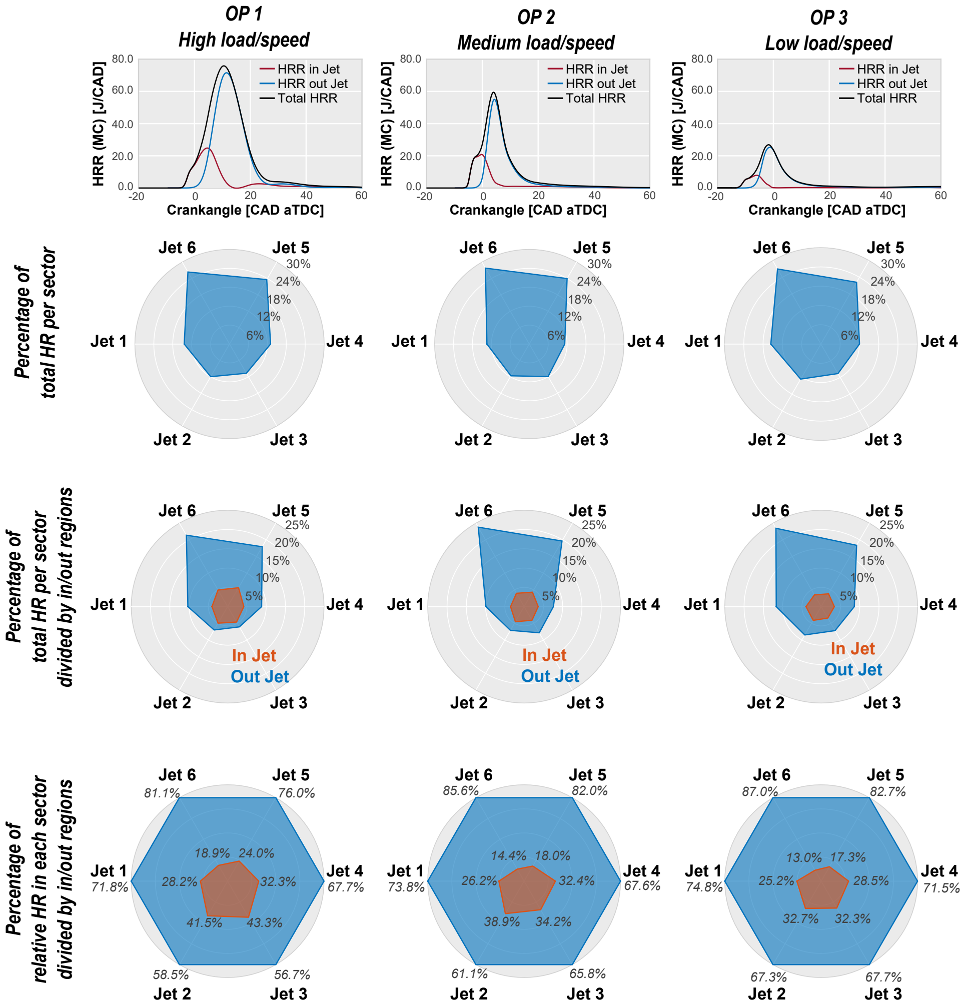

Figure 4.14: Analysis of the main chamber combustion. The HRR profiles are plotted at the top, divided into the contributions inside and outside of the jets. The amount of energy released by each jet is shown with the polar graphs below the HRR curves for each operating point.

and outside of the jets is similar for the three operating conditions, burning less than 30% of the fuel within the jet limits. This allows to confirm that the impact of the jets is less relevant when operating in un-diluted stoichiometric conditions, given that the main chamber fluid-dynamics and thermochemical properties allow the flame to consume the whole charge without any major problem and in a relatively short time-frame.

Nevertheless, this does not mean that the jets are inconsequential for the combustion process. In order to illustrate this remark, the polar graphs will be analyzed. The main chamber is discretized into six angular sectors corresponding to each jet, and as can be seen, sectors 5 and 6 is where the major part of the main chamber charge is consumed (around 50%). The first row of polar graphs reveals that the general energy distribution does not undergo significant changes when switching operating points. However, the middle and bottom rows show that as the engine load/speed decreases, the energy released by the jets becomes smaller. This can be attributed to the worsened ejection features coming from the pre-chamber combustion. In the case of OP3, jets 5 and 6 only consume 13% and 18% of the energy in their respective regions, leaving a large percentage of the main chamber volume un-swept.

Thus, having stronger jets is very helpful to drive the flame propagation along a higher portion of the main chamber volume, allowing the combustion to progress more quickly. This is particularly important for conditions where the turbulence and thermodynamic properties of the mixture downstream of the jets are compromised, as is the case when operating at low engine load/speeds or diluted conditions.

In order to obtain more information about the combustion evolution in the main chamber, Figure 4.15 shows a vertical visualization sequence of this process for each operating point. An axial cut-plane of Jet 6 was considered for this figure, in order to show the longest jet/flame path in the combustion chamber. The images are taken for three time-frames relative to the spark timing of each operating condition. As explained in Figure 4.6, the flame front is tracked with the source term of the energy equation, while the jet limits are highlighted in green with the user-defined dynamic tracer introduced in Section 3.3.4. Moreover, the temporal evolution of both the jet and the flame front in the main chamber are plotted at the bottom, relative to the wall distance. The crankangles of each snapshot are featured with vertical lines.

The penetration curves show that OP1 has the highest penetration rates, where at 10 CAD after triggering the spark both the jet and the flame have reached almost 70% of the wall distance, and 13 CAD after the spark timing the flame is able to progress outside of the jet boundaries at a high speed. In this case, by 20 CAD the flame has almost reached the chamber walls. Another interesting trend is the delay between the two curves (inert vs. reactive ejection), which is very short for OP1.

On the other hand, OP2 has a longer delay between the beginning of non-reacting flow (jet) and the start of reactive flow (flame). However, once the

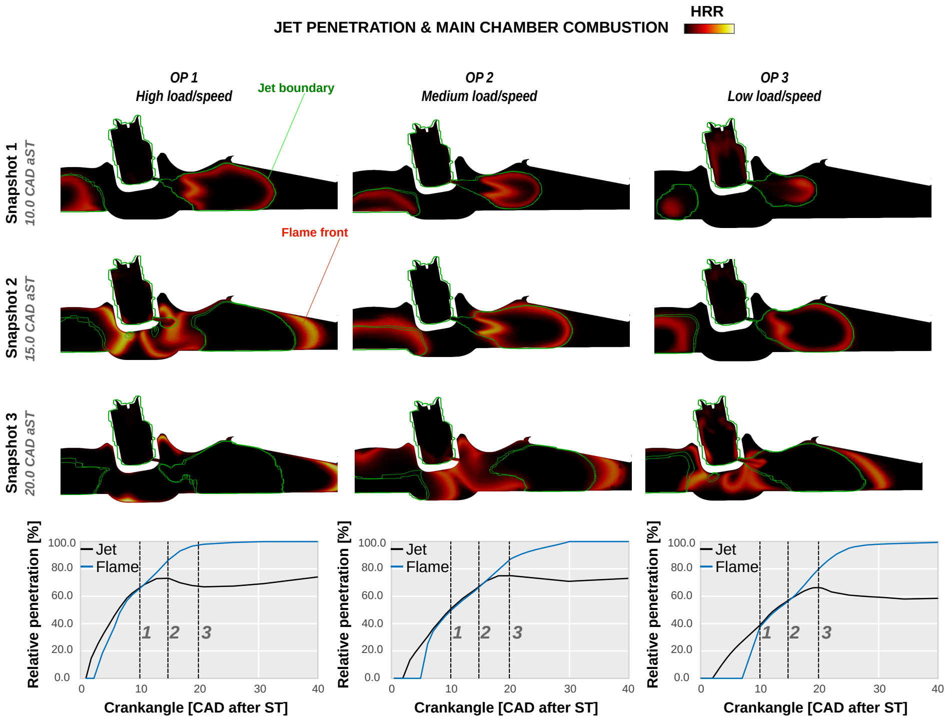

Figure 4.15: Evolution of the longest jet/flame (Jet 6) in the main chamber. The source term of the energy equation is colored to locate the flame, while the jet boundaries are highlighted in green by a dynamic tracer.

flame starts to penetrate into the chamber, it reaches the jet even sooner than OP1. Thereafter, the jet drives the flame for a longer period of time, and it is not able to surpass the jet limits until 18 CAD after the pre-chamber ignition time. Nevertheless, the relative penetration achieved by the jet in this point is very similar to OP1 (between 70%-80%).

Finally, OP3 shows the lowest penetration rates, particularly for the jet. although the flame is able to progress by itself before 20 CAD, the jet is barely able to surpass 60% of the wall distance. This confirms the aforementioned statement that the flame has to sweep a large section of the main chamber without the support of the turbulence generated by the jets. Additionally, this point also presents the longest lag between the start of the jet ejection and the beginning of the flame penetration, which has several negative implications for the concept's performance. One of these implications is that during this time, the flow-field in the main chamber can present higher variations at the beginning of combustion between consecutive cycles, which increases the possibility of having high cycle-to-cycle combustion variability (CCV).

The fundamental idea that is extracted from this section is the negative impact of reducing the engine load/speed on the characteristics of the ejected jets, and the subsequent combustion process in the main chamber. This aspect is critical since, at low loads, the inherent deterioration of the thermochemical and fluid-dynamic conditions in both chambers make it difficult to exploit the full potential of the passive pre-chamber concept. This is a major hurdle for the implementation of this ignition technology into passenger car engines, due to the loss of flexibility in this particular running point.

4.2.3 Detailed study at low engine load/speed conditions: compatibility with catalyst warm-up

Following the previous conclusion, a broader exploration of the low load/speed operating point is proposed. Particularly, a relevant issue found in the current literature [8] is the difficulty to stabilize the combustion process when delaying the spark timing in these conditions. Achieving a late combustion phasing is necessary to warm-up the three-way catalyst during cold-start operation.

This issue was encountered during the experimental campaigns performed for this research work. Figure 4.16 shows the spark timing sweep carried out in OP3, for the conventional SI concept and the passive pre-chamber concept. In this figure, the variability of the IMEP (σIMEP) is kept at low levels when operating with the pre-chamber, indicating a good combustion stability in a wide range of spark timings. However, the stability threshold is suddenly reached after -10 CAD, and, with a difference of only 2 CAD, the σIMEP levels become inadmissible, highlighting the concept's sensitivity to the ignition time.

Moreover, as the pre-chamber achieves faster combustion rates, the exhaust temperatures are also decreased compared to the SI system. Therefore, in order to obtain high enough temperatures to activate the three-way catalyst, the spark should be triggered very close to TDC, or even in the expansion stroke (at least for un-diluted stoichiometric conditions).

In order to understand the behavior of the concept as the ignition is delayed, additional simulations were prepared with the CFD model. Starting from the baseline MBT simulation for OP3, with the spark triggered at -22 CAD, and keeping the same configuration (boundary conditions and injected fuel mass), three retarded spark timings were simulated at -16, -8 and 0 CAD

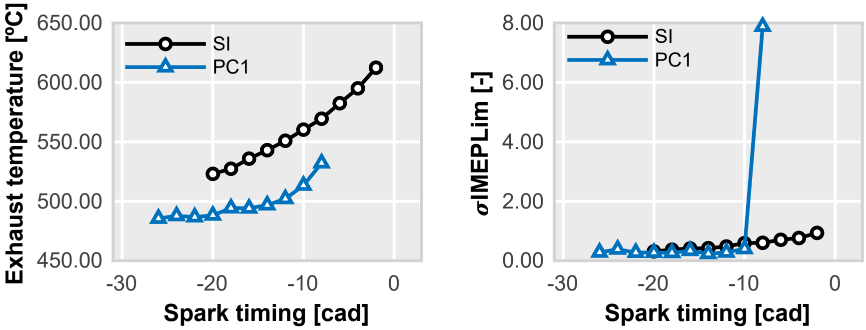

Figure 4.16: Spark timing sweep performed in the real engine at low load/speed conditions. The conventional SI and pre-chamber concepts are compared in terms of σIMEP and exhaust temperature.

respectively. The conditions of the last case, with the spark triggered at TDC, could not be implemented during the experimental campaign due to the extreme cyclic variability, however, this simulation provides additional information of great interest on the performance of the concept.

The accuracy of the numerical model is shown in Figure 4.17, where the main chamber pressure profiles are plotted. The general behavior of the combustion process as the spark is pushed towards TDC is well captured by the model, giving a good foundation for performing the analysis.

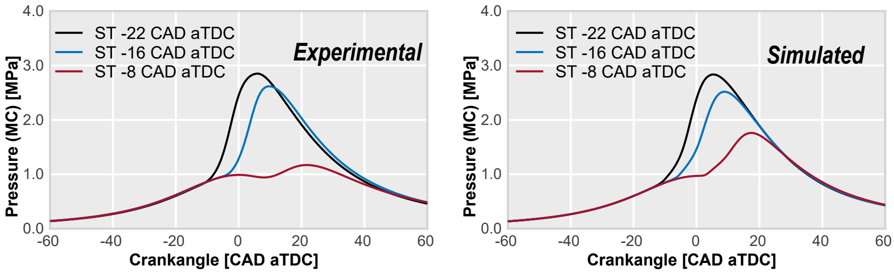

Figure 4.17: Comparison of the experimental and simulated pressure profiles for the spark timing sweep in OP3.

Figure 4.18 presents the pre-chamber HRR for each simulated spark timing, along with the ejection parameters (Δp and momentum flux). It is interesting that although the primary HRR during the ejection shows a similar behavior in terms of maximum burn rate and duration for the first three cases,

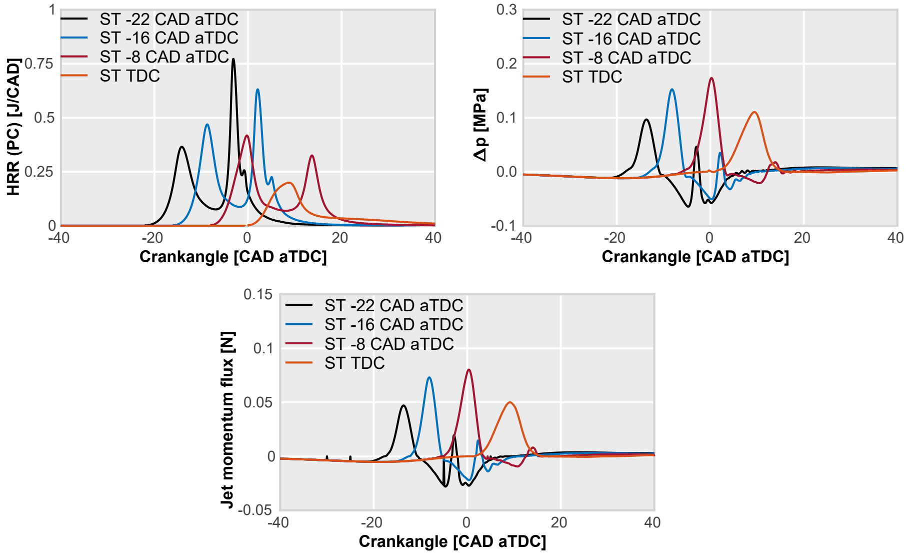

Figure 4.18: Pre-chamber HRR and ejection features for the spark timing sweep.

both the Δp and momentum profiles exhibit an increasing trend when delaying the spark timing. The maximum momentum flux achieved by triggering the spark at the stability threshold (-8 CAD), is 50% higher than the reference simulation (spark at -22 CAD). This can be explained by the higher fuel mass that fills the pre-chamber as the spark is pushed towards TDC. Moreover, by triggering the spark at TDC the HRR is considerably deteriorated, showing a longer combustion duration and almost half of the peak burn rates compared to the reference case. However, the peak momentum flux for the TDC case is at the same level as the baseline simulation.

This rising trend in the ejection parameters can be further analyzed by performing the pre-chamber energy balance. Thus, Figure 4.19 presents the absolute energy values at the beginning of the combustion process in the pre-chamber for each spark timing, as well as the relative share of each energy parameter that was described in Figure 4.10. From the left plot it is observed that the initial energy increases when delaying the spark. However, the actual energy that is used for main chamber ignition (EAE) barely changes among the 4 cases, being somewhat smaller for the TDC spark timing. Furthermore, the relative share of EAE decreases when pushing the spark towards TDC.

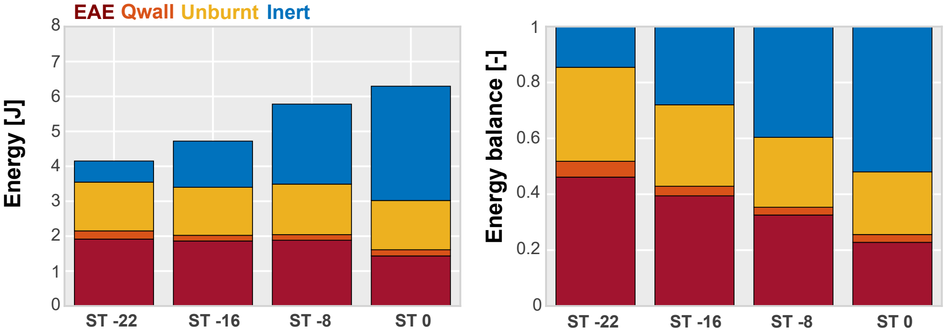

Figure 4.19: Pre-chamber energy balance for each simulated spark timing.

This means that all the extra energy that is available in the pre-chamber as the spark is delayed, is lost as cold/non-reactive flow.

Particularly, for the TDC case, over 70% of the energy is either lost during inert ejection or remains unburned inside the pre-chamber. These trends can be attributed to two main aspects. On one side, as part of the combustion process starts to take place during the expansion stroke, the fresh air-fuel mixture begins to prematurely leak from the pre-chamber, as a consequence of the downward piston motion. On the other hand, the levels of TKE inside the pre-chamber, which can be appreciated in Figure 4.20, sharply decrease when approaching TDC, and afterwards remain at very low values. These reduced levels of turbulence slow down the pre-chamber combustion process for very delayed spark timings, and the flame front takes more time to reach the bottom of the pre-chamber, which explains why so much mass is ejected under inert conditions.

It is interesting how the downward slope of the TKE curve in Figure 4.20 somehow matches the abrupt increase in the cycle-to-cycle variations observed during the experimental campaign (Figure 4.16). This leads to the idea that increasing the intensity of the turbulence field may help to improve the pre-chamber combustion stability when delaying the spark timing, by achieving faster burning rates in this region. A modification of the pre-chamber geometry can help to achieve this, therefore, this idea will be explored in Section 4.3.

The left-side plot of Figure 4.21 presents a comparison between the control spark timing (*setting ST*), defined as the moment when the control signal is activated in the ignition system, and the real ignition time (*effective ST*), defined as the moment when the ignition of the main chamber actually happens.

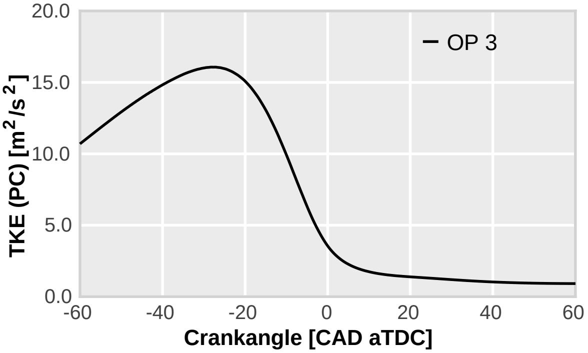

Figure 4.20: Pre-chamber average TKE at low load/speed conditions. The values are taken from the non-reactive simulation of OP3

This graph shows a diagonal line that represents an ideal scenario, where combustion in the main chamber starts at the exact moment the control signal is activated. However, there is always a lag between the control spark timing and the onset of combustion. Particularly, for the passive pre-chamber concept, three stages can be defined to describe and characterize the ignition sequence: (I) the start of combustion in the pre-chamber, (II) the onset of reactive ejection (when combustion products begin to penetrate into the main chamber) and (III) the start of combustion in the main chamber. These stages are represented by asterisks in Figure 4.21 for the spark timing sweep, and it can be seen how the time lag between them starts to widen as the control spark timing is moved towards TDC.

In the reference case (spark at -22 CAD), there is an interval of 9 CAD from the onset of combustion in the pre-chamber and the main chamber ignition, but, for the TDC spark timing, this interval is greater than 15 CAD. Thus, since there is a greater time interval between the *setting* ST and the *effective* ST, the local thermochemical and fluid-dynamic characteristics in both chambers may present greater variations between consecutive cycles. Consequently, both the ejection and combustion process in the main chamber can take place with very different flow conditions in each cycle, which can lead to higher cyclic dispersion.

As the right-side plot of Figure 4.21 shows, although the morphology of the momentum flux profiles is very similar for the reference simulation and the simulation with the spark at TDC (as was explained in Figure 4.18), the dashed lines drawn over each curve reveal an interesting difference between

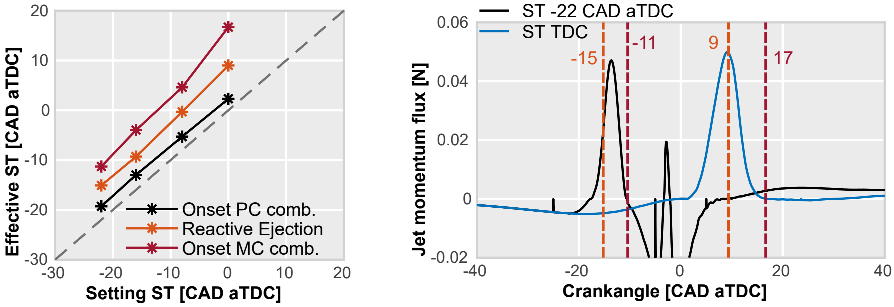

Figure 4.21: Analysis of the control spark timing and the main chamber ignition onset. The right plot shows the jet momentum flux for the reference spark timing (-22 CAD) and the most delayed spark timing (TDC)

these two cases. In accordance to the colors used to represent the three ignition stages of the concept, the dashed lines show the beginning of reactive ejection (orange) and the onset of combustion in the main chamber (red) for each case. From here, it can be seen that the reference simulation not only presents a shorter time difference between these two events (4 CAD), but also the momentum is still increasing at the beginning of reactive ejection. Furthermore, the concept is able to take advantage of stronger jets to produce the main chamber ignition, while sustaining the flame as it starts to develop in this region. On the other hand, the case with the spark triggered at TDC does not begin to eject hot products until reaching the maximum moment flux value. Therefore, the initial stages of the main chamber combustion are sustained by a lower jet momentum, and subsequently, by less turbulence. Moreover, the time gap between the onset of reactive ejection and the main chamber ignition increases from 4 CAD to 8 CAD in this case.

In order to better understand this last remark, Figure 4.22 shows the temporal and spatial evolution of the combustion process in the main chamber comparing the aforementioned cases (spark triggered at -22 CAD and at TDC). From the first and second snapshots, it can be seen that the jets are evolving in a similar way, but the reactive flow ejection is delayed for the TDC case. In addition, for the reference simulation, the third and fourth snapshots reveal the transition of the flame from inside to outside of the jet limits. After reaching these boundaries, the flame front again evolves through a conventional flame propagation process. On the other hand, the pattern for the delayed spark timing is quite different, given that the flame is not able

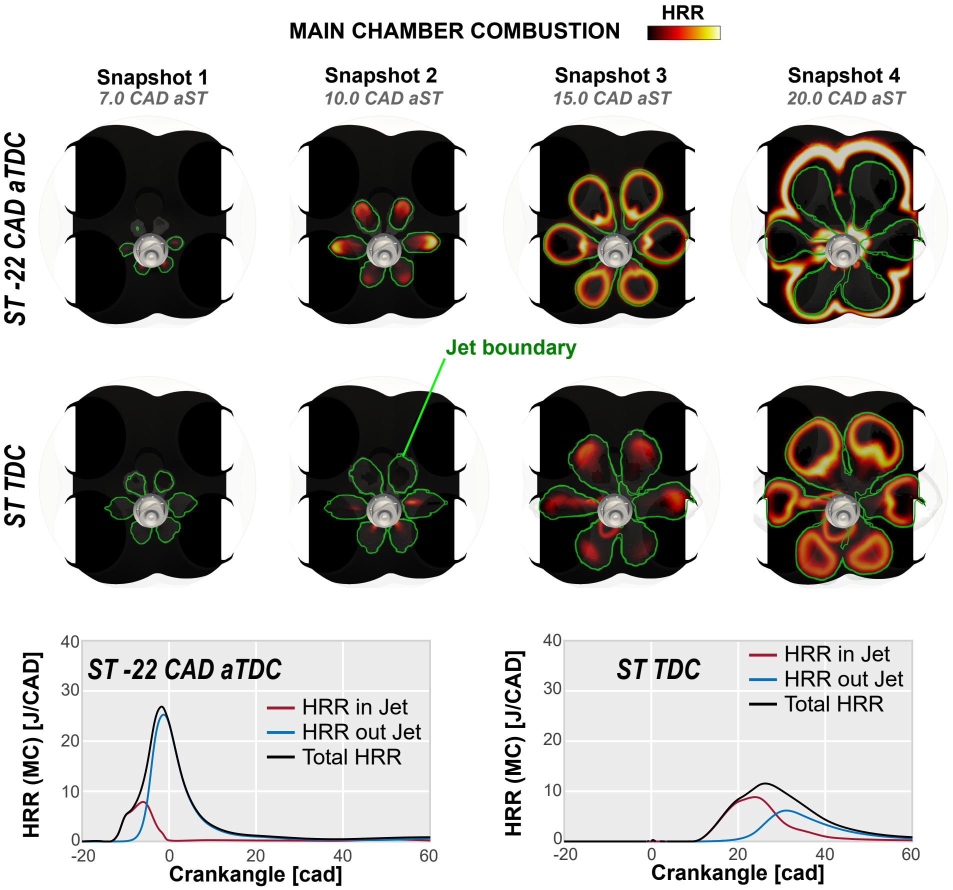

Figure 4.22: Evolution of the main chamber combustion for the reference spark timing (-22 CAD) and the most delayed spark timing (TDC). The HRR scale is the same for both snapshot sequences. The instantaneous evolution of the HRR profiles inside/outside of the jets are also included for both cases.

leave the limits of the jets in the considered time frame, and also the flame is noticeably less active.

This trend can be clearly observed in the evolution of the HRR in the main chamber, plotted at the bottom. The distribution of the energy released inside and outside of the jets changes significantly between the two considered cases. In the reference simulation, less than 20% of the main chamber charge is consumed within the jets, whereas for the TDC case this value rises above 50%. Therefore, the relevance of the jets in the combustion process of the main chamber, not only for ignition, is increased when the spark timing is delayed. However, precisely by delaying the spark, the start of reactive flow is also retarded, compromising the development and stability of the main chamber combustion process. In addition, once hot products are ejected during the expansion stroke, they will encounter less favorable thermodynamic and flow conditions downstream of the jets, which further compromises the ignition.

This study has shown that increasing the momentum flux of the jets does not guarantee an improvement in the combustion process of the main chamber if the majority of the jet is ejected in non-reactive conditions, without the ability to promote ignition. Therefore, increasing the combustion rates within the pre-chamber, to achieve an early ejection of reactive flow that is able to advance the moment of ignition in the main chamber, becomes critical. However, given the inherent decrease of turbulence levels and the loss of fuel due to the suction of the piston, achieving a fast pre-chamber combustion when retarding the spark timing at low load/speed conditions becomes very challenging, which compromises the compatibility of the concept with this catalyst activation strategy. Nevertheless, potential solutions for this problem include either an optimization of the ignition source inside the pre-chamber (using a higher energy igniter or optimizing the position of the spark plug), or an optimization of the pre-chamber geometry (internal design, volume, hole diameter, hole layout).

4.3 Impact of the pre-chamber geometry

The final section of this chapter will present a study of several geometric parameters of the pre-chamber, in order to understand their impact over the physical and thermochemical processes analyzed so far (scavenge and turbulence generation in the pre-chamber, combustion process in the pre-chamber and features of the ejected jets). Given that there were several designs available for performing the experimental campaign (as shown in Table 3.4), the first part of the analysis will make use of these test results to get an initial assessment of the general behavior of the different pre-chamber geometries, and then make use of the CFD model to better understand the experimental trends and draw conclusions.

4.3.1 Analysis of the pre-chamber A/V ratio

Figure 4.23 shows a 3D sketch of the pre-chamber geometries that were presented in Table 3.4. As it can be appreciated, the internal design was maintained among the four pre-chambers, changing only the basic geometric parameters: volume, number of holes and hole diameter. In addition, the tangential angle of the pre-chamber holes was also kept constant at 12.5°. The reference design that was used to perform the CFD model validation (PC1) has 6 holes of 0.7 mm and a volume of 600 mm^3. PC2 and PC3 have smaller volumes, both with 4 holes of 0.7 mm and 0.5 mm respectively, while PC4 has a larger volume with 6 holes of 0.5 mm. Therefore, a unique parameter to characterize and compare these four pre-chambers in terms of their performance is the relationship between the total cross-sectional area of the holes and the pre-chamber volume (the A/V ratio parameter also shown in Table 3.4).

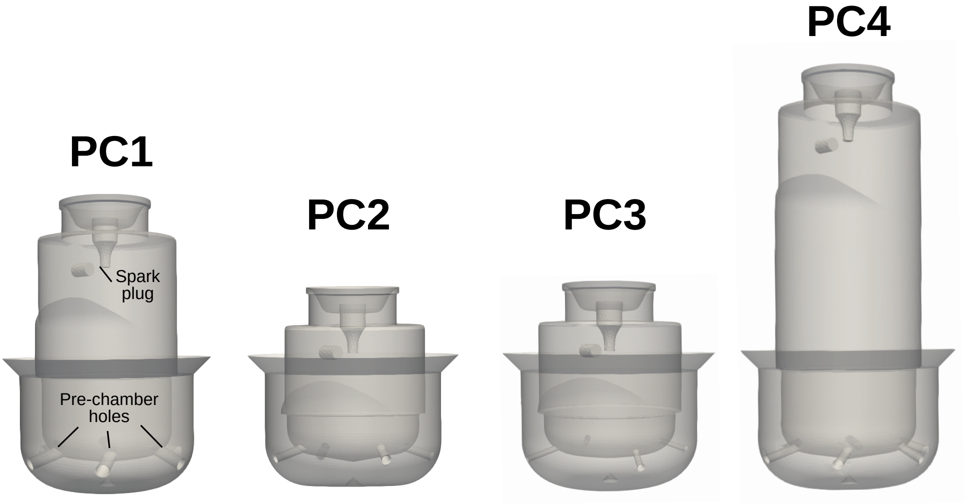

Figure 4.23: Pre-chamber designs that were used in the initial test campaign.

In order to begin the discussion, Figure 4.24 shows the experimental results for the different pre-chambers, contrasted with the results using the conventional spark plug. The temporal evolution of the in-cylinder pressure and the main chamber HRR are plotted at the top, for the tests performed at undiluted stoichiometric conditions. From here, the benefits of the pre-chamber concept are clearly observed, given that the four designs are able to achieve a better combustion phasing than the SI system, which leads to higher pressure profiles and an improved performance. This is highlighted in the bottom graphs, where the indicated efficiency and σIMEP values are plotted for the air and EGR dilution sweeps carried out during the test campaign. In un-diluted

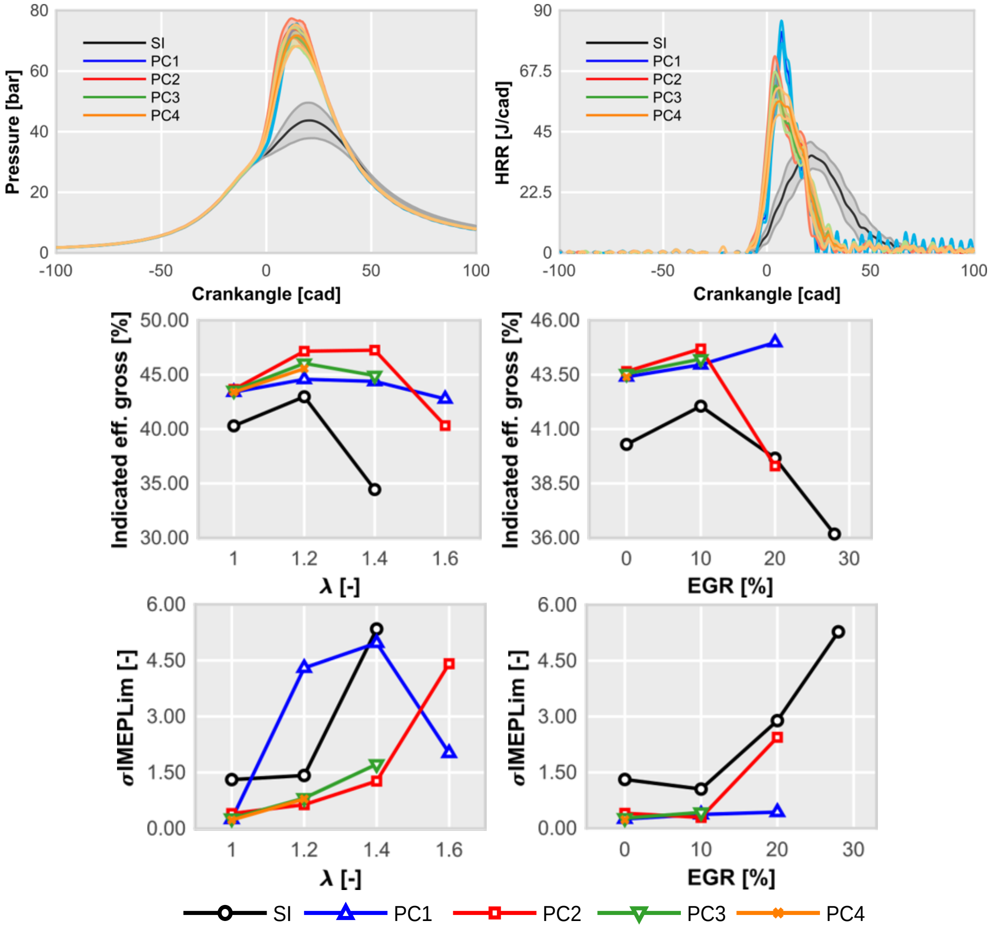

Figure 4.24: Experimental results for the different pre-chambers. The air dilution and EGR dilution sweeps are presented below the instantaneous curves for un-diluted stoichiometric conditions. The results with the conventional SI concept are also shown for reference.

conditions, all the pre-chambers manage to increase the levels of efficiency over 3% with respect to the SI concept, while also showing very low levels of σIMEP (good combustion stability). However, once the dilution rates start to increase, the differences among the four designs begin to emerge.

For the λ sweep it can be seen that PC1 and PC2 are able to extend the dilution limit of the conventional spark plug, keeping the levels of efficiency over 40% in the whole range. On the other hand, PC3 and PC4 are not able to extend this limit before reaching the combustion stability threshold. In particular, for PC4 only a λ of 1.2 is achieved before the σIMEP values become inadmissible. Thus, the pre-chambers exhibit a directly proportional trend between the A/V ratio and the dilution tolerance.

The EGR dilution sweep allows to further confirm this tendency. Here, not only is PC4 not able to reach even 10% of EGR dilution, but also PC1 and PC2 are no longer able to extend the dilution tolerance of the SI system. This leads to the thought that the issue could be both related to the A/V ratio and the amount of internal residuals that remain in each pre-chamber design. Therefore, in order to shed some light on this matter, non-reactive CFD simulations were prepared for the remaining 3 pre-chambers (PC2, PC3 and PC4).

The simulations were carried out in OP2, and the results of the pre-chamber scavenge are shown in Figure 4.25 for each design. The left-side plots of this figure show that PC1 and PC2, that have an A/V ratio of 3.9 m^{-1} and 4.4 m^{-1} respectively, present a very similar scavenge pattern with 12% of residuals left in the pre-chamber region at TDC. On the other hand, as the A/V ratio for PC3 and PC4 decreases (2.2 m^{-1} and 1.2 m^{-1} respectively) the residuals that remain in the pre-chamber start to increase. Moreover, while PC1 and PC2 are able to admit a short amount of fresh mixture during the intake stroke, the filling of PC3 and PC4 does not begin until the compression stroke (as shown by the right-side plots).

The A/V ratio is a parameter that allows to relate the amount of volume that needs to be filled by gases from the main chamber with the surface that is actually available for these gases to go through. Thus, as it becomes smaller, a larger portion of the pre-chamber region will remain un-scavenged. This matches the experimental results presented in Figure 4.24, since pre-chambers with low A/V ratios will inherently start the combustion process with a higher amount of residual gases, limiting the compatibility of the concept with EGR dilution. Nonetheless, after a given A/V ratio threshold, the average amount of residuals that remain in the pre-chamber no longer changes, as can be seen from the results of PC1 and PC2. At this point, the pre-chamber RGF is basically controlled by the engine operating conditions (load/speed).

In addition, another important aspect of reducing the A/V ratio is highlighted at the bottom of Figure 4.25, where the main chamber and pre-chamber pressure profiles are plotted for the non-reactive simulations of PC1 and PC4. Here, a relevant variation of the pressure difference between both chambers is observed. For PC1, this difference is barely noticeable, while for PC4 it considerably increases. Consequently, the combustion process in PC4 will have to

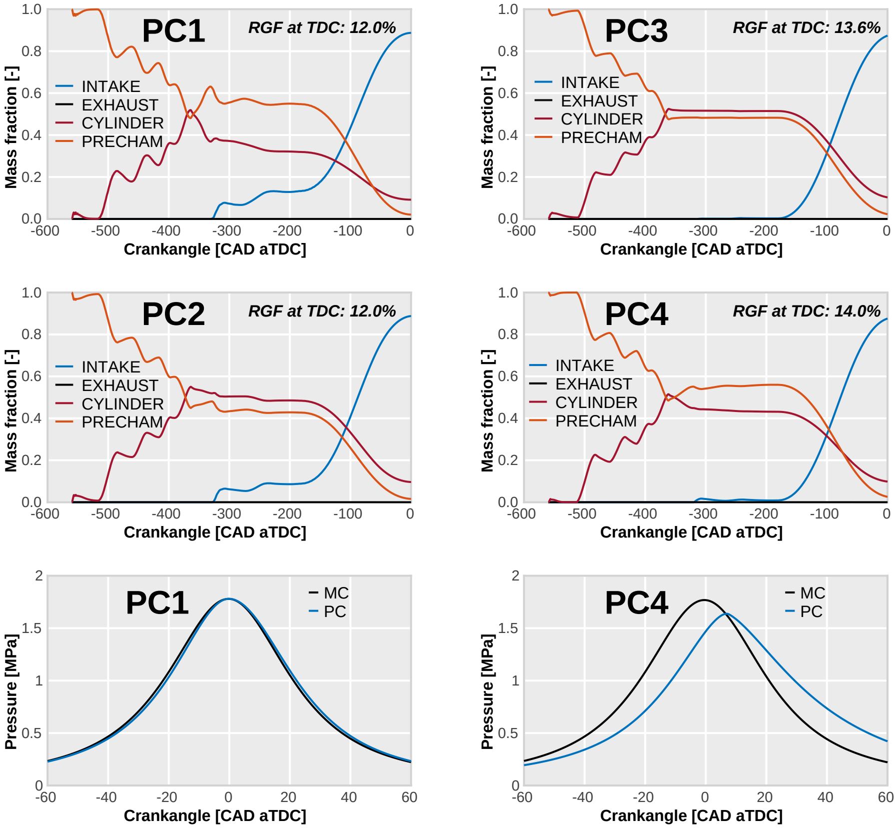

Figure 4.25: Scavenge of the different pre-chambers in OP2. The main chamber and pre-chamber pressures for PC1 and PC4 are shown at the bottom.

generate a higher Δp in order to invert the direction of the flow, which compromises the features of the ejected jets. This has significant implications for operating with higher levels of dilution, given that the thermodynamic conditions in the main chamber will already be compromised, and having weaker jets will not allow to achieve a suitable combustion process.

Going deeper into the analysis, Figure 4.26 shows the spatial distribution of residual gases in each pre-chamber. This figure reveals that the aforementioned scavenging issue of PC4 is even more critical in local terms. At -40 CAD, the central region of PC4 shows a concentration of residual gases over 30%, extending all the way towards the electrodes. Afterwards, as the piston approaches TDC, the local scavenging of PC1 and PC2 is notoriously improved

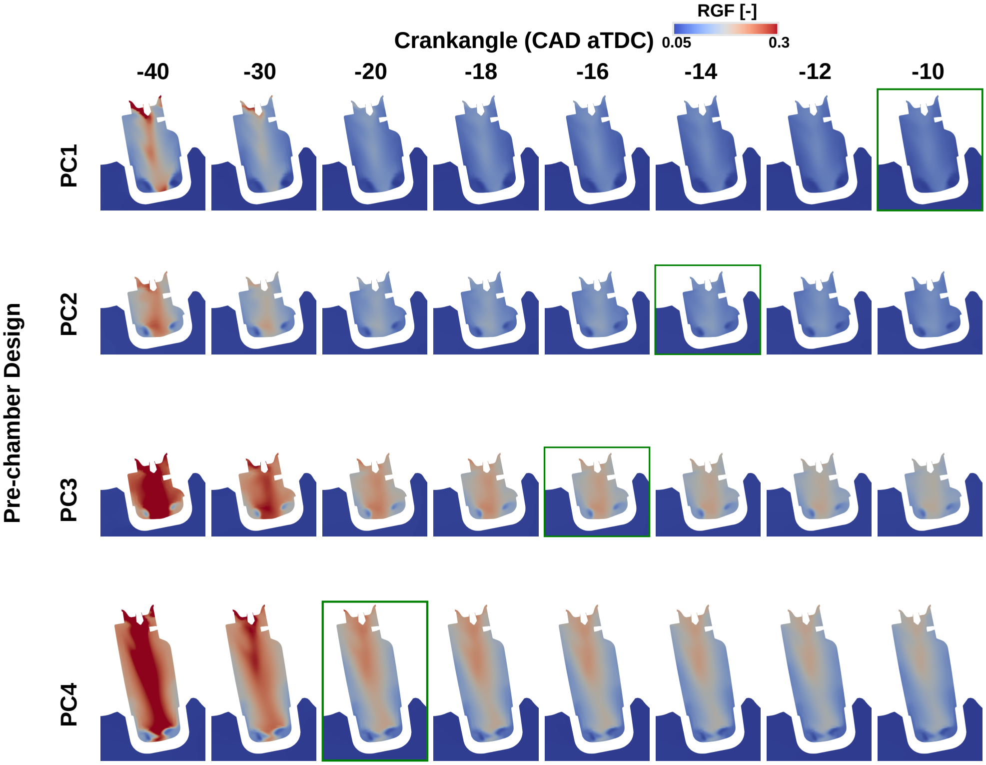

Figure 4.26: Local distribution of residual gases for each pre-chamber design from -40 CAD to -10 CAD.

with respect to PC3 and PC4. Additionally, the snapshots highlighted by a green square represent the spark timing that is required to reach MBT conditions with each pre-chamber design. It can be seen that as the pre-chamber A/V ratio decreases, an earlier spark advance is required to achieve an optimum combustion phasing, which makes sense as the combustion process will be slower for pre-chambers that present higher levels of RGF. Thus, as adding EGR will require triggering the spark at an earlier stage, the dilution limit will be reduced for pre-chambers that already have a very high concentration of internal residuals.

This study has demonstrated the importance of having a suitable pre-chamber A/V ratio to improve both the average and local scavenge of residual gases, in order to obtain the minimum RGF possible in this region at the beginning of the combustion process. Therefore, the following sections will present dedicated studies of different geometrical parameters by proposing pre-chamber designs that keep the same A/V ratio as PC1, in order to isolate the effects of each parameter. The proposed geometries are shown in Table 4.1, changing the pre-chamber volume, number of holes and the hole tangential angle, while keeping an A/V ratio of 3.9 m^{-1}. These simulations were carried out both in non-reacting and reacting conditions.

Table 4.1: Pre-chamber designs for the geometry study.

ID	Volume [mm^3]	Holes [-]	Diameter [mm]	Tangential angle [°]
PC1	**600**	**6**	**0.7**	**12.5**
PC1a	950	6	0.88	12.5
PC1b	950	10	0.7	12.5
PC1c	600	6	0.7	0

4.3.2 Impact of the pre-chamber volume

The first analyzed parameter is the pre-chamber volume, for which PC1 and PC1a are compared. Figure 4.27 shows the scavenging results of these two designs from the non-reacting CFD simulations. As was expected, the average amount of residual gases remaining at TDC barely changes between these pre-chambers, confirming that this value depends on the A/V ratio and the engine operating conditions. Moreover, the visualizations shown at the bottom correspond to the spatial distribution of residuals and the turbulent kinetic energy field at the spark timing. PC1a shows slightly higher levels of RGF in the spark plug region compared to PC1, however, contrasting these results with the ones observed for PC4 in Figure 4.26, a considerable improvement is achieved for this high volume pre-chamber. On the other hand, the TKE pattern is kept with respect to PC1, but, as PC1a has a longer axial length, the levels of turbulence in the upper part of the pre-chamber are significantly lower than the bottom region (higher TKE stratification).

Regarding the combustion process, Figure 4.28 shows the comparison of the reacting simulations for PC1 and PC1a in terms of HRR in both chambers (upper row), jet momentum and main chamber pressure (bottom row). It can be seen that the burning rates achieved with PC1a are twice as high as the ones for PC1. This is mainly due to the increased fuel mass available in the pre-chamber region due to the extra volume (higher amount of energy). However, an interesting result is that by triggering the spark at the same time, PC1a is able to keep the combustion phasing in the pre-chamber. This

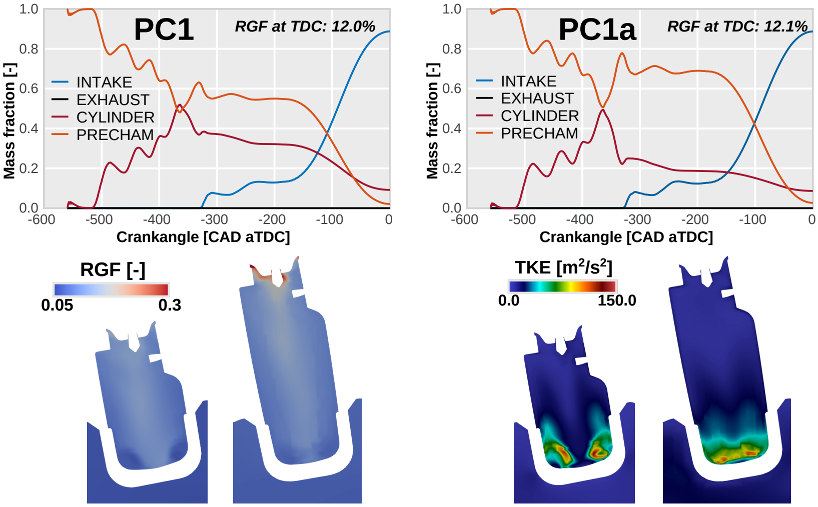

Figure 4.27: Analysis of the pre-chamber volume: RGF and TKE.

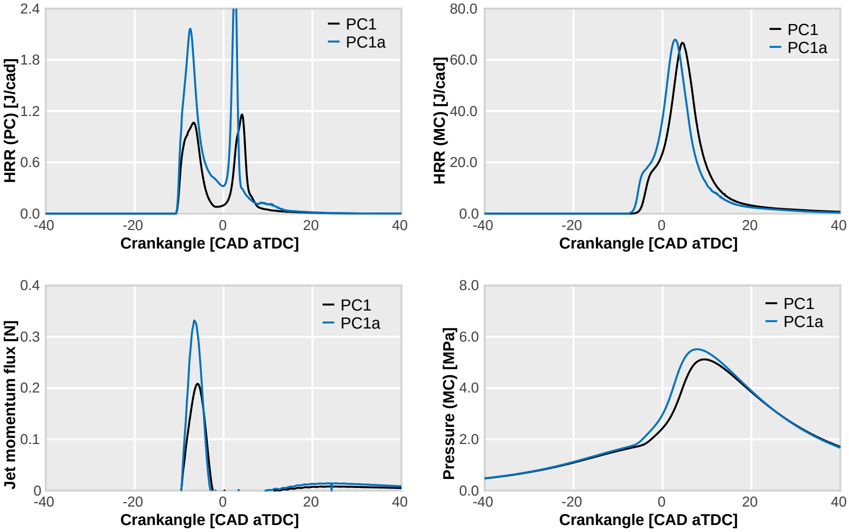

Figure 4.28: Analysis of the pre-chamber volume: combustion parameters.

implies that despite the longer axial length the flame is still able to sweep this volume quickly, which in term advances the onset of the main chamber combustion (as seen in the top-right plot) leading to an increased pressure profile. Additionally, the jet momentum achieved with PC1a is 50% higher than PC1 due to the faster burning rates, which also favors the combustion process in the main chamber.

Thus, having a higher pre-chamber volume allows to attain an increased engine performance, as long as a fast pre-chamber combustion is achieved. This is probably the most important challenge of the passive pre-chamber system, specially at low engine load/speeds where the burn rates are slower, and having a larger volume for the flame to sweep will further emphasize this problem. However, if the flame is able to consume the pre-chamber charge very quickly, then the high pre-chamber pressurization will lead to having strong jets and an early ejection of reactive products that are able to promote the ignition of the main chamber, overcoming the issues discussed so far and approximating its performance to the active pre-chamber system.

4.3.3 Impact of the number of holes

Moving on, the impact of the number of holes was evaluated by comparing PC1a and PC1b (both high volume pre-chambers). The same procedure that was followed in the previous section was used for this analysis.

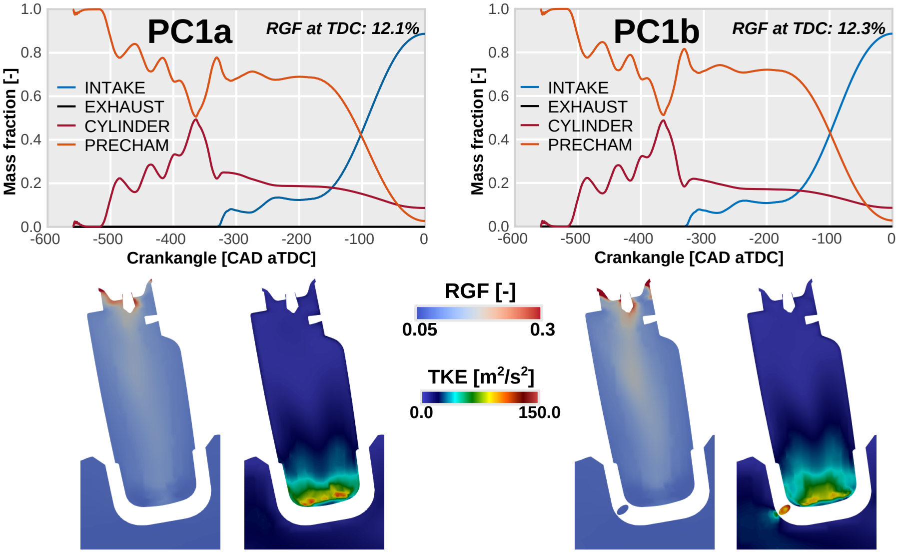

Figure 4.29: Analysis of the number of holes: RGF and TKE.

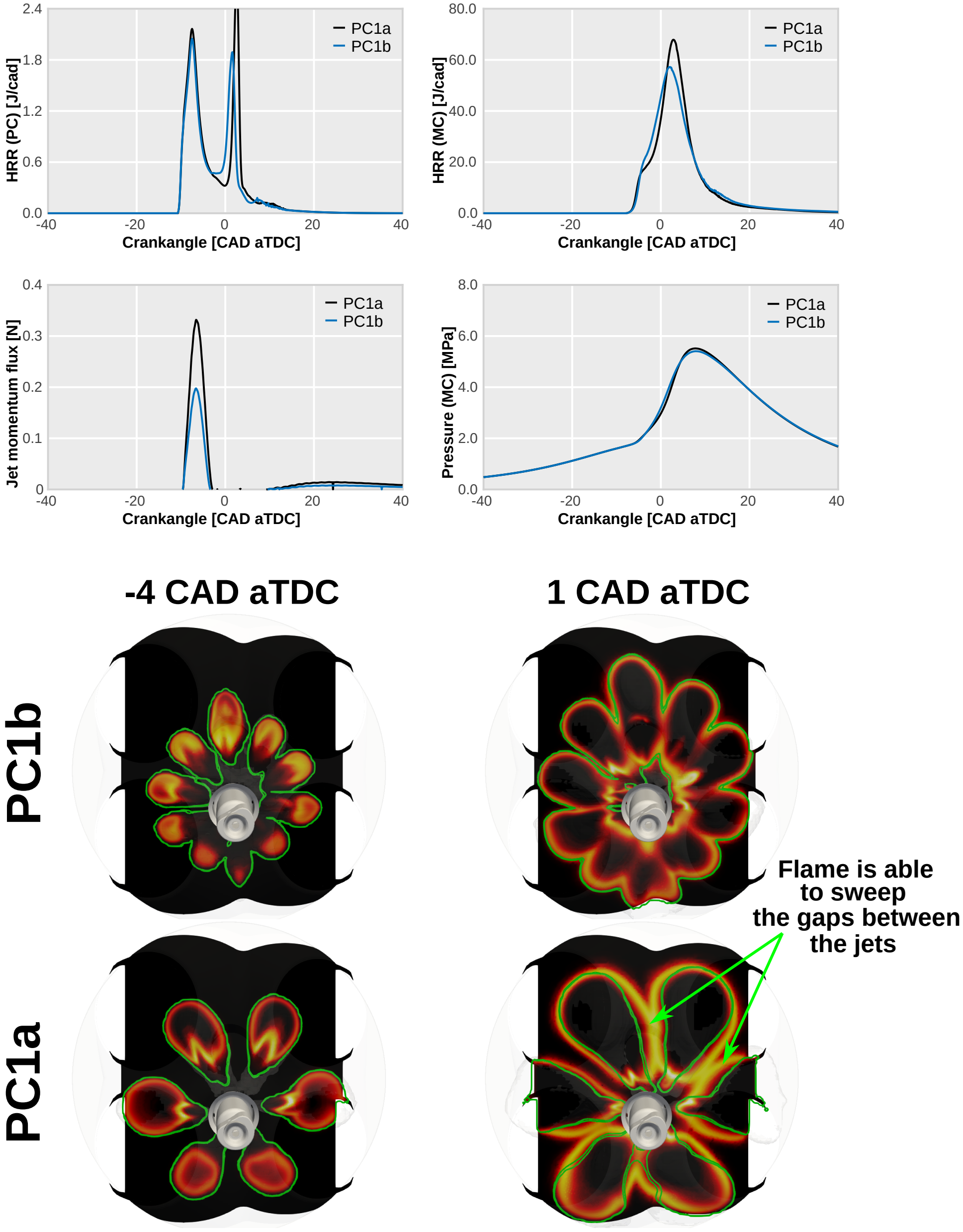

Figure 4.30: Analysis of the number of holes: combustion parameters.

Figure 4.29 shows the flow-field characteristics of these two pre-chambers (scavenge and turbulence generation). The left column of the figure corresponds to PC1a and the right column to PC1b. Little differences are perceived in the average amount of residual gases, however, the local stratification of the RGF presents more notable changes between the two designs. For PC1b, it appears that the residuals are more concentrated in the central part of the pre-chamber while the walls remain clean. This leads to having a slightly higher amount of RGF in the spark plug gap. Regarding the TKE, the same pattern is observed for both pre-chambers.

Nevertheless, analyzing the combustion process allows to distinguish more differences in the flame evolution. The upper part of Figure 4.30 shows the same distribution of plots that were presented in Figure 4.28. From here, although both designs have very similar pre-chamber combustion profiles, PC1b shows a considerably lower momentum peak than PC1a, given that the ejected mass is distributed in more holes. This in term leads to lower penetration values for the jets obtained with PC1b.

Moreover, despite not having a significant impact on the cylinder pressure profile, given that the main chamber combustion phasing is kept for both cases, an interesting distinction is observed in the flame propagation process. The bottom snapshots show the position of the flame front in two time frames for each pre-chamber, -4 CAD and 1 CAD after the TDC. It can be seen how the jets from PC1a penetrate faster and further into the main chamber, but also, in the second visualization image, the transition of the flame to outside of the jet limits is observed, and the gap between adjacent jets is swept very quickly. These results suggest that having highly penetrating jets, that are able to reach the proximities of the chamber walls, allows to achieve higher burn rates than having jets that sweep a wider circumferential region of the main chamber, given that the charge between the jets is consumed more easily than the charge downstream of the jets.

4.3.4 Impact of the tangential angle of the pre-chamber holes

The final geometrical parameter that was studied was the tangential angle of the holes. Until now, the holes of all the considered pre-chamber geometries have had an offset with respect to the pre-chamber center, that induces a swirling motion inside this volume. A schematic of the hole layout is presented in Figure 4.31, where the displaced holes of PC1 create a tangential angle with respect to the radial direction, in this case of 12.5°. On the other hand, PC1c faces the holes directly towards each other, eliminating the tangential offset.

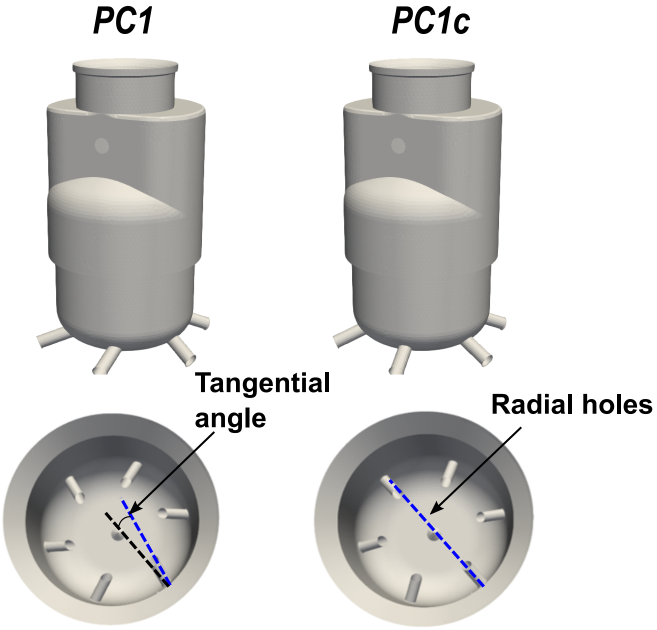

Figure 4.31: Schematic of the hole layout for PC1 and PC1c.

This is an interesting concept given that changing the hole orientation can result in very different fluid-dynamic conditions and flow patterns inside the pre-chamber.

Furthermore, Figure 4.32 shows the results of the non-reacting simulations for both designs. The similarities in the global scavenging process are again detected (average RGF at TDC remains constant). However, the pre-chamber visualizations at the spark timing reveal important differences between them. For the local scavenging of residuals, it is observed that the flow for PC1c now rises along the center of the pre-chamber, sweeping this region rather than the pre-chamber walls.

Additionally, the TKE levels of PC1c are notoriously higher in the whole volume. It can be seen that the radial hole layout creates a crashing flow in the bottom of the pre-chamber, which generates a highly turbulent flow in the central region that is even able to reach the pre-chamber top. These results match the findings of Bolla et al. [9], where a dedicated study of the turbulence field in a small pre-chamber with radial holes was performed in both RANS and LES frameworks, for a Rapid Compression Expansion Machine (RCEM).

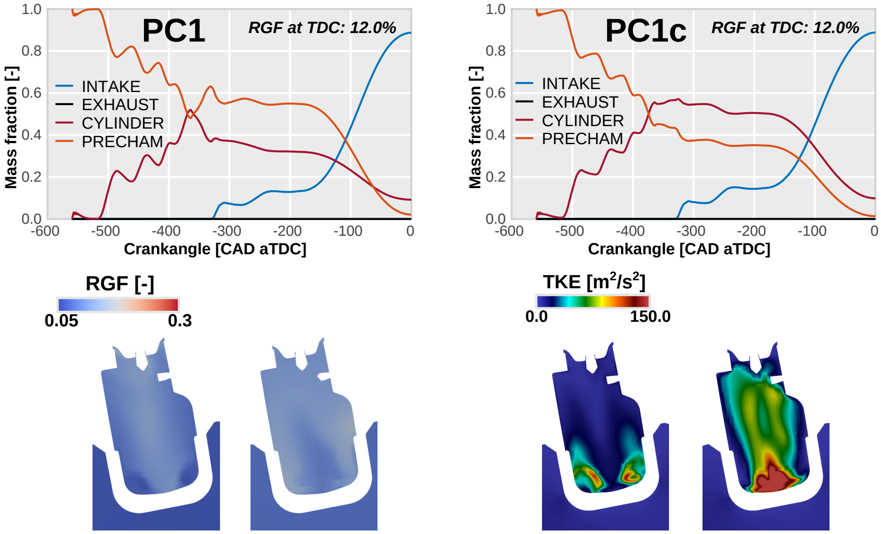

Figure 4.32: Analysis of the hole tangential angle: RGF and TKE.

The idea of increasing the levels of turbulence inside the pre-chamber for achieving faster burning rates was previously suggested in Section 4.2.3. Therefore, the impact of this particular internal flow-field over the combustion process was analyzed. Figure 4.33 shows the results for the reacting simulations, where a 50% increase in both the pre-chamber peak HRR and the maximum momentum flux is appreciated for PC1c. Thus, this new design has shown the potential to improve the engine performance by enhancing the pre-chamber combustion with higher TKE values. This is particularly interesting for low load/speed conditions, given that the flow properties in this running point are inherently worsened.

However, an important aspect to consider when significantly changing the flow field in ICE applications is the repercussions on multi-cycle combustion instabilities. Cycle-to-cycle variability is one of the major problems with SI engine technology, which has limited the use of these propulsive systems with strategies like EGR or air-dilution. Particularly, for the passive pre-chamber concept, CCV is also a relevant issue when delaying the spark timing at low engine load/speeds (as was explained in Section 4.2.3). Therefore, ensuring that the new pre-chamber flow-pattern is able to maintain a stable combustion process is mandatory to guarantee a good performance of the concept, and to extend the synergies with modern engine strategies.

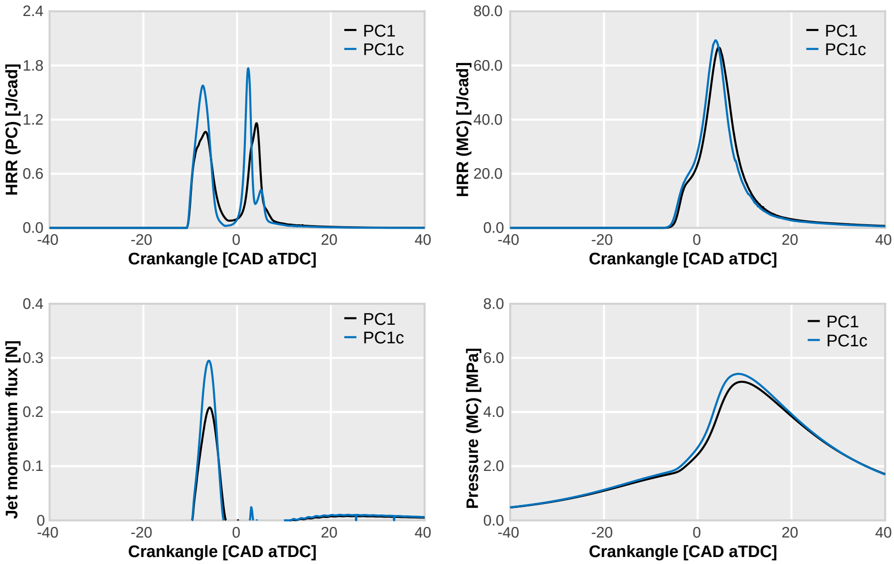

Figure 4.33: Analysis of the hole tangential angle: combustion parameters.

So far, the CFD simulations have been carried out in a RANS turbulence modelling framework (described in Section 3.3.2), since the turbulent scales estimated with this model are sufficient to ensure a reliable reproduction of the in-cylinder fluid-dynamics and the general behavior of the combustion process. Nevertheless, if more detailed phenomena such as cyclic dispersion are to be analyzed, the underlying hypothesis of the RANS model is not well suited to perform this task, as the flow-field variations in multiple engine cycles cannot be predicted. Hence, a LES turbulence model must be resorted to, given that it can resolve larger turbulent structures that condition the stability of the combustion process in all its phases.

Several researches have shown the potential of using a LES formulation in combination with the ECFM combustion model to predict the sources of CCV in SI engines, such as the work from Truffin et al. [10]. However, the main problem of doing simulations with LES models is the computational cost. These models require very fine meshes, which generate millions of cells in the computational domain, causing the associated computational time to increase significantly, even more so if there is an adaptive refinement applied to the mesh during the combustion process. For this reason, multi-cycle simulations using the complete engine geometry were unfortunately out of the reach with the available computational resources for this thesis.

Nevertheless, this study was still considered to be a necessary contribution for the research work, ergo, an innovative solution was formulated to carry it out. Given that the sources of cyclic variability phenomena can be traced back to the initial stages of the combustion process, the multi-cycle simulations can be performed by only considering the combustion in the pre-chamber region. This way, the computational domain is considerably reduced, and a small enough mesh can be used to solve a meaningful amount of the energy spectrum while maintaining reasonable computational times.

4.3.5 CCV analysis using multi-cycle LES simulations of the pre-chamber combustion

This section describes the methodology that was developed to perform the CCV studies of PC1 and PC1c, attributing the cyclic dispersion to changes in the pre-chamber flow conditions and combustion process. The simulations were carried out for both designs in OP3 (low load/speed conditions), since this is one of the most critical operating points related to the passive pre-chamber concept. The Dynamic Structure sub-grid model presented in Section 3.3.2 was considered for the LES framework.

Figure 4.34 shows the reduced computational domain, where the pre-chamber has been separated from the complete engine geometry and closed by inflow boundaries placed at the inlet of the holes. The base cell size in the pre-chamber region was set to 0.0625 mm. The calculations were again divided into non-reacting and reacting cases that will be described below.

The non-reacting case consisted in a single continuous simulation, initialized at the IVC with the same mixture stratification and thermodynamic conditions coming from the open-cycle RANS simulation of OP3. The main chamber pressure and temperature profiles of the RANS case were also imposed as inflow boundary conditions, to artificially replicate the piston motion for the pre-chamber filling/emptying. These profiles are shown at the right-side of Figure 4.34, perpetually reproduced for each cycle. The flow entering the pre-chamber was considered to have the same mixture composition of the main chamber at IVC in this particular running point. Furthermore, ten cycles were calculated for both PC1 and PC1c, with five instantaneous solutions generated near the TDC of each simulated cycle, corresponding to the crankangles of -25 CAD, -20 CAD, -15 CAD, -10 CAD and -5 CAD.

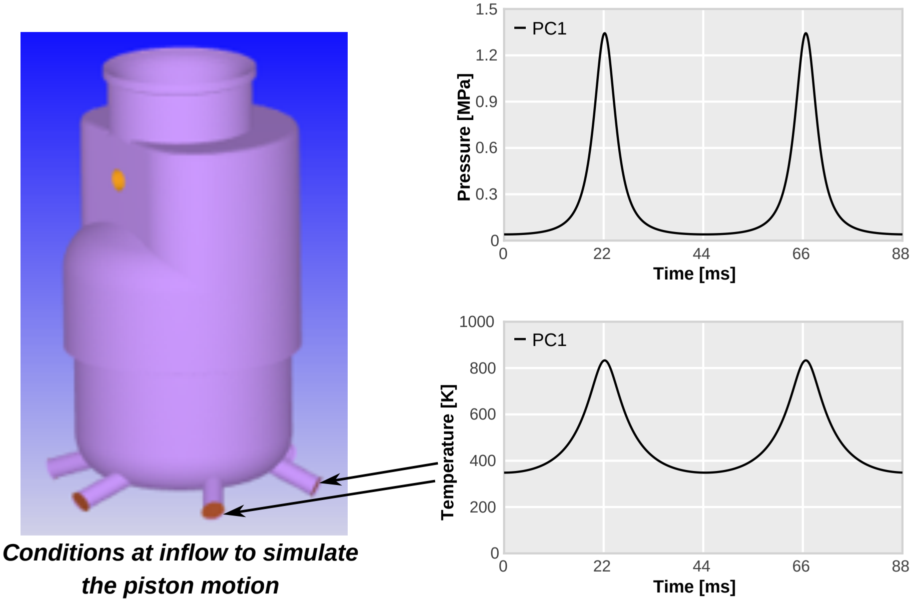

Figure 4.34: Computational domain and inflow conditions for the LES simulations.

Thereafter, the reacting simulations were done separately for each cycle, initialized by a mapping approach from the aforementioned instantaneous solutions of the non-reacting case. This way, the combustion process will initially develop within the characteristic flow-field of each cycle. The combustion model settings were kept equal to the reacting RANS simulation. Moreover, five ignition timings were calculated for every cycle with both pre-chambers, totalling one hundred simulations, with the reference spark timing being -20 CAD. This allowed to study the sensitivity of each pre-chamber to both advanced and delayed spark timings in terms of CCV, in order to compare these results with the experimental trends found for PC1.

Before diving into the results, several studies from the literature have shown strong correlations between the cycle-to-cycle variations of SI engines and the initial flow conditions in the proximities of the spark plug [11–13]. Therefore, the first part of the analysis will focus on characterizing the distribution of the flow variables in the whole pre-chamber and their deviations between cycles, paying special attention to the surroundings of the electrodes.

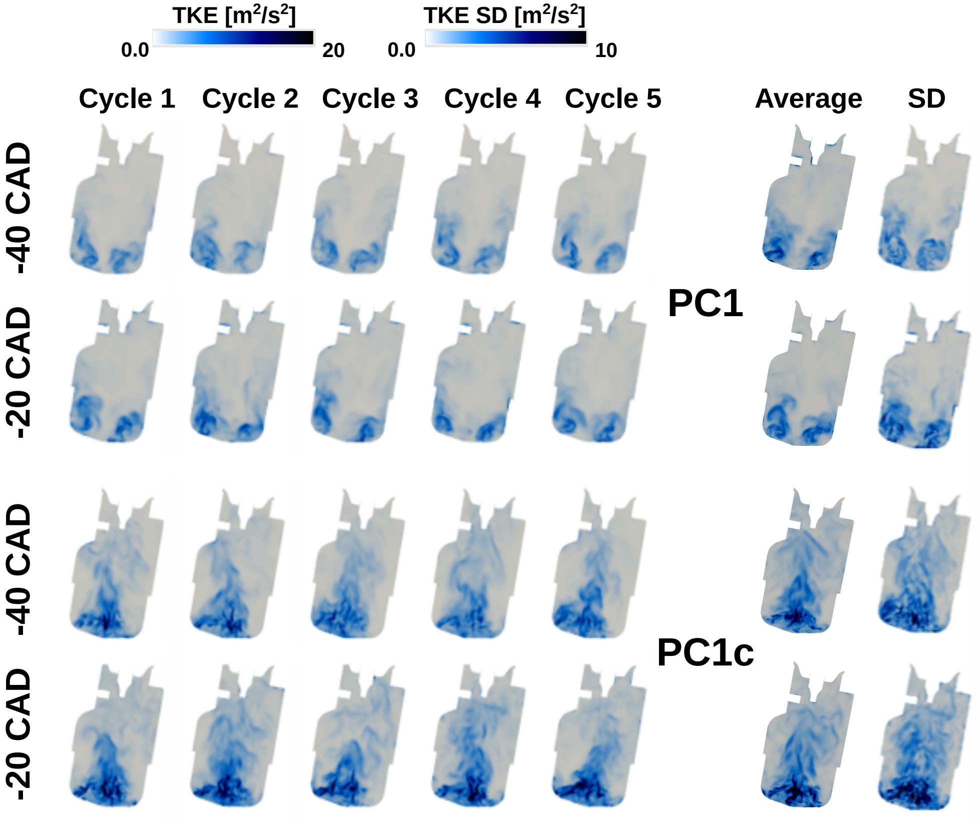

Figure 4.35: Generation of Turbulent Kinetic Energy inside the pre-chamber for the LES simulations. Snapshots for PC1 are shown in the upper rows for five cycles at two crankangles, and in the bottom rows for PC1c. The time averaged and standard deviation of this parameter over all cycles is shown at the right-side of the figure for each pre-chamber at the corresponding crankangle.

Figure 4.35 shows the TKE field for five consecutive cycles of PC1 (top rows) and PC1c (bottom rows). The snapshots are taken from the non-reacting simulations at an advanced crankangle (-40 CAD) and at the reference spark timing (-20 CAD). The right-side columns show the spatially averaged TKE field for all cycles and the standard deviation (SD) of the TKE in the full length of the pre-chamber. From here, the general behavior of the flow-field is maintained with respect to the RANS simulations, where the swirling motion of PC1 generates high TKE values at the bottom that quickly

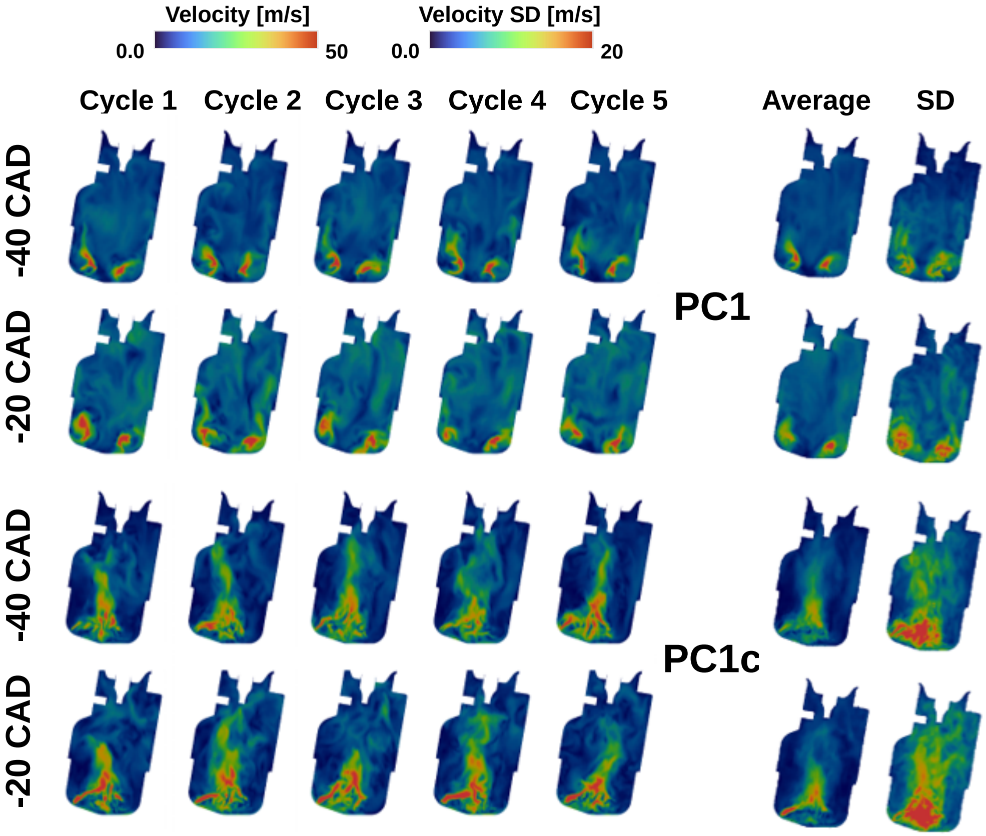

Figure 4.36: Velocity field inside the pre-chamber for the LES simulations. Snapshots for PC1 are shown in the upper rows for five cycles at two crankangles, and in the bottom rows for PC1c. The time averaged and standard deviation of this parameter over all cycles is shown at the right-side of the figure for each pre-chamber at the corresponding crankangle.

dissipate as the flow goes in the upwards spiral, while the crashing flow at the bottom of PC1c produces higher levels of turbulence that rise along the central part of the pre-chamber. However, the snapshots of PC1c exhibit more differences in both the local distribution of the TKE as it moves towards the spark plug, and the local intensity of the turbulence field. This is confirmed by the standard deviation column, where a much higher variation of the TKE between cycles is observed for PC1c compared to PC1.

Moreover, Figure 4.36 presents the same distribution of images but for the velocity field. It is interesting that despite showing the same pattern as the turbulence field, the local distribution of the velocity is much more uniform in the whole volume for PC1, without having such a high difference between the velocities at the bottom and at the top of the pre-chamber. On the other hand, PC1c shows a high stratification for this flow variable, where the velocities in the middle section of the pre-chamber are considerably higher than the near-wall regions. In addition, the consecutive snapshots also exhibit more differences compared to PC1, which is again highlighted by the standard deviation values. In this case, the levels of SD near the spark plug reach over 10 m/s for PC1c at -20 CAD, almost five times as high as the SD levels for PC1 in the same time frame.

From this initial assessment of the pre-chamber flow-field, PC1c starts to evidence a negative behavior in terms of CCV. However, the combustion simulations must be considered in order to complete the analysis. Therefore, Figure 4.37 shows an overview of the combustion process for each design, with the spark triggered at -20 CAD. The evolution of the flame can be observed in the visualization images, where five snapshots are taken for two consecutive cycles. Regarding PC1, the initial flame kernel is very similar between the two cycles, and given that the swirling motion of the holes generates a uniform flow pattern, the morphology of the combustion process as it starts to progress throughout the pre-chamber is also alike for both cycles. On the contrary, a different ignition spot is observed for the first snapshots of PC1c. Thus, the subsequent evolution of the flame presents higher differences between the two cycles of this geometry. In addition, the particular flow pattern of PC1c bends the flame towards one side of the pre-chamber as it develops in this region.

Below the snapshots of Figure 4.37, the HRR profiles of the ten combustion cycles are plotted, with the left column corresponding to PC1 and the right column to PC1c. From the top plots it is clearly seen that the stabilized flow pattern helps PC1 to achieve faster burning rates than PC1c, and the combustion phasing for all cycles is kept within a short range. Conversely, the HRR profiles of PC1c show further differences in terms of CA50, with an offset of approximately 2 CAD between the peak values of several cycles. This can be better observed in the bottom plots, where the average HRR of the ten cycles is presented for each pre-chamber, along with their corresponding standard deviations. Here, a higher SD is appreciated for PC1c, due to the more variations in the combustion process of each cycle.

Moving on, Figure 4.38 shows the cycle-averaged HRR of the five simulated spark timings, with their corresponding standard deviations. The black curves represent PC1 and the blue curves PC1c. For the reference case, with the ignition set to -20 CAD, the highest burn rates are achieved for both

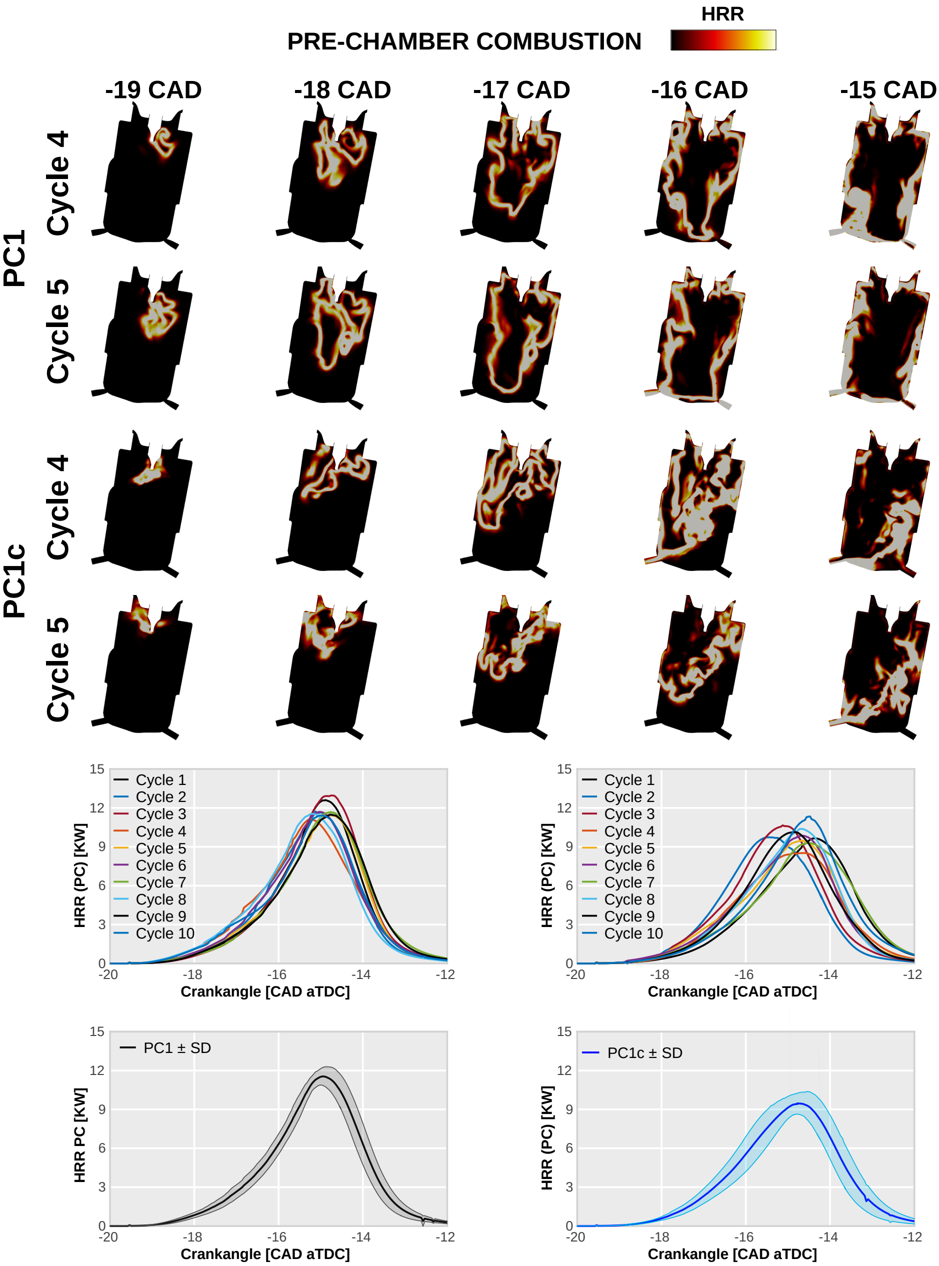

Figure 4.37: Analysis of the pre-chamber combustion in each cycle.

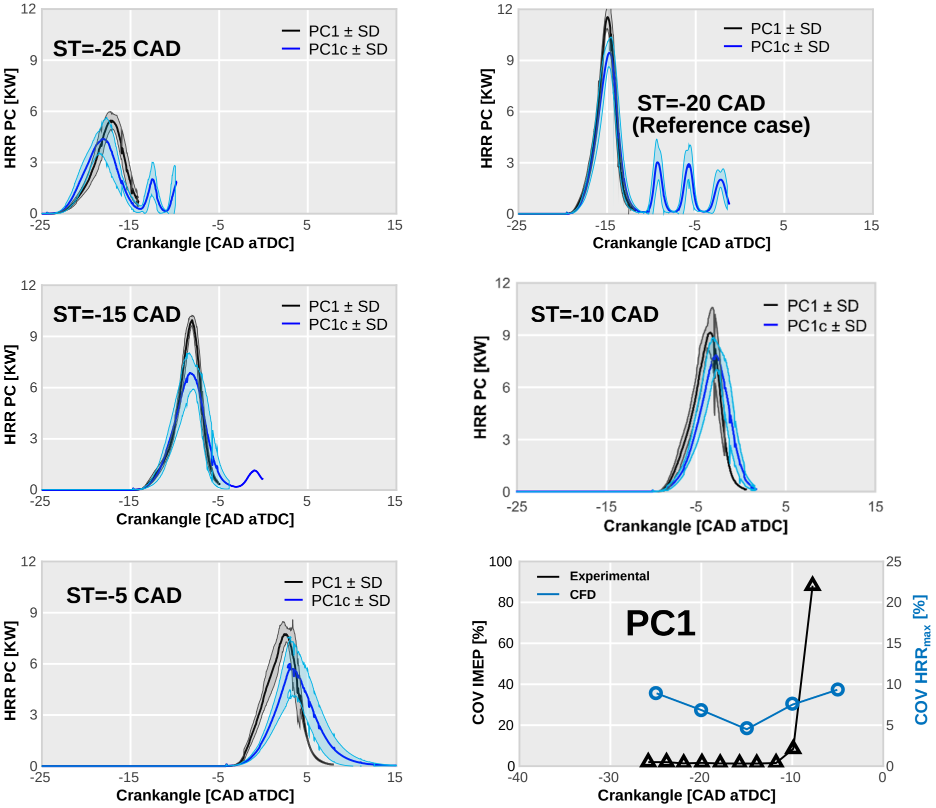

Figure 4.38: HRR averaged over ten combustion cycles with the corresponding standard deviation for each pre-chamber at five different spark timings. The bottom-right corner shows the COV IMEP for the spark timing sweep performed in the real engine with PC1 at the simulated operating conditions (OP3), along with the COV of the peak HRR for each simulated spark timing.

pre-chambers, showing also relatively low levels of dispersion. This matches the trends observed during the experimental campaign, given that the spark setting is the closest to the MBT conditions of OP3. However, when moving the ignition to either direction of this point, the SD values start to increase, specially for PC1c. At -5 CAD for example, a 50% variation is observed for the peak HRR of the aforementioned pre-chamber.

At this point, one of the major issues found for the multi-cycle LES methodology was the difficulty to effectively quantify the CCV. Considering that the cyclic dispersion is evaluated for the indicated parameters of the engine (σIMEP, COV IMEP), a suitable parameter for estimating the CCV was lacking from these simulations, given that only the pre-chamber combustion was modelled. For this purpose, the experimental spark timing sweep performed at low load/speed conditions (presented in Section 4.2.3) was contrasted with the results for the five simulated spark timings of PC1, in order to find a parameter that was able to reproduce the experimental trend.

In a first attempt, the maximum HRR value was considered. The bottom-right corner of Figure 4.38 shows the comparison of the experimental COV IMEP and the covariance of the peak HRR (COV $\mathrm{HRR}_{\mathrm{max}}$) for the ignition sweep. It is clearly seen that the real behavior of the engine is not captured with this parameter. Fairly similar levels of COV $\mathrm{HRR}_{\mathrm{max}}$ are obtained for each spark timing, showing the lowest value at -15 CAD, and failing to reproduce the flat tendency of the COV IMEP at early ignition times and the abrupt increase after -10 CAD. This can stem from the fact that the maximum HRR is not a parameter that directly relates to the ignition of the main chamber.

One of the phenomena that is usually overlooked when analyzing the pre-chamber system is the asymmetry with which the main chamber ignition can be generated. Considering that the flame can reach each hole at different time frames, as was observed in the flame evolution sequence of Figure 4.37, some jets would be ejected before others, which could cause the flame to be quenched in certain cycles due to a premature pressurization of the main chamber. The asymmetric combustion pattern can lead to high cyclical dispersion since the flame evolution would change significantly in every engine cycle. Consequently, a characteristic parameter "τ" can be defined as the time it takes for the flame to reach each hole. Thus, this variable would represent an estimation of the main chamber combustion onset, as well as the morphology of the ignition source.

In light of the previous statement, monitor boxes were placed at the entrance of each hole for both pre-chamber designs, in order to determine the time at which the ECFM progress variable reaches a value of 0.55, which is the usual threshold used to define the flame front separating the burned gases (where the progress variable has a value of 1) and the unburned mixture (where the progress variable is null).

The results of this study are presented in Figure 4.39 for the reference spark timing (upper row) and the most delayed spark timing (bottom row). These plots show the τ parameter in the vertical axis and the pre-chamber holes in the horizontal axis, labeled from 1 to 6. Each plotted line represents a combustion cycle, therefore, an ideal scenario would be characterized by over-

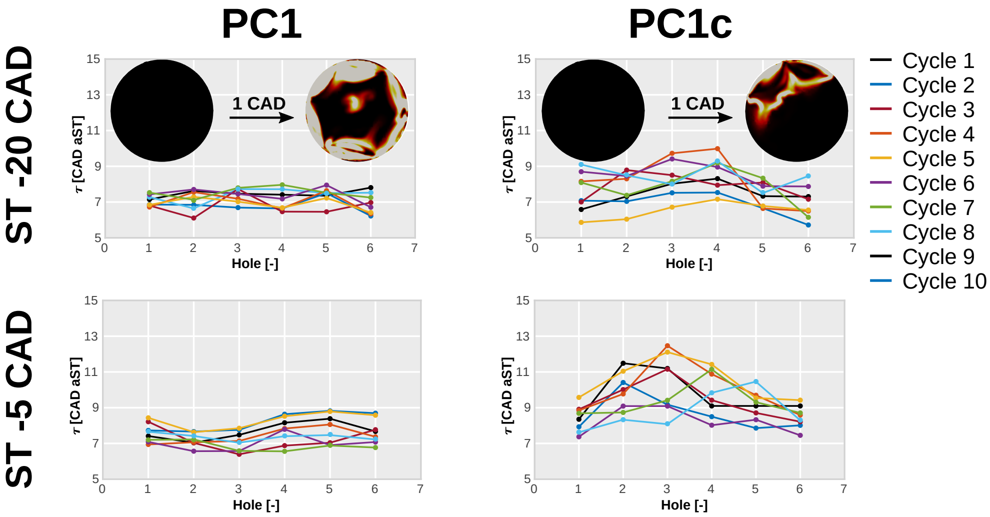

Figure 4.39: τ values for each cycle at the reference and most delayed spark timings. The snapshots are shown for a cut-plane perpendicular to the pre-chamber axis and 1mm over the position of the holes.

lapped horizontal lines, which indicates that the flame is reaching all the holes at the same time in every cycle. From here, the variations of the combustion process can be assessed in two directions (between holes and between cycles).

For PC1, the τ values are kept within a range of ±1 CAD between cycles at the reference spark timing, showing a good combustion stability. In addition, the behavior of τ in most cycles is relatively flat, with a variation of 0.5 CAD between holes, which also indicates a stable combustion evolution, leading to a uniform ignition of the main chamber. This can be further appreciated in the snapshots on the top plot of PC1, that are taken for a cut-plane perpendicular to the pre-chamber axis and just above the location of the holes. It can be seen that with a variation of only 1 CAD, the flame is able to reach the pre-chamber bottom and sweep the whole circumference, promoting the ejection of reactive products throughout the 6 holes in a similar time frame. Moreover, for the delayed spark timing the τ variations begin to increase (±2 CAD between cycles), however, the behavior of the flame pattern between holes is still kept within a short range.

On the other hand, the behavior of τ for PC1c is much more erratic in both considered spark timings. Firstly, the characteristic times for most cycles are higher than PC1, indicating that the flame takes longer to reach the pre-chamber bottom. This fact increases the energy losses due to non-reacting ejection of pre-chamber mixture, and also increases the delay between the ignition signal and the onset of main chamber combustion, which has negative implications for the concept as was discussed in Section 4.2.3. Secondly, the variations of τ between cycles are considerably higher, reaching a difference of up to 3 or even 4 CAD in both spark timings. Lastly, the variance of τ between holes is also very high for some cycles, which can be seen in the upper snapshots of PC1c, where the flame is clearly reaching some holes sooner than others, making for an asymmetrical main chamber ignition.

The analysis presented in this section suggests that PC1c is expected to have increased levels of CCV in a wide range of spark timings, compromising the performance of the engine. Nevertheless, the reliability of these results is yet to be verified. For this purpose, Figure 4.40 presents the covariance of the τ parameter compared to the COV IMEP, highlighting that the experimental trend is very well matched with this new variable. The simulations are able to qualitatively predict the global tendencies of the concept and the combustion stability threshold, proving the capacity of the developed multi-cycle LES methodology for assessing the sources of CCV in pre-chamber ignited engines.

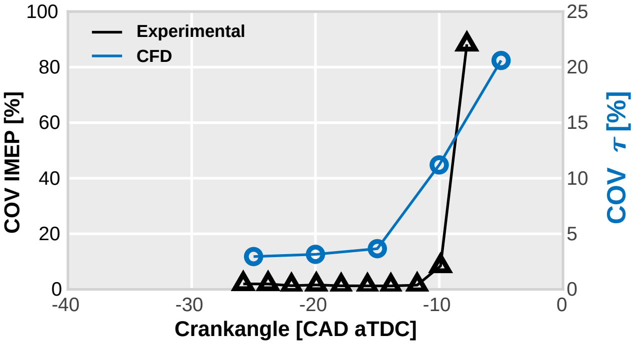

Figure 4.40: Validation of the τ parameter with the experimental trend for the COV IMEP.

Furthermore, in order to verify the previous statement, PC1c was manufactured and installed in the single-cylinder research engine for testing. Figure 4.41 shows the experimental results for PC1 and PC1c at low engine load/speed conditions. In this case, the operating conditions were not exactly the same as OP3 (see Table 3.5), given that these tests were performed long after the initial campaign and several of the engine settings had been changed.

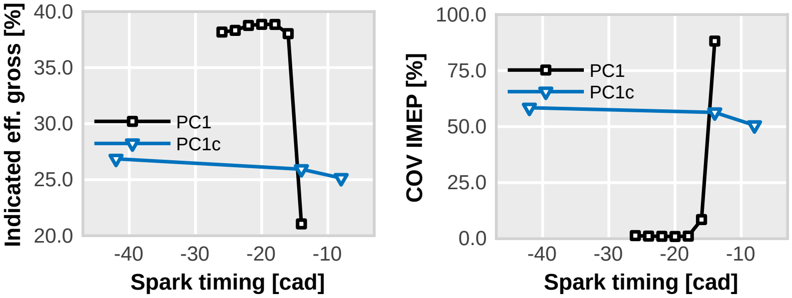

Figure 4.41: Experimental results for PC1 and PC1c at low engine load/speed conditions.

This explains the slightly different stability threshold achieved with PC1, however, the general behavior of this pre-chamber was maintained. These results confirm the exceedingly high variability faced during the experiments of PC1c, where only three points were measured with COV IMEP values over 50%.

Thus, this study has revealed an important conclusion related to the behavior of the passive pre-chamber concept in terms of cyclical dispersion. Although having higher levels of turbulence can (in principal) help to accelerate the pre-chamber turbulent flame speeds, which is a feature that can essentially help to improve the performance of the concept, generating a stable flow pattern inside this region is predominant in order to maintain a fast and stable combustion process. This can be achieved by providing a tangential angle to the layout of the holes, enabling the generation of a swirling vortex that stabilizes the flow-field. This is particularly important for small holes, given that the flow stretch through these nozzles will generate high turbulence levels as it enters the pre-chamber, and if the holes are facing each other, then extremely high TKE values will be propagated throughout the entire pre-chamber volume, promoting elevated variations of the flow conditions and the subsequent combustion process in both chambers.

4.4 Summary

In this chapter, an extensive characterization of the passive pre-chamber concept in un-diluted stoichiometric conditions has been performed by analyzing several features related to the engine operating conditions, phasing of the ignition signal and geometrical parameters of the pre-chamber, and their impact over the most relevant physical and thermochemical phenomena involved in this ignition system. For this purpose, the 3D-CFD model developed and validated in Chapter 3 was used to overcome the limitations of the experimental campaign, in order to further understand the behavior of the concept in the real engine.

Starting with the pre-chamber flow-dynamics, this aspect is mainly controlled by the force of the piston during the compression stroke, which also depends on the engine running point. Furthermore, due to the particular internal flow-field of the pre-chamber, the concept will have a high sensitivity to the ignition timing. Triggering the spark at an early stage will inherently imply an increase in the local stratification of residual gases in this region, particularly in the top of the pre-chamber where the electrodes are usually placed. On the other hand, for delayed spark timings the turbulence levels of the pre-chamber will sharply decrease, compromising the flame propagation speeds.

At λ=1 without dilution the pre-chamber jets act as a "super spark", igniting the main charge with a large flame surface distributed along the combustion chamber. Afterwards, as the thermochemical properties of the mixture are favorable in these conditions, the flame progresses quickly outside of the jet limits, consuming over 70% of the charge downstream of the jets. Moreover, if the cylinder head design doesn't allow the pre-chamber to be centered with respect to the cylinder axis, then some jets will not be able to reach the cylinder walls, forcing the flame to travel through a portion of the main chamber without the enhanced turbulence generated by the jets. This represents a potential issue when the conditions downstream of the jets are compromised (low engine load/speeds or diluted mixtures).

The flame structure of the passive pre-chamber concept follows a multi-regime evolution in the Borghi-Peters diagram. As the combustion progresses through the pre-chamber holes, the flame momentarily shifts towards the *thickened flames* regime, where the turbulent scales can lead to a flame extinction. Thereafter, as the main chamber ignites, the flame finishes developing in the *thickened wrinkled flames* and *corrugated flamelets* regime, which are characteristic for SI engines.

An energy balance of the pre-chamber during the ejection process was performed, dividing the total energy available in this region into four contributions: Energy used for main chamber ignition (EAE), heat losses during the pre-chamber combustion (Q_{wall}), unburned fuel remaining at the moment of flow inversion (Unburnt), and non-reacting mass ejected during the initial stages (Inert). Thus, in order to optimize the energy conversion and avoid losing fuel under inert conditions, the flame must sweep the entire pre-chamber volume in a short time frame, which can be achieved by enhancing the combustion process with higher turbulence, more energy during the ignition or more favorable thermochemical properties of the mixture.

The analysis at different operating conditions revealed several issues at low engine load/speeds that limit the concepts flexibility in this running point. The pre-chamber burn rates are considerably slowed down due to an inherent deterioration of the internal flow-field, with higher levels of residuals (close to 30% in the spark plug gap) and lower levels of TKE, and an inefficient energy management (less than 50% of the pre-chamber fuel is used for igniting the main charge). This leads to weaker jets penetrating into the main chamber, which slackens the flame development in this region.

Moreover, delaying the spark timing at low load/speed conditions further from the MBT results in the extra fuel that fills the pre-chamber to be lost under cold/non-reactive conditions. Thus, as the spark is triggered closer to TDC, most of the jet momentum is used to eject non-reacting flow, incapable of promoting the main chamber ignition. This leads to a longer time lag between the ignition signal and the onset of main chamber combustion, given that the reactive ejection is delayed and the thermodynamic conditions in the main chamber become less favorable as the piston starts to descend. In addition, delaying the onset of main chamber combustion can also result in an increased CCV, since the ignition lag gives more time for the flow field to present variations between cycles. This analysis explains, at least up to some extent, the low compatibility of the passive pre-chamber concept with catalyst warm-up under cold-start conditions.

The relationship between the total cross sectional area of the holes and the pre-chamber volume (A/V ratio) is a parameter that strongly conditions the scavenge of residual gases. Pre-chambers with low A/V ratios (small holes and large volumes) will not be able to evacuate most of the residuals from this region, particularly in the spark plug gap, which compromises both the performance of the concept and the tolerance to EGR dilution. A high enough A/V ratio must be used to assure the minimum amount of residuals to remain inside the pre-chamber for a given operating point.

Several geometric parameters of the pre-chamber were studied keeping a suitable A/V ratio, and it was found that:

- Having a larger pre-chamber volume allows to obtain better jets and an increased thermal efficiency, as long as the flame is able to burn the whole pre-chamber charge quickly, in order to take advantage of the higher fuel energy to eject reacting mixture.

- Having a lot of holes (>6) allows to sweep a larger circumferential portion of the main chamber, however, the penetration of the jets will be lower. This does not provide considerable benefits given that the charge between the jets is consumed more easily than the charge downstream of the jets.

- Removing the tangential angle of the holes and facing them directly towards each other allows to generate higher levels of turbulence in the whole pre-chamber volume, increasing the burn rates in this region. However, the resulting flow pattern is highly stratified and could prove to be a potential issue for CCV.

To prove this last remark, a clever methodology was devised to evaluate the cycle-to-cycle combustion variability of different pre-chamber designs by multi-cycle LES simulations. This approach attributed the sources of CCV to the pre-chamber combustion process, and thus only this region was simulated. Since the engine indicated parameters were not available with this methodology, the time for the flame to reach the pre-chamber holes (τ) was defined as a parameter to quantify the CCV of a given design, since it relates to the onset of main chamber combustion and its morphology. This parameter was able to qualitatively reproduce the experimental COV IMEP trend as the spark timing was delayed at low load/speed conditions for the reference pre-chamber (with swirl).

Thereafter, the predicted levels of CCV were much higher for the pre-chamber design without swirl. This was finally validated by manufacturing the aforementioned pre-chamber and testing it in the real engine. From this study it was concluded that generating a stable flow pattern inside pre-chamber is fundamental in order to maintain a suitable combustion stability. This can be achieved by providing a tangential angle to the layout of the holes, enabling the generation of a swirling vortex that stabilizes the flow-field.

References

[1] Benajes, J. et al. “Performance of the passive pre-chamber ignition concept in a spark-ignition engine for passenger car applications”. In: *SIA Power Train & Electronics*. Paris, France: SIA Power Train & Electronics, 2019.

[2] Novella, Ricardo et al. *Experimental and Numerical Analysis of Passive Pre-Chamber Ignition with EGR and Air Dilution for Future Generation Passenger Car Engines*. Tech. rep. SAE Technical Paper, 2020. DOI: `https://doi.org/10.4271/2020-01-0238`.

[3] Borghi, R. “On the structure and morphology of turbulent premixed flames”. In: *Recent advances in the Aerospace Sciences*. Springer, 1985, pp. 117–138.

[4] Peters, Norbert. “The turbulent burning velocity for large-scale and small-scale turbulence”. In: *Journal of Fluid mechanics* 384 (1999), pp. 107–132.

[5] Angelberger, C, Poinsot, T, and Delhay, B. *Improving near-wall combustion and wall heat transfer modeling in SI engine computations*. Tech. rep. SAE Technical Paper, 1997. DOI: `https://doi.org/10.4271/972881`.

[6] Benajes, J et al. “Evaluation of the passive pre-chamber ignition concept for future high compression ratio turbocharged spark-ignition engines”. In: *Applied Energy* 248 (2019), pp. 576–588. DOI: `https://doi.org/10.1016/j.apenergy.2019.04.131`.

[7] Benajes, J et al. “Computational assessment towards understanding the energy conversion and combustion process of lean mixtures in passive pre-chamber ignited engines”. In: *Applied Thermal Engineering* 178 (2020), p. 115501. DOI: `https://doi.org/10.1016/j.applthermaleng.2020.115501`.

[8] Zhu, Sipeng, Akehurst, Sam, Lewis, Andrew, and Yuan, Hao. “A review of the pre-chamber ignition system applied on future low-carbon spark ignition engines”. In: *Renewable and Sustainable Energy Reviews* 154 (2022), p. 111872.

[9] Bolla, Michele et al. “Numerical study of turbulence and fuel-air mixing within a scavenged pre-chamber using RANS and LES”. In: *SAE Technical Papers* 2019 (2019).

[10] Truffin, Karine, Angelberger, Christian, Richard, Stéphane, and Pera, Cécile. "Using large-eddy simulation and multivariate analysis to understand the sources of combustion cyclic variability in a spark-ignition engine". In: *Combustion and Flame* 162.12 (2015), pp. 4371–4390.

[11] Masouleh, M Ghaderi et al. "Flow and thermal field effects on cycle-to-cycle variation of combustion: scale-resolving simulation in a spark ignited simplified engine configuration". In: *Applied Energy* 230 (2018), pp. 486–505.

[12] Chen, Ceyuan et al. *LES analysis on cycle-to-cycle variation of combustion process in a DISI Engine.* Tech. rep. SAE Technical Paper, 2019.

[13] Masouleh, M Ghaderi et al. "Modeling cycle-to-cycle variations in spark ignited combustion engines by scale-resolving simulations for different engine speeds". In: *Applied Energy* 250 (2019), pp. 801–820.

Chapter 5

Combination of the passive pre-chamber with dilution strategies

"The future is eclectic", this is a popular quote that has been going around the ICE community during the past years. Nowadays many people claim that the use of electric-powered vehicles is the best alternative for reducing the environmental footprint of the transportation sector, however, aggressively replacing one technology with another has rarely panned out positively throughout history. Hence, the aforementioned quote suggests that, in the road towards decarbonization, research efforts should not be solely focused on the latest technological trends, but rather on the combination of the most appropriate technologies in order to develop the best vehicle possible.

ICE's still have an important role to play in transportation, and it is the integration of modern engine strategies that can help to achieve the goal of generating the lowest cradle-to-grave CO_2 emissions from passenger cars. In this sense, the use of diluted mixtures (lean burn or EGR) has been a highly demanded strategy for modern vehicles, due to its potential for reducing fuel consumption, tailpipe emissions and increasing the engine's thermal efficiency (as was explained in Chapter 2). However, the deterioration of the combustion process is the main bottleneck for this technology, which makes it necessary to incorporate a combustion enhancement strategy or a high energy ignition system like the pre-chamber concept. Nevertheless, the passive pre-chamber system has important drawbacks when operating with diluted mixtures, given that the usual problems that are found in the main chamber for the conventional SI concept are now translated to the pre-chamber.

Therefore, understanding the underlying thermochemical characteristics of the concept under diluted conditions becomes imperative to develop solutions for integrating these technologies in passenger car engines. Furthermore, this chapter makes use of the validated CFD model for different air and EGR dilutions rates, presented at the end of Chapter 3, to study the behavior of the concept in these conditions and understand its limitations.

5.1 Characteristics of the passive pre-chamber combustion with air dilution

The first section will focus on the combination of the passive pre-chamber concept with air dilution (lean burn). Particularly, this strategy has not been integrated into production engines due to its incompatibility with the Three-Way Catalyst for controlling tailpipe NO_x emissions, as it needs to be operated with a stoichiometric air-to-fuel equivalence ratio. Thus, achieving λ values of around 2.0 for conventional fuels (gasoline) is needed to maintain these emissions below the current European standards.

Figure 5.1 shows the experimental results for the λ sweep performed at high load/speed conditions, comparing the conventional SI system and the passive pre-chamber system (see Table 3.4 for reference on the pre-chamber designs). The instantaneous pressure signals and HRR are plotted in the top four graphs. According to these results, the sensitivity of both ignition concepts to air dilution is quite similar, showing a moderate impact on the combustion profile when going to a λ of 1.2, and afterwards experiencing an important deterioration of the HRR as the λ increases. Moreover, PC1 is able to extend the dilution limit from λ=1.4 to λ=1.6, achieving higher burn rates and pressure peaks in the whole dilution sweep.

The bottom plots of Figure 5.1 show the impact of air dilution on the indicated efficiency and the NO_x emissions for the four tested pre-chambers. All of the designs are able to obtain higher levels of efficiency compared to the conventional SI system, given that in these conditions the CA50 values of the SI concept are limited by knock, while the pre-chamber allows to overcome this issue. However, PC3 and PC4 are not able to extend the dilution limit (due to the reasons explained in Section 4.3.1), showing the importance of the pre-chamber geometry on the dilution tolerance.

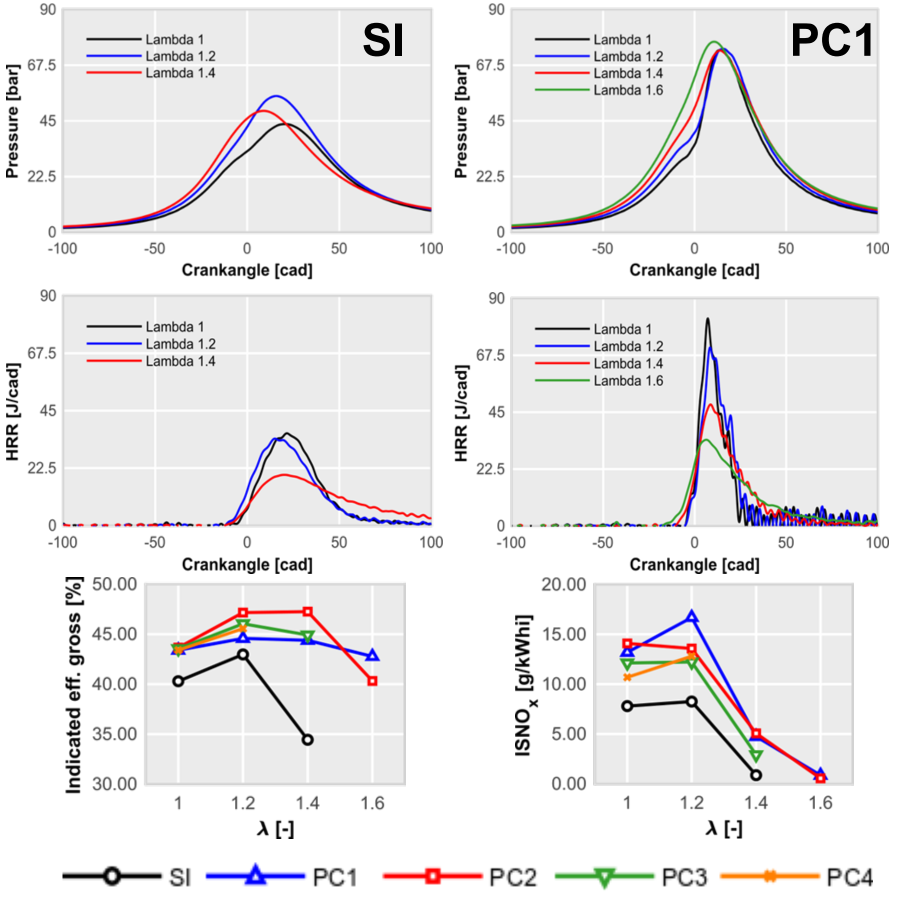

Figure 5.1: Experimental results for the air dilution sweep. The instantaneous pressure and HRR profiles are shown at the top for the conventional SI system and PC1. The indicated efficiency and NO_x emissions are shown at the bottom.

In addition, although PC1 is not able to achieve higher efficiency levels than PC2 at λ=1.2 and λ=1.4, it is able to keep the engine efficiency above 42% at λ=1.6. This is even more interesting when analyzing the NO_x emissions. From the bottom-right plot, it can be seen that the NO_x values are higher for the pre-chambers than the conventional SI system, because of the higher temperatures reached in the cylinder as a consequence of the faster combustion process. However, the NO_x values of PC1 at λ=1.6 are at the same level as the SI concept at λ=1.4, proving the potential of the passive pre-chamber concept to achieve low NO_x emissions while keeping high levels of efficiency. Nevertheless, this value of λ=1.6 is still far away from being enough to operate the engine without using the TWC. Thus, a deeper analysis of the concept's behavior at the dilution threshold can help to further understand these limitations.

5.1.1 Study of the concept at lean conditions

Considering the experimental trends, the CFD simulation for λ=1 was contrasted with the numerical results for λ=1.6, to study the fundamental differences in the combustion process. Figure 5.2 presents the combustion evolution in both chambers, using the same images that were introduced in Chapter 4 to highlight the location of the flame and the limits of the jets.

The snapshots for λ=1 show the characteristic pattern that was observed in Chapter 4, with a very fast pre-chamber combustion (in the range of 4 to 5 CAD) and a clear jet-driven ignition in the main chamber, where the flame is also able to evolve outside of the jet boundaries after a short time frame (around 8 to 10 CAD after the combustion onset). Moreover, the main chamber HRR profile plotted at the bottom, which is divided into the contributions inside and outside of the jet limits, shows that close to 80% of the fuel is consumed outside of the jets.

On the other hand, the flame evolution inside the pre-chamber for the lean simulation is considerably slower. In this case it takes the flame over 15 CAD to reach the bottom of the pre-chamber, which remarkably delays the main chamber ignition onset. Additionally, the morphology of the jets for λ=1.6 is also deteriorated, showing reduced penetrations and an ignition pattern more similar to the conventional SI concept. The main chamber snapshots for this simulation reveal that it takes the flame over 20 CAD after the start of combustion to leave the influential boundaries of the jets, in order to start progressing as a conventional SI flame front. Consequently, almost 40% of the main charge is burned inside of the jets in these conditions (as can be seen in the bottom plot).

To shed further light on the deteriorated main chamber combustion, the pre-chamber combustion features for λ=1.0 and λ=1.6 are presented in Figure 5.3. In a first glance, it can be appreciated how the pre-chamber HRR starts sooner for the lean simulation, since the spark timing of this case needs to be advanced from -10 CAD to -42 CAD in order to achieve a suitable CA50 in the main chamber. Moreover, The pre-chamber burn rates are considerably slower for λ=1.6, which leads to a lower pressure increase in this region. Ac-

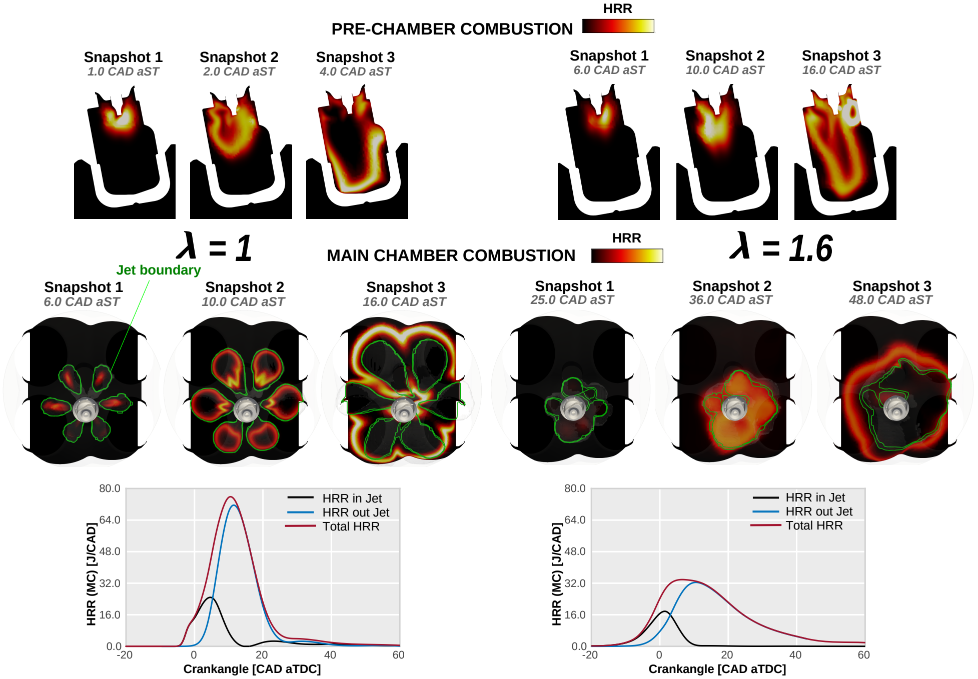

Figure 5.2: Combustion evolution in stoichiometric and lean conditions. The main chamber HRR inside and outside of the jets is shown at the bottom

cordingly, both the jet penetration rates and the maximum penetration values are also reduced.

This inherent need to advance the ignition signal has two very important consequences over the performance of the passive pre-chamber concept. The first is related to the energy available at the start of combustion, which is shown for both simulations in Figure 5.4. It can be observed how the pre-chamber fuel scavenge is interrupted for λ=1.6, due to the earlier flow inversion after triggering the spark, compromising the energy that will be used for igniting the main chamber.

The former remark can be better appreciated in the bottom bar graphs of Figure 5.4, where the energy conversion during the pre-chamber combustion and the ejection process was computed. This energy balance uses the same nomenclature that was introduced in Section 4.1.3, dividing the total energy into four contributions. Thus, not only is the energy available at the start of combustion over three times lower for λ=1.6, but also the real energy used for

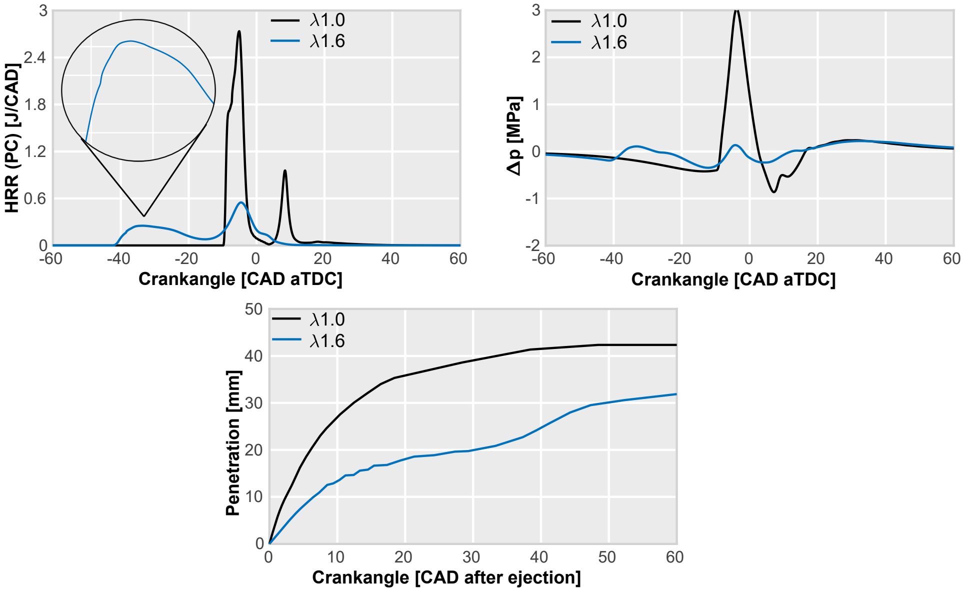

Figure 5.3: Pre-chamber combustion features for the stoichiometric and lean simulations.

main chamber ignition is close to four times lower in these conditions, given that a relevant part of the pre-chamber fuel is left unburned at the end of the jet ejection. This fact is due to the worsened local combustion process in the pre-chamber, which is a consequence of the deteriorated thermochemical properties of the flame that will be further explained below.

The second reason behind the slower burn rates shown in Figure 5.3 was extensively analyzed during Chapter 4, namely, the increase of internal residuals as the spark timing is advanced, which compromises the laminar flame speeds in the pre-chamber region. However, the properties of the flame are already in unfavorable conditions, since the lean mixture composition drastically reduces the flame speeds. This can be seen in the left-side plot of Figure 5.5, where the results from simple laminar flame speed calculations are shown for a λ sweep, using the 1D model described in Section 3.3.3. It can be observed that the jump from λ=1.0 to λ=1.6 entails a decrease of 50% in the laminar flame speed values. Therefore, enhancing the thermochemical properties of the mixture could be an interesting solution for improving the performance of the passive pre-chamber concept under lean conditions, and possibly allow to extend the dilution limit.

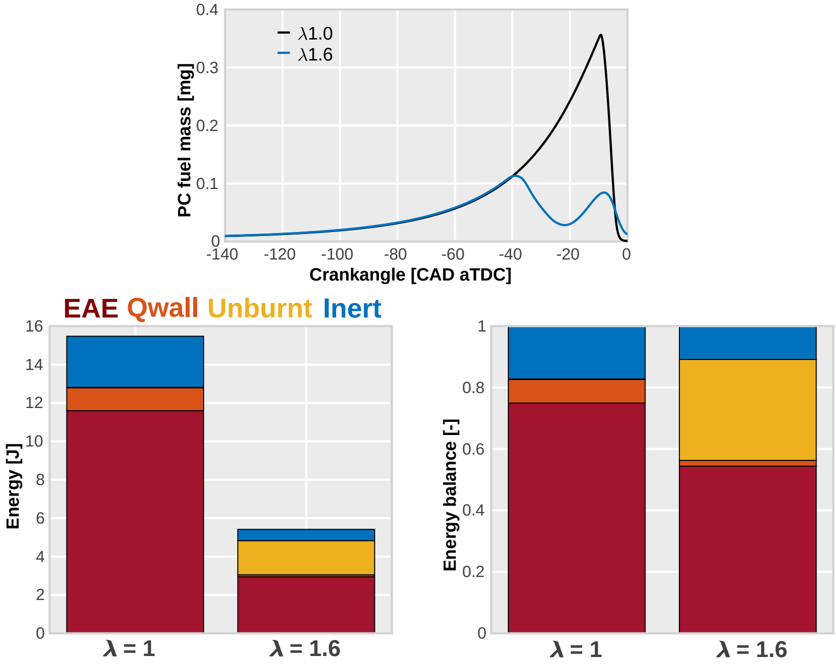

Figure 5.4: Pre-chamber energy conversion for the stoichiometric and lean simulations.

One way to achieve this is presented at the right-side of Figure 5.5, where a pathway is drawn to recover the laminar flame speeds of λ=1.0 when operating at λ=2.0 by increasing the mixture temperature. However, a previous study [1] has shown that the required temperature rise to reach these flame speeds would trigger an uncontrolled auto-ignition in the main chamber, that compromises the mechanical integrity of the engine, at least operating with gasoline. Thus, a different alternative developed for this thesis consisted in adding small amounts of hydrogen to the air-fuel mixture in the intake port, in order to increase the laminar flame speeds and enhance the burning rates in both chambers.

Recent studies [2, 3] have shown the capabilities of the ECFM model to accurately describe the combustion process of hydrogen in SI engines. In addition, the preliminary 1D studies presented in Section 3.3.3 showed that the laminar flame speeds of pure hydrogen and gasoline/hydrogen blends are well predicted with the chemical kinetics mechanism from Liu et al. [4], providing a good starting point to use the developed CFD model for analyzing the

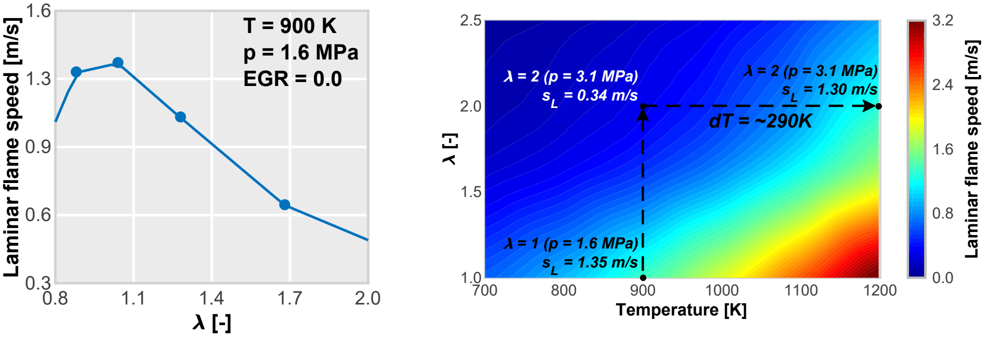

Figure 5.5: Sensitivity of the laminar flame speed to air dilution. The color map shows a path to recover the laminar flame speed values of λ=1.0 by increasing the temperature of the mixture at λ=2.0

combustion characteristics of the engine with hydrogen addition.

5.1.2 Using hydrogen to overcome the air dilution limit

A preliminary evaluation of the hydrogen fuel was performed to determine an optimum dilution level and the required H_2 amount for achieving competitive laminar flame speeds in these conditions. For this purpose, The 0D and 1D utilities described in Section 3.3.3 to generate the reference data tables for laminar flame speed and auto-ignition delay were used, in order to establish a suitable range for the hydrogen addition and to subsequently compute the new data tables for the selected gasoline/hydrogen blends.

The percentages of hydrogen are considered in volume fractions with respect to the total air admitted during the intake stroke. The results of the 1D laminar flame speed simulations are shown in the color maps of Figure 5.6. A λ sweep was performed extending from stoichiometric to λ=2.0 conditions, and the amount of hydrogen was also swept from 0% until 20% of the total air volume. The λ values shown in the map were simulated considering representative values of the in-cylinder pressure at the spark timing and a constant temperature of 800K. Both parameters were estimated by thermodynamic calculations based on engine tests and simulations. In addition, the total energy available in all fuel mixtures (gasoline+hydrogen) was kept constant.

The left plot of Figure 5.6 shows a pathway towards recovering the laminar flame speed of the λ=1.6 case without H_2 (experimental air-dilution limit).

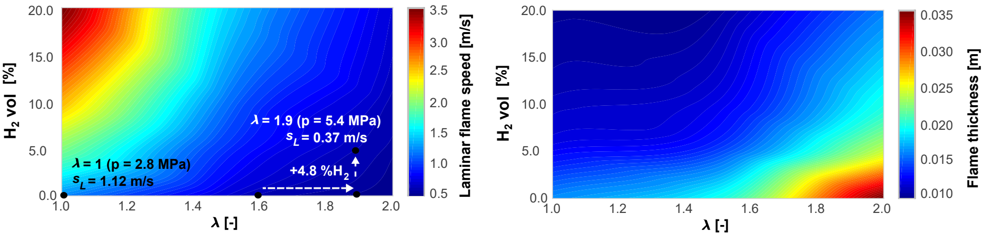

Figure 5.6: Laminar flame speed and flame thickness for several λ values and different percentages of hydrogen in the air-fuel mixture.

A λ value of 1.9 was considered to be a suitable dilution level for performing the CFD simulations, given that only 5% of hydrogen is required to achieve the same laminar flame speeds as the dilution threshold with pure gasoline. Additionally, the right-side plot shows that adding hydrogen also reduces the flame thickness, which is considerably enlarged when moving from λ=1.0 to λ=1.9. This has some relevant implications regarding the flame structure on the Borghi diagram, that will be explained later in this section.

Moreover, the auto-ignition delay calculations were also performed for the same λ and hydrogen sweeps. From previous investigations [5], it is known that the trends of the ignition delay pivot around a certain temperature value ($\sim$ 950K) when enriching the gasoline fuel with hydrogen. Thus, the impact of this enrichment could change drastically when considering values above or below this threshold.

Therefore, the temperatures of unburned gases were computed from the experimental tests at stoichiometric and λ=1.6 conditions to select an appropriate temperature for the 0D calculations. They are included in the right-side plot of Figure 5.7 for reference. From here, a temperature value of 900K was chosen as it is well representative of the maximum temperature reached by the fresh mixture as the combustion progresses in the main chamber.

Results of the 0D calculations for auto-ignition delay are shown in the color map plotted at the left-side of Figure 5.7. It is seen that the ignition delay values tend to decrease when considering higher dilution rates, due to the increased pressure achieved within the combustion chamber. However, the addition of hydrogen tends to increase the auto-ignition delay, thus reducing the knocking appearance.

This study has highlighted the thermochemical benefits of hydrogen for

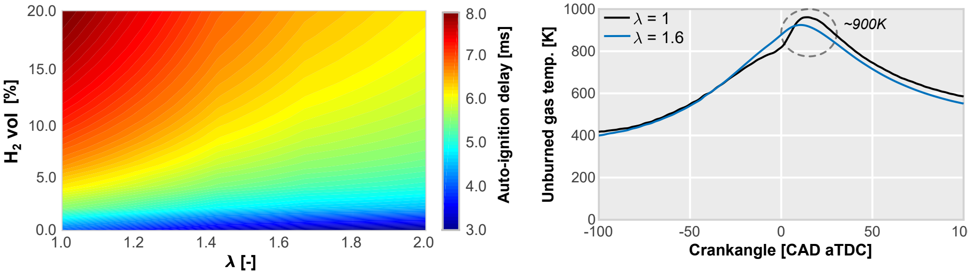

Figure 5.7: Auto-ignition delay values for different levels of air-dilution and different percentages of hydrogen, considering an unburned gas temperature of 900K.

enabling a successful lean operation of the engine. Therefore, the data tables of laminar flame speed and auto-ignition delay were generated considering the established hydrogen ranges, and a subsequent evaluation of the pre-chamber ignition concept enhanced with this strategy was performed with the CFD model.

After concluding the preliminary studies and generating the data tables, three simulations were calculated at λ=1.9, in order to evaluate different levels of hydrogen addition (2.5%, 4% and 5%) and their impact on the pre-chamber and main chamber combustion. These simulations were configured by considering the same methodology used in the experimental campaign. For this purpose, the mass of gasoline was adjusted in order to release the same amount of energy as the stoichiometric test, considering the specific amount of hydrogen added in each case. Thus, as the percentage of hydrogen increased, the mass of gasoline further decreased whereas the intake pressure was also increased to achieve the target air-to-fuel equivalence ratio.

Moreover, As no experimental data was available for these conditions, the spark timing used in each case was kept equal to the λ=1.6 simulation, given that the preliminary studies showed that the burning velocities should be similar to this case. Regarding the mixture formation process, a perfectly premixed mixture of gasoline/hydrogen and air is considered in the intake port region (no spray modeling is performed), and thus, the mixture enters the cylinder during the intake stroke without fuel stratification. Nevertheless, the stratification of residual gases is still considered in the simulations by initializing the cylinder region with burned gases from the previous cycle (as was explained in Section 3.3.4).

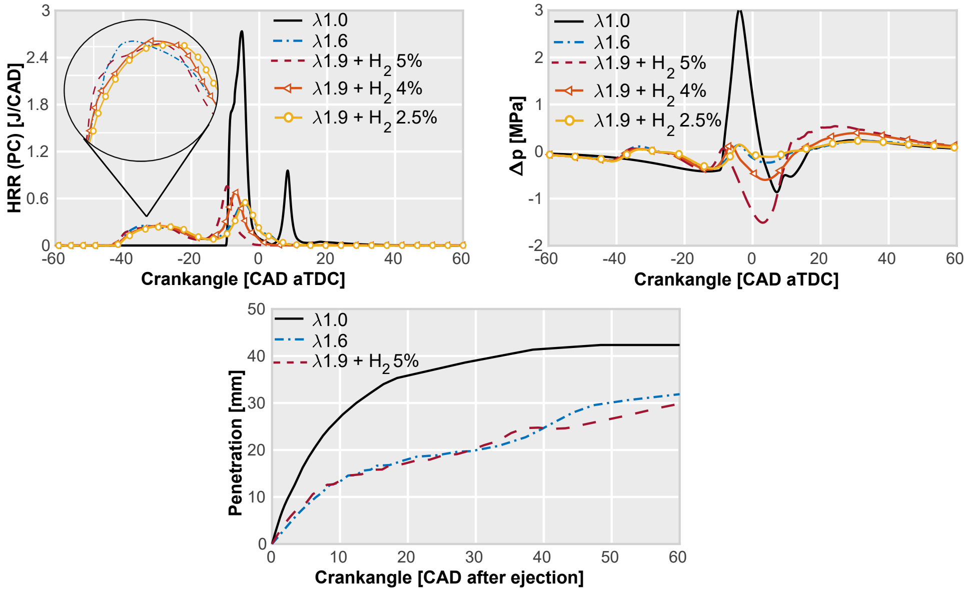

Figure 5.8: Pre-chamber combustion and jet characteristics for different levels of hydrogen enrichment.

Table 5.1: Pre-chamber burn durations.

Case	**Combustion duration [CAD]**
λ = **1.6**	22.8
λ = **1.9 + 2.5% H_2**	24.4
λ = **1.9 + 4.0% H_2**	22.7
λ = **1.9 + 5.0% H_2**	20.7

Results of the pre-chamber combustion and jet characteristics are shown in Figure 5.8. Here, the worsening of the HRR profile when moving from stoichiometric to λ=1.6 conditions is again observed, both reducing the maximum burning rate and increasing the combustion duration. However, with the hydrogen addition, the HRR profile no longer worsens when further increasing the air-dilution up to λ=1.9. As expected from the preliminary studies, the combustion profiles of the three levels of H_2 are very similar to the λ=1.6 case, achieving a slight improvement of 2 CAD in the combustion duration when considering 5% of hydrogen, as shown in Table 5.1. It can be seen that none of the diluted cases is able to achieve a suitable pressurization due to the very slow combustion process.

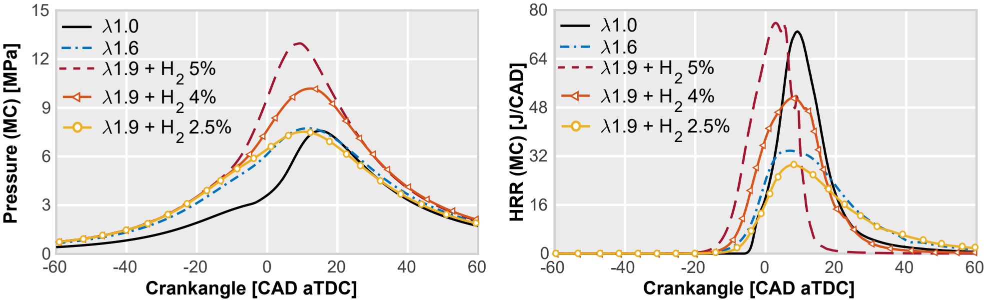

Figure 5.9: Main chamber combustion features for different levels of hydrogen enrichment. The simulated pressure profile and HRR are included.

The former remark is confirmed when analyzing the penetrations (referenced to the moment of ejection) plotted at the bottom of Figure 5.8, which correspond to the jet with the longest distance to travel within the main chamber. The faster combustion of the stoichiometric simulation results in considerably better jet features when compared to the lean cases, achieving much higher penetration rates in the first stages of the ejection process and reaching a higher maximum value in less time.

Moving on, the analysis of the main chamber combustion features in terms of in-cylinder pressure and HRR is presented in Figure 5.9. From these graphs it can be seen that, despite the initial assessment from the 1D flame speed calculations, adding 5% of hydrogen allows to achieve a similar combustion profile to the λ=1 case operating at λ=1.9. However, the main chamber ignition onset of the aforementioned hydrogen enriched lean case is advanced, leading to an increased pressure profile and a higher engine efficiency (around a 3% gain).

Thereafter, as the percentage of hydrogen enrichment decreases, the combustion tends to deteriorate. Nevertheless, even the smallest amount of H_2 considered in this study (2.5%) is able to burn at λ=1.9 similarly to the experimental dilution limit using pure gasoline. Thus, it is feasible that just by adding 2.5% of hydrogen in the intake port, the dilution limit could be extended up to $\lambda \sim$1.9.

Figure 5.10 shows the root causes of the observed combustion enhancement. In the left plot, the laminar flame speed is depicted. Here, the time scale is referred to the spark timing of each case. In the first stage, during the pre-chamber combustion, a large gap in the laminar flame speed is observed between the lean cases and the stoichiometric case. However, as

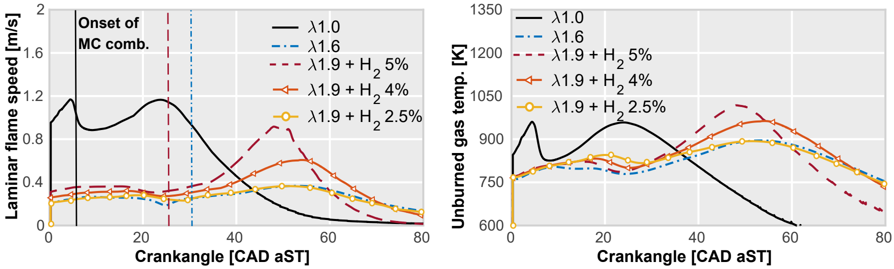

Figure 5.10: Laminar flame speed and temperature of unburned gases for the H_2 sweep. The time scale is referenced to the spark timing of each simulation.

expected from the 1D studies presented in Figure 5.6, the difference between the laminar flame speed of the dilution threshold (λ=1.6) and H_2-enriched cases (with 2.5%, 4% and 5%, respectively) is practically negligible when the flow temperature is kept constant. This is confirmed by inspecting the right-side graph of Figure 5.10, where the temperature of unburned gases is plotted and no remarkable differences are observed for the lean cases during the first stages of the combustion process. On the contrary, the laminar flame speed significantly increases after the onset of combustion in the main chamber, and the gap among the diluted cases becomes wider. This is attributed to the increase of the unburned gas temperature as the flame starts to develop in the main chamber. During this combustion stage, the temperature of fresh gases reaches higher values as the amount of hydrogen is progressively incremented. This effect causes an increase in the main chamber burn rates that, in some cases, can even exceed the values of the stoichiometric simulation (as was observed in Figure 5.9).

A detailed visualization of the main chamber combustion process is shown in Figure 5.11, in order to analyze the characteristics of the flame propagation in this region. The λ=1, λ=1.6 and λ=1.9 + 5% H_2 cases were considered. As with Figure 5.2, the heat release was colored by the source term of the energy equation to track the flame front, and the jet boundaries are highlighted as a green contour line. It is clearly observed in the ignition sequence of the stoichiometric case how the combustion is initially sustained by the jets, which helps to boost the early phases of the flame propagation. For the lean cases however, the poor jets play a small roll in the first stages of ignition, and the onset of combustion in the main chamber occurs later. In both lean cases the flame is able to progress outside of the jet boundaries, nevertheless, it

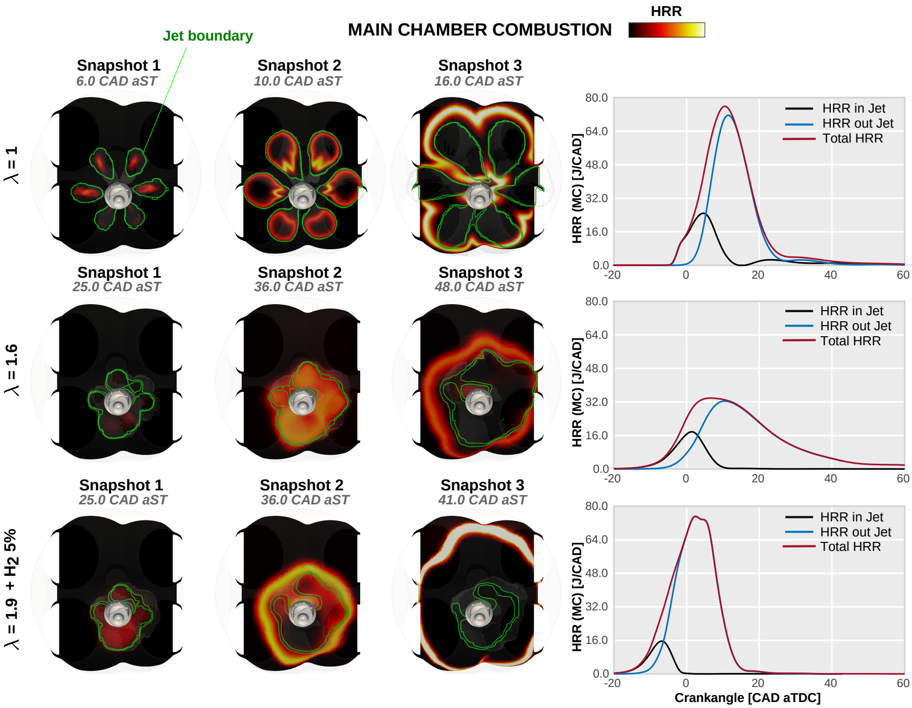

Figure 5.11: Main chamber ignition visualization at λ=1, λ=1.6 and λ=1.9 + 5% H_2. The HRR inside/outside of the jets is included besides each snapshot sequence

is noticeable that for the hydrogen enriched case the flame leaves the jets at an earlier stage, and progresses more actively due to the enhanced thermochemical properties of the mixture in the combustion chamber.

This last statement can also be observed in the plots on the right-side of Figure 5.11, which show the temporal evolution of the main chamber HRR for each case, considering the amount of energy released inside and outside of the jet boundaries. Both the λ=1 and λ=1.9 + 5% H_2 simulations follow the same trend, releasing a minor part of the total energy (less than 20%) inside the jets. However, the energy released within the jets for the hydrogen-enriched case is almost half of the corresponding energy of the stoichiometric case. This changes considerably the trend that was discussed for the λ=1.6 case in Figure 5.2, where over 30% of the combustion process took place within the jets due to the unfavorable conditions in the main chamber mixture.

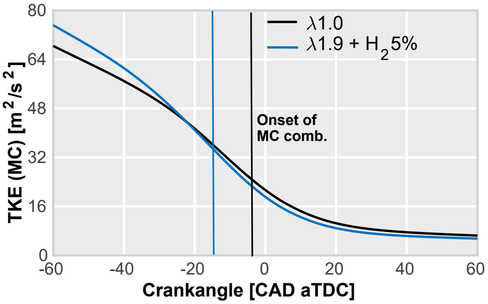

Figure 5.12: Main chamber TKE profiles for the non-reacting simulations of the λ=1 and λ=1.9 + 5% H_2 cases.

Another interesting remark comes from analyzing Figure. 5.12, where the spatially-averaged values of turbulent kinetic energy in the main chamber are plotted for the non-reacting simulations of the λ=1 and λ=1.9 + 5% H_2 cases. Small differences are observed between both curves, since the internal aerodynamics of the cylinder depends mostly on the intake port design and the engine running point (load/speed), which remain unchanged for the two simulations. However, the gap between the onset of combustion in the main chamber for both cases shows that the main chamber TKE levels are higher for the lean case. Thus, when enriching the mixture with 5% of hydrogen, not only the thermochemical properties favor the combustion process, but also the higher TKE levels at the onset of the main chamber combustion contribute to increase the burning rates.

In Figure 5.13 a Borghi-Peters diagram [6, 7] is included for analyzing the flame structure evolution of the λ=1, λ=1.6 and λ=1.9 + 5% H_2 cases. The computation of the required variables for generating this diagram (u', S_L, l_t and l_f) was explained at the end of Section 4.1.2. The colored dots represent the time frame respect to the spark timing of each simulation.

The stoichiometric combustion progresses initially in the *thickened wrinkled flames* regime, where the Kolmogorov scales are larger than the flame thickness and are thus only able to corrugate the flame, keeping a suitable structure for most of the operating conditions studied in SI engines. Later on, due to the nature of the passive pre-chamber combustion concept, the flame shifts momentarily towards the *thickened flames* regime, where some eddies can penetrate into the diffusive layer of the flame, enlarging the flame thickness and compromising its stability. However, after the main chamber

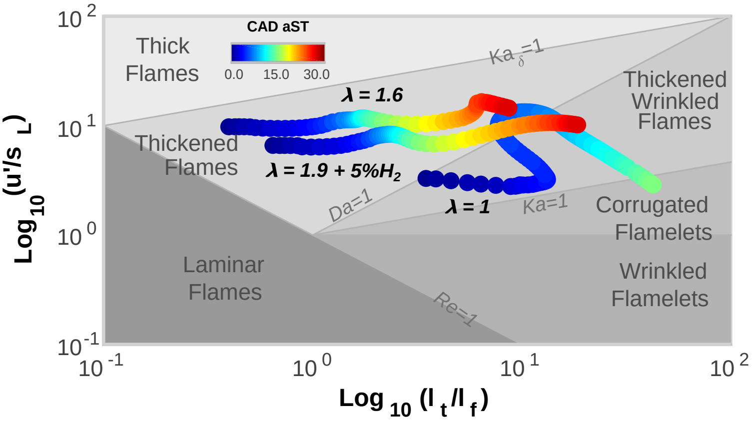

Figure 5.13: Evolution of the flame structure during the combustion process for the λ=1, λ=1.6 and λ=1.9 + 5% H_2 simulations.

combustion onset, the flame quickly stabilizes and returns to the *thickened wrinkled flames* regime.

On the other hand, the λ=1.6 case begins in a less favorable region of the diagram, deeper into the *thickened flames* regime. It can be seen that during the considered time frame, the flame of the λ=1.6 case is not able to shift towards the *thickened wrinkled flames* regime, showing that an important part of the combustion process takes place in conditions where the flame stability is compromised.

Moreover, the hydrogen enriched case improves slightly the initial flame structure when compared to the λ=1.6 case. Recalling Figure 5.6, this improvement is due to the combination of higher laminar flame speeds and lower flame thickness values. At the end of the hydrogen-enriched curve, the flame structure passes the Damköhler=1 line, progressing to a more favorable region of the diagram. Thus, the properties of H_2 can inherently help to achieve a more stable combustion process even at extremely diluted conditions.

Finally, Table 5.2 presents the indicated efficiency levels of the performed simulations. As it can be seen, the pressure profile generated in the λ=1.9 + 5% H_2 case increases the indicated efficiency by 3.6% with respect to the stoichiometric simulation, proving that despite introducing the same amount of energy, the combination of the employed technological bricks (high air-dilution, passive pre-chamber ignition and H_2 addition) provides considerable benefits in terms of engine performance.

Table 5.2: Indicated efficiency for the H_2 simulations.

Case	**Ind. efficiency** [%]
$\lambda = \mathbf{1}$	43.48
$\lambda = \mathbf{1.6}$	42.39
$\lambda = \mathbf{1.9 + 5\%\ H_2}$	47.12
$\lambda = \mathbf{1.9 + 4\%\ H_2}$	44.92
$\lambda = \mathbf{1.9 + 2.5\%\ H_2}$	42.07

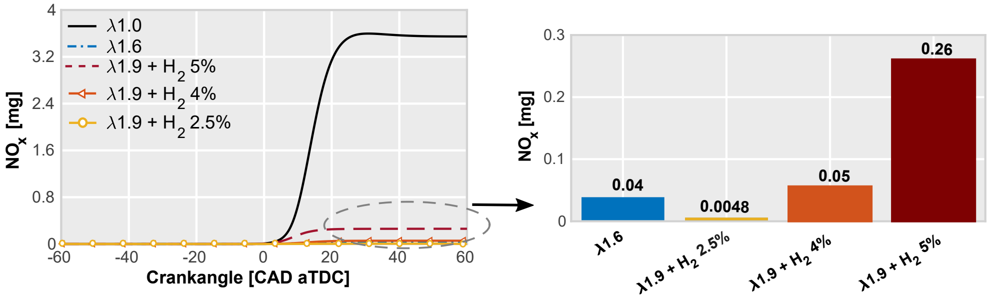

Figure 5.14: NO_x formation in the cylinder for all the simulated cases. The bar graphs represent the NO_x values of each lean case at the end of the simulation.

Additionally, the formation of NO_x in the cylinder is shown for each simulated condition in Figure 5.14. The left-side plot depicts the NO_x evolution during the closed cycle, while the right-side bar graphs show the final NO_x values of each lean case. Clearly, diluting the mixture with air considerably reduces the NO_x emissions with respect to the stoichiometric simulation. However, increasing the amount of hydrogen enrichment further increases the NO_x formation. This fact is due to the higher temperatures reached during the combustion process (discussed in Figure 5.10).

Nevertheless, an interesting analysis can be made by comparing the NO_x emissions of the hydrogen enriched cases with the λ=1.6 case. In this comparison, The NO_x values increase significantly (about seven times higher) by adding 5% of hydrogen. However, these values barely change when considering 4% of H_2, where the thermal efficiency of the engine is 1.5% higher than the stoichiometric case. Moreover, the NO_x emissions are reduced almost by a factor of ten just by considering 2.5% of H_2 enrichment. These results are encouraging as in the aforementioned condition the efficiency levels of the engine are maintained within a suitable range (over 42%).

Furthermore, this study has shown a potential strategy for operating the engine under conditions lean enough to achieve very low NO_x emissions without the use of the Three-Way Catalyst, while keeping high levels of efficiency. Nevertheless, this must be complemented with experimental activities that will be carried out in future research works.

5.2 Characteristics of the passive pre-chamber combustion with EGR dilution

The second part of this chapter focuses on analyzing the passive pre-chamber combustion characteristics when diluting the mixture with exhaust gases (EGR). This combination is very interesting since the mixture composition with EGR is still able to keep a stoichiometric air-to-fuel equivalence ratio, and thus the strategy is compatible with the TWC for controlling the engine NO_x emissions. Therefore, the validated CFD simulations at an intermediate dilution level (10% of EGR) and at the dilution limit (20% of EGR) were compared with the un-diluted stoichiometric simulation at medium load/speed conditions, following the same procedure that was used in Section 5.1.2, where the pre-chamber combustion features were first studied and afterwards their impact over the main chamber combustion.

5.2.1 Study of the concept at different EGR levels

Figure 5.15 shows the pre-chamber HRR traces, the Δp and the laminar flame speeds of the three considered simulations. From the burning profiles it is observed that the onset of combustion advances as the EGR rate increases. This is again due to the inherent need to trigger the spark at an earlier stage for higher dilution levels, in order to achieve a suitable combustion phasing in the main chamber. Thus, while the un-diluted case has a spark timing of -12 CAD, the EGR cases trigger the ignition at -17 CAD and -40 CAD respectively. Furthermore, the longer combustion duration and the reduced HRR peak as the EGR level rises are in part due to the loss of laminar flame speed shown at the bottom of the figure, which is again a product of the higher internal residuals as the spark is advanced and the higher external residuals added in the intake port.

Moreover, the pre-chamber pressurization is also compromised as the EGR rate increases. For the dilution limit (20% EGR), the pressure build up is extremely slow, which has a relevant impact on the ejected jets as will be

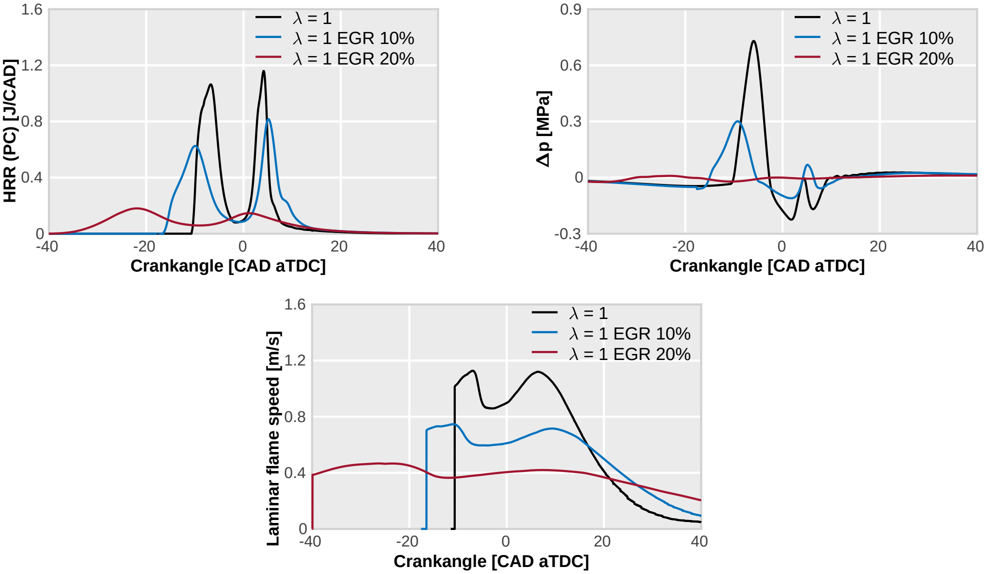

Figure 5.15: Pre-chamber combustion features for different EGR rates.

seen later. Nevertheless, the case with 10% of EGR is still able to generate a relatively fast Δp profile, but with a peak value that is less than half of the un-diluted case.

Going further in the pre-chamber combustion analysis, Figure 5.16 shows a visualization of the flame development in this region for the three simulations. It is interesting to note that the flame morphology is quite similar between the un-diluted and EGR=10% cases, with a similar ignition and propagation sequence and a modest temporal offset due to the slower burning rates of the diluted simulation. However, the flame thickness of the EGR=10% case is slightly enlarged with respect to the flame at stoichiometric conditions without EGR. This can be better appreciated in the snapshot sequence of the dilution threshold, where a clear flame front is never fully established and the combustion pattern pays resemblance to a homogeneous charge ignition. In this case, the flame thickness is considerably larger, and the ejection of reactive products is extensively delayed.

In order to elaborate on the former remark, Figure 5.17 presents the energetic analysis of the pre-chamber combustion process for the three simulations. The top plot shows the pre-chamber fuel scavenge during the compres-

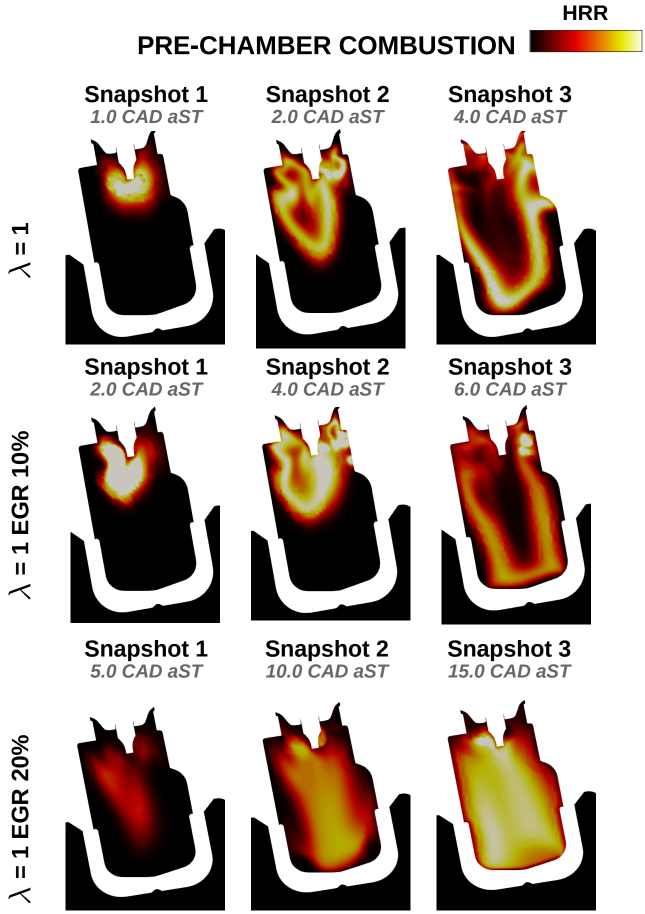

Figure 5.16: Visualization of the pre-chamber combustion in stoichiometric conditions with and without EGR dilution.

sion stroke, and similarly to what was observed in the air dilution analysis, the EGR=20% case starts with significantly less energy due to the advanced spark timing. The bottom bar graphs show the absolute energy values at the start of combustion (left) and the relative share of the four energy parameters to the total energy of each case (right). The EGR=10% simulation has a very moderate deterioration of the pre-chamber energy management, showing slightly higher energy losses in non-reacting (Inert) and unburned conditions since the flame speeds are slower. On the other hand, the impact of the worsened combustion process is more notable for the EGR=20% case, where almost 40% of the fuel is left unburned at the end of the main ejection. In this case however, the fuel lost under cold/non-reacting conditions is considerably reduced, as a

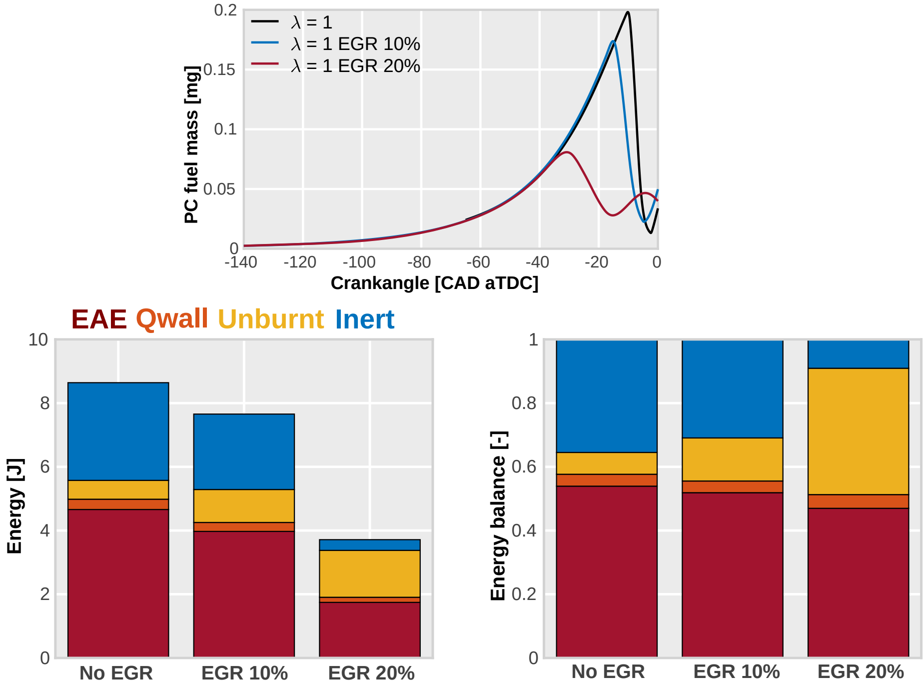

Figure 5.17: Energy conversion during the pre-chamber combustion process for different EGR rates.

consequence of the slower pressurization of the pre-chamber that delays the inversion of the flow as combustion develops in this region.

Moving on, a visualization of the main chamber combustion process is presented in Figure 5.18, along with the HRR profiles inside/outside of the jets for each simulation. In accordance to what was discussed in Figure 5.16, the ignition sequence for the un-diluted case and the simulation with 10% of EGR follow the same trend, showing a jet-driven combustion pattern which is moderately delayed for the latter case. Additionally, the enlargement of the flame thickness for the EGR=10% simulation is again observed (at least qualitatively). Nevertheless, both cases still burn the major part of the main charge outside of the jet limits.

Moreover, the flame evolution for the case with 20% of EGR is very different. Firstly, due to the slow pre-chamber combustion, the jet penetrations are contained in a small part of the main chamber. In addition, there is a considerable delay after the spark timing for the main chamber ignition to occur

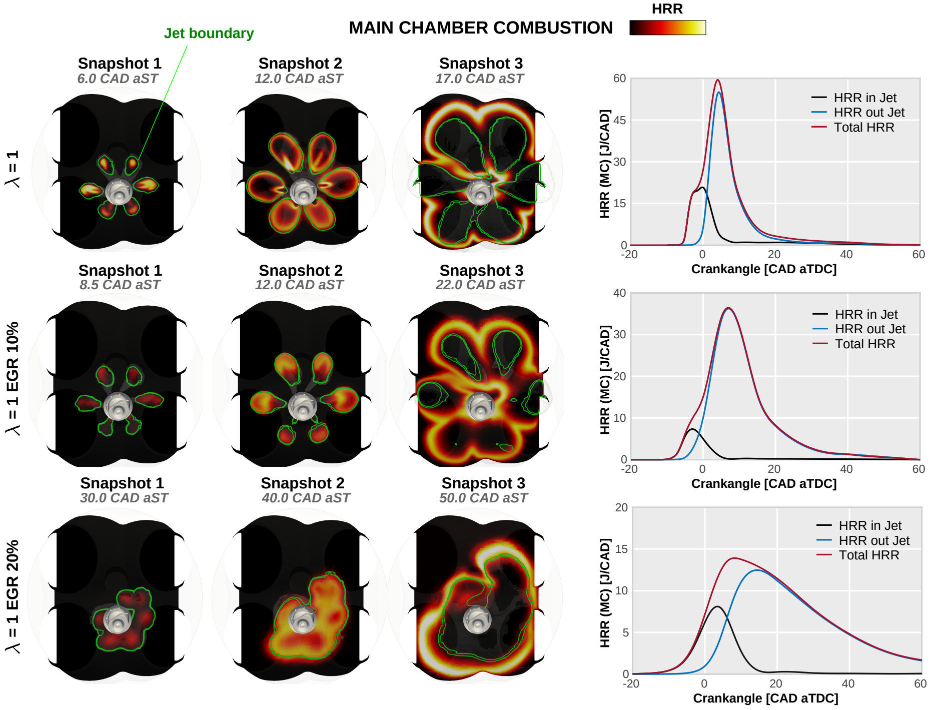

Figure 5.18: Main chamber combustion visualization for different EGR rates at stoichiometric conditions. The HRR inside/outside of the jets is included besides each snapshot sequence.

(around 25 to 30 CAD). Afterwards, as the combustion takes place inside of the jets, a significant enlargement of the flame is observed, taking up to 50 CAD after the ignition signal for a regular flame front to leave the jet boundaries. This pattern is numerically represented in the HRR plot, where a larger part of the combustion process develops inside of the jets when compared to the previous cases.

Finally, an analysis of the flame structure is presented in the Borghi-Peters diagram of Figure 5.19. Here, the characteristic multi-regime evolution of the flame is again observed for the un-diluted stoichiometric simulation, where the flame shifts briefly from the *thickened wrinkled flames* to the *thickened flames* regime as the jets penetrate into the main chamber, and then returns to a stable region of the diagram. What's more, the simulation with 10% of EGR shows a similar behavior. In this case the combustion begins in the *thickened flames* regime, but the flame is able to pass the Damköhler=1 line even before

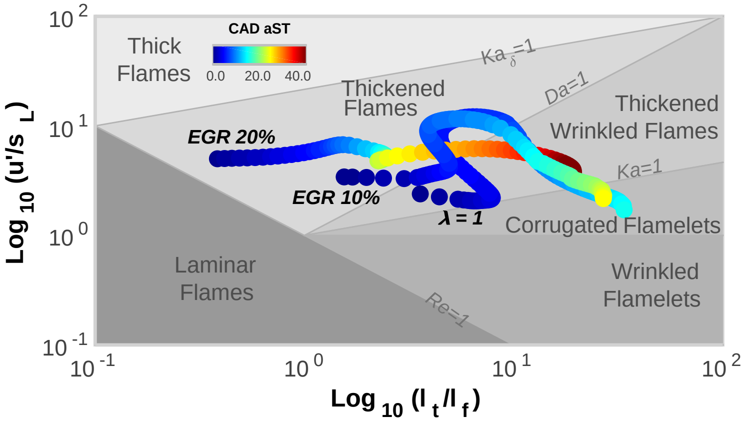

Figure 5.19: Evolution of the flame structure during the combustion process for the stoichiometric simulations with different EGR rates.

the pre-chamber combustion has ended. Thereafter, the particular loop of the passive pre-chamber concept is again perceived before the flame finishes developing in the *corrugated flamelets* regime.

On the other hand, the simulation with 20% of EGR shows a similar pattern to the one observed for the air-dilution threshold. In this case, the flame begins deep into the *thickened flames* regime, a very unfavorable region where the turbulent eddies can cause the flame extinction. However, the flame is still able to progress towards the *thickened wrinkled flames* regime in these conditions after approximately 30 CAD. Nevertheless, as a relevant part of the combustion process takes place in compromised conditions, slightly increasing the EGR rate can lead to an increased number of misfiring cycles and high levels of CCV.

5.2.2 Issues of the passive pre-chamber concept with EGR

Although the characterization of the passive pre-chamber concept at the EGR dilution threshold has shown similar tendencies to the air-dilution limit in terms of pre-chamber energy management, main chamber combustion pattern and evolution of the flame structure, using EGR has intrinsic drawbacks when compared to lean burn. One of these disadvantages is highlighted in the work of Benajes et al. [8] and presented in Figure 5.20, where the laminar flame speed and flame thickness computed from 1D simulations are shown for several air and EGR dilution levels, keeping the same pressure and temperature in

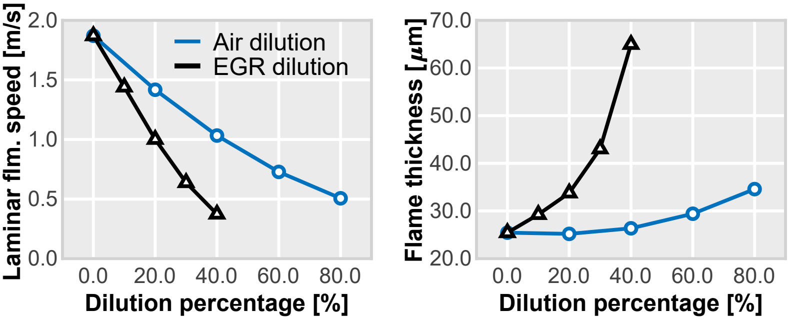

Figure 5.20: Laminar flame speed and flame thickness for different air and EGR dilution rates keeping the same mixture temperature and pressure [8].

the mixture. It is clearly seen that the flame properties are more sensitive to EGR, which consequently advances the dilution threshold and limits the potential benefits of this strategy for improving the overall performance of the engine.

However, the technological and economical convenience of EGR (since it can be used with the TWC) has made it a crucial strategy for the technical definitions of future SI engines. Thus, if the passive pre-chamber system is to be integrated in these vehicles, the synergies with EGR dilution must also be optimized. This leads to the most important issue of this combination, which was briefly discussed in Section 4.3.1 of Chapter 4, namely, the difficulty to achieve the same dilution limit as the conventional SI concept.

Figure 5.21 shows the results of the EGR sweep performed in the engine test campaign for several pre-chamber geometries and the SI system. Here, the aforementioned issue is highlighted, where PC1 and PC2 reach the dilution threshold much sooner than the regular spark plug, since after 20% of EGR a minimum rise of the dilution rate causes inadmissible CCV levels. This is due to the internal residuals of the pre-chamber, which depend on the pre-chamber design (as was explained in Section 4.3.1). Nevertheless, the benefits of the pre-chamber system in terms of indicated efficiency, HC and CO emissions are clearly observed in Figure 5.21. Therefore, a dedicated optimization of the pre-chamber geometry in order to achieve a best-case scenario where the internal residuals of the pre-chamber are close to the levels of residuals in the main combustion chamber, is an important thought to consider when designing passive pre-chambers for passenger car applications. This will be further elaborated in the next chapter.

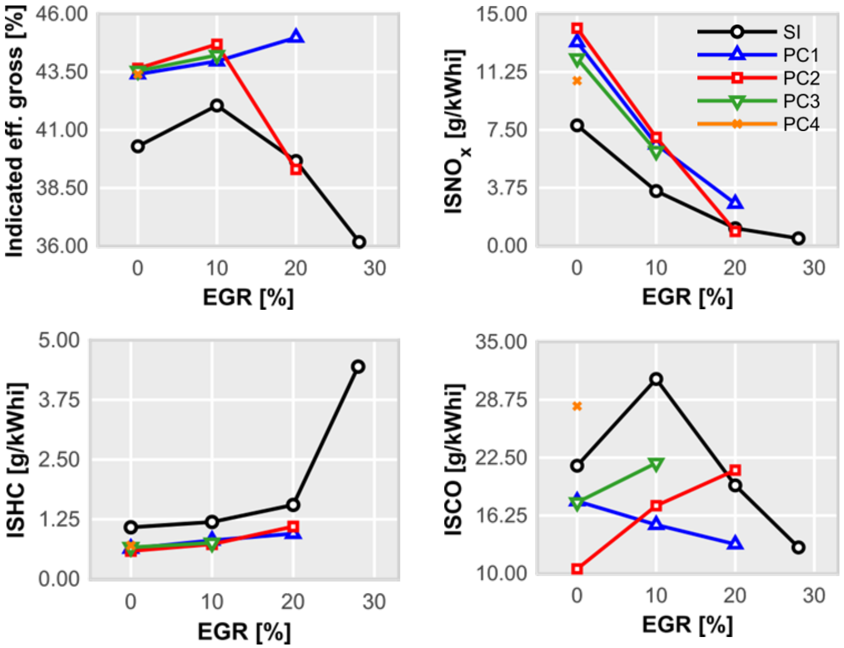

Figure 5.21: Experimental results for the EGR dilution sweep. The indicated efficiency, NO_x, HC and CO emissions are shown for the 4 pre-chamber designs used in the test campaign and the conventional SI system.

5.3 Summary

The combination of the passive pre-chamber concept with dilution strategies (both lean burn and EGR) has been evaluated in this chapter. For this purpose, a dedicated analysis of the combustion features in both chambers was performed with the CFD model, focusing on the fundamental differences between the flame evolution in un-diluted stoichiometric conditions and at the experimental air/EGR dilution thresholds.

From the experimental campaign it was observed that some pre-chamber designs were able to extend the air-dilution limit with respect to the conventional SI concept from λ=1.4 to λ=1.6, allowing to achieve similar $\mathrm{NO_x}$ emissions while keeping high levels of efficiency. However, these $\mathrm{NO_x}$ values were still not low enough to operate the engine without the use of the Three-Way Catalyst.

Furthermore, the simulation at λ=1.6 revealed a remarkable difference in the main chamber flame morphology with respect to the un-diluted case. while the stoichiometric simulation showed a jet-driven ignition pattern, the diluted case resembled a convention spark-ignition process, due to the deteriorated jet features. This is attributed to two main aspects that stem from the need of advancing the ignition signal to achieve a suitable CA50 in the main chamber. The first is the lower energy for producing the ignition, since the pre-chamber is filled with less fuel for advanced spark timings, and the second is the loss of flame speed due to the lean mixture composition and the higher internal residuals as the spark is advanced. Therefore, enhancing the thermochemical properties of the mixture to achieve higher laminar flame speeds arises as an interesting solution for overcoming the limitations of the concept at the dilution threshold.

In order to test the former remark, a special study was carried out by enriching the gasoline fuel with small amounts of hydrogen. Thus, a preliminary 0D/1D study was performed, and it was determined that adding up to 5% of H_2 (in volume fraction with respect to the total air) could allow to recover the laminar flame speeds of λ=1.6 by running the engine at λ=1.9. Hence, three simulations were configured in the CFD model to evaluate different levels of hydrogen enrichment (2.5%, 4% and 5%), keeping the total energy constant to make a fair comparison (reducing the amount of gasoline as the H_2 increased). The same spark timing as the λ=1.6 case was considered for the hydrogen simulations at λ=1.9.

Results from these studies showed a similar pre-chamber combustion and jet features between the hydrogen enriched cases and the λ=1.6 simulation with pure gasoline, which was expected from the preliminary 1D studies since the initial thermodynamic conditions (pressure/temperature) between these simulations were more or less the same. However, as the combustion started to develop in the main chamber, the burning profiles were considerably accelerated as the H_2 level increased. Particularly, the λ=1.9 + 5% H_2 case was able to achieve a similar HRR compared to the un-diluted stoichiometric simulation, leading to an elevated pressure profile and an indicated efficiency rise of approximately 3.5%. This combustion enhancement was a consequence of the higher temperatures of unburned gases reached in the cylinder as the hydrogen enrichment was increased.

Moreover, the addition of H_2 also showed and improvement in the flame structure evolution compared to the dilution threshold with pure gasoline (λ=1.6). In this case, although both simulations started in the *thickened flames* regime of the Borghi diagram, the λ=1.9 + 5% H_2 case enabled to shift the flame towards the *thickened wrinkled flames* regime in an earlier time frame, allowing the combustion process to develop in more stable conditions.

Ultimately, the NO_x emissions from the hydrogen simulations were estimated, and it was found that although the λ=1.9 + 5% H_2 case achieved higher levels of efficiency, the increased temperatures in the main chamber led to a considerable rise in the values of NO_x. However, the case with 2.5% of hydrogen allowed to keep relatively high levels of indicated efficiency (above 42%) while reducing the NO_x emissions almost by a factor of ten with respect to the λ=1.6 simulation.

Regarding the use of EGR, it was observed that for moderate dilution rates (EGR=10%) the flame evolution in both chambers followed the same trend as the stoichiometric case without EGR, with a relatively fast pre-chamber combustion (around 6 to 7 CAD) and a jet-driven ignition in the main chamber. On the contrary, the dilution threshold (EGR=20%) showed very different flame patterns. In this case, the combustion process in the pre-chamber was considerably slower, compromising the jet features, delaying the ejection of reactive products and leaving a significant amount (close to 40%) of unburned fuel in this region at the beginning of the backflow. What's more, the ignition sequence of the pre-chamber resembled a homogeneous charge ignition, with an enlarged flame thickness and without a clearly established flame front as the combustion progressed in this region. Afterwards, the ignition of the main chamber showed a similar behavior to the air-dilution threshold (λ=1.6), with the jets contained in a reduced portion of the main chamber and the flame developing within the jet limits for an extended period of time (over 40 CAD after the ignition signal) before leaving these boundaries as a regular SI flame front. Consequently, an important part of the combustion process develops in an unfavorable region of the Borghi diagram (the *thickened flames* regime).

Diluting the mixture with exhaust gases has inherent disadvantages with respect to air-dilution, given that the thermochemical properties of the flame are more sensitive to EGR. However, as this strategy has already been integrated into production vehicles, since it is fully compatible with the TWC, it is a key aspect of the technical definitions for future SI engines. This poses an important hurdle for integrating the passive pre-chamber concept, given that achieving the same EGR dilution limits as the conventional SI system is complicated with this ignition strategy. Therefore, special attention needs to be payed to optimizing the pre-chamber geometry in order to achieve a suitable scavenge of internal residuals (to keep them at a similar level as the main chamber residuals), but without compromising the pre-chamber combustion process or the jet ejection features.

References

[1] Benajes, J et al. “Computational assessment towards understanding the energy conversion and combustion process of lean mixtures in passive pre-chamber ignited engines”. In: *Applied Thermal Engineering* 178 (2020), p. 115501. DOI: `https://doi.org/10.1016/j.applthermaleng.2020.115501`.

[2] Iafrate, Nicolas, Matrat, Mickael, and Zaccardi, Jean-Marc. “Numerical investigations on hydrogen-enhanced combustion in ultra-lean gasoline spark-ignition engines”. In: *International Journal of Engine Research* 22.2 (2021), pp. 375–389.

[3] Benajes, J, Novella, R, Gomez-Soriano, J, Barbery, I, and Libert, C. “Advantages of hydrogen addition in a passive pre-chamber ignited SI engine for passenger car applications”. In: *International Journal of Energy Research* 45.9 (2021), pp. 13219–13237. DOI: `https://doi.org/10.1002/er.6648`.

[4] Liu, Yao-Dong, Jia, Ming, Xie, Mao-Zhao, and Pang, Bin. “Enhancement on a skeletal kinetic model for primary reference fuel oxidation by using a semidecoupling methodology”. In: *Energy & Fuels* 26.12 (2012), pp. 7069–7083. DOI: `https://doi.org/10.1021/ef301242b`.

[5] Broatch, A, Olmeda, P, Margot, Xandra, and Gómez-Soriano, Josep. “Numerical simulations for evaluating the impact of advanced insulation coatings on H2 additivated gasoline lean combustion in a turbocharged spark-ignited engine”. In: *Applied Thermal Engineering* 148 (2019), pp. 674–683.

[6] Borghi, R. “On the structure and morphology of turbulent premixed flames”. In: *Recent advances in the Aerospace Sciences*. Springer, 1985, pp. 117–138.

[7] Poinsot, Thierry and Veynante, Denis. *Theoretical and numerical combustion*. RT Edwards, Inc., 2005.

[8] Benajes, J et al. “Evaluation of the passive pre-chamber ignition concept for future high compression ratio turbocharged spark-ignition engines”. In: *Applied Energy* 248 (2019), pp. 576–588. DOI: `https://doi.org/10.1016/j.apenergy.2019.04.131`.

Chapter 6

Methodology for designing passive pre-chambers

"Without engineering, science is just philosophy", this phrase was written on a poster in the first office I started working in when my PhD studies began. However, this quote is not meant to discredit any of the hard sciences (who knows where humans would be without them), but rather to state that the synergies between theoretical constructs and engineering applications have always been necessary in order to achieve technological breakthroughs that push our society forwards. In the context of this research project, a lot of knowledge has been generated during Chapters 4 and 5 about the behavior and physico-chemical characteristics of the passive pre-chamber concept, and what better way to close this thesis than to develop a real-world application for the acquired knowledge.

Therefore, this chapter will present a methodology that was devised during this investigation to design and optimize the geometry of passive pre-chambers for passenger car applications, based on the combination of different numerical tools. The design process begins by explaining the way in which the 0D/1D models described in Sections 3.2.2 and 3.2.3 of Chapter 3 were combined to select a set of initial candidates that are able to generate, at least in principle, better jet features (momentum/penetrations) than those obtained with the reference pre-chamber (PC1 in Table 3.4). Subsequently, the CFD model is used to refine more detailed aspects of the pre-chamber geometry, and obtain a design that is able to fulfill the expected requirements in terms of combustion performance and tolerance to EGR dilution. Finally, the validation of this design methodology will be shown, presenting the results obtained in the test bench after manufacturing the optimized pre-chamber and installing it on the single-cylinder engine.

6.1 Implementation of the methodology

6.1.1 General outline of the pre-chamber design process

Before proceeding to explain the design process, it is important to highlight the most relevant conclusions drawn from Chapters 4 and 5 regarding the behavior and fundamentals of the passive pre-chamber concept, in order to understand the conceptual orientation of the designs obtained through the application of this methodology.

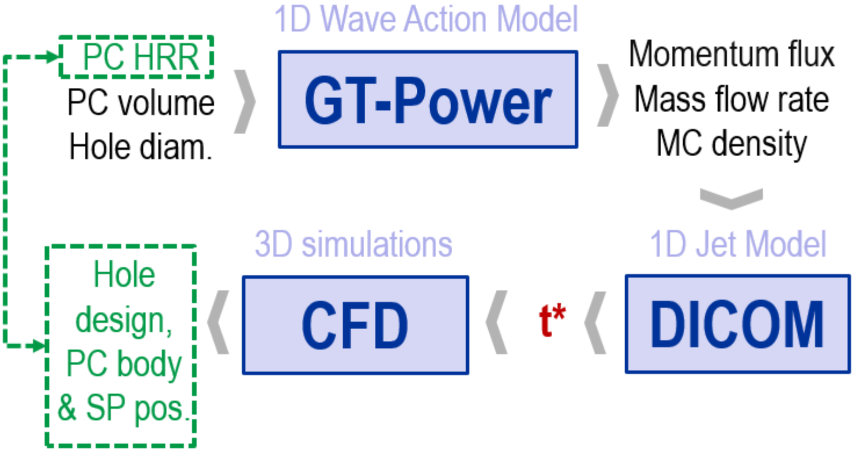

Figure 6.1: Pre-chamber design methodology workflow.

To optimize the performance of the passive pre-chamber ignition strategy two main aspects are required, on one hand, quickly consuming all of the charge contained within the pre-chamber volume, thus achieving a large sum of momentum flux evacuated through the holes and an early ejection of reactive products that are able to promote the main chamber ignition, and on the other hand, generating optimum conditions inside the pre-chamber in terms of turbulence and scavenging of residual gases, to improve the synergies of the concept with other engine strategies such as dilution with EGR and spark timing delay at low load/speed conditions.

With these two ideas in mind, a design procedure that allows to evaluate a large number of pre-chamber geometries in a reasonable period of time was developed, through the combination of the 0D/1D and CFD tools presented in the diagram of Figure 6.1. This procedure is based on using the outputs from one numerical tool as inputs for the following model, either to perform the next set of simulations or to verify the validity of the obtained results. With this methodology it has been possible to simulate fifty pre-chamber geometries in two engine operating points (high and low load/speed conditions), and carry out the optimization process until a final design in only three weeks. The workflow consists of three phases that will be explained below:

6.1.2 Description of each phase of the methodology

Phase 1: Selection of the pre-chamber geometric macroparameters (GT-Power + DICOM)

Since there are so many nuances regarding the design of the pre-chamber, this phase focuses on selecting the geometric macroparameters (volume and hole diameter) that are able to provide the best features in the ejected jets. For this purpose, the 0D/1D model of the engine (GT-Power) and the 1D gaseous jet model (DICOM) were used to evaluate a wide array of pre-chamber volumes and hole diameters for a specific number of pre-chamber nozzles. It is important to highlight that this phase was initially developed in another ongoing PhD thesis [1, 2], and it is complemented in this research work with the detailed CFD simulations performed during the following phases of the design methodology. Therefore, the development of the 0D/1D tools and the hypothesis/procedures considered during this stage will be better described in the aforementioned thesis, as well as the extracted conclusions.

In this investigation, a design of experiments (DOE) was proposed for the simplified simulations, considering a volume range between 600 mm^3 and 1200 mm^3 and a diameter range of 0.5 mm to 1.5 mm for 6 holes. Thus, applying the Full Factorial method, fifty combinations of pre-chamber volumes and hole diameters were obtained, resulting in one hundred cases for the initial set of 0D/1D calculations at high load speed conditions (12.8 bar IMEP @4500 rpm) and low load/speed conditions (2.8 bar IMEP @1350 rpm).

As was explained in Section 3.2.2, a very important detail of the GT-power simulations was the lack of a predictive model for the pre-chamber combustion, given that a pressure transducer for this region was not available and the diagnostics could only be performed from the in-cylinder pressure signal. Therefore, the pre-chamber HRR for these calculations was imposed by a Wiebe profile, modifying the combustion duration and maximum combustion rate. Particularly, the hypothesis considered for this design methodology was to keep the pre-chamber combustion as fast as possible, regardless of the pre-chamber volume. Thus, a fixed burn duration of 12 CAD was determined from previous experiences with the CFD model as a suitable length for the pre-chamber HRR. This assumption was evaluated in later stages with the 3D-CFD simulations, in order to verify that the selected pre-chambers are able to burn in a similar time frame compared to the reference design (PC1).

Thereafter, the flow properties obtained from the GT-Power simulations (mass flow rate, jet momentum flux and main chamber density) are used as inputs for the 1D gaseous jet model (as shown in Figure 6.1) to obtain the jet penetrations. Moreover, in order to quantify the impact of the jets in a simple way, the parameter t* has been defined, which represents the time that a free jet needs to reach the farthest wall distance of the main chamber (most unfavorable situation considering the asymmetric installation of the pre-chamber over the cylinder head) [2].

Figure 6.2 shows the results of a study where artificial profiles have been generated from a reference momentum flux profile (in black) by modifying the duration (α) and the peak value (β). Thus, the penetrations obtained in the right-side plot from the 1D simulations show the t* associated to each momentum profile, highlighting the importance of generating a fast combustion (high momentum peak and short duration) for the jets to reach the walls in a reduced time frame.

Finally, the maximum momentum flux values and the t* of each simulation are analyzed and used to pre-select a set of initial candidates to be evaluated in the following stages with the CFD model.

Phase 2: Evaluation of the design candidates and fine tuning of the final pre-chamber (CFD-RANS)

After selecting the initial candidates it must be verified that the designs are capable of fulfilling the requirements set in the first phase, namely, that the combustion process within the pre-chamber develops as quickly as possible. Therefore, during this second phase the proposed designs are implemented and simulated in the validated CFD model for each operating condition, in order to account for the real physics of the internal flow field and obtain a more reliable estimation of the flame development within this volume. The new geometries are then compared with the reference pre-chamber in terms of combustion

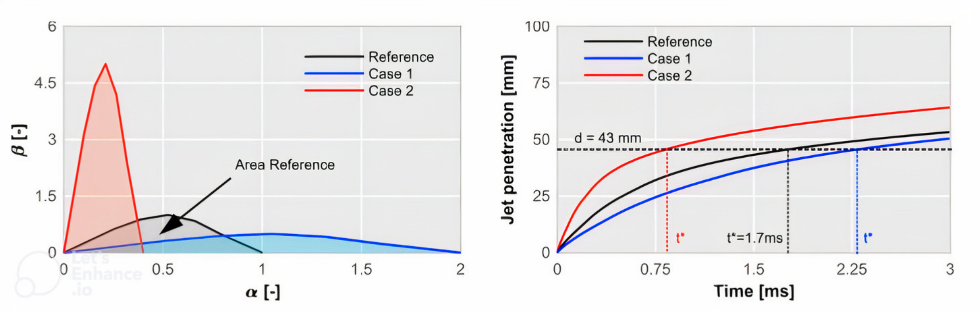

Figure 6.2: Definition of t^*.

duration, to discard those designs that are not able to consume the whole pre-chamber charge in a similar time frame than that of PC1. Finally, a candidate is selected for a final tuning of more detailed aspects of the geometry, such as the layout of the pre-chamber holes and the position of the electrodes.

Phase 3: CCV analysis of the final design (CFD-LES)

In the last phase, the optimized design is evaluated using the multi-cycle LES methodology developed in Chapter 4 to qualitatively compare the combustion stability with this new pre-chamber geometry against the reference pre-chamber. These simulations allow to better capture the details of turbulence and the flow-field variations between consecutive cycles, however, the required computational cost is considerably higher. For this reason, only the pre-chamber combustion was considered, and the CCV levels were quantified with the τ parameter defined in Section 4.3.5.

6.2 Application of the methodology

6.2.1 Phase 1 results

This section summarizes the results obtained after performing the one hundred 0D/1D calculations of the DOE corresponding to phase 1 of the methodology. The simulations were carried out at high load/speed and low load/speed conditions (fifty cases in each point). Figure 6.3 shows the jet penetrations for each case, highlighting with a horizontal dashed line the wall distance for determining the t*. From here, it is clearly seen how at high load/speeds (left-side plot)

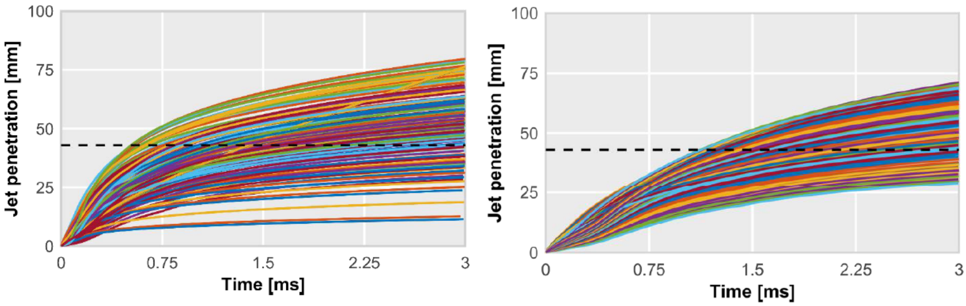

Figure 6.3: Jet penetrations obtained from the 50 1D jet simulations at high load speed conditions (left) and low load speed conditions (right) respectively.

the penetration rates are faster for several combinations of pre-camber volume and hole diameter, achieving earlier t* values compared to those obtained at low load/speed conditions (right-side plot).

Moreover, in order to better assess the numerical results, Figure 6.4 shows in the upper part the color maps for the maximum momentum flux values obtained from the GT-Power simulations, while in the lower part the color maps for t* are presented. All of the maps are plotted with the defined ranges for the pre-chamber volume and hole diameter.

The most interesting aspect observed in these graphs is how the optimum zone in terms of jet momentum and t* changes for both operating conditions. Furthermore, although it is true that the optimum regions are always found at higher volumes, which makes sense since the combustion duration is fixed and, as the volume increases, a greater amount of energy is available within the pre-chamber, it is clearly seen that operating at high engine load/speeds the ideal hole diameters are in a range of 1.1 mm and 1.3 mm, while at low load/speed conditions the diameters that give the best jet performance are around 0.7 mm. This leads to a very important conclusion: The design requirements of the pre-chamber change depending on the engine running point, which means that for a suitable performance of the concept in the entire engine map, a compromise solution (geometry) must be selected among the optimum pre-chambers in each operating condition.

Thus, the t* maps are used to simplify the determination of the compromise designs between the simulated operating points. In these graphs, several relevant iso-lines of t* are highlighted in black, translated into a crankangle time frame for each operating condition. From the experience gathered

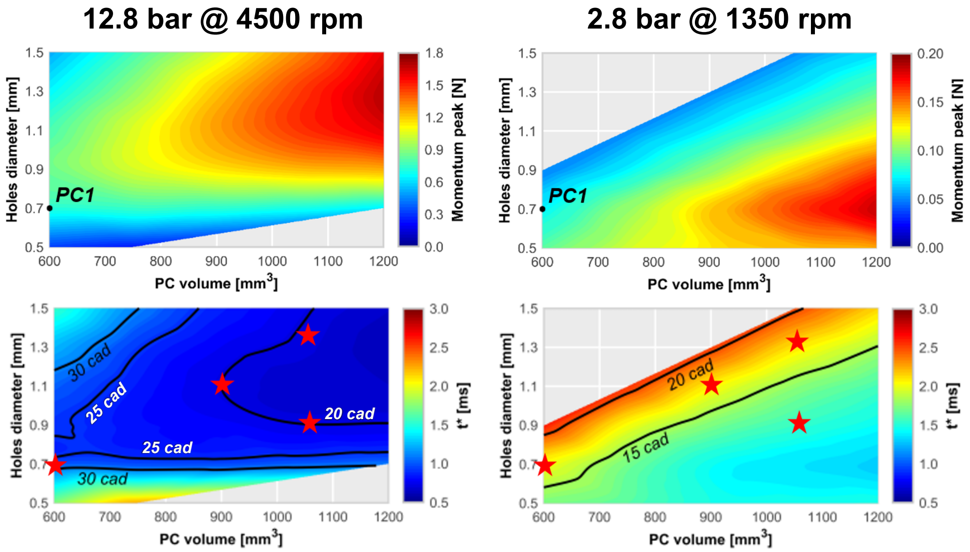

Figure 6.4: Color maps of maximum momentum flux and t obtained from the 0D/1D simulations at high load speed conditions (left) and low load speed conditions (right).*

during the experimental campaign and the CFD simulations of Chapter 4, it has been found that an optimum duration for the ejection process in this engine is around 20 CAD, regardless of the operating point. Therefore, the selected designs must comply with this restriction. In this way, three possible candidates have been identified and marked with red stars in the t* maps of Figure 6.4, along with the reference pre-chamber. It is clearly observed that in the high load/speed map the three designs are located in the iso-line of 20 CAD, however, at low load/speed conditions, it can be seen that one of the designs is much closer to the optimum zone for this operating point (t* $<$ 15 CAD).

The characteristics of the pre-chambers marked in Figure 6.4 are summarized in Table 6.1. These are the candidates selected from this initial phase to be evaluated in detail with the CFD model along the following stages.

Table 6.1: Initial design candidates from the first phase of the methodology.

ID	Volume [mm^3]	Holes [-]	Diameter [mm]	A/V ratio [1/m]
PC1	**600**	**6**	**0.7**	**3.9**
PCv900d1.1	900	6	1.1	6.3
PCv1050d0.9	1050	6	0.9	3.6
PCv1050d1.3	1050	6	1.3	7.6

6.2.2 Phase 2 results

The second part of the design methodology consists on simulating the pre-chambers obtained from phase 1 using the validated CFD model in the selected operating conditions. Thus, the simulations for the new designs were initialized considering the same settings as the reference pre-chamber in the corresponding operating point, that is, the injected fuel mass, initial thermodynamic conditions in each region and spark timing were kept constant.

Figure 6.5 shows the HRR in both chambers and the cylinder pressure for the simulations at high load/speed conditions. The pre-chamber combustion profiles are morphologically similar between the four designs, with faster burning rates for PCv900d1.1 and PCv1050d0.9. What's more, the main chamber combustion onset of the aforementioned designs is similar to PC1, but the slopes of the HRR curves are higher, which also leads to more elevated pressure profiles and an increased performance. However, this is not the case for PCv1050d1.3, given that the ignition of the main chamber is delayed with this geometry.

Moreover, the objective sought with the new designs was to burn the pre-chamber charge as quickly as possible, for which it must be verified that the combustion durations of the simulated geometries are equal to or shorter than the reference pre-chamber, thus fulfilling the hypothesis raised in phase 1 where the duration of the HRR profile was maintained for the 0D/1D simulations. For this purpose, Table 6.2 presents a parameter ΔCA10-90 defined as the difference between the combustion duration of each design and the combustion duration of PC1. Positive values indicate that the new pre-chamber burns slower than the reference, while negative values indicate that it burns faster. From here, it can be seen that the first two designs are relatively close to burning in the same time frame as PC1, however, the combustion duration for the last design (PCv1050d1.3) is prolonged. This explains the previously observed delay in the main chamber ignition onset.

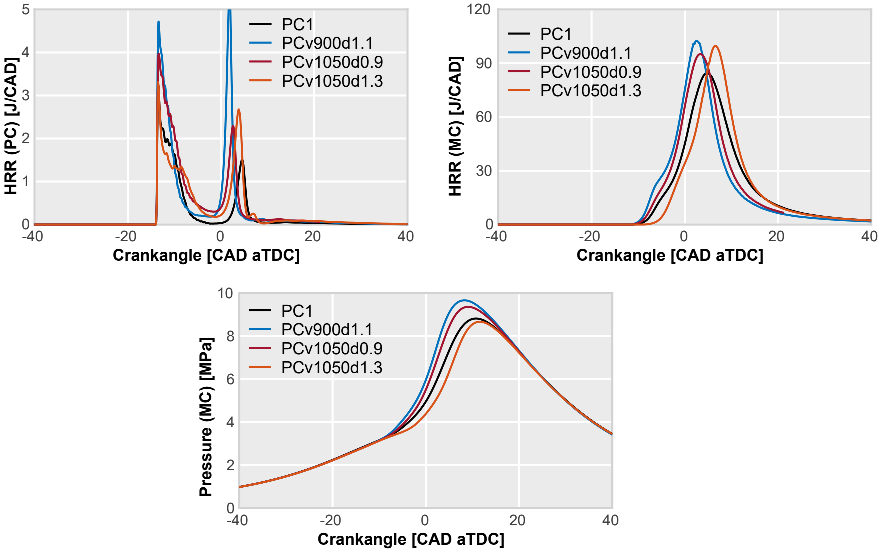

Figure 6.5: Combustion features of the new designs at high load/speed conditions.

Table 6.2: ΔCA10-90 for the new designs at high load/speed conditions.

ID	**ΔCA10-90 [CAD]**
PCv900d1.1	0.2
PCv1050d0.9	0.5
PCv1050d1.3	2.2

Going further, Figure 6.6 presents the resulting jet features for this set of simulations. In these plots, it can be appreciated how the momentum profile for PCv900d1.1 reaches higher values, since it is generated from the combination of a fast jet ejection with a high mass flow rate. On the other hand, the momentum flux values for PCv1050d0.9 and PCv1050d1.3 are at similar levels, given that the latter pre-chamber has increased mass flow rates (due to the bigger holes) but considerably slower jet velocities as the combustion process within this design is slower. Ultimately, the penetration rates for PCv900d1.1 are much faster, and due to the combination of these enhanced jet features and the fast pre-chamber combustion, the main chamber burning rates are accelerated, as was shown in Figure 6.5.

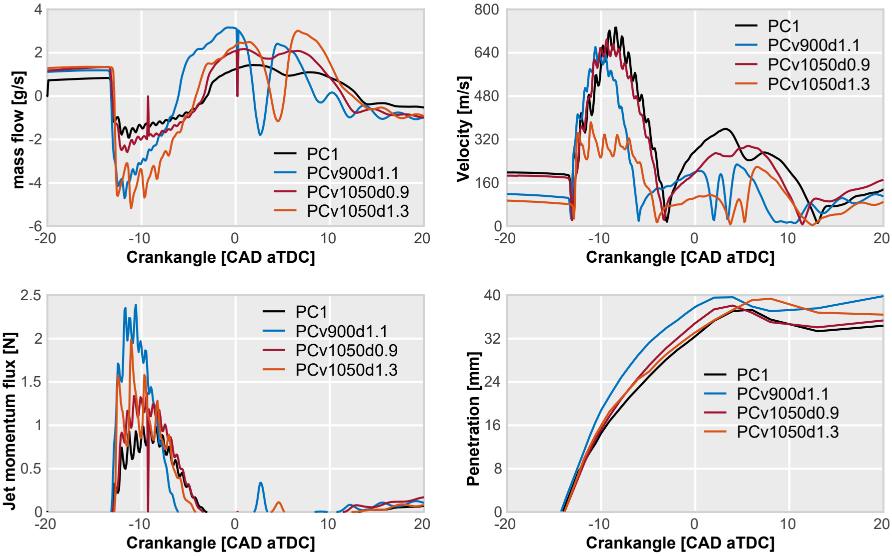

Figure 6.6: Jet features of the new designs at high load/speed conditions.

Performing the same study in a more compromised operating point (2.8 bar IMEP @1350 rpm) reveals very interesting trends. Recalling the analysis conducted in Section 4.2, at low load/speed conditions the amount of fuel in both chambers is reduced and both the scavenging of residuals and generation of turbulence are deteriorated, which can inherently cause issues for pre-chambers with large volumes. Furthermore, Figure 6.7 shows the combustion features of the new pre-chamber designs in the aforementioned operating point. From the pre-chamber HRR profiles it can be seen that, although the burning rates achieved with the new geometries are higher than PC1, the CA50 values are delayed. Consequently, the ignition of the main chamber is also retarded, specially for PCv1050d1.3 where the onset of combustion is produced very close to the TDC.

Table 6.3: ΔCA10-90 for the new designs at low load/speed conditions.

ID	ΔCA10-90 [CAD]
PCv900d1.1	-2.3
PCv1050d0.9	-2.5
PCv1050d1.3	1.7

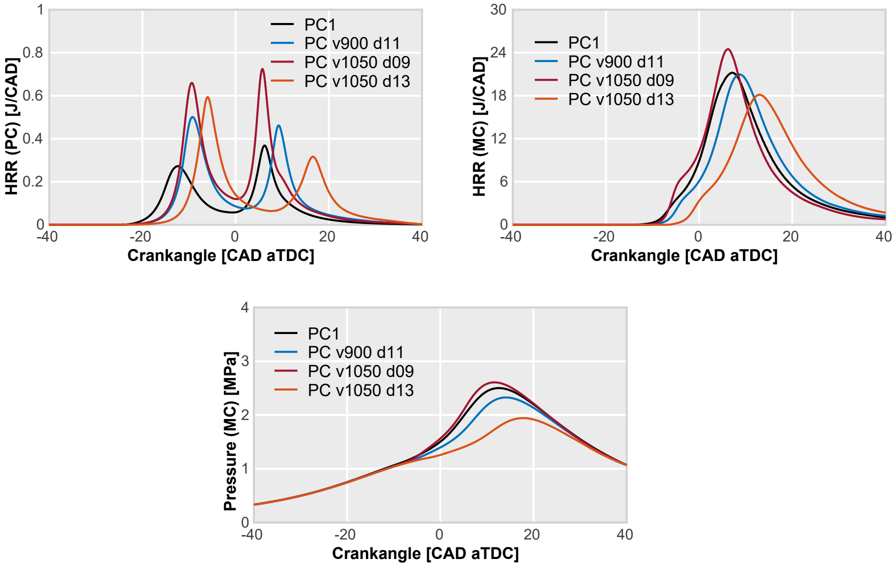

Figure 6.7: Combustion features of the new designs at low load/speed conditions.

Another interesting trend is found in Table 6.3. In these conditions, PCv900d1.1 and PCv1050d0.9 are able to burn faster than the reference design according to the ΔCA10-90 values, fulfilling the hypothesis considered for the 0D/1D simulations. Particularly, PCv1050d0.9 is able to generate a similar main chamber ignition onset compared to PC1, despite the delayed combustion in the pre-chamber. However, this is not the case for PCv900d1.1, where the combustion onset in the main chamber is slightly delayed, hindering the improvement of the engine performance as can be seen by the pressure profiles of Figure 6.7.

Moreover, Figure 6.8 shows the jet features of the simulated pre-chambers. From here, it can be observed that the delayed ignition of the pre-chamber also causes an offset in the ejection process. Thus, even though the peak momentum flux values are increased for the new designs, the penetration curves are delayed. Nevertheless, the penetration rates of the jets generated with PCv1050d0.9 allow to reach a farther distance in less time compared to the PC1 jet. This matches the results found in phase 1 of the methodology, where the performance of PCv1050d0.9 was expected to provide greater benefits at low load/speed conditions. Therefore, as this design has proven to be suitable

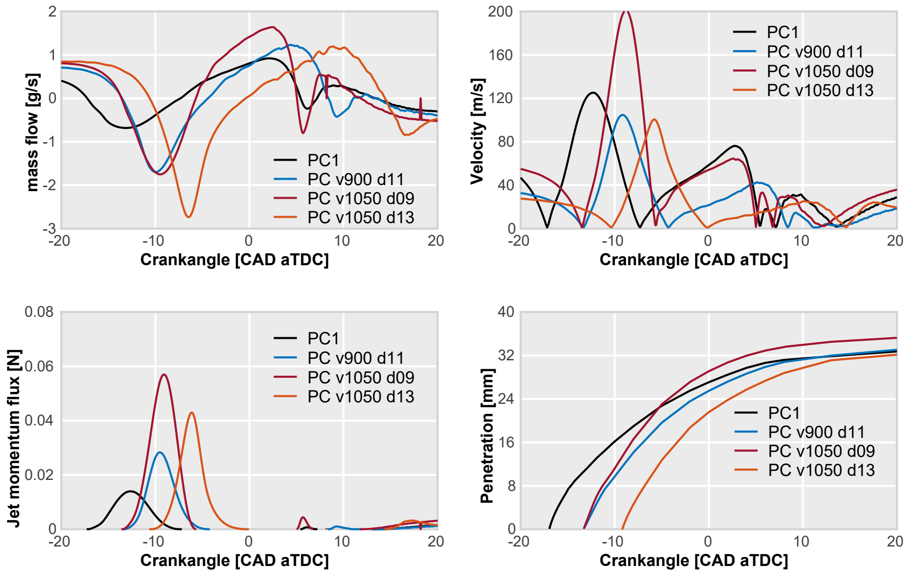

Figure 6.8: Jet features of the new designs at low load/speed conditions.

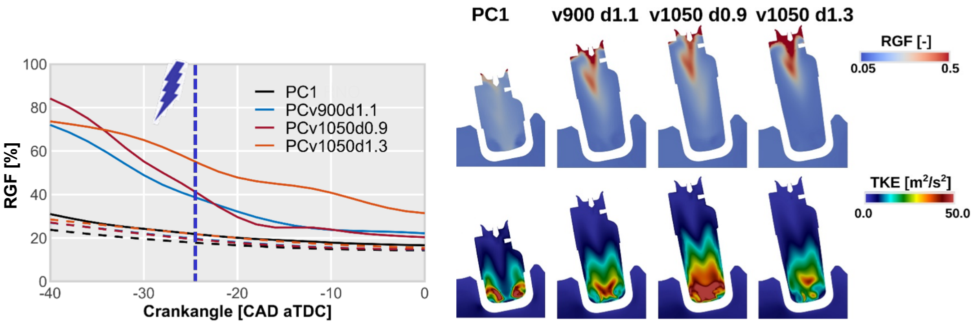

Figure 6.9: Stratification of residual gases and turbulence field at the spark timing for low load/speed conditions.

for both simulated operating points, it was selected as the best candidate to test in the real engine. However, the optimization process does not end here.

To shed further light on the aforementioned issue of the delayed pre-chamber combustion at low load/speed conditions, Figure 6.9 presents the temporal evolution of the residual gases in this region, highlighting the moment of ignition with a vertical line. The dashed curves represent the RGF averaged in the whole pre-chamber volume, while the solid lines correspond to the residuals averaged in a 1 mm side box located at the spark plug gap. Additionally, the local stratification of the RGF and the turbulence field at the spark timing are shown in the right-side snapshots. These images reveal the root cause of the retarded ignition onset in the pre-chamber, since the amount of residuals at the top of the large volume pre-chambers are considerably higher than the reference design, the initial stages of the combustion process are compromised. This represents a potential issue for the compatibility with EGR dilution, given that this strategy requires the spark to be advanced, causing the initial flame for the large volume designs to encounter even higher levels of residuals at the ignition timing. Nevertheless, PCv1050d0.9 is still able to achieve fast burning rates in the later stages of the combustion process, in part due to the higher TKE levels generated with this design at the bottom of the pre-chamber. Therefore, it is worth to evaluate alternatives for improving the scavenge of residuals with this design, thus extending the tolerance to the use of EGR.

The first alternative that was tested was to optimize the axial position of the electrodes. Since most of the residuals are stored in the upper part of the pre-chamber, it is logical to think that having the electrodes located in this area would be unfavorable for the first stages of the flame development. However, if the electrodes are placed closer to the holes, the regions with high concentrations of residual gases can be avoided. Following this idea, multiple simulations were carried out lowering the electrodes of PCv1050d0.9 in steps of 1 mm with respect to the initial location. Thus, Figure 6.10 shows the results of these simulations, plotting the residuals averaged in a 1 mm side box located at the spark plug gap, starting from 3 mm below the initial position. This figure also includes the RGF values for the reference pre-chamber in a dashed black line.

It can be seen that lowering the electrodes from 8 mm to 11 mm can significantly improve the scavenge of residual gases in the proximities of the spark plug for the new design, particularly in the range of -40 CAD to -10 CAD where the RGF values are kept below the levels of PC1. However, previous studies performed by Thelen et al. [3] have shown that it is not ideal to position the electrodes to close to the holes, as this could compromise the pressurization of the pre-chamber. In addition, having the spark plug near the pre-chamber bottom also causes the initial flame to encounter higher levels of turbulence (as can be seen in the bottom images of Figure 6.10), which could lead to an early flame extinction due to the blowing of the spark glow. For this reason, it was decided to place the electrodes 8 mm below the reference

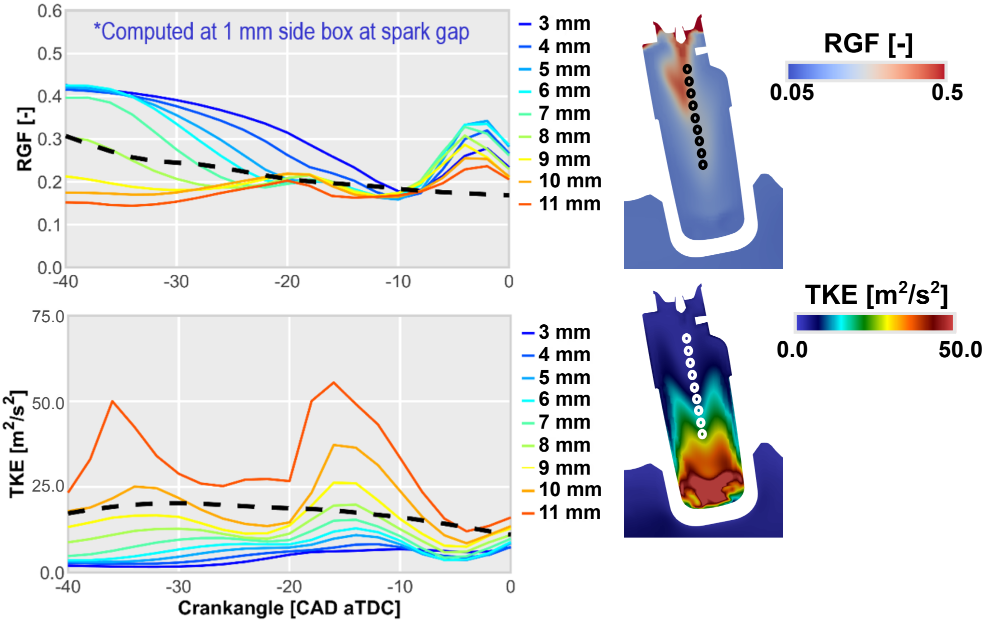

Figure 6.10: RGF and TKE evolution for the spark plug position sweep.

position, as it provides a good balance between the scavenging of residuals and the levels of TKE.

Thereafter, a combustion simulation was performed with the new spark location of PCv1050d0.9, and the results of this case are presented in Figure 6.11. It is clearly observed how the new spark plug position advances the ignition onset of the pre-chamber, while still managing to achieve a fast combustion process and higher burn rates compared to PC1. consequently, the jet ejection is also pushed forwards, leading to an early main chamber ignition and a considerable rise in the pressure profile. This study has shown the potential of optimizing the spark location for improving the performance of the concept.

Another strategy that was evaluated was the use of a central hole in the lower part of the pre-chamber. The idea with this design parameter is to have a flow pattern oriented towards the center of the pre-chamber (where the electrodes are located), in order to better sweep the residual gases in this direction. An investigation carried out by Sens et al. [4] proved that having a big hole in the pre-chamber bottom allows to improve the compatibility with spark timing delay. Additionally, Blankmeister et al. [5] performed studies

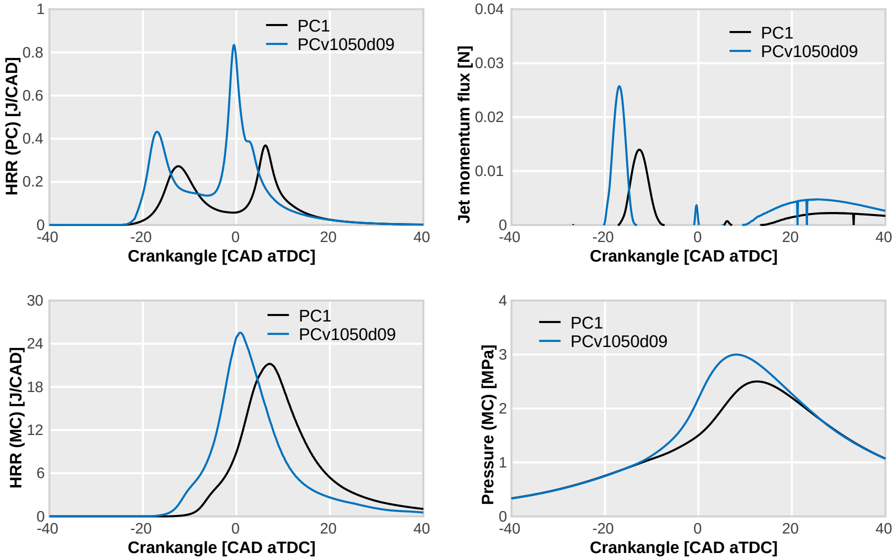

Figure 6.11: Results of the simulation with the new spark location of PCv1050d0.9 at low load/speed conditions.

with different pre-chamber configuration with a bottom hole, and found that having a slightly bigger diameter in the bottom orifice than the side-holes can provide benefits in terms of combustion performance, as long as a suitable A/V ratio is kept.

Thus, in order to implement this strategy and compare it with the original design of the PCv1050d0.9, the size of the 6 side-holes was reduced from 0.9 mm to 0.8 mm, in order to maintain the total A/V ratio after adding a 1 mm hole in the pre-chamber bottom. This new design was then simulated under the same conditions as PCv1050d0.9 at low engine load/speed, both with the electrodes at the top (without considering the optimization of this parameter). These results are shown in Figure 6.12, where the presented snapshots are taken at the spark timing. It can be seen that adding the central hole reduces the stratification of the RGF in the central and lower part of the pre-chamber, despite still having high concentrations of residual gases at the top. Additionally, the left-side plot shows the RGF evolution in a 1 mm side box at the spark location. From here, it is found that adding the hole at the bottom also achieves a better scavenge of the electrodes over

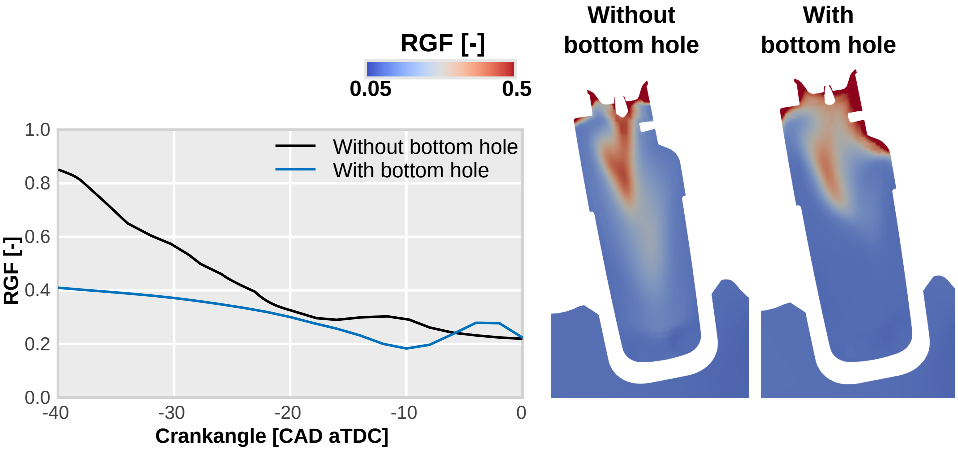

Figure 6.12: Scavenging of residual gases for PCv1050d0.9 with the addition of a bottom hole at low load/speed conditions.

a wide range of crankangles (from -40 to -10 CAD), even without optimizing the spark plug position.

These results are quite encouraging since by improving the scavenging of residuals inside the pre-chamber, particularly in the area of the electrodes and in wide ranges of crankangles, the concept's tolerance to EGR dilution can be increased. For this reason, it was decided to make these two final adjustments to the original design of the PCv1050d0.9 to obtain an optimized pre-chamber: Lowering the electrodes 8 mm with respect to the original position and adding a central hole of 1 mm by reducing the size of the side-holes to keep the pre-chamber A/V ratio. Thus, the final design is shown in Figure 6.13, where the most important characteristics are presented and also the specific aspects that each design parameter helps to improve.

6.2.3 Phase 3 results

Finally, since the hole layout of the optimized design (labeled as PCv1050d0.9opt) has been changed, the impact on cyclic variability must be evaluated to guarantee a suitable performance of the concept in terms of combustion stability, particularly at low engine load/speeds and EGR diluted conditions. Therefore, the last phase of the design process consists on performing multi-cycle LES simulations of PCv1050d0.9opt, following the

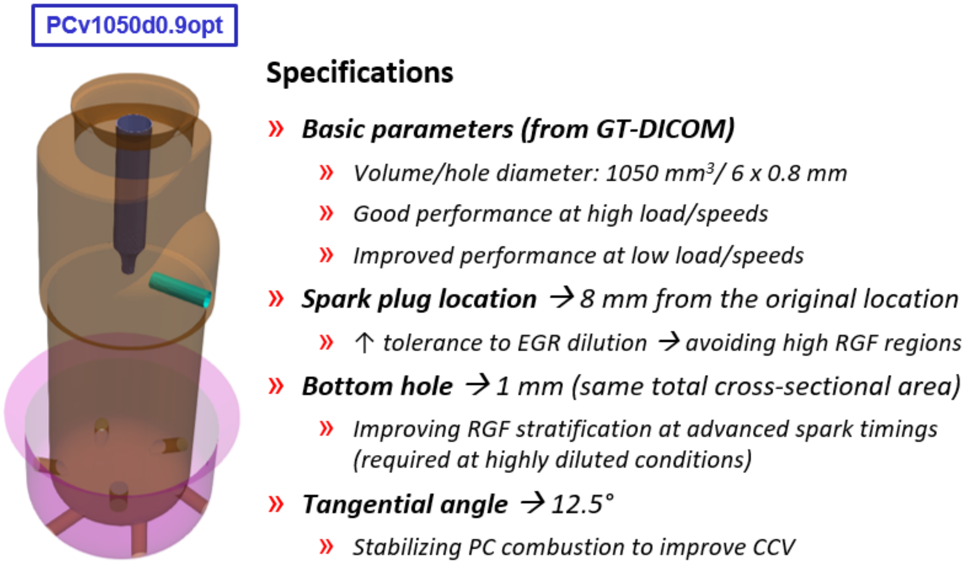

Specifications

- ***Basic parameters (from GT-DICOM)***
  - *Volume/hole diameter: 1050 mm^3/ 6 x 0.8 mm*
  - *Good performance at high load/speeds*
  - *Improved performance at low load/speeds*
- ***Spark plug location** → 8 mm from the original location*
  - *↑ tolerance to EGR dilution → avoiding high RGF regions*
- ***Bottom hole** → 1 mm (same total cross-sectional area)*
  - *Improving RGF stratification at advanced spark timings (required at highly diluted conditions)*
- ***Tangential angle** → 12.5°*
  - *Stabilizing PC combustion to improve CCV*

Figure 6.13: Specifications of the optimized design.

methodology developed in Section 4.3.5 of Chapter 4 for evaluating the CCV of passive pre-chambers.

This methodology attributes the cyclic dispersion phenomena to changes in the pre-chamber flow-field and the combustion process in this region. This way, only the pre-chamber is simulated, reducing considerably the computational domain and enabling the use of a very fine mesh for performing multiple high-fidelity LES simulations in a reasonable period of time. Thus, the non-reacting calculation of the optimized design is initialized at the IVC with the same mixture stratification and thermodynamic conditions coming from the open-cycle RANS simulation at low load/speed conditions. Thereafter, ten cycles are calculated, and two instantaneous solutions are generated in each cycle for performing the subsequent combustion simulations, corresponding to the crankangles of -20 CAD (reference spark timing) and -5 CAD, to evaluate the tolerance of the new pre-chamber to spark timing delay. Additionally, both PCv1050d0.9opt and PC1 are simulated at medium load/speed conditions (6.8 bar IMEP @2000 rpm) with 10% of EGR, to assess the performance of the new design with EGR dilution.

Considering that the CCV is usually evaluated for the engine indicated parameters and that in these simulations it is not possible to obtain these

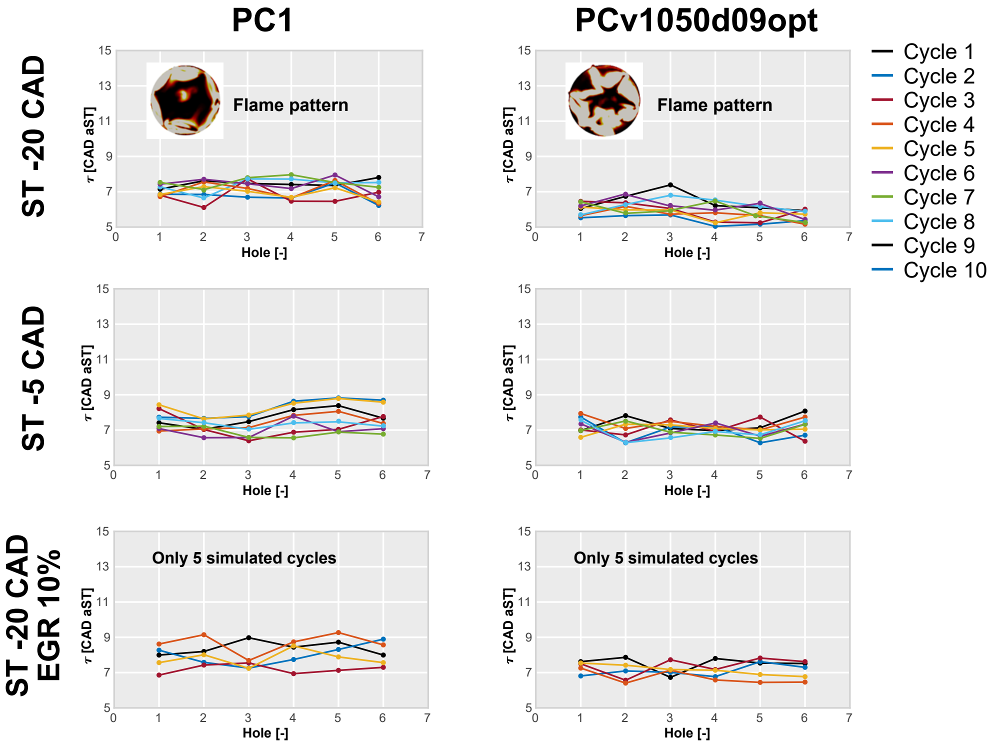

Figure 6.14: CCV study of the optimized design.

features (since only the pre-chamber combustion is simulated), a characteristic time τ was defined and validated in Chapter 4 as a suitable variable to quantify the cyclic variability. This parameter represents the time it takes for the flame to reach each hole of the pre-chamber, being related to both the main chamber combustion onset and the symmetry with which the ignition is produced.

The results of this study are summarized in Figure 6.14, where the τ values are plotted for the ten combustion cycles of PC1 and PCv1050d0.9opt at the reference and delayed spark timings. For the EGR simulations however, only five cycles were able to be calculated due limitations in the computational resources. From these graphs, it can be seen how the combustion varies not only cycle by cycle but also hole by hole. A large gap between curves indicates that there are significant cycle-to-cycle differences, while a large gap between points on the same curve indicates that the flame is reaching some holes before others.

At the reference spark timing, the stability levels of both pre-chambers are relatively similar, showing a maximum τ difference of ±1 CAD between holes and ±2 CAD between cycles. However, the τ values of the optimized design are lower than the reference, indicating that the flame reaches the holes in a shorter time frame. This is again observed at the delayed spark timing (-5 CAD), where additionally the pattern of the curves in each cycle are flatter for PCv1050d0.9opt compared to PC1, showing that the flame evolves symmetrically within the optimized pre-chamber, which leads to a uniform ignition of the main chamber. Moreover, the EGR simulations of PCv1050d0.9opt also show a better behavior in terms of combustion stability, with earlier τ values and less dispersion between cycles and between holes. Thus, this analysis has shown that the optimized design is able to maintain suitable levels of CCV at delayed spark timings and EGR diluted conditions, making it a promising candidate for improving the global performance of the passive pre-chamber concept.

6.2.4 Validation of the methodology

As a last step in the study, it is necessary to verify the validity of the developed numerical methodology for designing passive pre-chambers. For this purpose, the optimized design shown in Figure 6.13 was manufactured and installed on the engine. Subsequently, an experimental campaign was carried out to evaluate the use of this pre-chamber with EGR, in order to determine the dilution limit and confirm that the design purpose, which was to extend the tolerance to EGR dilution while keeping a good engine performance, is in fact fulfilled. It is important to point out that due to limitations in the experimental facilities, only these experiments were carried out for the optimized pre-chamber (EGR sweep at 2000 rpm and 6.8 bar IMEP).

The results of the experimental campaign are shown in Figure 6.15, where the optimized design (that was renamed as PC12) is compared with the reference pre-chamber (PC1) and the conventional SI concept. It can be seen that with PC12 the EGR dilution limit reaches 25%, where a stable pressure profile and HRR can still be achieved with low levels of COV IMEP and high combustion and indicated efficiency values. Thus, these results support the validity of the design methodology, given that the dilution limit has been extended by 5% with respect to the reference pre-chamber, that after an EGR rate of 20% begins to have critical stability issues that compromise the engine efficiency levels, which in this case are kept at similar levels as the SI concept given that in these conditions the engine is not limited by knock.

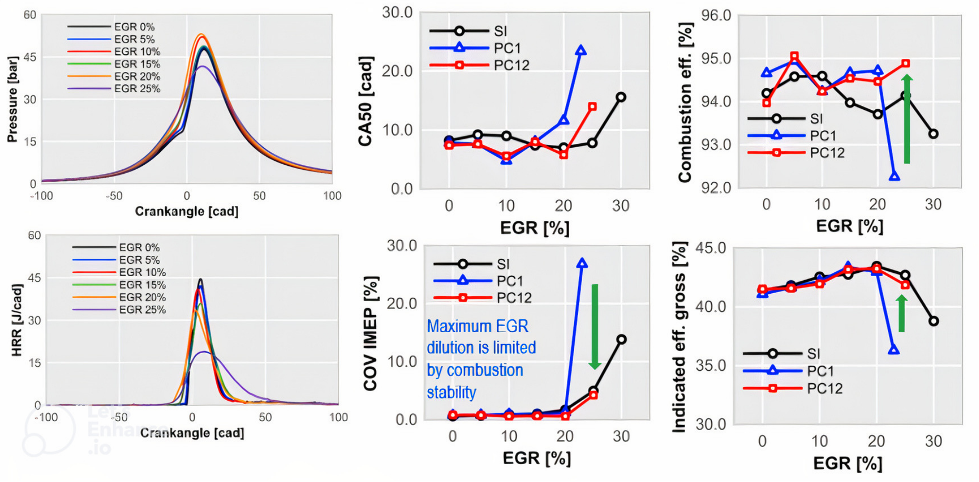

Figure 6.15: Results of the optimized design in the engine test bench at medium load/speed conditions with EGR.

This campaign has demonstrated the great value and usefulness of the design methodology developed during this research project, both for the scientific community and for real-world applications.

6.3 Summary

Along this chapter a pre-chamber design methodology for passenger car applications has been presented and validated with experimental activities. The design procedure is based on the combination of 0D/1D and CFD numerical tools to evaluate a wide set of pre-chamber geometries and perform the optimization process until a final design in a relatively short time frame (from three to four weeks with the available computational resources). Therefore, three distinct phases are defined in order to filter the pre-chamber candidates.

The first phase uses the 0D/1D model of the engine (GT-Power) and the 1D gaseous jet model that were described in Sections 3.2.2 and 3.2.3 of Chapter 3 to determine the geometric macroparameters of the pre-chamber (volume and hole diameter) that provide the best jet features (momentum, penetrations). In this part, a large number of simulations can be performed due to the reduced computational cost associated with these simple models. Thus, a design of experiments was proposed, resulting in fifty combinations of pre-chamber volumes and hole diameters for 6 pre-chamber nozzles. These fifty geometries were simulated at high load/speed conditions (12.8 bar IMEP @4500 rpm) and low load/speed conditions (2.8 bar IMEP @1350 rpm).

Particularly, an important hypothesis considered for the GT-Power simulations was to keep the pre-chamber burn duration constant regardless of the volume. This is a desired outcome given that one of the most relevant conclusions found in Chapter 4 was the need to achieve a fast pre-chamber combustion in order to take advantage of the concept. However, as the pre-chamber HRR profile is imposed by a Wiebe function for the 0D/1D simulations, this hypothesis must be verified in later stages with the 3D-CFD model considering the real physics of the combustion process.

After performing the GT-Power calculations, the obtained flow properties (mass flow rate, jet momentum flux and main chamber density) were used as input for the 1D gaseous jet simulations. From this model, the jet penetrations were obtained for each combination of pre-chamber volume and hole diameter. Thereafter, a parameter t* was defined in order to quantify the impact of the jets, which represents the time that a free jet needs to reach the farthest wall distance of the main chamber.

The results from this first phase revealed that the optimum regions for the jet features are found at high pre-chamber volumes, as long as a fast pre-chamber combustion is achieved. However, these regions change in terms of hole diameter depending on the operating condition. For high load/speeds, diameters between 1.1 mm and 1.3 mm provide a better performance, while at low load/speed conditions the optimum diameters are in the range of 0.7 mm to 0.9 mm. Therefore, three initial candidates were selected that are able to keep t* values below 20 CAD for both operating points, in order to assess their performance in more realistic simulations using the CFD model.

In the second stage of the methodology the selected pre-chambers from phase 1 were implemented in the validated CFD model for the considered operating conditions. Here, the pre-chamber burn durations for the new designs were contrasted against the reference pre-chamber (PC1 in Table 6.1), and it was found that two of the proposed candidates (PCv900d1.1 and PCv1050d0.9 in Table 6.1) are able to burn in a similar time frame compared to PC1, fulfilling the hypothesis considered for the 0D/1D calculations. At high load/speed conditions, PCv900d1.1 gave the best performance, while at low load/speed conditions this was achieved with PCv1050d0.9. Thus, the results allowed to confirm the previous conclusion from phase 1 regarding the pre-chamber design requirements at different operating points.

Moreover, a characteristic pattern found at low load/speed conditions for the new designs, all of which have larger volumes than PC1, was that the pre-chamber CA50 values were delayed. This is a consequence of the high concentrations of residual gases at the top of the pre-chamber (where the electrodes are placed), which compromise the initial stages of the flame development. Furthermore, this represents a potential issue for the compatibility of the concept with EGR dilution, given that the aforementioned strategy requires early spark timings where the internal residuals of the pre-chamber are even higher. Thus, as PCv1050d0.9 gave a suitable performance both at high and low load/speed conditions, it was selected for a final tuning to extend the tolerance to EGR dilution.

The first design aspect that was optimized was the axial position of the spark plug, given that if the electrodes are placed closer to the pre-chamber bottom then the high RGF regions can be avoided by the initial flame kernel. Several simulations were performed lowering the spark plug in intervals of 1 mm, and it was found that a position of 8 mm below the original location gave a good balance between the levels of residuals and TKE.

Another design aspect that was considered was the addition of a large hole at the bottom of the pre-chamber. The idea with this hole pattern is to orient the flow towards the center of the pre-chamber (where the electrodes are located), in order to better sweep the residual gases in this direction. Thus, the side-holes of PCv1050d0.9 were reduced to 0.8 mm in order to add a bottom hole of 1 mm and keep the same A/V ratio. Afterwards, the new design was simulated and the results showed an improved local stratification of the RGF in the bottom part of the pre-chamber. Moreover, the scavenging of residual gases at the spark plug was also improved at advanced crankangles. Therefore, a final design (PCv1050d0.9opt) was proposed with this new hole pattern and the optimized position of the electrodes, as it gave encouraging results for improving the tolerance to EGR dilution.

However, since the pre-chamber flow-field changes with the new layout of the holes, the last phase of the methodology was focused on evaluating this optimized design in terms of cyclic variability. In this stage, the multi-cycle LES methodology developed in Chapter 4 was used to simulate PCv1050d0.9opt at low load/speed conditions with two spark timings, in order to quantify the CCV levels of this pre-chamber with the τ parameter defined in Section 4.3.5. In addition, both PC1 and PCv1050d0.9opt were simulated at medium load/speed conditions (6.8 bar IMEP @2000 rpm) with 10% of EGR. The results showed an improved combustion stability for the optimized design at delayed spark timings and EGR diluted conditions, proving its potential for enhancing the global performance of the concept.

Finally, PCv1050d0.9opt was manufactured and tested in the real engine. An EGR sweep was performed at 2000 rpm and 6.8 bar IMEP, comparing the optimized design with the reference pre-chamber and the conventional SI concept. The results revealed that PCv1050d0.9opt was able to extend the dilution limit by 5% with respect to PC1, verifying the validity of the pre-chamber design methodology developed during this thesis.

References

[1] Benajes, J et al. “Evaluation of the passive pre-chamber ignition concept for future high compression ratio turbocharged spark-ignition engines”. In: *Applied Energy* 248 (2019), pp. 576–588. DOI: `https://doi.org/10.1016/j.apenergy.2019.04.131`.

[2] Novella, R, Gomez-Soriano, J, Martinez-Hernandiz, PJ, Libert, C, and Rampanarivo, F. “Improving the performance of the passive pre-chamber ignition concept for spark-ignition engines fueled with natural gas”. In: *Fuel* 290 (2021), p. 119971. DOI: `https://doi.org/10.1016/j.fuel.2020.119971`.

[3] Thelen, Bryce Charles and Toulson, Elisa. *A computational study of the effects of spark location on the performance of a turbulent jet ignition system.* Tech. rep. SAE Technical Paper, 2016.

[4] Sens, M et al. “Pre-chamber ignition and promising complementary technologies”. In: *27th Aachen colloquium automobile and engine technology.* 2018.

[5] Blankmeister, Matthias, Alp, Muhammed, and Shimizu, Eriko. “Passive pre-chamber spark plug for future gasoline combustion systems with direct injection”. In: *Proc., Ignition Systems for Gasoline Engines Conf.* 2018, pp. 149–174.

Chapter 7

Conclusions and future works

The most important remarks of this doctoral thesis are summarized in this final chapter along with several ideas for future investigations that could help to widen the knowledge of the passive pre-chamber concept, in order to overcome the current limitations of this ignition strategy for its use in future passenger car engines.

This research is meant to provide insight on the underlying physics of the passive pre-chamber system implemented in a representative light-duty single-cylinder SI engine. Thus, several objectives were defined for the investigation and fulfilled during Chapters 4, 5 and 6 by analyzing the characteristics of the combustion process, flow-dynamics, and energy management of this ignition strategy. Accordingly, the original contributions of the thesis can be divided into the scientific knowledge acquired and the developed methodological procedures for industry applications:

7.1 Scientific contributions of the research

The results obtained from the combination of experimental activities and the CFD model described in Chapter 3 have allowed to perform an extensive evaluation of the passive pre-chamber concept in several operating conditions of the engine map. In addition, an assessment of this ignition system with other engine strategies such as spark timing delay at low load/speed conditions for catalyst activation and air/EGR dilution has been performed, focusing on the physical and thermochemical characteristics of the concept. Furthermore, the main conclusions address different aspects of the system, including the pre-chamber combustion process, the jet development and main chamber combustion process, the pre-chamber geometric features and the compatibility with other strategies:

7.1.1 Conclusions of the pre-chamber combustion

- Starting with the gas exchange process, the pre-chamber flow-dynamics are mainly controlled by the force of the piston during the compression stroke, which also depends on the engine running point (load/speed). Therefore, as the engine load/speed decreases the pre-chamber flow conditions will be deteriorated, presenting higher levels of internal residuals and lower levels of turbulence that ultimately affect the burning rates in this region. This inherent deterioration of the flow properties makes the concept lose flexibility at low load/speed conditions.

- Moreover, the pre-chamber flow-field analysis has also revealed two important restrictions related to the phasing of the ignition signal: On one hand, triggering the spark at an early stage will inherently imply an increase in the local stratification of residual gases, particularly in the top of the pre-chamber where the electrodes are usually placed. On the other hand, for delayed spark timings the turbulence levels of the pre-chamber will sharply decrease, compromising the flame propagation speeds.

- The ability of the ejected jets to promote the main chamber ignition depends primarily on the momentum flux through the holes (jet morphology) and the composition/temperature of the ejected gases (thermochemical characteristics). Thus, achieving a fast pre-chamber combustion is critical in order to take advantage of the concept, given that if the flame is able to sweep the entire volume quickly, the energy losses through non-reactive ejection will be minimized while generating a high momentum profile composed mainly of reactive products.

7.1.2 Conclusions of the main chamber combustion

- In un-diluted stoichiometric conditions (λ=1) the pre-chamber combustion is usually fast, and the ejected jets act as a large spark plug promoting the combustion with a high flame surface distributed along the main chamber. Thus, the main parameters that drive the ignition process are the penetration rates of the jets and their temperature. In this scenario, the thermochemical properties of the mixture and fluid-dynamic conditions downstream of the jets are highly relevant, given that the flame is able to quickly leave the influential boundaries of the jets and a major part of the combustion process takes place outside of these limits (over 70%).

- Moreover, if the cylinder head design doesn't allow the pre-chamber to be centered with respect to the cylinder axis, then some jets will not be able to reach the cylinder walls, forcing the flame to travel through a large sector of the main chamber without the enhanced turbulence generated by the jets. This represents a potential issue when the conditions downstream of the jets are compromised (low engine load/speeds or diluted mixtures).

- The flame structure in un-diluted stoichiometric conditions follows a multi-regime evolution in the Borghi-Peters diagram, starting near the Damköhler=1 line and progressing towards the *corrugated flamelets* regime in its initial stages. Afterwards, as the flame passes through the holes and the jets begin to develop in the main chamber, the flame structure momentarily shifts towards the *thickened flames* regime, only to return to the *thickened wrinkled flames* regime as the flame reaches the jet boundaries.

7.1.3 Conclusions of the pre-chamber geometry features

- The relationship between the total cross sectional area of the holes and the pre-chamber volume (A/V ratio) is a parameter that strongly conditions the scavenge of residual gases. Pre-chambers with low A/V ratios (small holes and large volumes) will not be able to evacuate most of the residuals from this region, particularly in the spark plug gap, which compromises both the performance of the concept and the tolerance to EGR dilution. A high enough A/V ratio must be used to assure the minimum amount of residuals to remain inside the pre-chamber for a given engine operating point.

- A clever methodology was developed to evaluate the cycle-to-cycle combustion variability of different pre-chamber designs by high-fidelity multi-cycle LES simulations. This approach attributes the sources of CCV to the pre-chamber combustion process, and thus only this region is simulated. Furthermore, given that the engine indicated parameters are not available with this methodology, the time for the flame to reach the pre-chamber holes (τ) was defined as a parameter to quantify the CCV of a given design, since it relates to the onset of combustion in the main chamber and its morphology. After simulating ten combustion cycles for several spark timings, the τ parameter was able to qualitatively reproduce the experimental COV IMEP trend of the reference pre-chamber for the spark timing sweep performed at low load/speed conditions.

- From the multi-cycle LES study it was found that generating a stable flow pattern inside pre-chamber is fundamental in order to maintain a suitable combustion stability. Thus, providing a tangential angle to the layout of the holes, which generates a swirling vortex in the whole pre-chamber volume, is necessary to avoid the extreme velocity fluctuations that are produced by non-swirled small holes (≈0.7 mm), which ultimately compromise the CCV levels.

7.1.4 Conclusions of the compatibility with other engine strategies

- Delaying the spark timing at low load/speed conditions is critical for heating-up the Three-Way Catalyst during cold-start. However, the passive pre-chamber concept has some compatibility issues with this strategy, since delaying the ignition further from the MBT spark timing towards TDC results in the extra fuel that fills the pre-chamber to be lost under cold/non-reactive ejection. Thus, as the spark is triggered closer to TDC, most of the jet momentum is used to eject non-reacting flow, incapable of promoting the main chamber ignition. This leads to a longer time lag between the spark timing and the onset of main chamber combustion, given that the reactive ejection is delayed and the thermodynamic conditions in the main chamber become less favorable as the piston starts to descend. In addition, delaying the onset of main chamber combustion can also result in an increased CCV, since the ignition lag gives more time for the flow-field to present variations between cycles.

- Diluting the mixture with either air or EGR changes significantly the combustion characteristics of the concept when reaching the dilution limit. While the un-diluted stoichiometric case shows a jet-driven ignition pattern, the diluted cases resemble a convention spark-ignition process, with the jets contained in a small region of the main chamber due to the deteriorated pre-chamber combustion (lower laminar flame speeds due to the mixture composition and the higher internal residuals as the spark is advanced). In this scenario the flame development is much slower, and a larger part of the combustion process takes place within the jets compared to the λ=1 case without dilution. Thus, the jets act as a high temperature reactor, where the main parameters that drive the initial stages of the combustion process are the amount of main chamber charge that the jets are able to entrain and their temperature. Consequently, an important part of the combustion process develops in an unfavorable region of the Borghi diagram (the *thickened flames* regime), where some eddies can penetrate into the diffusive layer of the flame, enlarging the flame thickness and compromising its stability. This highlights the need to enhance the pre-chamber combustion process and generate jets that are able to entrain a larger part of the main chamber charge, in order to improve the combustion stability and the performance of the concept with high levels of dilution.

- The passive pre-chamber concept is able to extend the air-dilution limit from λ=1.4 to λ=1.6 compared to the conventional SI concept (at least for some pre-chamber designs). However, the generated NO_x levels with this λ value are still not low enough to operate the engine without the use of the Three-Way Catalyst. On this note, enriching the mixture with hydrogen arises as an interesting strategy to overcome the achieved air-dilution limit. Several studies performed with the CFD model revealed that adding only 2.5% of H_2 could allow to operate the engine at λ=1.9, with relatively high efficiency levels (over 42%) and much lower NO_x emissions.

- Diluting the mixture with exhaust gases is a highly demanded strategy for the technical definitions of future SI engines, given that this technology has already been integrated into production vehicles and it is fully compatible with the TWC. However, unlike air-dilution, the tolerance of the passive pre-chamber concept to EGR is lower than the conventional SI concept, since the pre-chamber will inherently have higher levels of residuals than the main chamber. Therefore, designing the pre-chamber geometry to optimize the scavenge of residual gases is a crucial aspect that must be considered for integrating this ignition system into passenger car engines.

7.2 Practical application of the acquired knowledge

In Chapter 6 of this thesis a real-world use for the information gathered along the research was introduced, namely, a methodology for designing passive pre-chambers for passenger car applications. The method is based on combining simplified 0D/1D numerical tools and more complex 3D-CFD models to evaluate a wide set of pre-chamber geometries in a relatively short time frame. The simulations are performed according to the characteristics and computational cost associated with each model, thus, to maximize the synergies between the numerical tools and minimize the overall time of the design process, three distinct phases were defined with a specific design purpose in each one:

- In the first phase the basic geometric parameters of the pre-chamber (volume and hole diameter) are determined with the use of the simple 0D/1D models described in Sections 3.2.2 and 3.2.3. During this stage, a large number of simulations can be performed for multiple combinations of pre-chamber volumes and hole diameters, considering a fixed number of pre-chamber nozzles. The goal of these simulations is to determine the combination that provides the best jet features. Therefore, a fixed pre-chamber combustion duration was considered for the GT-Power simulations, since the desired outcome is to keep a fast pre-chamber combustion regardless of the volume. Thereafter, the 1D gaseous jet model was used to calculate the jet penetrations and a parameter t* was defined as the time that a free jet needs to reach the farthest wall distance of the main chamber. This allows to quantify the impact of the jets in a simple way. Thus, the results from this study revealed that the optimum regions for the jet features (high momentum and low t*) are found at high pre-chamber volumes, as long as a fast pre-chamber combustion is achieved, but change in terms of hole diameter depending on the operating condition. For high load/speeds, diameters between 1.1 mm and 1.3 mm provide a better performance, while at low load/speed conditions the optimum diameters are in the range of 0.7 mm to 0.9 mm. Therefore, in order for the concept to perform suitably in the whole engine map, a compromise solution must be selected from the available pre-chamber candidates.

- In the second phase three to four pre-chambers from the first stage are simulated using the CFD model, to assess the detailed 3D combustion characteristics of the selected geometries. Here, the pre-chamber burn durations for the new designs are contrasted against the reference pre-chamber, to confirm the hypothesis considered for the 0D/1D GT-Power calculations. It was found that a pre-chamber with a volume of 1050 mm^3 and 6 holes of 0.9 mm in diameter improved the engine performance both at high and low load/speed conditions. However, in the latter operating point, the pre-chamber CA50 values were delayed as a consequence of the high concentrations of residual gases in the upper part of this region, which compromises the initial stages of the combustion process and represents a potential issue for the compatibility of the concept with EGR dilution. Thus, in order to improve this aspect two design solutions were proposed: On one hand lowering the axial position of the electrodes, to avoid the high RGF regions during the ignition, and on the other hand adding a larger hole at the bottom of the pre-chamber, which showed an improvement in the local stratification of residual gases at advanced spark timings.

- The third stage consists of evaluating the final pre-chamber design in terms of combustion stability with the developed multi-cycle LES methodology, since the changes in the geometry can also generate a very different internal flow-field. Here, the τ parameter defined in Section 4.3.5 (time that it takes the flame to reach the holes) is used to quantify the CCV levels. Ten combustion cycles were calculated for the optimized design, and the results showed an improved combustion stability compared to the reference pre-chamber at delayed spark timings and EGR diluted conditions.

Ultimately, the validity of the design methodology was confirmed by manufacturing the optimized pre-chamber and testing it in the real engine, where the results revealed that the new design was able to extend the EGR dilution limit by 5% with respect to the reference pre-chamber. In addition, it should be noted that this methodology has the advantage of allowing a quick response if phase 2 fails, since the corrective action consists of selecting other candidates from the already available database generated in phase 1.

7.3 Guidelines for future investigations

Based on the conclusions drawn from this thesis, several research paths have been identified that could potentially improve the performance of the passive pre-chamber concept. These paths are based on the identified limitations and drawbacks of this ignition system, especially in conditions where the operation of the engine with this technology is compromised.

Further optimizing the geometric features of the pre-chamber and extending the developed design methodology:

- Despite the fact that the desirable characteristics for the pre-chamber have been identified from a geometric design point of view, it is not yet known with certainty whether a truly optimized geometry has been evaluated, so it is undoubtedly necessary to continue in this direction by simulating and testing pre-chambers with very different internal designs, such as a narrow throat pre-chamber with a conical body. This will ultimately allow to to understand the real potential of the concept.
- Moreover, using the pre-chamber design procedure developed during this thesis to assess the performance of new pre-chamber bodies integrated in different engine architectures is also a research path that can help to develop this technology for passenger car applications, and further validate the robustness of the design methodology.

Improving the ignition process in the pre-chamber:

- In view of the obtained results, it is evident that the passive pre-chamber concept transfers the usual ignition issues of the conventional SI system in diluted conditions from the main chamber to the pre-chamber. Therefore, a potential solution to this problem is to study the use of unconventional ignition sources inside the pre-chamber, such as a corona igniter o a surface discharge system. This strategy could allow to overcome the deteriorated pre-chamber burning rates with diluted mixtures, generating better jets and resembling the operation with an active pre-chamber.

Improving the combustion process in the pre-chamber:

- An important conclusion that has been drawn from this work is the relevance of the combustion process in the pre-chamber for generating suitable jets and improving the performance of the concept. In this sense, several strategies are proposed to try to accelerate the pre-chamber burning rates.

  - Doping the pre-chamber mixture with fuels/chemical species that increase the flame speeds (H_2 is an ideal candidate).
  - Increasing the temperature of the gas in the pre-chamber by using surface coatings as thermal barriers to limit the heat transfer through the pre-chamber walls, or by using systems that allow to heat-up these walls (as long as the knocking phenomenon is controlled).
  - Improving the combustion process in the vicinity of the pre-chamber walls by using catalytic coatings on them.
  - Replacing the combustion process in the pre-chamber, moving from the conventional flame propagation to an auto-ignition concept, since it is not clear whether this transition is positive or negative and therefore it is necessary to evaluate this approach.

Replacing the combustion process in the main chamber:

- As has been mentioned, when the thermochemical properties of the mixture and fliud-dynamic conditions in the main chamber are compromised, the jets ejected from the pre-chamber must entrain a larger part of the main chamber charge, which is complicated due to the limited duration of the ejection and the subsequent physics of the combustion process. Therefore, combining the passive pre-chamber concept with combustion strategies such as Spark-Assisted Compression Ignition (SACI), where the conventional flame propagation process is replaced with an auto-ignition process when the combustion has reached a certain level of progress, seems to be an interesting approach to study.

Other lines of research that show potential, although they are not based on improving the performance of the passive pre-chamber ignition concept, are:

- Replacing the pre-chamber ignition system under certain conditions, for example during cold-start, where it is necessary to accelerate the activation of the catalyst. Here, the conventional SI concept offers obvious advantages, so both ignition strategies can be combined simply by integrating them into the engine and operating each one in the desired conditions, although it implies an increase in the complexity and cost of the ignition system.

- Replacing the thermal engine in certain conditions, for example at medium and low load/speeds, where the passive pre-chamber concept does not provide considerable advantages. In this case hybridizing the powerplant and using electric propulsion instead of the thermal engine arises as an interesting solution.

In outline, this thesis condenses a lot of information about the characteristics of the passive pre-chamber concept in light-duty engines. Furthermore, despite having a mechanical simplicity compared to the active system, several complex physical and thermodynamic phenomena, such as turbulence, the thermochemical properties of the mixture and even the pre-chamber design itself, play a more important role on the behavior of the concept due to the nature of the passive version. Thus, this research has done an excellent job in extracting key aspects of the pre-chamber scavenge and combustion processes, to improve the performance of the concept and extend the synergies with other engine strategies, such as the use of diluted mixtures (EGR or lean burn). Nevertheless, several hurdles still need to be overcome in order to implement the proposed solutions in a way that would make this technology viable for future generation passenger car engines.

In addition, the CFD modelling methodology developed during this thesis has also served as a basis to perform 3D simulations of other combustion-related topics, such as carbon-neutral fuels (H_2, NH_3) in ICE applications, that will be the focus of future investigations to be carried out at the IUI CMT-Research Institute.

Global Bibliography

(ACEA), European Association Of Automobile Manufacturers. *Data on motor vehicle sales in the European Union in 2021 and 2022, compiled by ACEA*. 2022 (cited on pages 3, 4).

(EEA), European Environment Agency. *Transport sector contribution to total GHG emissions (EEA-32)*. 2009 (cited on page 3).

(UN), United Nations. *World population projected to reach 9.8 billion in 2050, and 11.2 billion in 2100*. 2017 (cited on page 1).

Abdel-Gayed, RG, Bradley, D, and Lau, AKC. “The straining of premixed turbulent flames”. In: *Symposium (International) on Combustion*. Vol. 22. 1. Elsevier. 1989, pp. 731–738 (cited on page 18).

Adams, TG. “Theory and evaluation of auxiliary combustion (torch) chambers”. In: *SAE Transactions* (1978), pp. 2328–2339 (cited on page 35).

Adams, Tim G. *Torch ignition for combustion control of lean mixtures*. Tech. rep. SAE Technical Paper, 1979 (cited on page 35).

Alger, Terrence, Gingrich, Jess, Mangold, Barrett, and Roberts, Charles. “A continuous discharge ignition system for EGR limit extension in SI engines”. In: *SAE International Journal of Engines* 4.1 (2011), pp. 677–692 (cited on page 22).

Allison, PM, De Oliveira, M, Giusti, Andrea, and Mastorakos, Epaminondas. “Pre-chamber ignition mechanism: Experiments and simulations on turbulent jet flame structure”. In: *Fuel* 230 (2018), pp. 274–281 (cited on page 27).

Alvarez, Carlos Eduardo Castilla, Couto, Giselle Elias, Roso, Vinıcius Rückert, Thiriet, Arthur Braga, and Valle, Ramon Molina. “A review of prechamber ignition systems as lean combustion technology for SI engines”. In: *Applied Thermal Engineering* 128 (2018), pp. 107–120. DOI: `https://doi.org/10.1016/j.applthermaleng.2017.08.118` (cited on pages 25, 33).

Angelberger, C, Poinsot, T, and Delhay, B. *Improving near-wall combustion and wall heat transfer modeling in SI engine computations.* Tech. rep. SAE Technical Paper, 1997. DOI: `https://doi.org/10.4271/972881` (cited on pages 67, 113).

Ashok, B, Kumar, A Naresh, Jacob, Ashwin, and Vignesh, R. “Emission formation in IC engines”. In: *NOx Emission Control Technologies in Stationary and Automotive Internal Combustion Engines.* Elsevier, 2022, pp. 1–38. DOI: `https://doi.org/10.1016/B978-0-12-823955-1.00001-2` (cited on page 4).

Assanis, Dimitris, Engineer, Nayan, Neuman, Paul, and Wooldridge, Margaret. *Computational development of a dual pre-chamber engine concept for lean burn combustion.* Tech. rep. SAE Technical Paper, 2016 (cited on page 38).

Attard, William. *Turbulent jet ignition pre-chamber combustion system for spark ignition engines.* US Patent 8,857,405. 2014 (cited on page 33).

Attard, William P, Bassett, Michael, Parsons, Patrick, and Blaxill, Hugh. *A new combustion system achieving high drive cycle fuel economy improvements in a modern vehicle powertrain.* Tech. rep. SAE Technical Paper, 2011 (cited on page 25).

Attard, William P and Blaxill, Hugh. *A lean burn gasoline fueled pre-chamber jet ignition combustion system achieving high efficiency and low NOx at part load.* Tech. rep. SAE Technical Paper, 2012. DOI: `https://doi.org/10.4271/2012-01-1146` (cited on page 20).

Attard, William P and Blaxill, Hugh. “A single fuel pre-chamber jet ignition powertrain achieving high load, high efficiency and near zero NOx emissions”. In: *SAE International Journal of Engines* 5.3 (2012), pp. 734–746 (cited on page 26).

Attard, William P, Blaxill, Hugh, Anderson, Eric K, and Litke, Paul. “Knock limit extension with a gasoline fueled pre-chamber jet igniter in a modern vehicle powertrain”. In: *SAE International Journal of Engines* 5.3 (2012), pp. 1201–1215 (cited on page 26).

Attard, William P, Fraser, Neil, Parsons, Patrick, and Toulson, Elisa. “A turbulent jet ignition pre-chamber combustion system for large fuel economy improvements in a modern vehicle powertrain”. In: *SAE International Journal of Engines* 3.2 (2010), pp. 20–37 (cited on pages 27, 33, 34).

Attard, William P, Kohn, Jacob, and Parsons, Patrick. “Ignition energy development for a spark initiated combustion system capable of high load, high efficiency and near zero NOx emissions”. In: *SAE International Journal of Engines* 3.2 (2010), pp. 481–496 (cited on page 33).

Attard, William P, Konidaris, Steven, Hamori, Ferenc, Toulson, Elisa, and Watson, Harry C. *Compression Ratio Effects on Performance, Efficiency, Emissions and Combustion in a Carbureted and PFI Small Engine.* Tech. rep. SAE Technical Paper, 2007 (cited on page 25).

Attard, William P and Parsons, Patrick. “A normally aspirated spark initiated combustion system capable of high load, high efficiency and near zero NOx emissions in a modern vehicle powertrain”. In: *SAE International Journal of Engines* 3.2 (2010), pp. 269–287 (cited on page 33).

Attard, William P and Parsons, Patrick. “Flame kernel development for a spark initiated pre-chamber combustion system capable of high load, high efficiency and near zero NOx emissions”. In: *SAE International Journal of Engines* 3.2 (2010), pp. 408–427 (cited on pages 25, 33).

Ayala, Ferrán A, Gerty, Michael D, and Heywood, John B. *Effects of combustion phasing, relative air-fuel ratio, compression ratio, and load on SI engine efficiency.* Tech. rep. SAE Technical Paper, 2006 (cited on page 19).

Bagnulo, A. *Engine with Stratified Mixture.* U.S. Patent 2422610, Jun. 1947 (cited on page 29).

Barnard, A. and Brewer, C. D. *mprovements in or relating to internal combustion engines.* British Patent No. 948686, Feb. 1964 (cited on page 29).

Benajes, J, Novella, R, Gomez-Soriano, J, Barbery, I, and Libert, C. “Advantages of hydrogen addition in a passive pre-chamber ignited SI engine for passenger car applications”. In: *International Journal of Energy Research* 45.9 (2021), pp. 13219–13237. DOI: `https://doi.org/10.1002/er.6648` (cited on pages 72, 167).

Benajes, J et al. “Evaluation of the passive pre-chamber ignition concept for future high compression ratio turbocharged spark-ignition engines”. In: *Applied Energy* 248 (2019), pp. 576–588. DOI: `https://doi.org/10.1016/j.apenergy.2019.04.131` (cited on pages 57, 62, 64, 116, 183, 184, 191).

Benajes, J et al. “Computational assessment towards understanding the energy conversion and combustion process of lean mixtures in passive pre-chamber ignited engines”. In: *Applied Thermal Engineering* 178 (2020), p. 115501. DOI: https://doi.org/10.1016/j.applthermaleng.2020.115501 (cited on pages 66, 116, 167).

Benajes, J. et al. “Performance of the passive pre-chamber ignition concept in a spark-ignition engine for passenger car applications”. In: *SIA Power Train & Electronics*. Paris, France: SIA Power Train & Electronics, 2019 (cited on page 100).

Benajes, Jesús, Olmeda, Pablo, Martın, Jaime, and Carreño, Ricardo. “A new methodology for uncertainties characterization in combustion diagnosis and thermodynamic modelling”. In: *Applied Thermal Engineering* 71.1 (2014), pp. 389–399. DOI: https://doi.org/10.1016/j.applthermaleng.2014.07.010 (cited on page 78).

Benedikt, Walter, Latsch, Reinhard, and Schlembach, Hans. *Separately ignited internal combustion engine with at least one main combustion chamber and an ignition chamber*. US Patent 4,416,228. 1983 (cited on page 36).

Beyerlein, Steven W and Wojcicki, Stanislaw. “A lean-burn catalytic engine”. In: *SAE transactions* (1988), pp. 1040–1051 (cited on pages 35, 36).

Beyerlein, Steven Ware. *Catalytic charge activation in a lean-burn internal combustion engine*. Washington State University, 1987 (cited on page 35).

Biswas, Sayan and Qiao, Li. “Ignition of ultra-lean premixed H2/air using multiple hot turbulent jets generated by pre-chamber combustion”. In: *Applied Thermal Engineering* 132 (2018), pp. 102–114. DOI: https://doi.org/10.1016/j.applthermaleng.2017.11.073 (cited on pages 26, 86).

Biswas, Sayan and Qiao, Li. “Ignition of ultra-lean premixed hydrogen/air by an impinging hot jet”. In: *Applied energy* 228 (2018), pp. 954–964. DOI: https://doi.org/10.1016/j.apenergy.2018.06.102 (cited on page 26).

Blankmeister, Matthias, Alp, Muhammed, and Shimizu, Eriko. “Passive pre-chamber spark plug for future gasoline combustion systems with direct injection”. In: *Proc., Ignition Systems for Gasoline Engines Conf.* 2018, pp. 149–174 (cited on page 202).

Bolla, Michele et al. “Numerical study of turbulence and fuel-air mixing within a scavenged pre-chamber using RANS and LES”. In: *SAE Technical Papers* 2019 (2019) (cited on page 141).

Borghi, R. “On the structure and morphology of turbulent premixed flames”. In: *Recent advances in the Aerospace Sciences*. Springer, 1985, pp. 117–138 (cited on pages 14, 40, 71, 111, 175).

Borghi, Roland. “Turbulent combustion modelling”. In: *Progress in energy and combustion science* 14.4 (1988), pp. 245–292 (cited on page 71).

Boudier, P, Henriot, S, Poinsot, T, and Baritaud, T. “A model for turbulent flame ignition and propagation in spark ignition engines”. In: *Symposium (International) on Combustion*. Vol. 24. 1. Elsevier. 1992, pp. 503–510. DOI: `https://doi.org/10.1016/S0082-0784(06)80064-0` (cited on page 72).

Bounaceur, Roda et al. “Prediction of auto-ignition temperatures and delays for gas turbine applications”. In: *Journal of Engineering for Gas Turbines and Power* 138.2 (2016) (cited on page 74).

Bradley, D, Sheppard, CGW, Suardjaja, IM, and Woolley, R. “Fundamentals of high-energy spark ignition with lasers”. In: *Combustion and Flame* 138.1-2 (2004), pp. 55–77 (cited on page 23).

Brakora, Jessica and Reitz, Rolf D. *A comprehensive combustion model for biodiesel-fueled engine simulations*. Tech. rep. SAE Technical Paper, 2013. DOI: `https://doi.org/10.4271/2013-01-1099` (cited on page 75).

Brandstetter, Walter. “The Volkswagen lean burn pc-engine concept”. In: *SAE Transactions* (1980), pp. 1804–1821 (cited on page 35).

Brandstetter, Walter R et al. “THE VOLKSWAGEN PCI STRATIFIED CHARGE CONCEPT. RESULTS FROM THE 1, 6 LITER AIR COOLED ENGINE”. In: (1974) (cited on page 31).

Broatch, A, Olmeda, P, Margot, Xandra, and Gómez-Soriano, Josep. “Numerical simulations for evaluating the impact of advanced insulation coatings on H2 additivated gasoline lean combustion in a turbocharged spark-ignited engine”. In: *Applied Thermal Engineering* 148 (2019), pp. 674–683 (cited on pages 66, 169).

Broderson, N. O. *Method of operating internal-combustion engines*. U.S. Patent 2690741, Oct. 1954 (cited on page 29).

Bunce, Michael, Blaxill, Hugh, and Attard, William. *Turbulent jet ignition pre-chamber combustion system for spark ignition engines*. US Patent 9,353,674. 2016 (cited on page 33).

Bunce, Michael, Cairns, Alasdair, and Blaxill, Hugh. “The use of active jet ignition to overcome traditional challenges of pre-chamber combustors under low load conditions”. In: *International Journal of Engine Research* 22.11 (2021), pp. 3325–3339 (cited on page 34).

Cai, Liming and Pitsch, Heinz. “Optimized chemical mechanism for combustion of gasoline surrogate fuels”. In: *Combustion and flame* 162.5 (2015), pp. 1623–1637. DOI: `https://doi.org/10.1016/j.combustflame.2014.11.018` (cited on page 74).

Cant, RS. “SB Pope, Turbulent Flows, Cambridge University Press, Cambridge, UK”. In: *Combustion and Flame* 125 (2001), pp. 1361–1362. DOI: `http://dx.doi.org/10.1016/S0010-2180(01)00244-9` (cited on page 67).

Chen, Ceyuan, Pal, Pinaki, Ameen, Muhsin, Feng, Dengquan, and Wei, Haiqiao. “Large-eddy simulation study on cycle-to-cycle variation of knocking combustion in a spark-ignition engine”. In: *Applied Energy* 261 (2020), p. 114447 (cited on page 70).

Chen, Ceyuan et al. *LES analysis on cycle-to-cycle variation of combustion process in a DISI Engine*. Tech. rep. SAE Technical Paper, 2019 (cited on page 145).

Colin, O and Truffin, K. “A spark ignition model for large eddy simulation based on an FSD transport equation (ISSIM-LES)”. In: *Proceedings of the Combustion Institute* 33.2 (2011), pp. 3097–3104. DOI: `https://doi.org/10.1016/j.proci.2010.07.023` (cited on page 73).

CONVERGE 2.4 Theory Manual. CONVERGENT SCIENCE Inc. 2018 (cited on pages 65, 79).

Cooper, Adrian, Harrington, Anthony, Bassett, Michael, and Pates, David. *Knock Mitigation Benefits Achieved through the Application of Passive MAHLE Jet Ignition Enabling Increased Output under Stoichiometric Operation*. Tech. rep. SAE Technical Paper, 2021 (cited on pages 39, 40).

Cooper, Adrian, Harrington, Anthony, Bassett, Michael, Reader, Simon, and Bunce, Michael. *Application of the passive MAHLE jet ignition system and synergies with miller cycle and exhaust gas recirculation*. Tech. rep. SAE Technical Paper, 2020 (cited on pages 27, 39, 42).

d’Adamo, A, Breda, S, Berni, F, and Fontanesi, S. “The potential of statistical RANS to predict knock tendency: Comparison with LES and experiments on a spark-ignition engine”. In: *Applied Energy* 249 (2019), pp. 126–142 (cited on page 69).

d'Adamo, A, Iacovano, C, and Fontanesi, S. "Large-Eddy simulation of lean and ultra-lean combustion using advanced ignition modelling in a transparent combustion chamber engine". In: *Applied Energy* 280 (2020), p. 115949 (cited on page 71).

Dale, J De, Checkel, MD, and Smy, PR. "Application of high energy ignition systems to engines". In: *Progress in energy and combustion science* 23.5-6 (1997), pp. 379–398 (cited on page 23).

Date, T, Yagi, S, Ishizuya, A, and Fujii, I. *Research and Development of the Honda CVCC engine. SAE Paper 740605.* 1974 (cited on page 30).

Davidson, DF, Gauthier, BM, and Hanson, RK. "Shock tube ignition measurements of iso-octane/air and toluene/air at high pressures". In: *Proceedings of the Combustion Institute* 30.1 (2005), pp. 1175–1182 (cited on page 74).

Davis, GC, Krieger, RB, and Tabaczynski, Rodney J. "Analysis of the flow and combustion processes of a three-valve stratified charge engine with a small prechamber". In: *SAE Transactions* (1974), pp. 3534–3550 (cited on page 31).

Desantes, JM, Pastor, JV, Garcıa-Oliver, JM, and Pastor, JM. "A 1D model for the description of mixing-controlled reacting diesel sprays". In: *Combustion and Flame* 156.1 (2009), pp. 234–249 (cited on page 63).

Desantes, José M, Garcıa-Oliver, José M, Xuan, Tiemin, and Vera-Tudela, Walter. "A study on tip penetration velocity and radial expansion of reacting diesel sprays with different fuels". In: *Fuel* 207 (2017), pp. 323–335 (cited on page 63).

Desantes, Jose Maria, Payri, Raul, Salvador, Francisco Javier, and Gil, Antonio. "Development and validation of a theoretical model for diesel spray penetration". In: *Fuel* 85.7-8 (2006), pp. 910–917 (cited on page 64).

Dober, GG. "Modelling the flame enhancement of a HAJI equipped spark ignition engine". In: *SAE No. 99091* (1999) (cited on page 32).

Dodd, Robert et al. "Laser ignition of an IC test engine using an Nd: YAG laser and the effect of key laser parameters on engine combustion performance". In: *Lasers in Engineering* 17.3 (2007), pp. 1554–2971 (cited on page 25).

Duclos, JM and Colin, O. "(2-25) Arc and Kernel Tracking Ignition Model for 3D Spark-Ignition engine calculations ((SI-7) SI Engine Combustion 7-Modeling)". In: *The Proceedings of the International symposium on diagnostics and modeling of combustion in internal combustion engines 01.204*. The Japan Society of Mechanical Engineers. 2001, p. 46. DOI: `https://doi.org/10.1299/jmsesdm.01.204.46` (cited on page 73).

Extracted: *https://glanze.sakura.ne.jp/propagate.html* (cited on page 18).

Feyz, ME, Hasti, VR, Gore, JP, and Nalim, MR. "Large eddy simulation of hot jet ignition in moderate and high-reactivity mixtures". In: *Computers & Fluids* 183 (2019), pp. 28–37 (cited on page 71).

Fieweger, K, Blumenthal, Ro, and Adomeit, G. "Self-ignition of SI engine model fuels: a shock tube investigation at high pressure". In: *Combustion and Flame* 109.4 (1997), pp. 599–619. DOI: `https://doi.org/10.1016/S0010-2180(97)00049-7` (cited on page 74).

Galindo, J, Climent, H, Plá, B, and Jiménez, VD. "Correlations for Wiebe function parameters for combustion simulation in two-stroke small engines". In: *Applied thermal engineering* 31.6-7 (2011), pp. 1190–1199 (cited on page 62).

Garcia-Oliver, Jose Maria et al. "An experimental and one-dimensional modeling analysis of turbulent gas ejection in pre-chamber engines". In: *Fuel* 299 (2021), p. 120861 (cited on page 63).

Garret, Thomas Kenneth. *Automotive Fuels And Fuels Systems.* 1994 (cited on page 30).

Garrett, T Ken. "Porsche stratified charge engine". In: *Environmental Science & Technology* 9.9 (1975), pp. 826–830 (cited on page 30).

Ge, Haiwen et al. "CFD optimization of the pre-chamber geometry for a gasoline spark ignition engine". In: *Frontiers in Mechanical Engineering* 6 (2021), p. 599752 (cited on page 66).

Geiger, José, Pischinger, Stefan, Böwing, Robert, Koß, Hans-Jürgen, and Thiemann, Jörg. "Ignition systems for highly diluted mixtures in SI-engines". In: *SAE transactions* (1999), pp. 1099–1110 (cited on page 36).

Gentz, Gerald, Gholamisheeri, Masumeh, and Toulson, Elisa. "A study of a turbulent jet ignition system fueled with iso-octane: Pressure trace analysis and combustion visualization". In: *Applied energy* 189 (2017), pp. 385–394. DOI: `https://doi.org/10.1016/j.apenergy.2016.12.055` (cited on page 26).

Gentz, Gerald, Thelen, Bryce, Litke, Paul, Hoke, John, and Toulson, Elisa. "Combustion visualization, performance, and CFD modeling of a pre-chamber turbulent jet ignition system in a rapid compression machine". In: *SAE International Journal of Engines* 8.2 (2015), pp. 538–546 (cited on page 26).

Germane, Geoff J, Wood, Carl G, and Hess, Clay C. "Lean combustion in spark-ignited internal combustion engines-a review". In: (1983) (cited on pages 6, 20).

Gülder, Ömer L. "Turbulent premixed flame propagation models for different combustion regimes". In: *Symposium (International) on Combustion.* Vol. 23. 1. Elsevier. 1991, pp. 743–750 (cited on page 18).

Guo, Hengjie, Torelli, Roberto, Szybist, James P, and Som, Sibendu. "CFD modeling of pre-spark heat release in a boosted direct-injection spark-ignition engine". In: *International Journal of Engine Research* (2021), p. 14680874211044110 (cited on page 66).

Gussak, LA. "High chemical activity of incomplete combustion products and a method of prechamber torch ignition for avalanche activation of combustion in internal combustion engines". In: *SAE transactions* (1975), pp. 2421–2445 (cited on page 31).

Gussak, LA. *The role of chemical activity and turbulence intensity in prechamber-torch organization of combustion of a stationary flow of a fuel-air mixture.* Tech. rep. SAE Technical Paper, 1983 (cited on page 31).

Gussak, LA, Karpov, VP, and Tikhonov, YV. "The application of lag-process in prechamber engines: SAE paper 790692". In: *Passenger Car Meeting & Exposition, SAE International, Warrendale, PA, United States.* 1979 (cited on page 31).

Gussak, LA, Ryabikov, OB, Politenkova, GG, and Furman, GA. "Effect of adding individual combustion products on combustion of methane—Air mixture". In: *Bulletin of the Academy of Sciences of the USSR, Division of chemical science* 22 (1973), pp. 2128–2128 (cited on pages 31, 36).

Gussak, LA and Turkish, MICHAEL C. "LAG-process of combustion and its application in automobile gasoline engines". In: *Proc. IMechE C.* Vol. 257. 1976 (cited on page 31).

Han, Sung Bin, Choi, Kyu Hoon, Ra, Sung Oh, Lee, Sang Joon, and Lee, Jong Tai. *Ignitability and combustion characteristics of the multi spark capacitor discharge ignitor for a lean burn engine.* Tech. rep. SAE Technical Paper, 1995 (cited on page 22).

Han, Xiaoye, Yu, Shui, Tjong, Jimi, and Zheng, Ming. "Study of an innovative three-pole igniter to improve efficiency and stability of gasoline combustion under charge dilution conditions". In: *Applied Energy* 257 (2020), p. 113999 (cited on page 22).

Hansen, James et al. “Global temperature change”. In: *Proceedings of the National Academy of Sciences* 103.39 (2006), pp. 14288–14293 (cited on page 2).

Hayashi, Naoto, Sugiura, Akimitsu, Abe, Yuya, and Suzuki, Kotaro. “Development of ignition technology for dilute combustion engines”. In: *SAE International Journal of Engines* 10.3 (2017), pp. 984–994 (cited on page 22).

Heimel, Sheldon and Weast, Robert C. “Effect of initial mixture temperature on the burning velocity of benzene-air, n-heptane-air, and isooctane-air mixtures”. In: *Symposium (international) on combustion.* Vol. 6. 1. Elsevier. 1957, pp. 296–302 (cited on page 75).

Heise, Volker, Farah, Philippe, Husted, Harry, and Wolf, Edgard. *High frequency ignition system for gasoline direct injection engines.* Tech. rep. SAE Technical Paper, 2011 (cited on page 23).

Hese, Martin, Tschöke, Helmut, Breuninger, Tobias, Altenschmidt, Frank, and Winter, Harald. “Influence of a Multispark Ignition System on the inflammation in a Spray-guided Combustion Process”. In: *SAE International Journal of Fuels and Lubricants* 2.2 (2010), pp. 376–386 (cited on page 22).

Heyne, S., Meier, M., Imbert, B., and Favrat, D. “Experimental investigation of prechamber autoignition in a natural gas engine for cogeneration”. In: *Fuel* 88.3 (2009), pp. 547–552. DOI: `https://doi.org/10.1016/j.fuel.2008.09.032` (cited on pages 6, 25).

Heywood, John B. *Internal Combustion Engine Fundamentals. N. York: McGraw-Hill.* 1988 (cited on pages 6, 19).

Hlaing, Ponnya et al. “Effect of pre-chamber enrichment on lean burn pre-chamber spark ignition combustion concept with a narrow-throat geometry”. In: (2020) (cited on page 38).

Iafrate, Nicolas, Matrat, Mickael, and Zaccardi, Jean-Marc. “Numerical investigations on hydrogen-enhanced combustion in ultra-lean gasoline spark-ignition engines”. In: *International Journal of Engine Research* 22.2 (2021), pp. 375–389 (cited on page 167).

Issa, Raad I. “Solution of the implicitly discretised fluid flow equations by operator-splitting”. In: *Journal of computational physics* 62.1 (1986), pp. 40–65 (cited on page 67).

Jarosinski, J and Wojcicki, S. *Investigation of a lean-burn piston engine with catalytic prechamber and recirculation of combustion products.* Tech. rep. American Society of Mechanical Engineers, New York, NY (United States), 1995 (cited on page 35).

Jarosiński, Józef, Łapucha, Ryszard, Mazurkiewicz, Jacek, and Wójcicki, Stanisław. "Investigation of a lean-burn piston engine with catalytic prechamber". In: *SAE transactions* (1996), pp. 226–233 (cited on page 35).

Jerzembeck, S, Peters, N, Pepiot-Desjardins, Pitsch, and Pitsch, H. "Laminar burning velocities at high pressure for primary reference fuels and gasoline: Experimental and numerical investigation". In: *Combustion and Flame* 156.2 (2009), pp. 292–301. DOI: `https://doi.org/10.1016/j.combustflame.2008.11.009` (cited on page 75).

Kettner, Maurice et al. *The BPI flame jet concept to improve the inflammation of lean burn mixtures in spark ignited engines.* Tech. rep. SAE Technical Paper, 2004 (cited on page 37).

Kettner, Maurice et al. "A new flame jet concept to improve the inflammation of lean burn mixtures in SI engines". In: *SAE transactions* (2005), pp. 1549–1557 (cited on page 37).

Kim, Joohan et al. "Assessment of turbulent combustion models for simulating prechamber ignition in a natural Gas engine". In: *Journal of Engineering for Gas Turbines and Power* 143.9 (2021) (cited on pages 38, 71).

Kolmogorov, Andrey Nikolaevich. "The local structure of turbulence in incompressible viscous fluid for very large Reynolds numbers". In: *Cr Acad. Sci. URSS* 30 (1941), pp. 301–305 (cited on page 14).

Konishi, M., Nakamura, N., Oono, E., and Baika, T. "Effects of a Prechamber on NOx Formation Process in the SI Engine". In: *1979 Automotive Engineering Congress and Exposition.* SAE International, 1979. DOI: `https://doi.org/10.4271/790389` (cited on page 35).

Lapuerta, M., Armas, O., and Hernández, J.J. "Diagnosis of DI Diesel combustion from in-cylinder pressure signal by estimation of mean thermodynamic properties of the gas". In: *Applied Thermal Engineering* 19.5 (1999), pp. 513–529. DOI: `https://doi.org/10.1016/S1359-4311(98)00075-1` (cited on pages 58, 78).

Latsch, Reinhard. "The swirl-chamber spark plug: a means of faster, more uniform energy conversion in the spark-ignition engine". In: *SAE transactions* (1984), pp. 365–377 (cited on page 35).

Latsch, Reinhard and Schlembach, Hans. *Externally ignited internal combustion engine.* US Patent 4,218,992. 1980 (cited on page 36).

Latsch, Reinhard, Schlembach, Hans, and Scherenberg, Dieter. *Method for igniting lean fuel-air mixtures and an apparatus to perform the method.* US Patent 4,513,708. 1985 (cited on page 36).

Launder, Brian Edward and Spalding, Dudley Brian. “The numerical computation of turbulent flows”. In: *Numerical prediction of flow, heat transfer, turbulence and combustion.* Elsevier, 1983, pp. 96–116 (cited on page 67).

Lawrence, Jeremy and Watson, Harry C. “Hydrocarbon emissions from a HAJI equipped ultra-lean burn SI engine”. In: *SAE transactions* (1998), pp. 6–12 (cited on page 32).

Lefkowitz, Joseph K et al. “Schlieren imaging and pulsed detonation engine testing of ignition by a nanosecond repetitively pulsed discharge”. In: *Combustion and Flame* 162.6 (2015), pp. 2496–2507 (cited on page 22).

Liu, Yao-Dong, Jia, Ming, Xie, Mao-Zhao, and Pang, Bin. “Enhancement on a skeletal kinetic model for primary reference fuel oxidation by using a semidecoupling methodology”. In: *Energy & Fuels* 26.12 (2012), pp. 7069–7083. DOI: `https://doi.org/10.1021/ef301242b` (cited on pages 74–76, 88, 167).

López, JJ et al. “Advantages of the unscavenged pre-chamber ignition system in turbocharged natural gas engines for automotive applications”. In: *Energy* 218 (2021), p. 119466. DOI: `https://doi.org/10.1016/j.energy.2020.119466` (cited on page 57).

Lumsden, Grant and Watson, Harry C. “Optimum Control of an SI engine with a= 5 capability”. In: *SAE paper* 950689 (1995) (cited on page 32).

Malé, Quentin et al. “Large eddy simulation of pre-chamber ignition in an internal combustion engine”. In: *Flow, Turbulence and Combustion* (2019), pp. 1–19 (cited on pages 38, 66).

Mallory, M. *Internal Combustion Engine.* U.S. Patent 2121920, Feb. 1938 (cited on page 29).

Maly, Rudolf R and Herweg, Rüdiger. “Spark ignition and combustion in four-stroke gasoline engines”. In: *Flow and combustion in reciprocating engines.* Springer, 2008, pp. 1–66 (cited on page 23).

Mandilas, C, Ormsby, MP, Sheppard, CGW, and Woolley, R. “Effects of hydrogen addition on laminar and turbulent premixed methane and iso-octane–air flames”. In: *Proceedings of the combustion institute* 31.1 (2007), pp. 1443–1450 (cited on page 76).

Marble, Frank E and Broadwell, James E. *The coherent flame model for turbulent chemical reactions.* Tech. rep. PURDUE UNIV LAFAYETTE IN PROJECT SQUIDHEADQUARTERS, 1977 (cited on page 72).

Mariani, Antonio and Foucher, Fabrice. “Radio frequency spark plug: An ignition system for modern internal combustion engines”. In: *Applied energy* 122 (2014), pp. 151–161 (cited on page 23).

Masouleh, M Ghaderi et al. “Flow and thermal field effects on cycle-to-cycle variation of combustion: scale-resolving simulation in a spark ignited simplified engine configuration”. In: *Applied Energy* 230 (2018), pp. 486–505 (cited on page 145).

Masouleh, M Ghaderi et al. “Modeling cycle-to-cycle variations in spark ignited combustion engines by scale-resolving simulations for different engine speeds”. In: *Applied Energy* 250 (2019), pp. 801–820 (cited on page 145).

Mehl, Marco, Pitz, William J, Westbrook, Charles K, and Curran, Henry J. “Kinetic modeling of gasoline surrogate components and mixtures under engine conditions”. In: *Proceedings of the Combustion Institute* 33.1 (2011), pp. 193–200. DOI: `https://doi.org/10.1016/j.proci.2010.05.027` (cited on page 74).

Menon, S, Yeung, P-K, and Kim, W-W. “Effect of subgrid models on the computed interscale energy transfer in isotropic turbulence”. In: *Computers & fluids* 25.2 (1996), pp. 165–180 (cited on page 69).

Metghalchi, Mohamad and Keck, James C. “Burning velocities of mixtures of air with methanol, isooctane, and indolene at high pressure and temperature”. In: *Combustion and flame* 48 (1982), pp. 191–210 (cited on page 75).

Muller, Matias, Freeman, Corbin, Zhao, Peng, and Ge, Haiwen. “Numerical simulation of ignition mechanism in the main chamber of turbulent jet ignition system”. In: *Internal Combustion Engine Division Fall Technical Conference*. Vol. 51999. American Society of Mechanical Engineers. 2018, V002T06A010 (cited on page 38).

Nalley, S and LaRose, A. *International Energy Outlook 2021 (IEO2021)*. 2021 (cited on pages 1, 2).

Nishioka, Shin, Hanashi, Ken, and Okabe, Shinichi. *Super ignition spark plug with wear resistive electrode*. Tech. rep. SAE Technical Paper, 2008 (cited on page 23).

Noguchi, M., Sanda, S., and Nakamura, N. “Development of Toyota Lean Burn Engine”. In: *1976 Automobile Engineering Meeting*. SAE International, 1976. DOI: `https://doi.org/10.4271/760757` (cited on page 35).

Norbye, JP and Dunne, J. “Honda’s New CVCC Car Engine Meets’ 75 Emissions Now”. In: *Popular Science Magazine* (1973), pp. 79–81 (cited on page 30).

Novella, R, Gomez-Soriano, J, Barbery, I, and Libert, C. “Numerical analysis of the passive pre-chamber ignition concept for light duty applications”. In: *Applied Thermal Engineering* (2022), p. 118610 (cited on page 66).

Novella, R, Gomez-Soriano, J, Martinez-Hernandiz, PJ, Libert, C, and Rampanarivo, F. “Improving the performance of the passive pre-chamber ignition concept for spark-ignition engines fueled with natural gas”. In: *Fuel* 290 (2021), p. 119971. DOI: `https://doi.org/10.1016/j.fuel.2020.119971` (cited on pages 63, 64, 191, 192).

Novella, Ricardo et al. *Experimental and Numerical Analysis of Passive Pre-Chamber Ignition with EGR and Air Dilution for Future Generation Passenger Car Engines*. Tech. rep. SAE Technical Paper, 2020. DOI: `https://doi.org/10.4271/2020-01-0238` (cited on page 100).

O’Driscoll, Rosalind, Stettler, Marc EJ, Molden, Nick, Oxley, Tim, and ApSimon, Helen M. “Real world CO2 and NOx emissions from 149 Euro 5 and 6 diesel, gasoline and hybrid passenger cars”. In: *Science of the total environment* 621 (2018), pp. 282–290 (cited on page 4).

Olmeda, Pablo, Martın, Jaime, Novella, Ricardo, and Carreño, Ricardo. “An adapted heat transfer model for engines with tumble motion”. In: *Applied Energy* 158 (2015), pp. 190–202 (cited on page 58).

Pal, Pinaki, Keum, SeungHwan, and Im, Hong G. “Assessment of flamelet versus multi-zone combustion modeling approaches for stratified-charge compression ignition engines”. In: *International Journal of Engine Research* 17.3 (2016), pp. 280–290 (cited on page 71).

Pan, Jiaying et al. “LES analysis for auto-ignition induced abnormal combustion based on a downsized SI engine”. In: *Applied Energy* 191 (2017), pp. 183–192 (cited on page 5).

Pancheshnyi, Sergey V, Lacoste, Deanna A, Bourdon, Anne, and Laux, Christophe O. “Ignition of propane–air mixtures by a repetitively pulsed nanosecond discharge”. In: *IEEE Transactions on Plasma Science* 34.6 (2006), pp. 2478–2487 (cited on page 22).

Pastor, Jose V, Garcia-Oliver, Jose M, Pastor, Jose M, and Vera-Tudela, W. “One-dimensional diesel spray modeling of multicomponent fuels”. In: *Atomization and sprays* 25.6 (2015) (cited on page 63).

Pastor, José V, López, J Javier, Garcıa, José M, and Pastor, José M. “A 1D model for the description of mixing-controlled inert diesel sprays”. In: *Fuel* 87.13-14 (2008), pp. 2871–2885 (cited on page 63).

Payri, F., Molina, S., Martín, J., and Armas, O. "Influence of measurement errors and estimated parameters on combustion diagnosis". In: *Applied Thermal Engineering* 26.2 (2006), pp. 226–236. DOI: `https://doi.org/10.1016/j.applthermaleng.2005.05.006` (cited on page 58).

Payri González, Francisco and Desantes Fernández, José Mª. *Motores de combustión interna alternativos.* Editorial Universitat politécnica de valencia, 2011 (cited on page 19).

Peters, Nathan, Subramanyam, Sai Krishna Pothuraju, Bunce, Michael, Blaxill, Hugh, and Cooper, Adrian. "Optimization of lambda across the engine map for the purpose of maximizing thermal efficiency of a jet ignition engine". In: *SAE International Journal of Advances and Current Practices in Mobility* 2.2020-01-0278 (2020), pp. 3140–3150 (cited on pages 26, 34).

Peters, Norbert. "The turbulent burning velocity for large-scale and small-scale turbulence". In: *Journal of Fluid mechanics* 384 (1999), pp. 107–132 (cited on pages 14, 40, 111).

Peters, Norbert. *Turbulent combustion.* Cambridge university press, 2000 (cited on page 67).

Pickett, Lyle M et al. "Relationship between diesel fuel spray vapor penetration/dispersion and local fuel mixture fraction". In: *SAE International Journal of Engines* 4.1 (2011), pp. 764–799 (cited on page 64).

Poinsot, Thierry and Veynante, Denis. *Theoretical and numerical combustion.* RT Edwards, Inc., 2005 (cited on pages 14, 71, 175).

Poinsot, TJ, Haworth, Daniel Connell, and Bruneaux, Gilles. "Direct simulation and modeling of flame-wall interaction for premixed turbulent combustion". In: *Combustion and flame* 95.1-2 (1993), pp. 118–132 (cited on page 86).

Pomraning, Eric and Rutland, Christopher J. "Dynamic one-equation nonviscosity large-eddy simulation model". In: *AIAA journal* 40.4 (2002), pp. 689–701 (cited on page 70).

Pomraning, Eric Douglas. *Development of large eddy simulation turbulence models.* The University of Wisconsin-Madison, 2000 (cited on page 69).

Pope, Stephen B. "Ten questions concerning the large-eddy simulation of turbulent flows". In: *New journal of Physics* 6.1 (2004), p. 35 (cited on page 69).

Posch, Stefan, Winter, Hubert, Zelenka, Jan, Pirker, Gerhard, and Wimmer, Andreas. “Development of a tool for the preliminary design of large engine prechambers using machine learning approaches”. In: *Applied Thermal Engineering* 191 (2021), p. 116774. DOI: `https://doi.org/10.1016/j.applthermaleng.2021.116774` (cited on page 71).

Quader, Ather A. “Lean combustion and the misfire limit in spark ignition engines”. In: *SAE transactions* (1974), pp. 3274–3296 (cited on page 20).

Ravi, Sankaranarayanan and Petersen, Eric L. “Laminar flame speed correlations for pure-hydrogen and high-hydrogen content syngas blends with various diluents”. In: *International Journal of Hydrogen Energy* 37.24 (2012), pp. 19177–19189 (cited on page 76).

Ravindran, Arun C and Kokjohn, Sage L. “Combining machine learning with 3D-CFD modeling for optimizing a DISI engine performance during cold-start”. In: *Energy and AI* 5 (2021), p. 100072 (cited on page 66).

Ravindran, Arun C and Kokjohn, Sage L. “The challenges of using detailed chemistry model for simulating direct injection spark ignition engine combustion during cold-start”. In: *International Journal of Engine Research* (2021), p. 14680874211045968 (cited on page 71).

Ravindran, Arun C, Kokjohn, Sage L, and Petersen, Benjamin. “G-equation based ignition model for direct injection spark ignition engines”. In: *International Journal of Engine Research* 23.8 (2022), pp. 1339–1352 (cited on page 69).

Redlich, Otto and Kwong, Joseph NS. “On the thermodynamics of solutions. V. An equation of state. Fugacities of gaseous solutions.” In: *Chemical reviews* 44.1 (1949), pp. 233–244 (cited on page 67).

Reitz, Rolf D et al. *IJER editorial: The future of the internal combustion engine.* 2020 (cited on page 22).

Ricardo, Harry R. “Recent research work on the internal-combustion engine”. In: *SAE Transactions* (1922), pp. 1–93 (cited on page 28).

Richardson, Lewis Fry. *Weather prediction by numerical process.* University Press, 1922 (cited on page 14).

Rychter, TJ, Saragih, R, Lezański, T, and Wojcicki, S. “Catalytic activation of a charge in a prechamber of a SI lean-burn engine”. In: *Symposium (International) on Combustion.* Vol. 18. 1. Elsevier. 1981, pp. 1815–1824 (cited on page 35).

Sanal, Sangeeth et al. *A Numerical Study on the Ignition of Lean CH 4/Air Mixture by a Pre-Chamber-Initiated Turbulent Jet.* Tech. rep. SAE technical paper, 2020 (cited on page 38).

Sanda, S. and Nakamura, N. *Internal combustion engine provided with precombustion chamber.* U.S. Patent 4048973, Sep. 1977 (cited on page 35).

Santos, Nathália Duarte Souza Alvarenga, Alvarez, Carlos Eduardo Castilla, Roso, Vinıcius Rückert, Baeta, José Guilherme Coelho, and Valle, Ramon Molina. “Combustion analysis of a SI engine with stratified and homogeneous pre-chamber ignition system using ethanol and hydrogen”. In: *Applied Thermal Engineering* 160 (2019), p. 113985 (cited on page 28).

Scussel, AJ, Simko, AO, and Wade, WR. “The Ford PROCO engine update”. In: *SAE Transactions* (1978), pp. 2706–2725 (cited on page 31).

Sens, M et al. “Pre-chamber ignition and promising complementary technologies”. In: *27th Aachen colloquium automobile and engine technology.* 2018 (cited on pages 28, 202).

Sens, Marc and Binder, Emanuel. “Pre-chamber ignition as a key technology for future powertrain fleets”. In: *MTZ worldwide* 80.2 (2019), pp. 44–51 (cited on page 39).

Shih, Tsan-Hsing, Liou, William W, Shabbir, Aamir, Yang, Zhigang, and Zhu, Jiang. “A new k- eddy viscosity model for high reynolds number turbulent flows”. In: *Computers & fluids* 24.3 (1995), pp. 227–238 (cited on page 68).

Shiraishi, Taisuke, Urushihara, Tomonori, and Gundersen, Martin. “A trial of ignition innovation of gasoline engine by nanosecond pulsed low temperature plasma ignition”. In: *Journal of Physics D: Applied Physics* 42.13 (2009), p. 135208 (cited on page 23).

Silva, Mickael et al. *Effects of geometry on passive pre-chamber combustion characteristics.* Tech. rep. SAE Technical Paper, 2020 (cited on pages 38, 71).

Silva, Mickael et al. “Computational assessment of effects of throat diameter on combustion and turbulence characteristics in a pre-chamber engine”. In: *Applied Thermal Engineering* 212 (2022), p. 118595 (cited on page 66).

Sodja, Jurij. “Turbulence models in CFD”. In: *University of Ljubljana* (2007), pp. 1–18 (cited on page 67).

Stadler, Andreas, Wessoly, Maximilian, Blochum, Sebastian, Härtl, Martin, and Wachtmeister, Georg. “Gasoline fueled pre-chamber ignition system for a light-duty passenger car engine with extended lean limit”. In: *SAE International Journal of Engines* 12.3 (2019), pp. 323–340 (cited on page 20).

Suess, M, Guenthner, M, Schenk, M, and Rottengruber, HS. “Investigation of the potential of corona ignition to control gasoline homogeneous charge compression ignition combustion”. In: *Proceedings of the Institution of Mechanical Engineers, Part D: Journal of Automobile Engineering* 226.2 (2012), pp. 275–286 (cited on page 23).

Summers, C. E. *Internal Combustion Engine.* U.S. Patent 1568638, Jan. 1926 (cited on page 29).

Syrovatka, Zbynek, Vitek, Oldrich, Vavra, Jiri, and Takats, Michal. *Scavenged pre-chamber volume effect on gas engine performance and emissions.* Tech. rep. SAE Technical Paper, 2019 (cited on page 72).

Tang, Qinglong et al. “Optical diagnostics on the pre-chamber jet and main chamber ignition in the active pre-chamber combustion (PCC)”. In: *Combustion and Flame* 228 (2021), pp. 218–235 (cited on page 27).

Tanoue, Kimitoshi et al. “Development of a novel ignition system using repetitive pulse discharges: application to a SI Engine”. In: *SAE International Journal of Engines* 2.1 (2009), pp. 298–306 (cited on page 22).

Thelen, Bryce Charles, Gentz, Gerald, and Toulson, Elisa. *Computational study of a turbulent jet ignition system for lean burn operation in a rapid compression machine.* Tech. rep. SAE Technical Paper, 2015 (cited on page 38).

Thelen, Bryce Charles and Toulson, Elisa. *A computational study of the effects of spark location on the performance of a turbulent jet ignition system.* Tech. rep. SAE Technical Paper, 2016 (cited on pages 38, 201).

Torregrosa, A, Olmeda, P, Degraeuwe, By, and Reyes, M. “A concise wall temperature model for DI Diesel engines”. In: *Applied Thermal Engineering* 26.11-12 (2006), pp. 1320–1327. DOI: `https://doi.org/10.1016/j.applthermaleng.2005.10.021` (cited on page 78).

Toulson, Elisa. *Applying alternative fuels in place of hydrogen to the jet ignition process.* University of Melbourne, Department of Mechanical Engineering, 2008 (cited on page 32).

Toulson, Elisa, Schock, Harold J, and Attard, William P. *A review of pre-chamber initiated jet ignition combustion systems.* Tech. rep. SAE Technical Paper, 2010. DOI: `https://doi.org/10.4271/2010-01-2263` (cited on pages 6, 25).

Toulson, Elisa, Watson, Harry C, and Attard, William P. “The effects of hot and cool EGR with hydrogen assisted jet ignition”. In: *Asia Pacific Automotive Engineering Conference.* 2007-01-3627. 2007 (cited on page 21).

Truffin, Karine, Angelberger, Christian, Richard, Stéphane, and Pera, Cécile. "Using large-eddy simulation and multivariate analysis to understand the sources of combustion cyclic variability in a spark-ignition engine". In: *Combustion and Flame* 162.12 (2015), pp. 4371–4390 (cited on page 143).

Turkish, Michael C. "3-valve stratified charge engines: Evolvement, analysis and progression". In: *SAE Transactions* (1974), pp. 3483–3503 (cited on page 29).

Turkish, Michael C. "Prechamber and valve gear design for 3-valve stratified charge engines". In: *SAE Transactions* (1975), pp. 2827–2856 (cited on page 29).

Turns, Stephen R et al. *Introduction to combustion.* Vol. 287. McGraw-Hill Companies New York, NY, USA, 1996 (cited on page 71).

Vermorel, Olivier et al. "Towards the understanding of cyclic variability in a spark ignited engine using multi-cycle LES". In: *Combustion and flame* 156.8 (2009), pp. 1525–1541 (cited on page 70).

Versteeg, Henk Kaarle and Malalasekera, Weeratunge. *An introduction to computational fluid dynamics: the finite volume method.* Pearson education, 2007 (cited on pages 7, 67).

Wang, Hu, Yao, Mingfa, and Reitz, Rolf D. "Development of a reduced primary reference fuel mechanism for internal combustion engine combustion simulations". In: *Energy & Fuels* 27.12 (2013), pp. 7843–7853. DOI: `https://doi.org/10.1021/ef401992e` (cited on pages 74, 75).

Wang, Jihui, Chen, Hong, Hu, Zhicheng, Yao, Mingfa, and Li, Yongdan. "A review on the Pd-based three-way catalyst". In: *Catalysis Reviews* 57.1 (2015), pp. 79–144 (cited on pages 4, 25).

Wang, Zhi, Huang, Jian, Wang, Qiang, Hou, Lingyun, and Zhang, Guixin. "Experimental study of microwave resonance plasma ignition of methane–air mixture in a constant volume cylinder". In: *Combustion and Flame* 162.6 (2015), pp. 2561–2568 (cited on page 23).

Watson, Harry C. *Internal combustion engine ignition device.* US Patent 5,611,307. 1997 (cited on page 32).

Watson, HC. *International Patent. Application PCT/AU92/00552.* Tech. rep. PCT/AU92/00552, 1992 (cited on page 32).

Wei, Haiqiao, Zhu, Tianyu, Shu, Gequn, Tan, Linlin, and Wang, Yuesen. "Gasoline engine exhaust gas recirculation–A review". In: *Applied energy* 99 (2012), pp. 534–544 (cited on page 21).

Weng, Volker et al. "Investigation on the Bowl-Prechamber-Ignition (BPI) Concept in a Direct Injection Gasoline Engine at Part Load". In: *Design of Racing and High-Performance Engines—1998-2003* (1999), p. 463 (cited on page 36).

Wilcox, David C et al. *Turbulence modeling for CFD.* Vol. 2. DCW industries La Canada, CA, 1998 (cited on page 67).

Wilcox, David C. "Formulation of the kw turbulence model revisited". In: *AIAA journal* 46.11 (2008), pp. 2823–2838 (cited on page 68).

Wyczalek, Floyd A, Frank, Daniel L, and Neuman, John G. "Plasma jet ignition of lean mixtures". In: *SAE Transactions* (1975), pp. 856–868 (cited on page 35).

Wyczalek, Floyd A, Harned, John L, Maksymiuk, S, and Blevins, Jerry R. *EFI prechamber torch ignition of lean mixtures.* Tech. rep. SAE Technical Paper, 1975 (cited on pages 30, 31).

Xu, Guoqing, Hanauer, Christophe, Wright, Yuri M, and Boulouchos, Konstantinos. *CFD-simulation of ignition and combustion in lean burn gas engines.* Tech. rep. SAE Technical Paper, 2016 (cited on page 66).

Xu, Guoqing, Kotzagianni, Maria, Kyrtatos, Panagiotis, Wright, Yuri M, and Boulouchos, Konstantinos. "Experimental and numerical investigations of the unscavenged prechamber combustion in a rapid compression and expansion machine under engine-like conditions". In: *Combustion and Flame* 204 (2019), pp. 68–84 (cited on pages 26, 28).

Xu, Guoqing, Wright, Yuri Martin, Schiliro, Michele, and Boulouchos, Konstantinos. "Characterization of combustion in a gas engine ignited using a small un-scavenged pre-chamber". In: *International Journal of Engine Research* (2018), p. 1468087418798918. DOI: `https://doi.org/10.1177/1468087418798918` (cited on pages 38, 71).

Yakhot, Victor and Orszag, Steven A. "Renormalization group analysis of turbulence. I. Basic theory". In: *Journal of scientific computing* 1.1 (1986), pp. 3–51. DOI: `https://doi.org/10.1007/BF01061452` (cited on page 68).

Yamaguchi, Shigeki, Ohiwa, Norio, and Hasegawa, Tatsuya. "Ignition and burning process in a divided chamber bomb". In: *Combustion and flame* 59.2 (1985), pp. 177–187 (cited on page 86).

Ye, Ying et al. "A Mapping Approach for Efficient CFD Simulation of Low-Speed Large-Bore Marine Engine with Pre-Chamber and Dual-Fuel Operation". In: *Energies* 14.19 (2021), p. 6126 (cited on page 66).

Yu, Shui and Zheng, Ming. “Future gasoline engine ignition: A review on advanced concepts”. In: *International Journal of Engine Research* 22.6 (2021), pp. 1743–1775 (cited on pages 23, 24).

Yusuf, Siti Nurul Akmal, Asako, Yutaka, Sidik, Nor Azwadi Che, Mohamed, Saiful Bahri, and Japar, Wan Mohd Arif Aziz. “A short review on rans turbulence models”. In: *CFD Letters* 12.11 (2020), pp. 83–96 (cited on page 67).

Zhongming, Zhu, Linong, Lu, Xiaona, Yao, Wangqiang, Zhang, Wei, Liu, et al. “Transport: increasing oil consumption and greenhouse gas emissions hamper EU progress towards environment and climate objectives”. In: (2020) (cited on page 3).

Zhu, Sipeng, Akehurst, Sam, Lewis, Andrew, and Yuan, Hao. “A review of the pre-chamber ignition system applied on future low-carbon spark ignition engines”. In: *Renewable and Sustainable Energy Reviews* 154 (2022), p. 111872 (cited on pages 28, 123).